Title

Utilizing data science for insight into soil-water interactions

Author

BASSET, CHRISTELLE Nabil

Publication Date

2024

Peer reviewed|Thesis/dissertation

Utilizing data science for insight into soil-water interactions

By

CHRISTELLE BASSET

DISSERTATION/THESIS

Submitted in partial satisfaction of the requirements for the degree of

DOCTOR OF PHILOSOPHY

in

Soil And Biogeochemistry

in the

OFFICE OF GRADUATE STUDIES

of the

UNIVERSITY OF CALIFORNIA

DAVIS

Approved:

_____

Majdi Abou Najm, Chair

_____

Anthony Toby O'Geen

_____

Andre Daccache

Committee in Charge

2024

Acknowledgements

This dissertation would not have been possible without the guidance, support, and encouragement of many individuals. I would like to take this opportunity to express my deepest gratitude to them.

First and foremost, I extend my heartfelt thanks to my supervisor, Dr. Majdi Abou Najm, for their continued support throughout my PhD journey. I have worked with Dr. Majdi even before joining their lab at the department of Land, Air, and Water Resources at UC Davis. Their expertise and guidance have been nothing but invaluable in shaping my research and helping me grow on a personal and professional level.

I am also deeply grateful to my committee members, Dr. Anthony O'Geen, and Dr. Andre Daccache, for their timely responses, valuable feedback, and constructive suggestions, which have greatly enhanced the quality of my research.

A special thank you goes to friends, lab mates, and colleagues for their friendship, support, and for creating a collaborative and enjoyable work environment over these years.

I would like to acknowledge the financial support provided by The University of California – Davis, Agricultural Experiment Station and the Multistate Hatch Program W4188 of the USDA, National Institute of Food and Agriculture. without which this research would not have been possible.

I am deeply indebted to my family for their love, sacrifices, and encouragement. My parents, Nabil Basset and Latife Sarrouf, have always believed in me and supported me in all my endeavors. My only sister, Joelle Basset, has been my pillar of strength and patience.

To all those who have contributed to this journey in various ways, thank you.

Dedication

I dedicate my PhD research to the memory of Karim Majdi Abou Najm.

Karim inspired me, his father, his family, and friends to ask the right questions and to be critical thinkers. Karim’s journey ended on April 29, 2023, but his legacy continues. As a brilliant computer science student, he enjoyed working on solutions for the betterment of humanity.

My first conversation with Karim in 2021 was about machine learning. Despite my frustration and lack of knowledge on the subject, Karim's enthusiasm for data science to potentially address global challenges was infectious. His words motivated me to take a machine learning course, which I thoroughly enjoyed. I ended up applying many concepts about machine learning to my PhD research which shaped our understanding of soil-water interactions using data science.

As a cherished friend to many, Karim had helped many friends realize their full potentials, including myself. I am honored to dedicate my work to his memory.

Abstract

My PhD research celebrates nearly two centuries of theoretical advancements in soil-water interactions, specifically focusing on soil infiltration. Over time, mathematical models and experimental techniques have enriched our understanding of infiltration processes, contributing to improved water management, soil conservation, and environmental practices. Despite the proliferation of models enhancing our understanding of soil-water interactions, the diversity of available options poses challenges in model selection and data analysis. To address these challenges, I first conducted a detailed literature review tracing the theoretical and historical evolution of infiltration models. This review categorized 138 models based on their conceptual and empirical foundations, covering a wide spectrum of applications to guide researchers in selecting appropriate models and challenge existing theories to advance infiltration modeling. Building on this review, I addressed the uncertainty in extracting soil hydraulic properties, such as saturated hydraulic conductivity (Ks) and sorptivity (S) from experimental infiltration data to evaluate the physical meaning of these estimated properties across various infiltration models. As such, I performed a metadata analysis using a global database of 5,023 cumulative infiltration curves to assess the variability in (Ks) and (S) parameters across various one- and three-dimensional models and extraction techniques. My analysis revealed insights into the robustness of current practices applied in soil water parameter estimation. Another key finding from my literature review on infiltration modeling is the significant gap in theoretical frameworks studying the impact of soil structure on infiltration. To this end, I conducted a meta-analysis systematic review to establish correlations between infiltration rates and soil structural properties, emphasizing the need for integrated approaches. As we advance, leveraging large databases and advanced analytics can enhance our understanding of soil-water interactions and address real-world challenges. My research calls for continued scientific rigor and curiosity to uncover new relationships of dominant processes in soil science.

Table of Contents

List of Figures

List of Tables

CHAPTER 1: Mapping the Terrain: An Overview of the Dissertation

Today we celebrate almost two centuries of theoretical advancements in soil-water interactions, particularly soil infiltration. This effort has resulted in sophisticated mathematical models and experimental techniques that mark a rich history that has deepened our understanding of infiltration processes, contributing to more effective water management strategies, soil conservation, and environmental practices.

Looking ahead, I truly believe there is no better time to study soil infiltration than today with all the exciting modeling advancements, technologies, and applications. The proliferation of models has indeed advanced our collective ability to understand infiltration processes. However, this wide array of modeling options has presented a real challenge for researchers to select which model to use, and what procedures to follow for analyzing experimental infiltration data and extracting soil hydraulic properties. While many reviews have covered different aspects of infiltration processes and modeling, until now there has not been a comprehensive and objective examination of infiltration models in the literature.

This gap motivated me to develop a detailed review that summarized and mapped conceptual and empirical infiltration models' development through historic and theoretical lenses over the last two centuries. First, I started by tracing the evolution of the basic and fundamental physical flow models for rigid (non-swelling) soils that researchers have built on and used as steppingstones to model infiltration. Then I extended my review beyond the rigid soil's theory to encompass the characterization of water movement through deformable (swelling) soils. Moving from these pioneering concepts, I collected and identified 138 infiltration models spanning from early theories to the most recent models, including their mathematical equations along with their underlying philosophies and concepts. These infiltration models were categorized into a wide spectrum of

formats and applications from conceptual to empirical equations, rigid to non-rigid swelling soils, one-dimensional to multi-dimensional infiltration, from pre-ponding to completely saturated porous media.

Despite the hundreds of infiltration models that were developed, they all clustered theoretically around major milestones that were achieved by six or seven major contributions, starting with the early theoretical work of Navier-Stoke and Hagen-Poiseuille at the pore scale moving into Darcy and Richard-Richards-Buckingham at the core scale, then opening into dual and multiple domains. Around the 1990's, as models started to build on each other for advancing models' ability to predict infiltration, they tended to treat earlier classic models like Darcy and Richard as absolute laws. This paradigm was clearly evidenced by a decline in citations of these foundational models within papers introducing new theoretical models. At this stage, we take our review as an opportunity to reopen a dialogue in the soil physics and soil science community, inspiring researchers to ask critical questions, as well as to challenge and improve the current theory as we aspire to advance modeling of infiltration. Achieving this requires treating all theories with the critical lens of a curious scientist and becoming less "comfortable" with some of our assumptions, theories, and boundary conditions.

At this stage, my review offers a unique examination of the evolution of infiltration modeling, guiding researchers in selecting the most appropriate infiltration model tailored to their specific application, as well as inspiring them to challenge existing theories. However, the uncertainty researchers encounter when determining appropriate procedures for analyzing experimental infiltration data and extracting soil hydraulic properties has not been addressed yet. Put simply, it's essential to address the accuracy of extracting soil hydraulic properties, such as saturated hydraulic conductivity K_s (LT^{-1}) and sorptivity S ($LT^{-0.5}$) across different infiltration models. These

properties play crucial roles in infiltration modeling as they govern movement and retention of water through soil.

The accuracy of K_s (LT^{-1}) and S ($LT^{-0.5}$) estimates depends on various factors, including the degree to which steady flow is attained within the system being studied, ability of each experimental method to account for various theoretical and practical constraints associated with representing the physical system using a particular infiltration model, and robustness of the parameter estimation techniques employed. Using experimental infiltration data, researchers often employ various extraction methods, such as inverse modeling or curve fitting algorithms to estimate K_s (LT^{-1}) and S ($LT^{-0.5}$). When employing the same extraction method, different infiltration models may yield similar estimates of K_s (LT^{-1}) and S ($LT^{-0.5}$), particularly if they are based on comparable theoretical frameworks and parameterization techniques. However, variations in model complexity, input data requirements, and applied extraction techniques, especially given the evolving landscape of infiltration databases, as well statistical and numerical data analysis, can lead to differences in estimated K_s (LT^{-1}) and S ($LT^{-0.5}$) values. A comprehensive and unbiased assessment of these similarities and discrepancies has been lacking till now.

Given these aspects, I carried out a metadata analysis using a global infiltration database of 5,023 cumulative infiltration curves to assess variability of the estimated infiltration characteristics, K_s (LT^{-1}) and S ($LT^{-0.5}$) across eleven one-dimensional (1D) and four three-dimensional (3D) infiltration models, considering different extraction techniques applied to estimate those characteristics. By examining the differences in predictions of K_s (LT^{-1}) and S ($LT^{-0.5}$) among infiltration models using diverse data analysis methods, we gained insight into the robustness of available applied practices in estimating soil hydraulic parameter through multi-dimensional infiltration modeling.

My PhD journey focused on discovering and assessing infiltration modeling, one key observation that I found very interesting, yet insightful, is the significant absence of and the need for theoretical frameworks studying the impacts of soil structure on water infiltration. Soil structure plays a crucial role in governing the movement and distribution of water within the soil profile, yet there is a notable gap in the existing literature in terms of theoretical frameworks specifically addressing this aspect of infiltration modeling.

Motivated by growing availability of large databases of soil properties, I further explored how soil structural properties control soil infiltration capacity, while using statistical modeling methods through a meta-analysis systematic review. My systematic review again highlighted the dominance of field-scale experimental studies comparing field responses under different soil practices or treatments over the modeling efforts studying the effects of soil structure on water infiltration.

To conduct this meta-analysis systematic review, I formulated the following question: "How does soil structure affect water infiltration?". From there, I built a literature search strategy, applying specific inclusion and exclusion criteria to collect and analyze data from the most relevant research on soil structure and water infiltration. Several pedo-transfer functions were developed, revealing significant correlations (R^2>0.5) between infiltration rate and soil structural properties (such as bulk density, wet aggregate stability, mean weight diameter, organic carbon, and porosity), highlighting the positive effects of improving soil structure on water infiltration and the dynamic nature of infiltration response. Structure and soil texture assessed together lead to stronger predictability of soils infiltration characteristics than when each soil property is considered alone.

As I conclude my PhD journey, I strongly believe that our scientific rigor and curiosity as a community should continue to guide us through the discoveries of new relationships and the understanding of more dominant soil-water processes. From the inherent variability of soil systems

to preferential flows, water repellency and surface processes, the pursuit of practical and adaptive infiltration models should persist. As we move forward in today's world governed by "big data", we could draw some inspiration from the growing availability of large databases and advanced data analytics. Eventually, we can develop comprehensive theoretical frameworks that not only advance our knowledge but also enhance the relevance of soil-water interactions in addressing real-world challenges.

CHAPTER 2: Evolution of Infiltration Modeling: Theory and Historical Perspectives

2.1. Abstract

Infiltration regulates the movement and storage of water at the soil-atmosphere interface and is, therefore, a key component of many related physical and biogeochemical processes. Numerous studies have examined infiltration over the past two centuries. These efforts have resulted in the development of numerous models that capture the effects of specific soil properties and initial and boundary conditions. This proliferation of models has advanced our collective ability to understand infiltration processes but has also made it challenging for researchers to select appropriate approaches for analyzing experimental infiltration data or for conducting basic research on soil parameters like saturated hydraulic conductivity or sorptivity. Here, we aimed to reduce this uncertainty by developing a comprehensive literature review of published infiltration models, including their underlying philosophies and evolution across the years. Through this effort we compiled and examined 138 unique infiltration models. We grouped models into two major categories, empirical and conceptual, noting boundaries between those two categories are at times debatable. We considered conceptual approaches as those built based upon earlier concepts, mainly derived from fundamental flow models, resulting in analytical solutions applied to the infiltration problem. We classified empirical models as those that solved the infiltration problem by curve-fitting measured data with algebraic equations. After classifying and providing a full historical retrospective of these models, we examined specific model parameters and how their usage has changed with time. We also reviewed different methods applied to estimate infiltration parameters, as well as the challenges that arise when using such methods.

2.2. Introduction

Water infiltration is one of the most important processes of the hydrologic cycle for assessing runoff, soil moisture, groundwater recharge, nutrient leaching, plant growth and many other soil-related processes (Zadeh et al., 2007; Singh, 2010; Fodor et al., 2011). Because of its importance, infiltration has been widely studied for over two centuries (Ghorbani et al., 2009). This attention led to development of numerous infiltration models, classified into two categories: conceptual and empirical models. Conceptual models are derived from fundamental and physical theories and typically account for soil properties and specific boundary and initial conditions, while empirical models are based on fitting experimentally measured data using defined mathematical functions (Assouline, 2013; Jacka et al., 2016).

Among the conceptual models, most equations were derived from Darcy's law and substantially influenced by approximating solutions and assumptions of Buckingham and Richardson-Richards. Although some researchers have questioned the validity of Buckingham's assumptions and Richardson-Richards' equations (Hunt et al., 2013; Beven 2018; Abou Najm et al., 2019; Germann, 2021), several extensions and new applications of Darcy-Buckingham–Richardson-Richards paradigm for saturated and unsaturated flow (hereafter referred to as Darcy-BRR and explained in depth in the following section) were developed as an attempt to estimate infiltration. For example, flow in infiltration models was mostly derived from an abstracted and often overly simplified soil pore-structure of a bundle of capillary tubes. Comparatively rare are advancements reporting progress in percolation theory, network models, and Stokes viscous approach (Hunt et al., 2013; Beven, 2018; Germann, 2021).

The abundancy of developed equations motivated other researchers to build reviews that investigate different infiltration models. Some of these reviews were comprehensive summaries of

various conceptual and empirical equations (Kutilek and Nielsen, 1994; Clothier, 2001; Raats et al., 2002; Delleur, 2006; Barry et al., 2007). Others provided insight of the historical evolution of infiltration theory, including the classic solutions of Richards' equation (Youngs, 1995), or more generally, simple physical models (Assouline, 2013). Building on these reviews (Youngs, 1995; Assouline, 2013), other researchers have worked to identify which models are satisfactory for field applications. Typically, such models were fitted to measured infiltration data (e.g., cumulative infiltration vs. time of infiltration) for estimation of the parameters of fitted infiltration models. Ease and accuracy of estimated parameters were further assessed through evaluation techniques that identify the best-fit infiltration models for different datasets (Fodor et al., 2011; Jacka et al., 2016; Nie at al., 2017b; Bayabil et al., 2019).

Most reviews on infiltration theory provided a comprehensive evaluation of the commonly used infiltration models developed over the past century, highlighting the seminal works of Green and Ampt (1911), Philip (1957a, b), Parlange et al. (1982), Swartzendruber (1987), and Haverkamp et al. (1990, 1994), along with key empirical equations by Kostiakov (1932), Horton (1940), Mezencev (1948), and Holtan (1961). These models are still extensively studied and applied. However, in the last two decades, substantial efforts have been built on the above-mentioned models, leading to theoretical improvements and a wider body of research on modeling infiltration. These advancements have ultimately led to a larger and more diverse set of infiltration models and to more open discussions on the validity and application of some of the dominant theoretical frameworks. To this end, it became challenging for researchers to select appropriate approach(es) for analyzing experimental infiltration data or for conducting basic research on soil parameters like saturated hydraulic conductivity or sorptivity. Therefore, a comprehensive and current review covering both past and recent model development is still needed.

Here, we present a comprehensive critical review that traces the development of conceptual and empirical models over the past two centuries through both historical and theoretical lenses. With this review, our objectives are to 1) build an inclusive historical retrospective of the evolution of the infiltration problem and its solutions, 2) highlight the diversity in form, origin, and theory among reviewed infiltration models, and 3) explore methods applied to estimate the basic model parameters, including saturated hydraulic conductivity and sorptivity. To this end, we aimed for models that provided theoretical advancements, novel frameworks, and unique empirical fits, and excluded papers that focused on iterative or incremental advancements of existing models, as well as papers that adapted these models to other uses (e.g., hydraulic characterization).

2.3. Underlying physics of infiltration processes

Water, lying upon or below the soil surface, infiltrates principally because of two forces of comparable importance, capillarity, and gravity (Buckingham, 1907). Absorption of water due to capillarity, namely sorptivity S ($LT^{-0.5}$), controls water movement at the early state of infiltration; then at transient state, hydraulic conductivity K (LT^{-1}) comes into play and dominates the infiltration process at steady state, which is mainly driven by gravity (Philip 1957b). The hydraulic conductivity, K (LT^{-1}), varies rapidly and nonlinearly with matric head, ψ (L) (Richards, 1931). Integration of K (LT^{-1}) over a range of ψ (L) is defined as matric flux potential, φ (L^2T^{-1}), which provides an interesting approach to the infiltration problem in unsaturated soils (Raats, 1971). The relative importance of capillarity over gravity during water infiltration in unsaturated soils is expressed by a scaling factor defined as the capillary length, λ_c (L) (Philip, 1985). λ_c (L) is equal to the inverse of a parameter α (L^{-1}) introduced by Gardner (1958) as a general description of soil textural and structural characteristics. α tends to be small in fine-textured soils with capillarity dominant, while large in coarse-textured soils where gravity is important. Typically, α is about $1\ m^{-1}$, and the range 0.1 to $5\ m^{-1}$ can be representative of the full moisture range in real soils (Philip, 1984). Elrick and Reynolds (1992) suggested four values i.e., $\alpha = 36, 12, 4$ and $1\ m^{-1}$ for practical use of permeameters and infiltrometers in soils varying from coarse sands to compacted clays. The reader should note that the larger values (i.e., 12 and 36 m^{-1}) are for "sand fractions" and/or apply over small capillary ranges.

Infiltration, at both local and field scales, can be treated as a one-dimensional (1D) process assuming water flow below the water source at soil surface or subsurface is directionally restricted. Otherwise, a multi-dimensional infiltration including two-dimensional (2D) flow through planar or axi-symmetrical domains, and fully three-dimensional (3D) flow can be established.

To determine water infiltration into soils, it is necessary to impose appropriate boundary conditions. These conditions include concentration, pressure, or flux-based depictions. Such boundaries may be summarized as:

1) The concentration type boundary condition states that there is an infiltration flow that corresponds to the value of water content at the soil surface below saturation (but above the initial water content of the soil profile) and that the pressure head is fixed to negative or zero since the boundary is unsaturated.
2) When water is ponding at the soil surface imposing hydrostatic head pressure, h_0 (L), at the boundary between the soil and the constant or falling water in a furrow, lake, or river, infiltration is governed by a pressure type boundary condition.
3) When a water flux, q_0 (LT^{-1}), occurring primarily in sprinkling irrigation or rain is imposed across the boundary, a flux boundary condition can be applied as long as q_0 is below the soil infiltration capacity. As soon as infiltration capacity decreases below the imposed water flux, runoff may be generated at the soil surface.

The boundary conditions may change from prescribed flux to prescribed head type conditions (and vice-versa). For instance, when the precipitation or irrigation rate q_0 (LT^{-1}) exceeds infiltration capacity of the soil, ponding will occur. In this case, infiltration rate is no longer controlled by precipitation rate, but instead by infiltration capacity of soil.

Finally, soil characteristics greatly affect water infiltration. Some soil characteristics with relatively high importance include:

- Rigid vs. deformable or shrink-swell soils
- Isotropic vs. anisotropic soils
- Homogeneous vs. scale-heterogeneous or heterogeneous soils

- Non-hydrophobic vs. hydrophobic soils
- Single- vs. dual- or multi-porosity domains
- One- vs. two- or multi-layer soil profiles
- Flat vs. sloping soil surfaces

Infiltration models are mostly designed to characterize infiltration into simplistic soils, i.e., rigid, homogeneous, isotropic, and non-hydrophobic soils. These soils have idealized conditions with no water-repellency, preferential flow, or any other factors where the cumulative infiltration curves reflect a characteristic concave shape. The concave curve demonstrates higher infiltration capacity at early stages that reaches a constant slope at steady state. However, different soil and field conditions can alter this behavior leading to cumulative infiltration curves that exhibit convex, mixed, or non-standard shapes (e.g., Chen et al., 2020; Abou Najm et al., 2021; Pachepsky and Karahan, 2022).

Altogether, the physics underlying infiltration processes are highly complex. To be able to select and apply the most appropriate model(s), it is important to understand how variables such as flow direction and dimensionality, driving forces, non-uniformities in drivers and media, and boundary conditions all interact. To guide the model selection process, we emphasized, in the first section of our review, the underlying physics of infiltration processes that encompass dimensions and directions, forces, convex vs. concave curves, homogeneity vs. heterogeneity and non-uniform flow drivers, as well as a brief discussion of common boundary conditions. In the following sections, we provided a narrative of the history and evolution of major infiltration models, divided into 1) empirical models and 2) conceptual models divided as macro-scale depictions of flow in rigid versus deformable soils. Across the years, modeling infiltration shifted from an extensive use

of analytical approaches to numerical computations, which aligned with the development of mathematics and resolving techniques throughout history.

2.4. Evolution of the basic flow models for rigid soils

We summarized basic and fundamental physical flow models used as the foundations for modeling infiltration in rigid (non-swelling) soils (**Error! Reference source not found.**2.1). Below, we present the main fundamental equations that were used as steppingstones in most of the infiltration models reviewed in this paper.

The Navier-Stokes equation was the first fundamental concept, developed by Navier (1823) and Stokes (1850), that described laminar motion of incompressible fluids flowing through homogeneous and smooth surfaces in both horizontal and vertical directions:

$$\rho\left(\frac{\partial\vec{v}}{\partial t}+(\vec{v}.\nabla)\vec{v}\right)=-\nabla P+\rho\vec{g}+\mu\nabla^2\vec{v} \quad [2.1]$$

where v (LT^{-1}) is velocity, $\frac{dv}{dt}$ (LT^{-2}) is the change of velocity with respect to time t (T), ∇P ($ML^{-2}T^{-2}$) is the pressure gradient, ρ (ML^{-3}) is fluid density , μ ($ML^{-1}T^{-1}$) is the dynamic viscosity of the fluid, and g (LT^{-2}) is the acceleration of gravity, and ∇ stand for the nabla operator where $\nabla=\frac{\partial}{\partial x}\overrightarrow{e_x}+\frac{\partial}{\partial y}\overrightarrow{e_y}+\frac{\partial}{\partial z}\overrightarrow{e_z}$

Based on Navier's work, Poiseuille (1844) derived a physical law, known as Hagen–Poiseuille equation, that describes the pressure drop, ΔP ($ML^{-1}T^{-2}$), in an incompressible and Newtonian fluid with laminar volumetric flow, Q (L^3T^{-1}), flowing through a cylindrical pipe of length l (L) and radius r (L):

$$Q=\frac{\pi\Delta P r^4}{8\mu l} \quad [2.2]$$

While the concept of infiltration was discussed and described in the literature before Darcy's work, Darcy (1856) formulated the first empirical quantitative description of flow through a saturated

porous medium, known as **Darcy's law**, based on water infiltration experiments through sand beds, valid for both horizontal and vertical flow:

$$q = -K_s \nabla h \quad [2.3]$$

where q (LT^{-1}) is the flux, K_s (LT^{-1}) is the saturated hydraulic conductivity, ∇h (LL^{-1}) is the hydraulic gradient describing the difference in total hydraulic head h (L) between any two points within the porous medium.

A few decades after Darcy, Buckingham (1907) built on the earlier work of Lyman Briggs, his senior colleague at the U.S. Bureau of Soil, who introduced capillary flow due to capillary gradient. Buckingham's work resulted from deviations of the equilibrium between gravity and capillarity in unsaturated soils (Briggs, 1897). More about this development can be found in Germann (2021). Buckingham, who apparently did not notice the work of Darcy (Beven, 2018), extended Briggs' concepts and drew an analogy with Ohm's law and Fourier's law to define unsaturated water flow as a function of a gradient of attraction and a constant of proportionality, namely "capillary conductivity", based on two main assumptions:

1. The driving force for water flow in isothermal, rigid, unsaturated soil containing no solute membranes and zero air pressure potential is the gradient between two points of the combination of matric ψ (L) and gravitational z (L) potentials, i.e., $h = \psi + z$
2. The hydraulic conductivity of unsaturated soil is a function of water content θ (L^3L^{-3}) or matric potential ψ (L).

Based on Buckingham's approach, vertical and 3D infiltration processes are generally considered to be in response to a combination of gravity and capillarity, and horizontal infiltration considered to be driven exclusively by capillarity. To this end, Buckingham's assumptions have tremendously

advanced the theory of water flow and become the fundamental "depictions of the underlying physics".

$$q = -K(\psi)(\nabla\psi + 1) = -K(\theta)(\nabla\psi + 1) \qquad vertical\ flow \qquad [2.4]$$

$$q = -K(\psi)(\nabla\psi) = -K(\theta)(\nabla\psi) \qquad horizontal\ flow \qquad [2.5]$$

where $\nabla\psi$ (LL^{-1}) is the matric hydraulic gradient, and $K(\psi)$ and $K(\theta)$ (LT^{-1}) are the unsaturated hydraulic conductivities as respective functions of ψ (L) and water content θ (L^3L^{-3}). Equation 2.4 and/or 2.5 can be viewed as a generalization of Darcy's Law and can be referred to as the **Buckingham-Darcy law**.

In 1911, the flow theory witnessed the conceptualization of a "wetting front potential" by Green and Ampt who quantified the capillary force resulting from the matric potential of unsaturated soils. Green and Ampt (1911) assumed a constant wetting front that goes downward at constant water content and, thus, constant matric potential ψ (L), as well as constant hydraulic conductivity K ($L\ T^{-1}$), since water always moves within a saturated soil. The Green-Ampt model works best when a relatively sharp wetting front exists throughout the infiltration process. Such a distinct wetting front was adopted later by several infiltration models, such as those developed by Mein and Larson (1973), Li et al. (1976), Beven (1984), Selker et al. (1999a), Swartzendruber (2000), Selker and Assouline (2017), Stewart (2019). Consequently, the Green-Ampt model has proven to be one of the governing equations in understanding and predicting infiltration.

The next advancement in theory was to combine these steady-state flow theories to non-steady conditions, in which soil water content can change over time and space. Two different scientists (Richardson, 1922; Richards, 1931) independently developed similar solutions to this problem through a second order convection-diffusion equation, conventionally known as Richards'

equation (Equation 2.6 or 2.7). However, the resulting equation should rightly be called the **Richardson-Richards' equation**. Unfortunately, Richardson's work was barely noticed in the soil physics or hydrology literature, most likely because it was presented as part of a book on weather prediction (Raats and Knight, 2018).

As Richards (1931) attempted to extend Darcy-Buckingham work, he defined "the essential difference between flow through a porous medium which is saturated and flow through a medium which is unsaturated is that under the latter condition the pressure is determined by capillary forces and the conductivity depends on the moisture content of the medium" (Richards 1931, page 323). However, Richards constrained his derivation to low pressure gradients, and highlighted the need for different model approximations for high pressure gradients: "For low pressure gradients it has been found by numerous investigators that this law (Darcy) is in exact agreement with experiment, and it is entirely analogous to the well-known law of Poiseuille for the flow of liquids through capillary tubes. However, both laws fail to hold for high pressure gradients. The limit within which they are true and the modifications which a second approximation requires can be determined only by exhaustive experiments on a wide range of materials." (Richards 1931). The validity problem of Richards' assumption is related to the validity of Darcy's law. Very large hydraulic gradients will induce rapid flows where Darcy's law is no longer valid. These fluxes appear under certain conditions where the Reynolds number varies from 1 to 10. Therefore, different scenarios where **Darcy-BRR** fails to apply include i) the appearance of turbulence for high-speed flows (e.g., cascade flows in macropores), ii) the problem of air entrapment and the need to account for air pressure gradients, iii) the need for connectedness of both the water and air phases.

Theoretically, Richards' nonlinear partial differential equation for water flow can be derived by simply combining Darcy's equation and conservation of mass along with Buckingham's paradigm under isothermal conditions in a homogeneous and rigid porous medium.

$$\frac{\partial \theta}{\partial t} = \nabla[D(\theta)\nabla\theta] + \nabla K(\theta) \quad [2.6]$$

Richards' equation is also written in the following head-based form:

$$C(\psi)\frac{\partial \psi}{\partial t} = \nabla[K(\psi)\nabla\psi] + \nabla K(\psi) \quad [2.7]$$

The soil infiltration characteristics are hydraulic conductivity $K(\theta)$ or $K(\psi)$ (LT^{-1}), hydraulic diffusivity $D(\theta) = K(\psi)\frac{\partial \psi}{\partial \theta}$ (L^2T^{-1}), and water holding capacity $C(\psi) = \frac{\partial \theta}{\partial \psi}$ (L^{-1}).

The concept of water movement as a diffusion phenomenon, implicit in Buckingham's approach, and later in that of Richards as well as Green and Ampt's model, was explicitly proposed by Childs (1936a, 1936b) who studied the hypothesis of constant diffusivity. Later, Childs and Collis-Georges (1950) introduced the concept of concentration-dependent diffusivity characterized by the strong dependence of diffusivity on water content. Embracing this concept, Philip (1957a) developed, based on a Taylor Series expansion of Equation 2.6, the first specific quasi-analytical solution of the non-linear Richards' equation, in the form of a power series in $t^{1/2}$ describing infiltration in a homogeneous, isotropic, and rigid porous medium. However, Philip's time expansion series converges only for finite *t*; thus, the solution becomes unreliable at infinite times. To this end, Philip (1957b) approximated his equation by the two first terms, describing one-dimensional, unsaturated infiltration for relatively short times. At this point, he defined the first term as "sorptivity" or "a term embracing both absorption and desorption". In his words, it is "a measure of the capillary uptake or removal of water". Later, in 1969, Philip showed that sorptivity

can be determined from horizontal infiltration where water flow is mostly controlled by capillary absorption (Philip, 1969a). The second term in Philip's two-term equation reflects gravity effects and can be assumed equal to the saturated hydraulic conductivity multiplied with a constant between 1/3 and 2/3 (Davidoff and Selim, 1986; Swartzentruber and Young, 1974; Ghorbani et al., 2009).

Following on Philip's work, Parlange obtained, in a different series of papers, a quasi-analytical solution for water infiltration, by first developing a one-dimensional absorption equation (Parlange, 1971a), which was then extended to infiltration to include gravity effects (Parlange, 1971b), and further extended in subsequent papers to problems in two and three dimensions (Parlange 1971c, 1972a, 1972b).

The series of papers published by Philip and Parlange more than fifty years ago remains today the basis of our understanding of infiltration theory. However, a serious limitation of applying their quasi-analytical solutions emerges from the representativity of the initial and boundary conditions (described in detail in Section 2.8).

Later, the analysis of the highly non-linear flow problem has been simplified and made tractable by applying the matric flux potential using Kirchhoff transformation. Raats (1971) defined the matric flux potential, φ ($L^2 T^{-1}$), by: $\varphi = \int_{\psi_i}^{\psi} K(\bar{\psi}) d\bar{\psi} = \int_{\theta_i}^{\theta} D(\bar{\theta}) d\bar{\theta}$; subscript i denotes the initial state. Using this definition, Redinger et al. (1984) and Campbell (1985) were the first to apply the Kirchhoff transform (K transform) of the matric potential ψ (L) to linearize the second-order spatial term in Richards' equation (Equation 2.7). Their method introduced a simple but efficient method of solution for homogeneous unsaturated soils. However, K transform depends on the soil hydraulic properties and will therefore vary spatially with any spatial change in the hydraulic

properties. Therefore, to characterize scale-heterogeneous soils, Ross (1990) used an inverse hyperbolic sine transform of ψ (L) in preference to the K transform. Later, Ross and Bristow (1990) capitalized on the numerical advantages of using the K transform to solve Richards' equation for water flow in scale-heterogeneous soils when the appropriate correction to spatial changes in soil properties is made.

Clearly, Richards' equation quickly became the mainstream approach for modeling flow in unsaturated soils. Two factors contributed to the success and rapid adoption of Richards' equation that are discussed in detail below.

First, researchers quickly developed simplified analytical approximations over the next few decades following Richards paper, and later, thanks to advancements in numerical computation, developed robust numerical models, particularly the HYDRUS software packages, which simulate water, heat and solute movement in 1-D, 2-D or 3-D porous media and provide numerical solutions to Richards' equation (Simunek et al., 1998, 1999, 2005, 2006). HYDRUS uses linear finite elements to numerically solve Richardson-Richards' equation for saturated or unsaturated water flow under uniform or nonequilibrium conditions, as well as Fickian-based advection–dispersion equations for solute transport. In 2008, Simunek and his coworkers described the entire history of the development of the various HYDRUS programs with related models and tools (Simunek et al., 2008a). Later, Simunek et al. (2016) reviewed recent developments and applications of the HYDRUS program implemented after 2008.

Second, the ubiquity and ease-of-use of Richards-based model frameworks, including HYDRUS, led Richards' equation to dominate the theory of unsaturated flow, thus transitioning research in infiltration and unsaturated flow almost exclusively from a theoretical search for a better infiltration theory into an expanded field of highly applied and practical research. Therefore, many

researchers have been applying Richards' equation to understand processes or develop solutions addressing environmental, agricultural, and ecological issues like irrigation efficiency, pollutant and nutrient transport, heat transfer, water recharge, and stormwater management (Lassabatere et al., 2010; Kandelous and Simunek, 2010; Goutaland et al., 2013; Slimene et al., 2017; Stewart et al., 2017a, b; Autovino, 2018; Coppola et al., 2019; Fields et al., 2020).

Despite its widespread adoption, Richards' equation fails to adequately describe infiltration in different flow situations and scales (e.g., Hunt et al., 2013; Beven, 2018; Germann, 2021). Fundamentally, the Richards' equation was developed using equilibrium-based measurements, such that equilibrium between soil pressure head and water content is instantaneous, opposite to non-equilibrium conditions that occur during rapid flow (Simunek et al.,2003). Based on the theoretical dominance of capillary forces in unsaturated flow, Richards proposed an elegant hierarchy of active-inactive pores in which larger pores empty while smaller pores conduct water in partially saturated soils. He stated that if "there is a steady flow of liquid through a porous medium which is only partially saturated, then the larger pore spaces contain air and the effective cross-sectional area of the water conducting region is reduced" (Richards 1931). This hierarchy completely deactivates those larger pores "If these air spaces could in some way be filled with solid, the condition of the flow would be unchanged" (Richards 1931). On the other hand, Germann's last published work was critical of Richards experiment "which relied on the application of air pressure to ensure that larger pores were empty at each potential and flow rate, was simply the wrong experiment for flows under more natural conditions." (Germann 2021). Germann's stated that "while capillary flow relies on the strongest force extended on water in an unsaturated soil, the weaker force of viscosity can dominate during infiltration as a result of formation of film flows at and near the soil surface." (Germann 2021). Similar criticism was levied

by Hunt et al. (2013) and Beven (2018). Additionally, while HYDRUS is widely used to simulate water movement in variably saturated media, the software presents challenges for researchers to obtain accurate results in clay rich soils and soils with perched water table or restrictive layers. HYDRUS does not natively handle the dynamics aspects of soil swelling and shrinking processes or soil with restrictive layers. However, it could provide relatively reliable results under these specific conditions if the model was calibrated with specific soil data pertaining to these conditions. In the case of restrictive layers, Hydrus can simulate these effects if the hydraulic properties of each layer, such as Ks or soil water characteristic curves of each layer, were accurately defined. The same case applies for shrink/swell soils; as their hydraulic properties are different, accurate parameterization is needed at this stage. So, more specific input is needed under these conditions, presenting challenges for researchers.

The inadequacies of **Darcy-BRR** framework were also becoming apparent as interests increased in depicting preferential flow processes through a wide range of theoretical advancements (Simunek et al., 2003; Jarvis, 2007; Simunek et al., 2008b). Studies were increasingly noting pollutant and nutrient transport processes that were happening at faster rates or over greater distances than seemed possible based on the depictions provided by BRR-based models (Zehe and Fluhler, 2001; Reichenberger et al., 2002; Zheng and Gorelick, 2003; Beven, 2010). Other work at hillslope and watershed scales also indicated that BRR-based models did not accurately capture soil wetting and streamflow responses to precipitation, even when treated with parameter values deemed as “effective” for the larger scales (van Schaik et al., 2008; James et al. 2010; Nimmo et al., 2021).

These issues were first raised by Beven and Germann (1982), who demonstrated the importance of macropores and preferential water flow in soils, as well as identified the need for future

comprehensive characterization of flow that goes beyond Richards' equation. Beven and Germann's pioneering work (1982) led to a mainstream recognition and acknowledgement to the limitations of current physical theory. Thirty years later, many of the same discrepancies persisted, as noted by the revised work in Beven and Germann (2013).

The first theoretical attempt at addressing the discrepancies of Darcy-BRR framework was held by Beven and Germann (1981), who described flow in high-permeability domains by the kinematic wave approach. To this end, Beven and Germann (1981) developed a one-dimensional model of bulk flow in a combined micropore/macropore system by approximating the micropore (subscript m) flow, q_{m} ($\mathrm{LT^{-1}}$)**,** for various arrangements of macropores (subscript f) at different water contents, θ_f ($\mathrm{L^3L^{-3}}$):

$$q_{\mathrm{m}} = a_1 {\theta_f}^{b_1} \qquad [2.8]$$

And the flow in macropores, q_f ($\mathrm{L\ T^{-1}}$), by:

$$q_f = K_f a_2 {\theta_f}^{b_1} \qquad [2.9]$$

where: K_f ($\mathrm{L\ T^{-1}}$) is the hydraulic conductivity of the macropores, a_1 ($\mathrm{L\ T^{-1}}$), a_2, and b_1 (dimensionless) are fitting parameters.

Recognizing the importance of preferential and non-equilibrium flow that is not captured by Darcy-BRR framework, Gerke and van Genuchten (1993) transformed Richards' equation into a dual permeability model that describes two single-permeability media, one associated with macropores (fracture, inter-porosity domain) of high permeability, and the other associated with micropores (matrix, intra-porosity domain) of low permeability, with exchange possible through a permeable interface. This approach assumed constant fluid densities, no hysteresis in the hydraulic

properties, no effects of swelling, shrinking, temperature, air pressure, and solute concentration on water flow. Based on Richards' equations, Gerke and van Genuchten (1993) model uses the flow equations for the fast-flow region (subscript f) and the matrix (subscript m), respectively as follows:

$$\frac{\partial \theta_f(\psi_f)}{\partial t} = \nabla\left[K_f(\psi_f)\left(\nabla\psi_f + 1\right)\right] - s_f(\psi_f) - \frac{\Gamma_w}{w_f} \quad [2.10]$$

And

$$\frac{\partial \theta_m(\psi_m)}{\partial t} = \nabla[K_m(\psi_m)(\nabla\psi_m + 1)] - s_m(\psi_m) - \frac{\Gamma_w}{1-w_f} \quad [2.11]$$

where $s(\psi)$ (T^{-1}) is the sink–source term, w_f (L^3L^{-3}) is the ratio of the volume occupied by the fast-flow region and relative to the total volume, and Γ_w (T^{-1}) is a space- and time-dependent exchange term describing the transfer of water between the two pore systems.

Other further approaches for modeling preferential and non-equilibrium flow in the vadose zone have used the kinematic approach (Jarvis, 1994; Jarvis and Larsson, 1998; Larsbo and Jarvis, 2003), Darcy-BRR (Lewandowska et al., 2004), or Green and Ampt (Weiler, 2005; Stewart, 2018) by describing water movement in the soil matrix in combination with a depiction of water flow through macropores.

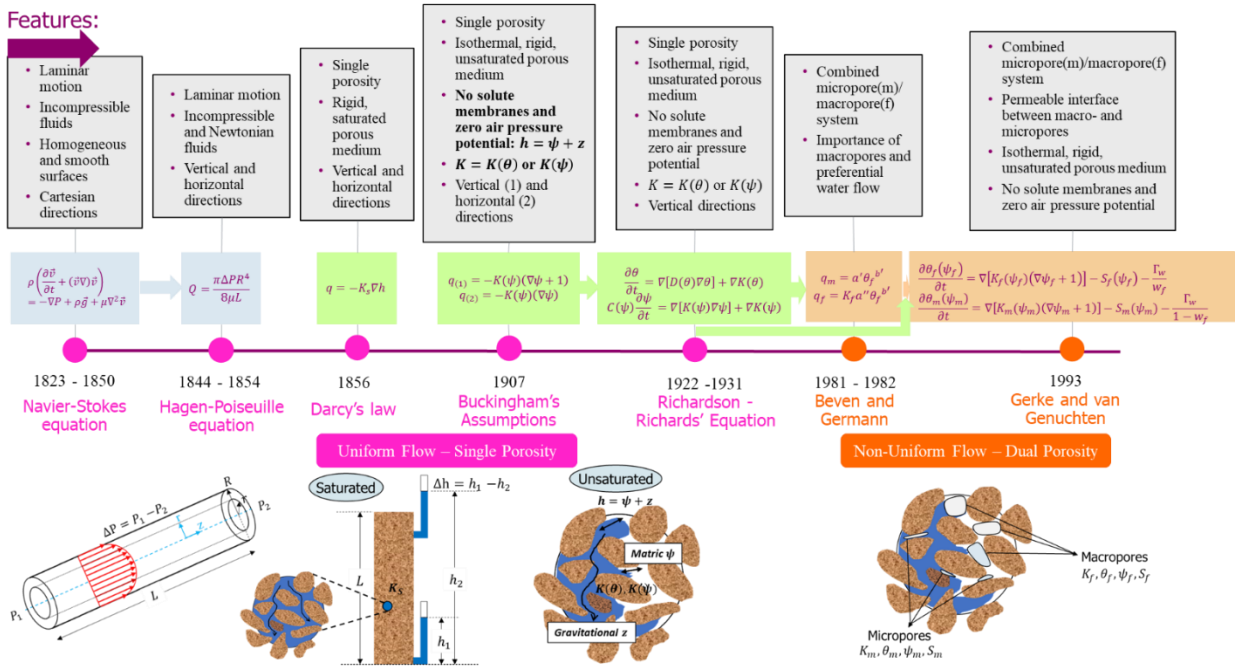

Figure 2.1: Evolution of the basic flow models for rigid (i.e., non-swelling) soils. It is worth noting that non-uniform preferential flows were recognized long before the equilibrium concepts of Buckingham and Richardson-Richards (Schumacher, 1864; Lawes et al., 1882; Kubiena, 1938; Brewer, 1960). However, the non-uniform flow was not modeled until early 1980s.

2.5. Evolution of basic flow characterization for deformable soils

Many soils have clay minerals or other particles (e.g., organic substrates) that change volume when wetting and drying, which causes the soil matrix to deform and typically leads to excessive error when infiltration models developed for rigid soils are applied. Therefore, substantial research efforts have been devoted to characterizing water movement through deformable soils with time-variable pore structures. In the context of water infiltration into soils, deformable soils are known as shrink/swell soils which expand when they absorb water and shrink when they dry out. These specific soils could be distinguished in the field by their wide deep cracks, their rough soil surface, and typically feel sticky and plastic when wet.

Here, we list the basic conceptual models developed to characterize water flow into deformable soils (Figure 2.2).

Using Darcy's law, Biot (1955) first described the flow of fluids in deformable anisotropic soils by studying the problem of soil consolidation through the mixture theory in the absence of gravity effects:

$$v_{liquid} - v_{solid} = -\frac{k}{\theta\mu}\nabla P \qquad [2.12]$$

where: v_{liquid} and v_{solid} are the vertical velocity components of the liquid and solid phases, respectively, and k (L^2) is the solid permeability.

Then, mass conservation of the solid (Equation 2.13) and liquid (Equation 2.14) phases, yielded (Bowen, 1980):

$$\frac{\partial\theta}{\partial t} - \nabla[(1-\theta)v_{solid}] = 0 \qquad [2.13]$$

$$\frac{\partial\theta}{\partial t} + \nabla\left(\theta v_{liquid}\right) = 0 \qquad [2.14]$$

Later, researchers' attention was skewed towards characterizing soils that shrink and swell in volume when drying and wetting, namely shrink-swell soils. To understand the behavior of shrink-swell soils, the soil shrinkage curve (SSC) was developed describing the change in soil volume as function of the change in water content from a fully saturated state to a completely dry state. The soil shrinkage curve is generally sigmoidal in shape and is represented by numerous models (McGarry and Malafant, 1987; Tariq and Durnford, 1993; Braudeau et al., 1999; Crescimanno and Provenzano, 1999; Chertkov 2000, 2003; Peng and Horn, 2005; Cornelis et al., 2006a, b; Lu and Dong, 2017; Chen and Lu, 2018; Gupt et al., 2021).

Different modeling analogs of Richardson-Richards' equation were developed to study and solve the problem of infiltration into shrink-swell soils. For instance, Philip (1969b) modified Richardson-Richards' equation for a rigid soil and developed the standard Fokker–Planck equation (FPE - Equation 2.15) describing flow in unsaturated swelling media:

$$\frac{\partial \theta}{\partial t} = \nabla[D(\theta)\nabla\theta] + \nabla[(1-\gamma_w)K(\theta)] \qquad [2.15]$$

where γ_w (dimensionless) is the wet specific gravity of the swelling soil.

Smiles and Raats (2005) reformulated the standard (FPE) by including the dimensionless constant, here called α_{swell}, defined as a water content-dependent value and as an average over a defined pressure range, to deal with curvilinearity in the shrinkage curve:

$$\frac{\partial \theta}{\partial t} = \nabla[D(\theta)\nabla\theta] + \nabla[(1-\alpha_{swell}\gamma_w)K(\theta)] \qquad [2.16]$$

Furthermore, a special form of the (FPE) was investigated by Su (2009), who considered the inclusion of dimensionless parameter β_{swell}, the order of fractional derivative, which enables a clear explanation of the anomalous infiltration into swelling porous media:

$$\frac{\partial^{\beta_{swell}}\theta}{\partial t^{\beta_{swell}}} = \nabla[D(\theta)\nabla\theta] + \nabla[(1 - \alpha_{swell}\gamma_w)K(\theta)] \quad [2.17]$$

Another governing equation for water movement in swelling soils was provided by Giraldez and Sposito (1985) who used a generalized version of the Richardson-Richards equation:

$$\frac{\rho_b}{\rho}\frac{\partial\theta}{\partial t} = \nabla[D(\theta)\nabla\theta] + \nabla H \quad [2.18]$$

where: ρ_b (ML^{-3}) is the soil bulk density and ρ (ML^{-3}) is the fluid density. H (LT^{-1}) is a gravity-envelope-pressure parameter given by:

$$H = K(\theta)\left(1 - \rho_{b,w}\bar{V}\right) \quad [2.19]$$

where: $\rho_{b,w}$ (ML^{-3}) is the wet bulk density (subscript w), and $\bar{V}$ (L^3M^{-1}) is the slope of the shrinkage curve.

Furthermore, Feddes et al. (1988) extended Richardson-Richards' equation to characterize water flow in swelling/cracked soils by adding two sink-source terms, s_r (T^{-1}) quantifying the volume of water extracted from soil by roots, and s_f (T^{-1}) quantifying the horizontal infiltration from soil cracks (subscript f) into the soil matrix:

$$\frac{\partial\theta}{\partial t} = \nabla[K(\psi)(\nabla\psi + 1)] - s_r + s_f \quad [2.20]$$

Shifting from Richardson-Richards' equation, Davidson (1984), and later Weiler (2005), built on the classic Green-Ampt model to characterize infiltration into macroporous soils. Neither approach, however, describes the dynamic shrinkage and swelling processes. In response, Stewart (2018) combines the Green-Ampt model with a multidomain framework previously developed by Stewart, Abou Najm, et al. (2016), allowing for variations in properties of the different porosity domains, and therefore a better characterization of the dynamic properties of shrink-swell soils.

Another approach towards modeling water movement through shrink-swell soils was developed by Bennethum and Cushman (1996) who derived a new constitutive theory for multiphase, multicomponent, three-scale, swelling systems with interfaces. This effort resulted in a generalized form of Darcy's law where flow is governed by gravity and the Gibbs free energy, temperature, and concentration gradients:

$$q = \kappa^L \left[-\phi^L \rho^L \nabla \left(\tilde{A}^L - \frac{1}{\rho^L} \sigma \right) + \left(\frac{1}{\rho^L} \sigma^L + \frac{1}{\rho^L} P^L \right) \nabla (\phi^L \rho^L) + \phi^L \rho^L g^L - \phi^L \rho^L \mathrm{E}^L \nabla T^0 + \sum_{j=1}^{N-1} \phi^L \rho^L \tilde{\mu}^{L_j} \nabla \mathrm{C}^{L_j} \right] \quad [2.21]$$

Where: $L=lA$ refers to the fluid phase in the particle at the macroscale, *B* and *C* refer to the liquid and air phase at the mesoscale respectively, κ (L^3TM^{-1}) is second order positive semi-definite tensor, ϕ (L^3L^{-3}) is the volume fraction, ρ (ML^{-3}) is the fluid density, E ($L^2T^{-2}T^{0(-1)}$) is the entropy, $\tilde{A}$ (L^2T^{-2}) is the specific Helmholtz free energy, ∇T^0 (T^0) is the temperature gradient, $\tilde{\mu}$ (L^4MT^{-2}) is the chemical potential, and $\nabla \mathrm{C}$ (ML^{-4}) is the concentration gradient.

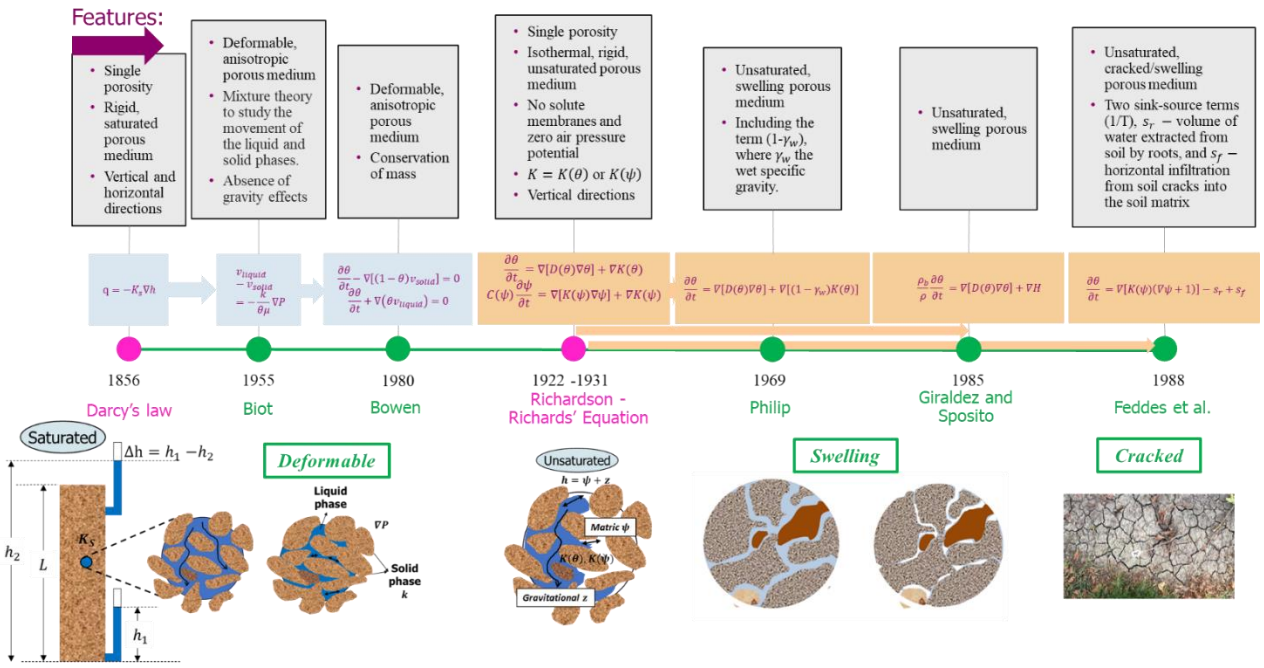

Figure 2.2: Evolution of the basic flow models for deformable (i.e., swelling) soils

2.6. Pore-scale models

The infiltration process in soils through which air is replaced by water is typically investigated using Richards' equation at the continuum scale, which requires the determination of soil hydraulic properties, such as water retention and unsaturated hydraulic conductivity curves. During infiltration within the complex structure of soils, one observes phenomena such as irregular wetting front and hydraulic non-equilibrium that are controlled by pore-scale characteristics of soils. Therefore, to better understand infiltration at the continuum scale, one should first investigate it at the pore scale - the scale of processes taking place within porous media. Different visualization tools were used to investigate the pore scale such as X-ray microcomputed tomography, confocal microscopy, and optical microscopy (Krummel et al., 2013; Geistlinger and Ataei-Dadavi, 2015; Liu and Song, 2015; Song et al., 2020).

Several pore-scale approaches emerged to address fluid flow and transport in the complex geometry and topology of porous media, as well as to solve physics within the given domain at the pore scale (Wilkinson, 1984; Martys and Hagedorn, 2002; Valvatne and Blunt, 2004; Liu et al., 2006; Prodanovic and Bryant, 2006; Blunt et al., 2013). The most widely used approaches for pore-scale modeling are Lattice Boltzmann Methods (BME), smoothed particle hydrodynamics approach, computational fluid dynamics-based techniques, and pore-network models (Blunt, 2017).

Here, we present a summary of the emergence of pore-scale models and their co-evolution to broaden our review aspects, as well as our understanding of the modelling and application of flow into porous media. Mapping the pore space of porous media into a network of connected pores was first developed by Fatt (1956a, b, c) who stressed the inadequacy of parallel tube models to describe the complex structure of soils and rocks. Fatt (1956a) proposed a regular 2D network of

tubes with various pore size distributions, which evolved to a ball-and-stick network proposed by Chandler et al. (1982) and Koplik (1982), and then to a biconical pore network proposed by Toledo et al. (1994). Recognizing that real porous media are three-dimensional, Rose (1957) developed the first computer-based network characterized by 3D lattices which were further used to study hysteresis (Nicholson, 1968), dispersion (Torelli and Scheidegger, 1971) and waterfloods (Simon and Kelsey, 1971, 1972).

Since 1980s up to now, research in pore-scale modeling evolved from the computation of simple two-phase flow processes and relative permeability (Larson et al., 1981; Heiba et al. 1984; Koplik and Lasseter, 1985; Blunt and King, 1991; Blunt et al., 1992; Mogensen and Stenby, 1998) to a huge range of pore-scale events e.g. wettability, three-phase flow, hysteresis, mass transfer between phases, and to a more accurate abstraction of porous media (Wilkinson and Willemsen, 1983; Blunt and Scher; 1995; Blunt 2001; Blunt et al. 2002; Joekar-Niasar et al., 2008, 2009; Dong and Blunt, 2009; Raoof and Hassanizadeh, 2010; Bultreys et al., 2015).

For instance, Pomchaitaward et al. (2003) applied a lattice-Boltzmann method to study capillary infiltration in porous spheres and cubes. They further validated their approach by comparing the results of their lattice-Boltzmann simulations with those obtained from a continuum model based on the kinetic of capillary infiltration. Later, Tzavaras et al. (2017) used pore-network modeling to simulate infiltration at the pore scale. In their study, the structure of pores and their topology were adapted from a loess soil sample. Using the same pore size distribution, they generated two types of pore networks: structured and random. The former was based on the measured topology, while the latter was based on random pore connection. Their pore networks, however, were only composed of 16×16×32 nodes. The authors compared their pore-scale simulation from pore-network modeling with the continuum-scale simulations obtained by solving the Richards'

equation. More specifically, the horizontally averaged dynamics of water content and water potential at the two scales were compared. Although reasonable agreements were found, the authors stated that assuming fluid phases were immiscible and incompressible led to unrealistic air trapping in the studied pore networks.

2.7. Percolation theory

Concepts from the percolation theory were widely applied in conjunction with network modelling to study flow and transport in complex porous media (Hunt, 2014; Sahimi, 2011; Hunt and Sahimi, 2017). Percolation theory addresses the effect of geometrical and topological properties of the pore space, particularly pore size distribution and connectivity at both small and large scales. An important feature within percolation theory is the presence of a percolation threshold (critical fraction) below which the network is not connected and, therefore, there is no macroscopic flow or transport. The basic concept of percolation threshold has also been broadly referred to in soil physics using other terms such as residual water saturation or critical air-filled porosity.

Early percolation models were based on networks (or lattices) composed of bonds and sites. Bonds act like links (or pore throats) connecting sites (or pore bodies). The early advancement in percolation theory for vertical downward infiltration was described by Glass and Yarrington (1996) as "gravity fingering in porous media" emphasizing that water mainly percolates due to gravity. More specifically, Glass and Yarrington (1996) proposed a modified invasion percolation approach for the immiscible displacement of a nonwetting fluid (e.g., air) by a wetting one (e.g., water). They further found that their modified invasion percolation model yielded substantially different structures in wetting front compared to the standard invasion percolation. Within their framework, gravity, and capillary fingering, as well as capillary facilitation, contributed to the determination of wetting front and its structure. In their own words, they stated that, "results suggest capillary forces to stabilize downward infiltration events either in very narrow or very wide pore-size distribution media. While this stabilization is intuitive for wide pore-size distributions, gravity fingering has generally been considered to dominate as the pore-size distribution narrows."

Later, Glass et al. (2000) expanded these efforts and developed a macroscale growth "structural" model to model invasion percolation at the near pore scale. Under non-negligible viscous forces conditions, Glass et al. (2000) redefined (1) the total pore filling pressure to incorporate viscous losses within the invading phase (e.g., water) from one hand, and (2) the viscous effect to reduce randomness caused by capillary forces at the front. By comparing their simulations with CO_2-water experiments where viscous forces were negligible, Glass et al. (2000, 2001) found a fair agreement between simulations and experimental data. However, for trichloroethylene-water experiments, discrepancies between simulations and measured data were considerable. It is worth mentioning that the viscosity of trichloroethylene is nearly 40 times greater than that of CO_2.

Another approach towards modeling infiltration was developed by Hunt (1997) who presented random percolation theory and accordingly applied statistics of clusters showing that cumulative infiltration was analogous to electrical polarization. Using such an analogy, Hunt (1997) derived a general expression for cumulative infiltration including the two-term Philip (1957b) model as a special case (see his Eq. 40).

More recently, Hunt et al. (2017) developed a theoretic model for vertical infiltration using concepts from random percolation theory. They proposed a two-term relationship for transient and steady-state infiltration. Hunt et al. (2017) assumed that the transient term describes solute transport under saturating conditions and the steady-state term represents advection fluid.

$$I(t) = \frac{x_0}{t_{x0}} t + \frac{x_0}{t_{x0}^{1/D_b}} t^{\frac{1}{D_b}} \qquad [2.22]$$

where D_b = 1.861 is the backbone fractal dimension in three dimensions (Hunt et al., 2014), x_0 is the typical length scale (e.g., typical pore diameter), and t_{x0} is the time for fluid to traverse the distance x_0. By setting D_b = 1.861, one finds the exponent in the transient term equal to 0.54 (=

1/1.861) which is close to 0.5 in the Philip (1957b) derivation. Using experimental data from Sharma et al. (1980), Hunt et al. (2017) scaled infiltration data and demonstrated that a much better agreement with actual data was obtained when infiltration data were scaled using the percolation theory exponent (e.g., 0.54). They concluded that the exponent 0.54 might be a better approximation than 0.5.

2.8. Bundle of capillary tubes approach

Most of the fundamental flow concepts (described in sections 2.2 and 2.3) modeled water flow into porous media while characterizing the pore space with bundles of capillary tubes of either similar or varying radii. By simplifying the pore space topology, such models do not capture the fundamental randomness of porous media characterized by a wide distribution of interconnected channels and pore sizes. However, the different models based on bundles of capillary tubes can still provide improved representation of complex pore structures while their formulation remains an open theoretical and experimental challenge.

One of the early infiltration models based on the bundle of capillary tubes approach was developed by Chu (1993). In his study, first soil water retention data were used to determine pore size distribution. Then, the Hagen-Poiseuille equation was applied to calculate hydraulic conductivity of each individual tube. Chu (1993) considered a scale factor to match theoretical and experimental saturated hydraulic conductivities. He generalized the Green-Ampt model to describe water flow in all tubes determined from water retention data, and then applied the van Genuchten model to derive a special case. Chu (1993) showed that his model captured spatial variation in the wetting front - an improvement over the traditional Green-Ampt model which assumes a constant depth front. In another study, Chu (1994) used the same approach but replaced the van Genuchten model with the Brooks-Corey model to represent water retention data. Using a Yolo light clay soil sample, he compared his theoretical results with those by the Philip model and found reasonable agreement between the two models.

Recently, a more advanced approach based on the bundle of capillary tubes was proposed to predict pore size distribution using non-Newtonian fluids offering new possibilities for improving porous media characterization (Abou Najm and Atallah, 2016; Atallah and Abou Najm, 2019; Basset et

al., 2019; Hauswirth et al., 2019). Experimental evidence was presented validating the ability of a non-Newtonian fluid at different concentrations to infer the pore structure of simple and synthetic porous media using the ANA model (Atallah and Abou Najm, 2019; Hauswirth et al., 2019) and that of dual-porosity media using the dual-permeability ANA-2 model (Basset et al., 2019).

2.9. Summary of the infiltration models

Building on the fundamental physical flow models for rigid and deformable/swelling soils (sections 2.2 and 2.3), several concepts were derived across the years to estimate infiltration for a specific porous media under specific boundary and initial conditions. Empirical models were also developed describing infiltration with fitted data derived from either field or laboratory experiments. Here, we present a comprehensive summary of the evolution of 138 infiltration models. Our summary is by no means an exhaustive list of all the attempts of infiltration modeling in literature.

We illustrated the historical evolution of infiltration models as listed in Table 2.1, in an ascending historical order based on their year of publication. Table 2.1 summarizes those models based on their category, origin, and assumptions, as well as type and behavior of infiltration. For additional information and formulation, Table 2.1 was further expanded into Tables 2.5 and 2.6 in the Appendix to describe the model parameters, equations, and concepts.

Table 2.1: Summary of 138 infiltration models

Model	Category	Soil Type	Porosity Domain	Type of Infiltration	Infiltration Behavior	Boundary Conditions			Assumptions			Cited [Mentioned in text] Origins
						Concentra-tion	Flux	Pressure Head	Step-function moisture profile	Diffusivity $D(\theta)$ ($L^2 T^{-1}$) and/or Hydraulic Conductivity $K(\theta)$ or $K(\psi)$ ($L T^{-1}$)	Driving forces for infiltration	
Green and Ampt (1911)	Conceptual	Rigid, Homogeneous, Isotropic, Non-hydrophobic, Flat surface	Single	1D, Local scale, Surface	Early and Steady-State			x [Constant head]	Yes	Rapidly varying D, nearly constant K	Hydrostatic Pressure, Capillarity and Gravity	Darcy (1856) - Buckingham (1907)
Kostiakov (1932)	Empirical	Arbitrary	Arbitrary	1D, Local and Field-scale, Surface	Early and Transient State							Experimental infiltration data
Horton (1941)	Empirical	Arbitrary	Arbitrary	1D, Local and Field-scale, Surface	Early and Steady-State							Experimental infiltration data
Mezencev (1948)	Empirical	Arbitrary	Arbitrary	1D, Local and Field-scale, Surface	Early, Transient and Steady-State							Experimental infiltration data - Kostiakov (1932)
Hansen (1955)	Conceptual	Rigid, Homogeneous, Isotropic, Non-hydrophobic, Flat surface	Single	1D, Local scale, Surface	Early, Transient and Steady-State			x [Constant head]	No	K is constant within the transmission zone, then K within the wetting zone decreases toward the wetting front	Capillarity and Gravity	[Darcy's law]
Philip (1957a)	Conceptual	Rigid, Homogeneous, Isotropic, Non-hydrophobic, Flat surface	Single	1D, Local scale, Surface	Early and Transient (implicit)	x			No	D and K are non-linear, strongly varying functions of θ	Capillarity and Gravity	Buckingham (1907) - Richards (1931)
Philip (1957b)	Conceptual	Rigid, Homogeneous, Isotropic, Non-hydrophobic, Flat surface	Single	1D, Local scale, Surface	Early, Transient and Steady-State (explicit)	x			No	D approaches a delta function	Capillarity and Gravity	Philip (1957a)

Holtan (1961)	Empirical	Arbitrary	Arbitrary	1D, Local and Field-scale, Surface	Early, Transient and Steady-State							Experimental infiltration data
Overton (1964)	Semi-Empirical	Arbitrary	Arbitrary	1D, Local and Field-scale, Surface	Early, Transient and Steady-State							Holtan (1961)
Huggins and Monke (1966)	Semi-Empirical	Arbitrary	Arbitrary	1D, Local and Field-scale, Surface	Early, Transient and Steady-State							Holtan (1961)
Fok and Hansen (1966)	Conceptual	Rigid, Homogeneous, Isotropic, Non-hydrophobic, Flat surface	Single	1D, Local scale, Surface (Furrow)	Early, Transient and Steady-State			x [Constant head]	No	K is constant within the transmission zone, then within the wetting zone K decreases toward the wetting front	Capillarity and Gravity	Hansen (1955) [Darcy's law]
Philip (1967)	Conceptual	Rigid, Scale-Heterogeneous, Anisotropic, Non-hydrophobic, Flat surface	Single	1D, Field-scale, Surface	Early and Transient	x			No	K varies spatially with ψ in a mutually consistent way	Capillarity and Gravity	Richards (1931) - Philip (1957a, b) [Darcy's law]
Philip (1968)	Conceptual	Rigid, Homogeneous, Isotropic, Non-hydrophobic, Flat surface	Single	3D, Local scale, Subsurface (Point sources and spherical cavities)	Steady-State	x			No	D is constant, K represented by an exponential function of ψ (Gardner, 1958)	Capillarity and Gravity	Richards (1931) [Darcy's law]
Wooding (1968)	Conceptual	Rigid, Homogeneous, Isotropic, Non-hydrophobic, Flat surface	Single	3D, Local scale, Surface (Shallow Pond)	Steady-State	x			No	D is constant, K represented by an exponential function of ψ (Gardner, 1958)	Capillarity and Gravity	Richards (1931) - Philip (1968) [Darcy's law]
Philip (1969a)	Conceptual	Rigid, Homogeneous, Isotropic, Non-hydrophobic, Flat surface	Single	1D, 2D and 3D, Local scale, Surface and Subsurface (Cylindrical and spherical cavities)	Early, Transient and Steady-State	x			No	(A) D and K are non-linear, strongly varying functions of θ (B) D is constant, K represented	Capillarity and Gravity	Darcy (1856) - Buckingham (1907) - Richards (1931) - Philip (1957a, b, 1967, 1968)

										by an exponential function of ψ (Gardner, 1958) (C) D approaches delta function, very sharp peak in K then K varies very slowly near saturation		
Parlange (1971a)	Conceptual	Rigid, Homogeneous, Isotropic, Non-hydrophobic, Flat surface	Single	1D, Local scale, Surface	Early and Transient	x			No	D vary markedly with θ and rapidly near saturation	Capillarity	Philip (1957a, b, 1969a)
Parlange (1971b)	Conceptual	Rigid, Homogeneous, Isotropic, Non-hydrophobic, Flat surface	Single	1D, Local scale, Surface	Early, Transient and Steady-State	x			No	D vary markedly with θ and rapidly near saturation, very sharp peak in K then K varies very slowly near saturation	Capillarity and Gravity	Philip (1957a, 1969a) - Parlange (1971a)
Parlange (1971c)	Conceptual	Rigid, Homogeneous, Isotropic, Non-hydrophobic, Flat surface	Single	2D and 3D, Local scale, Surface	Early and Transient	x			No	Arbitrary	Capillarity	Philip (1969a) - Parlange (1971a, b)
Philip (1971)	Conceptual	Rigid, Homogeneous, Isotropic, Non-hydrophobic, Flat surface	Single	2D and 3D, Local scale, Surface and Subsurface (Point and line sources)	Steady-State		x [Constant rainfall rate]		No	D is constant, K represented by an exponential function of ψ (Gardner, 1958)	Capillarity and Gravity	Philip (1968, 1969a)
Parlange (1972a)	Conceptual	Rigid, Homogeneous, Isotropic, Non-hydrophobic, Flat surface	Single	2D and 3D, Local scale, Subsurface (Cavity)	Steady-State	x			No	D and K strongly depend on θ	Capillarity and Gravity	Philip (1968, 1969a) -Parlange (1971a, b, c)

Parlange (1972b)	Conceptual	Rigid, Homogeneous, Isotropic, Non-hydrophobic, Flat surface	Single	2D and 3D, Local scale, Subsurface (Cavity)	Early and Transient	x			No	D and K strongly depend on θ	Capillarity and Gravity	Philip (1969a) - Parlange (1971a, b, c, 1972a)
Smith (1972)	Semi-Empirical	Arbitrary	Arbitrary	1D, Local and Field-scale, Surface	Steady-State							Extensive numerical solutions of Richards (1931)
Philip (1972)	Conceptual	Rigid, Scale-Heterogeneous, Anisotropic, Non-hydrophobic, Flat surface	Single	2D and 3D, Field-scale, Surface and Subsurface (Point and line sources)	Steady-State		x [Constant rainfall rate]		No	D is constant, K depends exponentially on ψ and z	Capillarity and Gravity	Philip (1967, 1968, 1969a, 1971)
Talsma and Parlange (1972)	Conceptual	Rigid, Homogeneous, Isotropic, Non-hydrophobic, Flat surface	Single	1D, Local scale, Surface	Early, Transient and Steady-State	x			No	(1) D approaches a delta function, very sharp peak in K then K varies very slowly near saturation (2) $dK/d\theta$ and D are proportional (3) D is constant	Capillarity and Gravity	Philip (1957a, b, 1969a) – Parlange (1971a, b)
Parlange (1972c)	Conceptual	Rigid, Homogeneous, Isotropic, Non-hydrophobic, Flat surface	Single	1D, Local scale, Surface	Early, Transient and Steady-State		x [Constant rainfall rate]		No	D and K strongly depend on θ	Capillarity and Gravity	Philip (1969a) - Parlange (1971a, b)
Mein and Larson (1973)	Conceptual	Rigid, Homogeneous, Isotropic, Non-hydrophobic, Flat surface	Single	1D, Local scale, Surface	Early and Steady-State		x Before ponding [Constant rainfall rate]	x After ponding [Constant head]	Yes	Rapidly varying D, very sharp peak in K to a constant K near saturation	Hydrostatic Pressure, Capillarity and Gravity	Green and Ampt (1911) [Darcy's law]
Smiles (1974)	Conceptual	Swelling, Homogeneous, Isotropic, Non-hydrophobic, Flat surface	Single	1D, Local scale, Surface	Transient State	x			No	Arbitrary	Capillarity and Gravity	Philip (1969a, b) [Darcy's law]
Turner and Parlange (1974)	Conceptual	Rigid, Homogeneous, Isotropic, Non-	Single	1D, Local scale, Surface	Early State	x			No	Arbitrary	Capillarity and Gravity	Parlange (1971a) - Talsma and Parlange (1972)

		hydrophobic, Flat surface										
Swartzendruber (1974)	Conceptual	Rigid, Homogeneous, Isotropic, Non-hydrophobic, Flat surface	Single	1D, Local scale, Surface	Early and Steady-State		x Before ponding [Constant rainfall rate]	x After ponding [Constant head]	Yes	Rapidly varying D, very sharp peak in K to a constant K near saturation	Hydrostatic Pressure, Capillarity and Gravity	Green and Ampt (1911) - Mein and Larson (1973)
Morel-Seytoux and Khanji (1974)	Conceptual	Rigid, Homogeneous, Isotropic, Non-hydrophobic, Flat surface	Single	1D, Local scale, Surface	Early and Steady-State			x [Constant head]	Yes	Rapidly varying D, very sharp peak in K to a constant K near saturation	Hydrostatic Pressure, Capillarity, Gravity, and Air resistance	Green and Ampt (1911) - Mein and Larson (1973) [Darcy's law]
Morel-Seytoux (1976)	Conceptual	Rigid, Homogeneous, Isotropic, Non-hydrophobic, Flat surface	Single	1D, Local scale, Surface	Early, Transient and Steady-State		x Before ponding [Arbitrary rainfall rate]	x After ponding [Arbitrary head]	No	Arbitrary	Hydrostatic Pressure, Capillarity, Gravity, and Air resistance	Mein and Larson (1973) - Morel-Seytoux and Khanji (1974) [Darcian sense]
Li et al. (1976)	Conceptual	Rigid, Homogeneous, Isotropic, Non-hydrophobic, Flat surface	Single	1D, Local scale, Surface	Early and Steady-State			x [Constant head]	Yes	Rapidly varying D, nearly constant K	Hydrostatic Pressure, Capillarity and Gravity	Green and Ampt (1911)
Brutsaert (1977)	Conceptual	Rigid, Homogeneous, Isotropic, Non-hydrophobic, Flat surface	Single	1D, Local scale, Surface	Early and Steady-State	x			Yes	D and K are represented by Averjanov-Irmay formula (1964)	Capillarity and Gravity	Green and Ampt (1911) - Richards (1931) - Philip (1957a, 1969a) - Parlange (1971a)
Collis-George (1977)	Empirical	Arbitrary	Arbitrary	1D, Local and Field-scale, Surface	Early, Transient and Steady-State							Experimental Infiltration data
Hachum and Alfaro (1977)	Conceptual	Rigid, Homogeneous, Isotropic, Non-hydrophobic, Flat surface	Single	1D, Local scale, Surface	Early and Steady-State		x Before ponding [Variable rainfall rate]	x After ponding [Variable head]	Yes	Rapidly varying D, very sharp peak in K to a constant K near saturation	Hydrostatic Pressure, Capillarity and Gravity	Green and Ampt (1911) - Mein and Larson (1973) [Darcy's equation]
Smith and Parlange (1978)	Conceptual	Rigid, Homogeneous, Isotropic, Non-hydrophobic, Flat surface	Single	1D, Local scale, Surface	Early, Transient and Steady-State		x Before ponding [Arbitrary rainfall rate]	x After ponding [Arbitrary head]	No	(1) D approaches a delta function, very sharp peak in K	Hydrostatic Pressure, Capillarity and Gravity	Green and Ampt (1911) - Philip (1957b, 1969a) - Parlange (1971b) - Talsma and Parlange (1972)

										then K varies very slowly near saturation (2) $dK/d\theta$ and D increase rapidly and in similar fashion, K varies rapidly near saturation		
Batu (1978)	Conceptual	Rigid, Homogeneous, Isotropic, Non-hydrophobic, Flat surface	Single	2D, Local scale, Surface (Single and periodic strip sources)	Steady-State	x			No	D is constant, K represented by an exponential function of ψ (Gardner, 1958)	Capillarity and Gravity	Philip (1968, 1969a, 1971)
Kutilek (1980)	Conceptual	Rigid, Homogeneous, Isotropic, Non-hydrophobic, Flat surface	Single	1D, Local scale, Surface	Early, Transient and Steady-State	x After saturation ($h_0 = 0$)	x Before ponding [Constant rainfall rate]		No	D approaches a delta function	Capillarity and Gravity	Philip (1957a)
Parlange (1980)	Conceptual	Rigid, Homogeneous, Isotropic, Non-hydrophobic, Flat surface	Single	1D, Local scale, Surface	Early, Transient and Steady-State	x ($h_0 \leq 0$)		x ($h_0 > 0$) [Constant head]	No	(1) D approaches a delta function, very sharp peak in K then K varies very slowly near saturation (2) $dK/d\theta$ and D increase rapidly and in similar fashion	Hydrostatic Pressure, Capillarity and Gravity	[Darcy's law]
Parlange et al. (1982)	Conceptual	Rigid, Homogeneous, Isotropic, Non-hydrophobic, Flat surface	Single	1D, Local scale, Surface	Early and Steady-State	x			No	D approaches a delta function, very sharp peak in K then K varies	Capillarity and Gravity	Philip (1957a, 1969a) - Parlange (1980)

										very slowly near saturation		
Scotter et al. (1982)	Conceptual	Rigid, Homogeneous, Isotropic, Non-hydrophobic, Flat surface	Single	3D, Local scale, Surface	Steady-State			x [Constant head]	No	D is constant, K represented by an exponential function of ψ (Gardner, 1958)	Hydrostatic Pressure, Capillarity and Gravity	Wooding (1968)
Fok et al. (1982)	Conceptual	Rigid, Homogeneous, Isotropic, Non-hydrophobic, Flat surface	Single	2D, Local, Surface (Furrow)	Early, Transient and Steady-State			x [Constant head]	No	K is constant within the transmission zone, then within the wetting zone K decreases toward the wetting front	Hydrostatic Pressure, Capillarity and Gravity	Hansen (1955) - Fok and Hansen (1966) [Darcy's law]
Brakensiek and Rawls (1983)	Conceptual	Rigid, Heterogeneous, Two-layer (surface crust + subsoil), Isotropic, Non-hydrophobic, Flat surface	Dual	1D, Local scale, Surface	Early and Steady-State		x Before ponding [Constant rainfall rate]	x After ponding [Constant head]	Yes	Rapidly varying D, very sharp peak in K to a constant K near saturation	Hydrostatic Pressure, Capillarity and Gravity	Green and Ampt (1911)
Reynolds et al. (1983)	Conceptual	Rigid, Homogeneous, Isotropic, Non-hydrophobic, Flat surface	Single	3D, Local scale, Subsurface (Well)	Steady-State			x [Constant head]	No	Constant saturated K	Hydrostatic Pressure and Gravity	[Darcy's law]
Novak and Soltesz (1984)	Empirical	Swelling/ Cracked, Heterogeneous, Anisotropic, Non-hydrophobic, Flat surface	Multi	1D, Local and Field-scale, Surface	Early, Transient and Steady-State							Experimental infiltration data
Fok and Chiang (1984)	Conceptual	Rigid, Homogeneous, Isotropic, Non-hydrophobic, Flat surface	Single	2D, Local scale, Surface (Furrow)	Early, Transient and Steady-State			x [Constant head]	No	K is constant within the transmission zone, then within the wetting zone K decreases toward the wetting front	Hydrostatic Pressure, Capillarity and Gravity	Fok and Hansen (1966) - Fok et al. (1982)

Philip (1984a)	Conceptual	Rigid, Homogeneous, Isotropic, Non-hydrophobic, Flat surface	Single	2D, Local scale, Subsurface (Cylindrical cavities)	Steady-State	x			No	D is constant, K represented by an exponential function of ψ (Gardner, 1958)	Capillarity and Gravity	Philip (1957a, 1968, 1969a)
Philip (1984b)	Conceptual	Rigid, Homogeneous, Isotropic, Non-hydrophobic, Flat surface	Single	3D, Local scale, Subsurface (Spherical cavities)	Steady-State	x			No	D is constant, K represented by an exponential function of ψ (Gardner, 1958)	Capillarity and Gravity	Philip (1968, 1969a) - Philip (1984a)
Beven (1984)	Conceptual	Rigid, Scale-Heterogeneous, Anisotropic, Non-hydrophobic, Sloping surface	Single	1D, Field-scale, Surface	Early and Steady-State		x Before ponding [Constant rainfall rate]	x After ponding [Constant head]	Yes	Rapidly varying D, saturated K decreases as an exponential function of depth	Hydrostatic Pressure, Capillarity and Gravity	Green and Ampt (1911) - Mein and Larson (1973) [Darcy's law]
Germann (1985)	Conceptual	Rigid, Heterogeneous, Isotropic, Non-hydrophobic, Flat surface	Multi	1D, Local scale, Surface	Steady-State		x [Constant rainfall rate]		No	Kinematic K	Gravity	Beven and Germann (1981, 1982)
Warrick et al. (1985)	Conceptual	Rigid, Homogeneous, Isotropic, Non-hydrophobic, Flat surface	Single	1D, Local scale, Surface	Early, Transient and Steady-State	x			No	Arbitrary	Capillarity and Gravity	Richards (1931) - Philip (1957a)
Reynolds et al. (1985)	Conceptual	Rigid, Homogeneous, Isotropic, Non-hydrophobic, Flat surface	Single	3D, Local scale, Subsurface (well)	Steady-State			x [Constant head]	No	D is constant, K represented by an exponential function of ψ (Gardner, 1958)	Hydrostatic Pressure, Capillarity and Gravity	Scotter et al. (1982) - Reynolds et al. (1983)
Parlange et al. (1985)	Conceptual	Rigid, Homogeneous, Isotropic, Non-hydrophobic, Flat surface	Single	1D, Local scale, Surface	Early, Transient and Steady-State	x ($h_0 \leq 0$)		x ($h_0 > 0$) [Constant head]	No	$dK/d\theta$ and D increase rapidly and in similar fashion	Hydrostatic Pressure, Capillarity and Gravity	Parlange (1980)
Chu (1985)	Conceptual	Rigid, Heterogeneous, Three-layer	Triple	1D, Local scale, Surface	Early and Steady-State		x Before ponding	x After ponding	Yes	Rapidly varying D, very sharp	Hydrostatic Pressure,	Green and Ampt (1911) -

		(surface crust + till layer + subsoil), Isotropic, Non-hydrophobic, Flat surface					[Arbitrary rainfall rate]	[Arbitrary head]		peak in K to a constant K near saturation	Capillarity and Gravity	Brakensiek and Rawls (1983)
Waechter and Philip (1985)	Conceptual	Rigid, Homogeneous, Isotropic, Non-hydrophobic, Flat surface	Single	2D and 3D, Local scale, Subsurface (Cylindrical and spherical cavities)	Steady-State	x			No	D is constant, K represented by an exponential function of ψ (Gardner, 1958)	Capillarity (weak) and Gravity	Philip (1957a, 1968, 1969a, 1984a, b)
Philip (1985)	Conceptual	Rigid, Homogeneous, Isotropic, Non-hydrophobic, Flat surface	Single	2D and 3D, Local scale, Subsurface (Cavities)	Steady-State	Any			No	D is constant, K represented by an exponential function of ψ (Gardner, 1958)	Capillarity and Gravity	Van de Hulst (1949) - Philip (1957a, 1968, 1969a, 1984a, b) - Waechter and Philip (1985)
Philip (1986a)	Conceptual	Rigid, Homogeneous, Isotropic and Anisotropic, Non-hydrophobic, Flat surface	Single	3D, Local scale, Subsurface (Spheroidal cavities)	Steady-State	x			No	D is constant, K represented by an exponential function of ψ (Gardner, 1958)	Capillarity and Gravity	Philip (1957a, 1968, 1969a, 1984a, b, 1985)
Philip (1986b)	Conceptual	Rigid, Homogeneous, Isotropic, Non-hydrophobic, Flat surface	Single	2D and 3D, Local scale, Subsurface (Discs, cylinders, spheres)	Steady-State	x			No	D is constant, K represented by an exponential function of ψ (Gardner, 1958)	Capillarity and Gravity	Van de Hulst (1949) - Philip (1957a, 1968, 1969a, 1984a, b, 1985, 1986a)
Kutilek and Krejca (1987)	Conceptual	Rigid, Homogeneous, Isotropic, Non-hydrophobic, Flat surface	Single	1D, Local scale, Surface	Early and Transient State	x			No	Arbitrary	Capillarity and Gravity	Philip (1957a)
Swartzendruber (1987a)	Conceptual	Rigid, Homogeneous, Isotropic, Non-hydrophobic, Flat surface	Single	1D, Local scale, Surface	Early and Steady-State			x [Constant head]	Yes	Rapidly varying D, nearly constant K	Hydrostatic Pressure, Capillarity and Gravity	Darcy (1856) - Green and Ampt (1911)

Swartzendruber (1987b)	Conceptual	Rigid, Homogeneous, Isotropic, Non-hydrophobic, Flat surface	Single	1D, Local scale, Surface	Early, Transient and Steady-State	x ($h_0 \leq 0$)		x ($h_0 > 0$) [Constant head]	No	Arbitrary	Hydrostatic Pressure, Capillarity and Gravity	Richards (1931) - Philip (1957a)
Broadbridge and White (1988)	Conceptual	Rigid, Homogeneous, Isotropic, Non-hydrophobic, Flat surface	Single	1D, Local scale, Surface	Early, Transient and Steady-State		x Before ponding [Constant rainfall rate]	x After ponding [Constant head]	No	D and K depend on a single free parameter C and readily measured soil hydraulic properties	Hydrostatic Pressure, Capillarity and Gravity	[Darcy-Buckingham approach]
Yeh (1989)	Conceptual	Rigid, Heterogeneous, Isotropic, Non-hydrophobic, Flat surface	Multi	1D, Local scale, Surface	Early and Steady-State	x			No	K represented by an exponential function of ψ (Gardner, 1958)	Capillarity and Gravity	[Buckingham]
Reynolds and Elrick (1990)	Conceptual	Rigid, Homogeneous, Isotropic, Non-hydrophobic, Flat surface	Single	3D, Local scale, Surface	Steady-State			x [Constant head]	No	K represented by an exponential function of ψ (Gardner, 1958)	Hydrostatic Pressure, Capillarity and Gravity	[Darcy - Buckingham relationships]
Haverkamp et al. (1990)	Conceptual	Rigid, Homogeneous, Isotropic, Non-hydrophobic, Flat surface	Single	1D, Local scale, Surface	Early, Transient and Steady-State	x ($h_0 \leq 0$)		x ($h_0 > 0$) [Constant head]	No	D approaches a delta function, $dK/d\theta$ and D increase rapidly and in similar fashion, K varies rapidly near saturation	Hydrostatic Pressure, Capillarity and Gravity	Parlange et al. (1985)
Smith (1990)	Conceptual	Rigid, Heterogeneous, Two-layer (surface crust + subsoil), Isotropic, Non-hydrophobic, Flat surface	Dual	1D, Local scale, Surface	Early, Transient and Steady-State		x Before ponding [Variable rainfall rate]	x After ponding [Variable head]	No	K represented as function of θ using Brooks and Corey (1964) and van Genuchten (1980)	Hydrostatic Pressure, Capillarity and Gravity	Philip (1957b) - Parlange (1971b) - Talsma and Parlange (1972) - Smith and Parlange (1978) [Darcy's law], [Richards' equation]

Schmid (1990)	Conceptual	Rigid, Homogeneous, Isotropic, Non-hydrophobic, Flat surface	Single	1D, Local scale, Surface	Early and Steady-State		x Before ponding [Variable rainfall rate]	x After ponding [Variable head]	Yes	Rapidly varying D, very sharp peak in K to a constant K near saturation	Hydrostatic Pressure, Capillarity and Gravity	Mein and Larson (1973)
Ankeny et al. (1991)	Conceptual	Rigid, Homogeneous, Isotropic, Non-hydrophobic, Flat surface	Single	3D, Local scale, Surface	Steady-State	x			No	D is constant, K represented by an exponential function of ψ (Gardner, 1958)	Capillarity and Gravity	Wooding (1968)
Swartzendruber and Hogarth (1991)	Conceptual	Rigid, Homogeneous, Isotropic, Non-hydrophobic, Flat surface	Single	1D, Local scale, Surface	Early and Steady-State			x [Constant head]	No	Arbitrary	Hydrostatic Pressure, Capillarity and Gravity	Richards (1931) - Swartzendruber (1987b)
Philip (1992)	Conceptual	Rigid, Homogeneous, Isotropic, Non-hydrophobic, Flat surface	Single	1D, Local scale, Surface	Early and Steady-State			x [Falling head]	Yes	Rapidly varying D, nearly constant K	Hydrostatic Pressure, Capillarity and Gravity	Green and Ampt (1911)
White et al. (1992)	Conceptual	Rigid, Homogeneous, Isotropic, Non-hydrophobic, Flat surface	Single	3D, Local scale, Surface	Steady Flow	x			No	D is constant, K represented by an exponential function of ψ (Gardner, 1958)	Capillarity and Gravity	Wooding (1968) [Darcy's equation]
Barry et al. (1993)	Conceptual	Rigid, Homogeneous, Isotropic, Non-hydrophobic, Flat surface	Single	1D, Local, Surface	Early, Transient and Steady-State	x ($h_0 \leq 0$)		x ($h_0 > 0$) [Constant head]	No	D represented as function of θ using Bruce and Klute (1956), K depends strongly on the soil moisture characteristic curve	Hydrostatic Pressure, Capillarity and Gravity	Richards (1931) [Darcy's law]
Fonteh and Podmore (1993)	Conceptual	Rigid, Homogeneous, Isotropic, Non-hydrophobic, Flat surface	Single	2D, Local scale, Surface (Furrow)	Early and Steady-State			x [Constant head]	Yes	Rapidly varying D, very sharp peak in K to a constant K	Hydrostatic Pressure, Capillarity and Gravity	Green and Ampt (1911) - Hansen (1955) - Fok and Chiang (1984)

										near saturation		
Smith et al. (1993)	Conceptual	Rigid, Homogeneous, Isotropic, Non-hydrophobic, Flat surface	Single	1D, Local scale, Surface	Early, Transient and Steady-State	x During rainfall hiatus	x Before ponding/ post hiatus [Arbitrary rainfall rate]	x After ponding [Arbitrary head]	No	K represented as function of θ using Brooks and Corey (1964)	Hydrostatic Pressure, Capillarity and Gravity	Parlange et al. (1982) [Darcy flow] [Richards' equation]
Philip (1993)	Conceptual	Rigid, Homogeneous, Isotropic, Non-hydrophobic, Flat surface	Single	1D, Local scale, Surface	Early and Steady-State		x Before ponding [Arbitrary rainfall rate]	x After ponding [Arbitrary head]	Yes	Rapidly varying D, very sharp peak in K to a constant K near saturation	Hydrostatic Pressure, Capillarity and Gravity	Green and Ampt (1911)
Stone et al. (1994)	Conceptual	Rigid, Homogeneous, Isotropic, Non-hydrophobic, Flat surface	Single	1D, Local scale, Surface	Early and Steady-State			x [Constant head]	Yes	Rapidly varying D, constant K near saturation	Hydrostatic Pressure, Capillarity and Gravity	Green and Ampt (1911) - Philip (1957a)
Mandal and Waechter (1994)	Conceptual	Rigid, Homogeneous, Isotropic, Non-hydrophobic, Flat surface	Single	2D, Local scale, Subsurface (Cylinders)	Steady-State	x			No	Arbitrary	Capillarity and Gravity	Philip (1968, 1984a, b, 1985) - Waechter and Philip (1985)
Fallow et al. (1994)	Conceptual	Rigid, Homogeneous, Isotropic, Non-hydrophobic, Flat surface	Single	1D, Local scale, Surface	Early, Transient and Steady-State	x ($h_0 \leq 0$)		x ($h_0 > 0$) [Constant and Falling head]	No	D is constant, K represented by an exponential function of ψ (Gardner, 1958)	Capillarity	Philip (1957a - 1969a)
Basha (1994)	Conceptual	Rigid, Homogeneous, Isotropic, Non-hydrophobic, Flat surface	Single	1D, 2D and 3D, Local scale, Surface and subsurface	Early and Steady-State		x Before ponding [Arbitrary rainfall rate]	x After ponding [Arbitrary head]	No	D is constant, K represented by an exponential function of ψ (Gardner, 1958)	Capillarity and Gravity	Buckingham (1907) - Richards (1931) - Greenberg (1971)
Salvucci and Entekhabi (1994)	Conceptual	Rigid, Homogeneous, Isotropic, Non-hydrophobic, Flat surface	Single	1D, Local scale, Surface	Early and Steady-State			x [Constant head]	Yes	Rapidly varying D, constant K near saturation	Hydrostatic Pressure, Capillarity and Gravity	Green and Ampt (1911) - Philip (1957a)
Corradini et al. (1994)	Conceptual	Rigid, Homogeneous, Isotropic, Non-	Single	1D, Local scale, Surface	Early, Transient and Steady-State		x		No	K represented as function	Capillarity and Gravity	Parlange et al. (1982, 1985) - Smith et al. (1993)

		hydrophobic, Flat surface					[Arbitrary rainfall rate]			of θ using Brooks and Corey (1964)		[Richards' equation]
Smettem et al. (1994)	Conceptual	Rigid, Homogeneous, Isotropic, Non-hydrophobic, Flat surface	Single	3D, Local scale, Surface	Early State	x			No	D increases sharply with increasing θ, K varies rapidly near saturation	Capillarity	Parlange (1971a) - Turner and Parlange (1974)
Haverkamp et al. (1994)	Conceptual	Rigid, Homogeneous, Isotropic, Non-hydrophobic, Flat surface	Single	1D and 3D, Local scale, Surface	Early, Transient and Steady-State	x ($h_0 \leq 0$)		x ($h_0 > 0$) [Constant head]	No	$dK/d\theta$ and D increase rapidly and in similar fashion, K varies rapidly near saturation	Hydrostatic Pressure, Capillarity and Gravity	Parlange et al. (1982) - Smetten et al. (1994) - Haverkamp et al. (1990)
Barry et al. (1995)	Conceptual	Rigid, Homogeneous, Isotropic, Non-hydrophobic, Flat surface	Single	1D, Local scale, Surface	Early and Steady-State			x [Constant head]	No	$dK/d\theta$ and D increase rapidly and in similar fashion, K varies rapidly near saturation	Hydrostatic Pressure, Capillarity and Gravity	Richards (1931) - Philip (1957a) - Parlange et al. (1982, 1985) - Haverkamp et al. (1990)
Elrick et al. (1995)	Semi-Empirical	Arbitrary	Single	1D, Local and Field-scale, Surface	Transient and Steady-State			x [Falling head]				Experimental Infiltration data – Richards (1931)
Sommer and Mortensen (1996)	Conceptual	Deformable, Homogeneous, Anisotropic, Non-hydrophobic, Flat surface	Single	1D, Local scale, Surface	Early and Steady-State			x [Constant head]	Yes	Rapidly varying D, nearly constant K	Liquid Pressure or Hydrostatic Pressure, and Capillarity	Biot (1955) [Darcy's law]
Srivastava et al. (1996)	Conceptual	Rigid, Homogeneous, Isotropic, Non-hydrophobic, Flat surface	Single	1D, Local scale, Surface	Early and Steady-State			x [Constant head]	Yes	Rapidly varying D, nearly constant K	Hydrostatic Pressure, Capillarity and Gravity	Green and Ampt (1911) - Mein and Larson (1973)
Preziosi et al. (1996)	Conceptual	Deformable, Homogeneous, Anisotropic, Non-hydrophobic, Flat surface	Single	1D, Local scale, Surface	Early and Steady-State			x [Constant head]	Yes	Rapidly varying D, nearly constant K	Liquid Pressure or Hydrostatic Pressure, and Capillarity	Darcy (1856) - Bowen (1980)
Corradini et al. (1997)	Conceptual	Rigid, Homogeneous, Isotropic, Non-hydrophobic, Flat surface	Single	1D, Local scale, Surface	Early, Transient and Steady-State	x During rainfall hiatus	x Before ponding/ post hiatus	x After ponding [Arbitrary head]	No	K represented as function of θ using	Hydrostatic Pressure, Capillarity and Gravity	Parlange et al. (1985) - Smith et al. (1993) - Corradini et al. (1994)

							[Arbitrary rainfall rate]			Brooks and Corey (1964)		[Darcy's law] [Richards' equation]
Parlange et al. (1997)	Conceptual	Arbitrary	Arbitrary	1D, Local scale, Surface	Early and Steady-State	Any			No	D approaches a delta function, very sharp peak in K then K varies very slowly near saturation	Hydrostatic Pressure, Capillarity and Gravity	Parlange et al. (1982, 1985) [Richards' equation]
Wu and Pan (1997)	Conceptual	Rigid, Homogeneous, Isotropic, Non-hydrophobic, Flat surface	Single	3D, Local scale, Surface	Early, Transient and Steady-State	x ($h_0 \leq 0$)		x ($h_0 > 0$) [Constant head]	No	K represented by an exponential function of ψ (Gardner, 1958)	Hydrostatic Pressure, Capillarity and Gravity	Richards (1931) - Warrick et al. (1985) - Reynolds and Elrick (1990)
Wang et al. (1997)	Conceptual	Rigid, Homogeneous, Isotropic, Non-hydrophobic, Flat surface	Single	1D, Local scale, Surface	Early and Steady-State			x [Constant head]	Yes	Rapidly varying D, nearly constant K	Hydrostatic Pressure, Capillarity, Gravity, and Air entrapment effects	Green and Ampt (1911)
Enciso-Medina et al. (1998)	Conceptual	Rigid, Heterogeneous, Three-layer (surface seal + till layer + subsoil), Isotropic, Non-hydrophobic, Flat surface	Triple	1D, Local scale, Surface (Furrow)	Early and Steady-State			x [Constant head]	Yes	Rapidly varying D, nearly constant K	Hydrostatic Pressure, Capillarity and Gravity	Green and Ampt (1911) [Darcy's law]
Philip (1998)	Conceptual	Rigid, Heterogeneous, Two-layer (surface crust + subsoil), Anisotropic, Non-hydrophobic, Flat surface	Dual	1D, Local scale, Surface	Early, Transient and Steady-State	x ($h_0 \leq 0$)		x ($h_0 > 0$) [Constant head]	No	D and K are nonlinear functions of θ in the crust and in the soil	Hydrostatic Pressure, Capillarity and Gravity	Philip (1957a, b, 1967, 1969a) [Darcy's law]
Smith et al. (1999)	Conceptual	Rigid, Heterogenous, Two-layer (surface crust + subsoil),	Dual	1D, Local scale, Surface	Early, Transient and Steady-State	x During rainfall hiatus	x Before ponding/ post hiatus	x After ponding [Arbitrary head]	No	K represented as function of θ using Brooks and	Hydrostatic Pressure, Capillarity and Gravity	Smith et al. (1993) - Corradini et al. (1994, 1997)

		Isotropic, Non-hydrophobic, Flat surface					[Arbitrary rainfall rate]			Corey (1964) – Upper layer has always the lowest K		[Darcy's law] [Richards' equation]
Selker et al. (1999a)	Conceptual	Rigid, Scale-Heterogeneous, Anisotropic, Non-hydrophobic, Flat surface	Single	1D, Field-scale, Surface	Early and Steady-State			x [Constant head]	Yes	Rapidly varying D, saturated K function of depth following linear, power law and exponential relationship	Hydrostatic Pressure, Capillarity and Gravity	Green and Ampt (1911) - Beven (1984)
Wu et al. (1999)	Conceptual	Rigid, Homogeneous, Isotropic, Non-hydrophobic, Flat surface	Single	3D, Local scale, Surface	Early, Transient and Steady-State	x ($h_0 \leq 0$)		x ($h_0 > 0$) [Constant head]	No	K represented by an exponential function of ψ (Gardner, 1958)	Hydrostatic Pressure, Capillarity and Gravity	Philip (1957a) - Reynolds and Elrick (1990) - Wu and Pan (1997) [Richards' equation]
Novak et al. (2000)	Conceptual	Swelling/ Cracked, Heterogeneous, Isotropic, Non-hydrophobic, Flat surface	Multi	1D, Local scale, Surface	Early, Transient and Steady-State	x ($h_0 \leq 0$)		x ($h_0 > 0$) [Constant head]	No	Arbitrary	Hydrostatic Pressure, Capillarity and Gravity	Green and Ampt (1911) - Feddes et al. (1988) [Darcy's law] [Richards' equation]
Corradini et al. (2000)	Conceptual	Rigid, Heterogeneous, Two-layer (surface crust + subsoil), Isotropic, Non-hydrophobic, Flat surface	Dual	1D, Local scale, Surface	Early, Transient and Steady-State	x During rainfall hiatus	x Before ponding/ post hiatus [Arbitrary rainfall rate]	x After ponding [Arbitrary head]	No	K represented as function of θ using Brooks and Corey (1964) – Either layer may be less permeable	Hydrostatic Pressure, Capillarity and Gravity	Smith et al. (1993, 1999) - Corradini et al. (1994, 1997) [Darcy's law] [Richards' equation]
Swartzendruber (2000)	Conceptual	Rigid, Homogeneous, Isotropic, Non-hydrophobic, Flat surface	Single	1D, Local scale, Surface	Early and Steady-State			x ($h_0 > 0$) [Variable head]	Yes	Rapidly varying D, nearly constant K	Hydrostatic Pressure, Capillarity and Gravity	Darcy (1856) - Green and Ampt (1911)
Govindaraju et al. (2001)	Semi-analytical	Rigid, Scale-Heterogeneous (at the field scale), Anisotropic, Non-	Single	1D, Local and Field-scale, Surface	Early, Transient and Steady-State		x Before ponding [Arbitrary rainfall rate]	x After ponding [Arbitrary head]	(1) Yes (2) No	(1) At the local scale, rapidly varying D, constant K near saturation,	Hydrostatic Pressure, Capillarity and Gravity	Green and Ampt (1911)

		hydrophobic, Flat surface								(2) At the field-scale, saturated K varies spatially and represented by a correlated lognormal random field		
Serrano (2001)	Conceptual	Rigid, Homogeneous, Isotropic, Non-hydrophobic, Flat surface	Single	1D, Local scale, Surface	Early and Steady-State			x [Constant head]	Yes	Rapidly varying D, nearly constant K	Hydrostatic Pressure, Capillarity and Gravity	Green and Ampt (1911)
Corradini et al. (2002)	Semi-analytical	Rigid, Scale-Heterogeneous, Anisotropic, Non-hydrophobic, Sloping surface	Single	1D, Field-scale, Surface	Early, Transient and Steady-State	x Downslope after ponding (no run-on) (1)	x Before ponding [Arbitrary rainfall rate]	x After ponding [Arbitrary head]	No	(1) Saturated K varies spatially and represented as a log-distributed random variable with PDF (2) Effective Saturated K represented empirically	Hydrostatic Pressure, Capillarity and Gravity	Govindaraju et al. (2001)
Elrick et al. (2002)	Conceptual	Rigid, Homogeneous, Isotropic, Non-hydrophobic, Flat surface	Single	1D, Local scale, Surface	Early and Steady State			x (Constant- and Falling-head)	Yes	Rapidly varying D, very sharp peak in K to a constant K near saturation	Hydrostatic Pressure, Capillarity and Gravity	Green and Ampt (1911) - Philip (1957b) - Elrick et al. (1995)
Parlange et al. (2002)	Conceptual	Rigid, Homogeneous, Isotropic, Non-hydrophobic, Flat surface	Single	1D, Local scale, Surface	Early and Steady-State	x ($h_0 = 0$)			No	D and K lie between the assumption of sharp wetting front and the assumption of D and $dK/d\theta$ proportional	Capillarity and Gravity	Green and Ampt (1911) - Philip (1969a) - Talsma and Parlange (1972) - Parlange (1980) - Parlange et al. (1982)
Warrick et al. (2005)	Conceptual	Rigid, Homogeneous, Isotropic, Non-	Single	1D, Local scale, Surface	Early and Steady-State			x (Variable head)	Yes	Rapidly varying D,	Hydrostatic Pressure,	Green and Ampt (1911)

		hydrophobic, Flat surface								nearly constant K	Capillarity and Gravity	
Weiler (2005)	Conceptual	Rigid, Heterogeneous, Isotropic, Non-hydrophobic, Flat surface	Dual	1D, Local scale, Surface	Early and Steady-State			x [Constant head]	Yes	Rapidly varying D, nearly constant K	Hydrostatic Pressure, Capillarity and Gravity	Green and Ampt (1911) [Buckingham-Darcy law]
Govindaraju et al. (2006)	Semi-analytical	Rigid, Scale-Heterogeneous, Anisotropic, Non-hydrophobic, Sloping surface	Single	1D, Field-scale, Surface	Early, Transient and Steady-State	Downslope after ponding (no run-on)	x Before ponding [Variable rainfall rate]	x After ponding [Variable head]	No	Saturated K varies spatially and represented as a log-distributed random variable with PDF	Hydrostatic Pressure, Capillarity and Gravity	Govindaraju et al. (2001) - Corradini et al. (2002)
Morbidelli et al. (2006)	Semi-analytical	Rigid, Scale-Heterogeneous, Anisotropic, Non-hydrophobic, Sloping surface	Single	1D, Field-scale, Surface	Early, Transient and Steady-State		x Before ponding [Variable rainfall rate]	x After ponding [Variable head]	No	Saturated K varies spatially and represented as a log-distributed random variable with PDF	Hydrostatic Pressure, Capillarity and Gravity	Govindaraju et al. (2001, 2006) - Corradini et al. (2002)
Lassabatere et al. (2006)	Conceptual	Rigid, Homogeneous, Isotropic, Non-hydrophobic, Flat surface	Single	3D, Local scale, Surface	Transient and Steady-State	x			No	K represented as function of θ using Brooks and Corey (1964)	Capillarity and Gravity	Philip (1969) - Smetten et al. (1994) - Haverkamp et al. (1994)
Chen and Young (2006)	Conceptual	Rigid, infinitely deep, Homogeneous, Isotropic, Non-hydrophobic, Sloping surface	Single	1D, Local scale, Surface	Early and Steady-State		x Before ponding [Arbitrary rainfall rate]	x After ponding [Arbitrary head]	Yes	Rapidly varying D, very sharp peak in K to a constant K near saturation	Hydrostatic Pressure, Capillarity and Gravity	Green and Ampt (1991) [Darcy's law]
Warrick and Lazarovitch (2007)	Conceptual	Rigid, Homogeneous, Isotropic, Non-hydrophobic, Flat surface	Single	2D, Local scale, Surface (Strip source)	Early, Transient and Steady-State			x [Constant head]	No	Arbitrary	Hydrostatic pressure, Capillarity and Gravity	Turner and Parlange (1974) - Smetten et al. (1994) - Haverkamp et al. (1994) [Richards' equation]
Warrick et al. (2007)	Conceptual	Rigid, Homogeneous, Isotropic, Non-hydrophobic, Flat surface	Single	2D, Local scale, Surface (Furrow)	Early, Transient and Steady-State			x [Constant head]	No	Arbitrary	Hydrostatic pressure, Capillarity and Gravity	Haverkamp et al. (1994) - Warrick and Lazarovitch (2007) [Richards' equation]

Assouline et al. (2007)	Conceptual	Arbitrary	Arbitrary	Arbitrary	Early, Transient and Steady-State		x Before ponding [Variable rainfall rate]	x After ponding [Variable head]	No	Arbitrary	Hydrostatic Pressure, Capillarity and Gravity	Smith et al. (2002) - Brutsaert (2005)
Germann et al. (2007)	Conceptual	Rigid, Heterogeneous, Isotropic, Non-hydrophobic, Flat surface	Multi	1D, Local scale, Surface	Steady-State		x [Constant rainfall rate]		Yes	Saturated K is time-variant	Gravity	[Stokes flow]
Essig et al. (2009)	Conceptual	Rigid, Homogeneous, Isotropic, Non-hydrophobic, Sloping surface	Single	1D, Local scale, Surface	Early and Steady-State	x Before ponding and after saturation ($h_0 = 0$)	x Before ponding [Constant rainfall rate]	x After ponding [Constant head]	Yes	Rapidly varying D, very sharp peak in K to a constant K near saturation	Hydrostatic Pressure, Capillarity and Gravity	[Darcy - Buckingham law] [Darcy's law]
Valiantzas (2010)	Conceptual	Rigid, Homogeneous, Isotropic, Non-hydrophobic, Flat surface	Single	1D, Local scale, Surface	Early, Transient and Steady-State	x ($h_0 \leq 0$)		x ($h_0 > 0$) [Constant head]	No	D and K lie between the assumption of sharp wetting front and the assumption of D and $dK/d\theta$ proportional	Hydrostatic Pressure, Capillarity and Gravity	Philip (1975a, b) - Talsma and Parlange (1972) [Darcy's law] [Richards' equation]
Su (2010)	Conceptual	Swelling, Heterogeneous, Isotropic, Non-hydrophobic, Flat surface	Multi	1D, Local scale, Surface	Early, Transient and Steady-State	x			No	Constant D and linear K as function of θ (Fleming et al., 1984)	Capillarity and Gravity	Philip (1969b) - Smiles and Raats (2005) – Su (2009) [Richards' equation]
Corradini et al. (2011)	Conceptual	Rigid, Heterogeneous, Two-layer (surface crust + subsoil), Isotropic, Non-hydrophobic, Flat surface	Dual	1D, Local scale, Surface	Early, Transient and Steady-State	x During rainfall hiatus	x Before ponding/ post hiatus [Arbitrary rainfall rate]	x After ponding [Arbitrary head]	No	K represented as function of θ using Brooks and Corey (1964) – Upper layer is more permeable	Hydrostatic Pressure, Capillarity and Gravity	Smith et al. (1993) - Corradini et al. (1997, 2000) [Richards' equation]
Swamee et al. (2012)	Conceptual	Rigid, Homogeneous, Isotropic, Non-hydrophobic, Flat surface	Single	1D, Local scale, Surface	Early and Steady-State	x ($h_0 \leq 0$)		x ($h_0 > 0$) [Constant head]	(1) Yes (2) No	(1) Rapidly varying D, nearly constant K (2) $dK/d\theta$ and D are proportional	Hydrostatic Pressure, Capillarity and Gravity	Richards (1931) - Green and Ampt (1911) - Taslma and Parlange (1972)

Govindaraju et al. (2012)	Conceptual	Rigid, Scale-Heterogeneous, Anisotropic, Non-hydrophobic, Flat surface	Single	1D, Local and Field-scale, Surface	Early, Transient and Steady-State		x Before ponding [Arbitrary rainfall rate]	x After ponding [Arbitrary head]	(1) Yes (2) No	(1) At the local scale, saturated K continuously decreasing with depth according to a power law (2) At the field-scale, saturated K represented spatially by a correlated lognormal random field	Hydrostatic Pressure, Capillarity and Gravity	Green and Ampt (1911)
Ali et al. (2013)	Conceptual	Rigid, Homogeneous, Isotropic, Non-hydrophobic, Flat surface	Single	1D, Local scale, Surface	Early and Steady-State			x [Constant head]	Yes	Rapidly varying D, nearly constant K	Hydrostatic Pressure, Capillarity and Gravity	Green and Ampt (1911)
Almedeij and Esen (2014)	Conceptual	Rigid, Homogeneous, Isotropic, Non-hydrophobic, Flat surface	Single	1D, Local scale, Surface	Early and Steady-State		x Before ponding [Constant rainfall rate]	x After ponding [Constant head]	Yes	Rapidly varying D, very sharp peak in K to a constant K near saturation	Hydrostatic Pressure, Capillarity and Gravity	Green and Ampt (1911) - Mein and Larson (1973)
Bautista et al. (2014)	Conceptual	Rigid, Homogeneous, Isotropic, Non-hydrophobic, Flat surface	Single	2D, Local scale, Surface (Furrow)	Early, Transient and Steady-State			x [Variable head]	No	Arbitrary	Hydrostatic pressure, Capillarity and Gravity	Richards (1931) - Haverkamp et al. (1994) - Warrick and Lazarovitch (2007) - Warrick et al. (2007)
Lassabetere et al. (2014)	Conceptual	Rigid, Heterogeneous, Isotropic, Non-hydrophobic, Flat surface	Dual	1D and 3D, Local scale, Surface	Early, Transient and Steady-State	x			No	K represented as function of θ using van Genuchten - Mualem model (Mualem, 1976; van Genuchten, 1980)	Capillarity and Gravity	Gerke and van Genuchten (1993) -Haverkamp et al. (1994) [Buckingham - Darcy law] [Richards' equation]

Vatankhah (2015)	Conceptual	Rigid, Homogeneous, Isotropic, Non-hydrophobic, Flat surface	Single	1D, Local scale, Surface	Early and Steady-State			x [Arbitrary head]	Yes	Rapidly varying D, very sharp peak in K to a constant K near saturation	Hydrostatic Pressure, Capillarity and Gravity	Green and Ampt (1911) - Almedeij and Esen (2014)
Bautista et al. (2016)	Conceptual	Rigid, Homogeneous, Isotropic, Non-hydrophobic, Flat surface	Single	2D, Local scale, Surface (Furrow)	Early, Transient and Steady-State			x [Variable head]	No	Arbitrary	Hydrostatic pressure, Capillarity and Gravity	Richards (1931) - Haverkamp et al. (1994) - Warrick and Lazarovitch (2007) - Warrick et al. (2007) - Bautista et al. (2014)
Nie et al. (2017a)	Conceptual	Rigid, Homogeneous, Isotropic, Non-hydrophobic, Flat surface	Single	1D, Local scale, Surface	Early and Steady-State			x [Constant head]	Yes	Rapidly varying D, nearly constant K	Hydrostatic Pressure, Capillarity and Gravity	Green and Ampt (1911), Valiantzas (2010) [Darcy's equation]
Selker and Assouline (2017)	Conceptual	Rigid, Homogeneous, Isotropic, Non-hydrophobic, Flat surface	Single	1D, Local scale, Surface	Early State			x [Constant head]	Yes	Rapidly varying D, nearly constant K	Hydrostatic Pressure, Capillarity and Gravity	Green and Ampt (1911)
Stewart and Abou Najm (2018)	Conceptual	Rigid, Homogeneous, Isotropic, Non-hydrophobic, Flat surface	Single	3D, Local scale, Surface	Transient and Steady-State	x ($h_0 \leq 0$)		x ($h_0 > 0$) [Constant head]	No	K represented as function of ψ using Brooks and Corey (1964)	Hydrostatic Pressure, Capillarity and Gravity	Philip (1957a) - Philip (1969a) - Reynolds and Elrick (1990) - Wu and Pan (1997) - Wu et al. (1999)
Stewart (2018)	Conceptual	Shrink-swell, Heterogeneous, Isotropic, Non-hydrophobic, Flat surface	Dual	1D, Local scale, Surface	Early and Steady-State		x Before ponding [Constant rainfall rate]	x After ponding [Constant head]	Yes	Rapidly varying D, very sharp peak in K to a constant K near saturation	Hydrostatic Pressure, Capillarity and Gravity	Green and Ampt (1911) - Selker and Assouline (2017)
Rahmati et al. (2019)	Conceptual	Rigid, Homogeneous, Isotropic, Non-hydrophobic, Flat surface	Single	1D, Local scale, Surface	Early and Transient State	x			No	Arbitrary	Hydrostatic Pressure, Capillarity and Gravity	Richards (1931) - Philip (1957a) - Parlange et al. (1982) - Haverkamp et al. (1994)
Stewart (2019)	Conceptual	Rigid, Heterogeneous, Isotropic, Non-hydrophobic, Flat surface	Dual	1D, Local scale, Surface	Early and Steady-State		x Before ponding [Constant rainfall rate]	x After ponding [Constant head]	Yes	Rapidly varying D, very sharp peak in K to a constant K	Hydrostatic Pressure, Capillarity and Gravity	Green and Ampt (1911) - Beven and Germann (1982) - Gerke and Van Genuchten (1993) - Selker

										near saturation		and Assouline (2017) [Darcy's law]
Baiamonte (2020)	Conceptual	Rigid, Homogeneous, Isotropic, Non-hydrophobic, Flat surface	Single	1D, Local scale, Surface	Early, Transient and Steady-State		x [Constant rainfall rate]		No	(1) K represented using Torricelli's law (2) K represented as function of ψ using Brooks and Corey (1964)	Gravity	Richards (1931)
Su et al. (2020)	Conceptual	Deformable, Scale-Heterogeneous, Anisotropic, Non-hydrophobic, Flat surface	Single	1D, Local scale, Surface	Early, Transient and Steady-State	x ($h_0 \leq 0$)		x ($h_0 > 0$) [Constant head]	No	K represented as function of θ using van Genuchten model (1980)	Hydrostatic Pressure, Capillarity and Gravity	Richards (1931)
Poulovassilis and Argyrokastritis (2020)	Conceptual	Rigid, Homogeneous, Isotropic, Non-hydrophobic, Flat surface	Single	1D, Local scale, Surface	Early, Transient and Steady-State	x			No	Arbitrary	Capillarity and Gravity	Richards (1931) - Philip (1957a, b)
Abou Najm et al. (2021)[a]	Semi-Conceptual	Arbitrary	Arbitrary	Arbitrary	Arbitrary	Any			No	Arbitrary	Arbitrary	-
Di Prima et al. (2021)[a]	Conceptual	Rigid, Homogeneous, Isotropic, Hydrophobic, Flat surface	Single	3D, Local scale, Surface	Transient and Steady-State	x			No	K represented as function of θ using Brooks and Corey (1964)	Capillarity and Gravity	Haverkamp et al. (1994) - Lassabatere et al. (2006) - Abou Najm et al. 2021)

[a]All models illustrate a concave cumulative infiltration curve I(t), except for Abou Najm et al. (2021) and Di Prima et al. (2021) which allow both the representation of either concave or convex I(t) curves.

From a historic timeline demonstrating the evolution of knowledge from earlier theories into the most recent conceptual models based on citations (Figure 2.3), we identified areas that witnessed the most developments vs. areas that have been understudied. Studies based on Darcy's law, the Richardson-Richards-Buckingham paradigm and the Green-Ampt models, are very common, while models based on Stokes' work and other earlier theories are areas for possible investigation and advancements.

One additional finding from our inclusive survey is that almost all infiltration models for early- and transient-time behavior, except for Abou Najm et al. (2021) and Di Prima et al. (2021), were designed to reflect typical infiltration results from infiltration experiments revealing a concave cumulative infiltration curve. The concave curve demonstrates higher infiltration capacity at early stages that reaches a constant slope at steady state. This concave shape mimics what we call "perfect" infiltration conditions with no water-repellency, preferential flow, or any other factors present. However, different soils and field conditions can alter this behavior leading to cumulative infiltration curves that exhibit convex, mixed, or non-standard shapes. More recently, Pachepsky and Karahan (2022) analyzed the global infiltration database called SWIG developed by Rahmati et al. (2018). By analyzing 5023 infiltration curves, they found 12 types of cumulative infiltration curve shapes. Nearly one third of the SWIG database showed non-classic shape. They applied a classification tree approach to divide those data with non-classic shapes. Their results showed that measurement method, clay content, and organic matter were among the most influential predictors of the shape type. In fact, non-classic shapes were previously reported and associated to soil structure and hydrophobicity (Angulo-Jaramillo et al., 2019). Given different land use and field conditions, different structural interactions come into play such as soil water-repellency, hydrophobicity, and preferential flow paths. As an attempt to model infiltration behavior covering the full range of shapes, Abou Najm et al. (2021) introduced a soil water-repellency parameter, α_{WR} (T^{-1}) that can be used with any infiltration model. α_{WR} accounts for water repellency using an exponential scaling factor that mimics the attenuation of infiltration rates observed at start of infiltration (Figure 2.4). The α_{WR} family of models originated by Abou Najm et al. (2021) presented a macroscopic approach addressing water repellency (Di Prima et al., 2021; Yilmaz et al., 2022); other more microscopic and process-based approaches can be found in Shillito et al. (2020) and Hammecker et al. (2022).

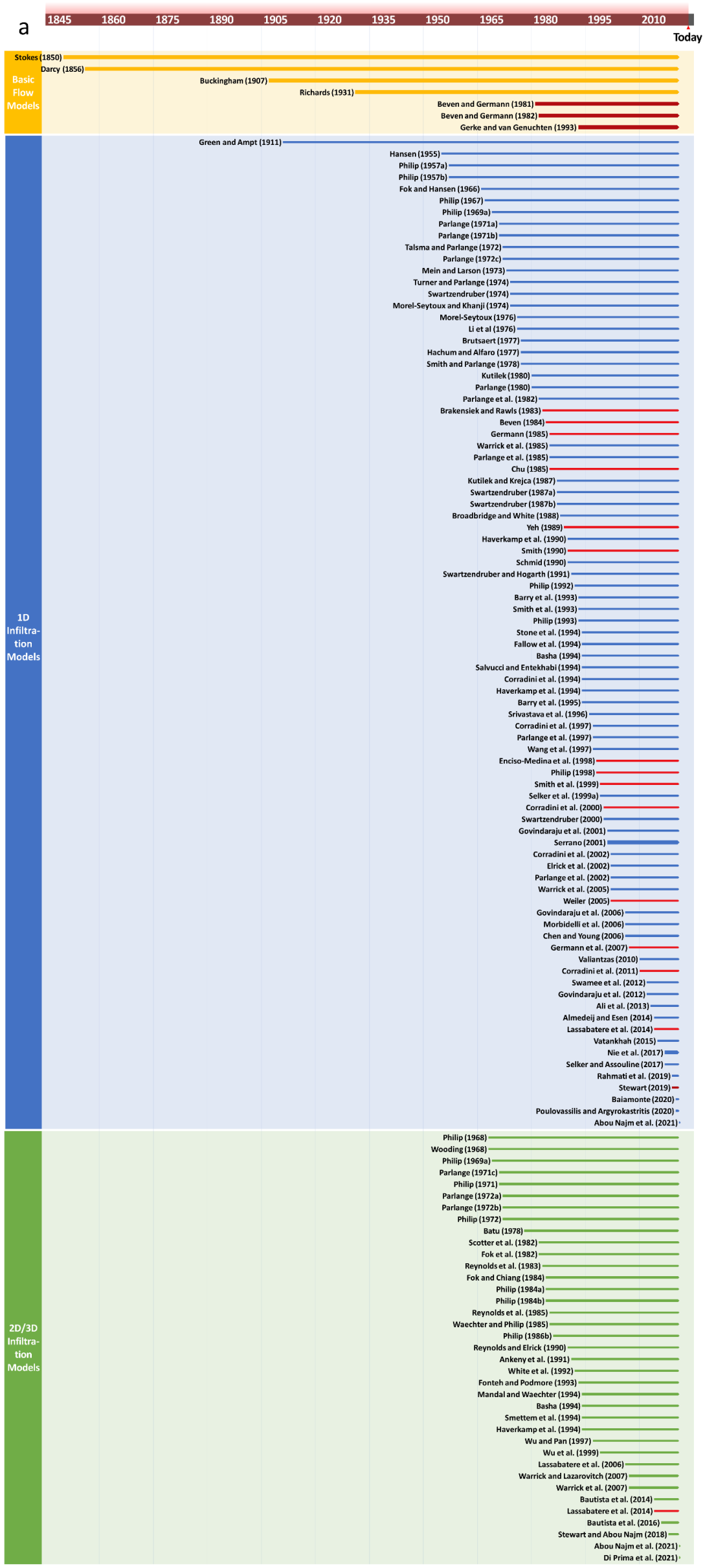
a
1845
1860
1875
1890
1905
1920
1935
1950
1965
1980
1995
2010
Today
Basic Flow Models
Stokes (1850)
Darcy (1856)
Buckingham (1907)
Richards (1931)
Beven and Germann (1981)
Beven and Germann (1982)
Gerke and van Genuchten (1993)
1D Infiltra-tion Models
Green and Ampt (1911)
Hansen (1955)
Philip (1957a)
Philip (1957b)
Fok and Hansen (1966)
Philip (1967)
Philip (1969a)
Parlange (1971a)
Parlange (1971b)
Talsma and Parlange (1972)
Parlange (1972c)
Mein and Larson (1973)
Turner and Parlange (1974)
Swartzendruber (1974)
Morel-Seytoux and Khanji (1974)
Morel-Seytoux (1976)
Li et al (1976)
Brutsaert (1977)
Hachum and Alfaro (1977)
Smith and Parlange (1978)
Kutilek (1980)
Parlange (1980)
Parlange et al. (1982)
Brakensiek and Rawls (1983)
Beven (1984)
Germann (1985)
Warrick et al. (1985)
Parlange et al. (1985)
Chu (1985)
Kutilek and Krejca (1987)
Swartzendruber (1987a)
Swartzendruber (1987b)
Broadbridge and White (1988)
Yeh (1989)
Haverkamp et al. (1990)
Smith (1990)
Schmid (1990)
Swartzendruber and Hogarth (1991)
Philip (1992)
Barry et al. (1993)
Smith et al. (1993)
Philip (1993)
Stone et al. (1994)
Fallow et al. (1994)
Basha (1994)
Salvucci and Entekhabi (1994)
Corradini et al. (1994)
Haverkamp et al. (1994)
Barry et al. (1995)
Srivastava et al. (1996)
Corradini et al. (1997)
Parlange et al. (1997)
Wang et al. (1997)
Enciso-Medina et al. (1998)
Philip (1998)
Smith et al. (1999)
Selker et al. (1999a)
Corradini et al. (2000)
Swartzendruber (2000)
Govindaraju et al. (2001)
Serrano (2001)
Corradini et al. (2002)
Elrick et al. (2002)
Parlange et al. (2002)
Warrick et al. (2005)
Weiler (2005)
Govindaraju et al. (2006)
Morbidelli et al. (2006)
Chen and Young (2006)
Germann et al. (2007)
Valiantzas (2010)
Corradini et al. (2011)
Swamee et al. (2012)
Govindaraju et al. (2012)
Ali et al. (2013)
Almedeij and Esen (2014)
Lassabatere et al. (2014)
Vatankhah (2015)
Nie et al. (2017)
Selker and Assouline (2017)
Rahmati et al. (2019)
Stewart (2019)
Baiamonte (2020)
Poulovassilis and Argyrokastritis (2020)
Abou Najm et al. (2021)
2D/3D Infiltra-tion Models
Philip (1968)
Wooding (1968)
Philip (1969a)
Parlange (1971c)
Philip (1971)
Parlange (1972a)
Parlange (1972b)
Philip (1972)
Batu (1978)
Scotter et al. (1982)
Fok et al. (1982)
Reynolds et al. (1983)
Fok and Chiang (1984)
Philip (1984a)
Philip (1984b)
Reynolds et al. (1985)
Waechter and Philip (1985)
Philip (1986b)
Reynolds and Elrick (1990)
Ankeny et al. (1991)
White et al. (1992)
Fonteh and Podmore (1993)
Mandal and Waechter (1994)
Basha (1994)
Smettem et al. (1994)
Haverkamp et al. (1994)
Wu and Pan (1997)
Wu et al. (1999)
Lassabatere et al. (2006)
Warrick and Lazarovitch (2007)
Warrick et al. (2007)
Bautista et al. (2014)
Lassabatere et al. (2014)
Bautista et al. (2016)
Stewart and Abou Najm (2018)
Abou Najm et al. (2021)
Di Prima et al. (2021)

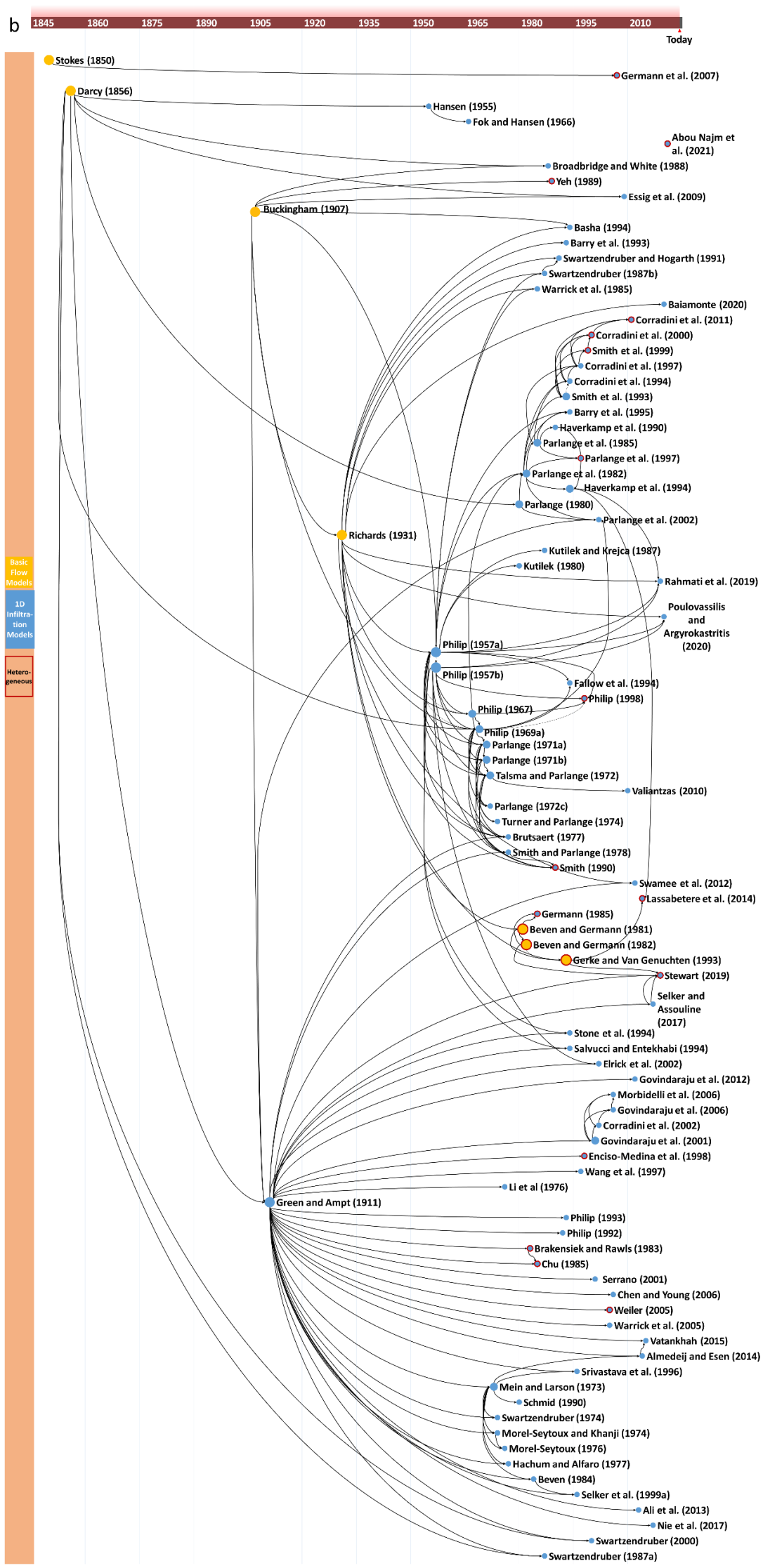

Figure 2.3: Schematic overview of (a) the historical evolution of infiltration theory from basic flow models to 1D and 3D infiltration models, and (b) the evolution of knowledge from earlier theories into the most recent infiltration models. Red symbols refer to infiltration models characterizing heterogenous pore domains.

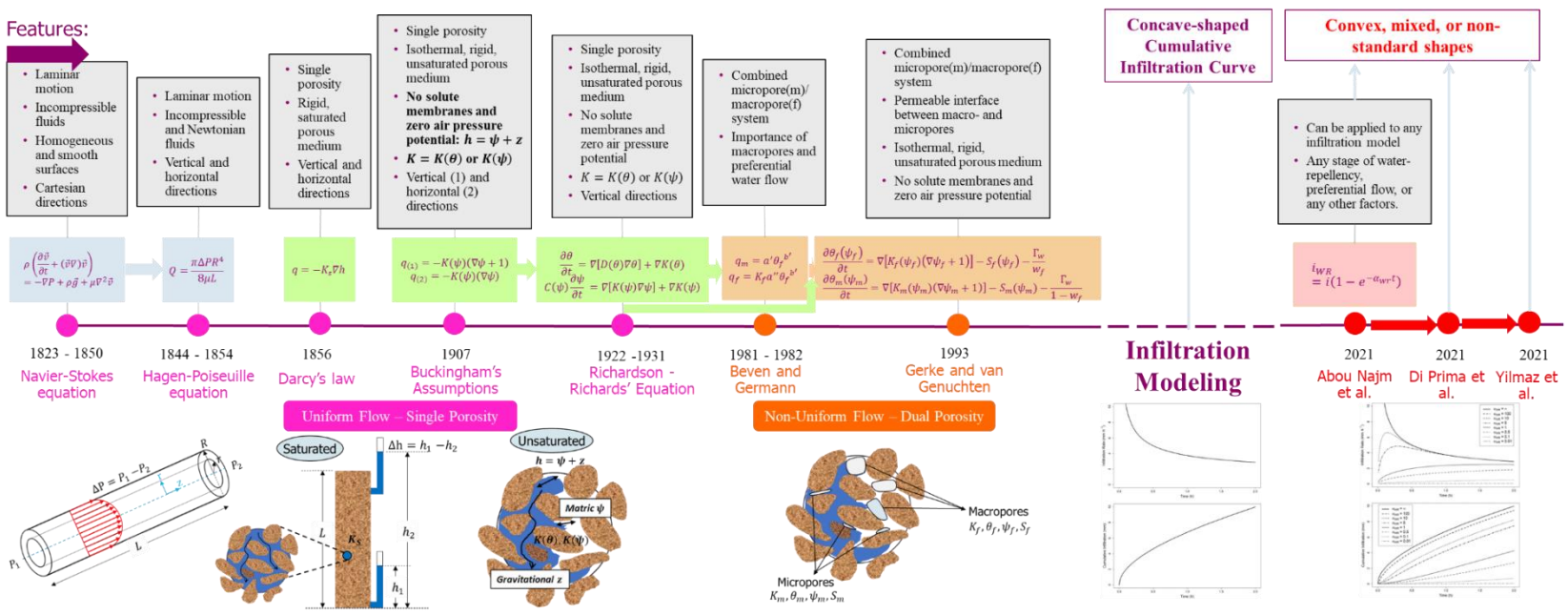

Figure 2.4: All infiltration models are based on the basic physical flow models and mimic the concave shape infiltration curve, except for Abou Najm et al. (2021), Di Prima et al. (2021), and Yilmaz et al. (2021) who captured the multi-shaped cumulative infiltration curve behavior in water-repellent soils

Figure 2.5, which illustrates arc diagrams tracing the evolution of model advancements using the citations within the manuscripts in Table 2.1, further showed how conceptual models are interrelated and how newer models built on the foundations of previous models, particularly Darcy, Buckingham, Richardson-Richards and Green & Ampt (GA). However, we noticed that starting around 1990 the citations of these classic works began to decrease. Instead, new models started to build on one another, citing only earlier works that are one or two steps away, but not many of those models compiled the entire chain of references to the original or fundamental source. This is evidenced by the fact that the blue arc/links should have been denser on the left side; instead, Figure 2.5 demonstrates the relatively small number of citations that the original flow papers received (for example, Darcy or Buckingham), with the interesting exception of the GA model.

Therefore, literature has tended to treat earlier classic models like Darcy and Richardson-Richards as accepted laws rather than fundamental studies to be cited. Another way to interpret this result is that the origins of many infiltration models became obscured and overlooked as model variations proliferated. To this end, Figure 2.5 clearly provides alarming evidence, not only for the observation that papers Darcy and Richardson-Richards are no longer cited regularly (of course we believe they should), but for what this can imply, which is a general belief, that flow theory in porous media is resolved and related macroscopic laws are utterly determined, and that the challenges are more on the application and mathematical interpretation of current theories.

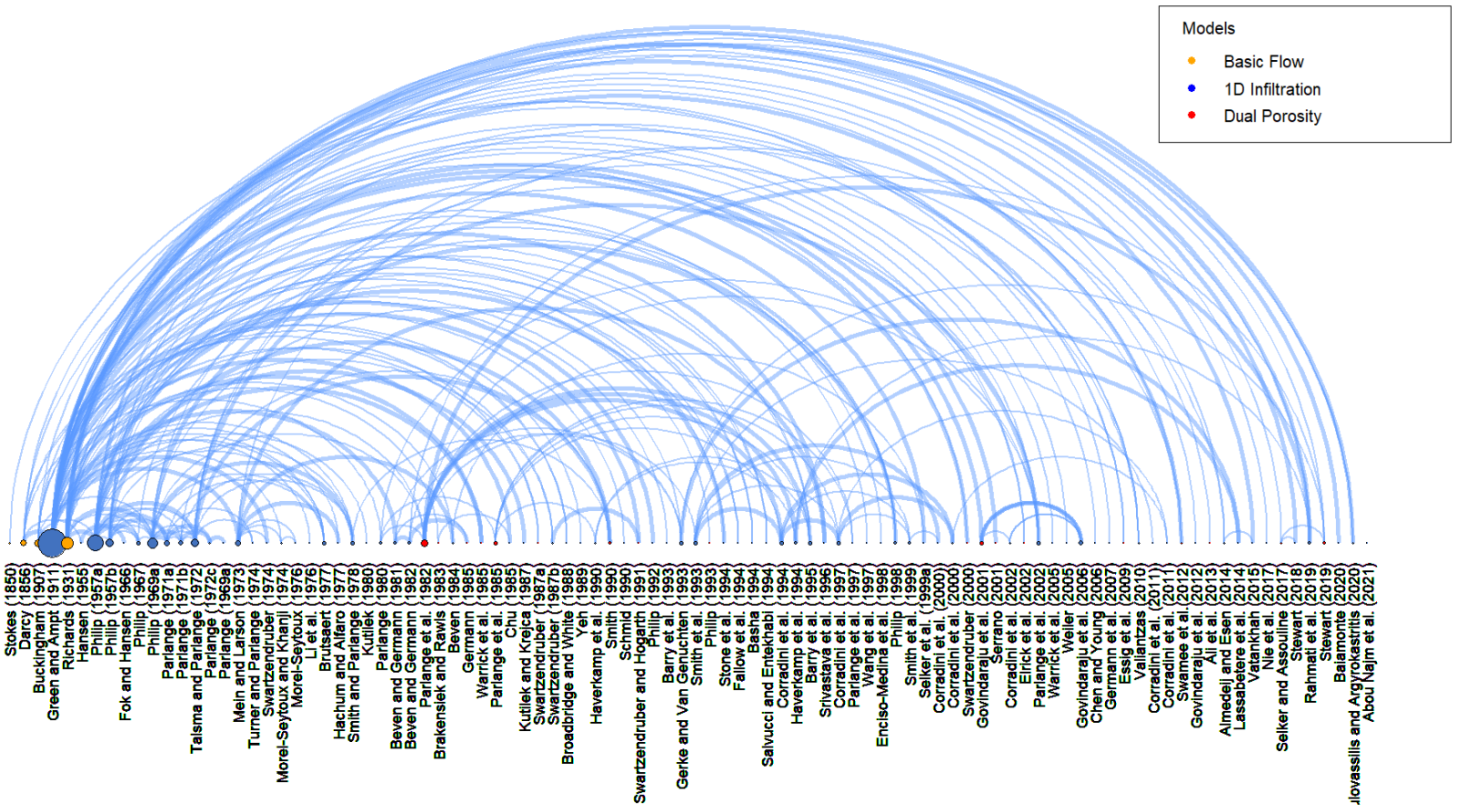

Figure 2.5: Arc diagrams constituted by nodes that represent the conceptual infiltration models displayed as nodes along a single axis in an ascending historical order, and links that show connections between those models. Each node was assigned a size weight based on how many links (N) connect the represented model with the other nodes along each diagram. The diagram connects the represented models to their target sources cited in the corresponding papers.

To demonstrate this issue further, we built Table 2.2 that gathers some data from a literature search carried out in Google Scholar and Scopus. The first two columns in Table 2.2 represent the actual number of citations to the papers that we considered (Column 1), whereas the last two columns refer to the number of mentions of those references in papers (with or without citations). Table 2.2 shows how the literature refers to Darcy and Richards' work using key terms such as law, model, equation, or theory and in many instances not citing them. For example, Darcy (1856) was cited 8,067 times, but the terms Darcy law or Darcy model or Darcy equation were mentioned a total of 21,381 times in the literature. We noticed that the keyword "law" is used more commonly to represent Darcy, while the keyword "equation" generally represents Richards. On the other hand, soil water characteristic models, which are required to model infiltration processes under the Darcy-BRR paradigm, gained wide adoption. For example, Table 2.2 shows the citation impact of the van Genuchten model, which had 32,113 citations or nearly four times as many citations than either Darcy (1856) and Richards (1931). This result suggests that the van Genuchten (1980) model was published recently enough in the literature to continue being cited as a primary source.

Therefore, our analysis raises the question of the reliability and validity of citations as quality indicators in infiltration research. We conclude that assessment of infiltration theory in literature based on citations does not often reflect its impact and relevance for the new concepts being addressed.

*Table 2.2: Citation analysis involving Darcy, Richards, and van Genuchten theories (the asterisk * is used as a trick for a better Scopus search – can search for the alternative spellings of the same word)*

Cited theory (references list)	**Number of Records by Google Scholar [Scopus]** *(on September 26th, 2023)*	**Theory mentioned in text**	**Number of Records by Scopus** *(on September 26th, 2023)*
Darcy (1856)	8,067 [ND]	"Darcy* law" OR "Darcy* model*" OR "Darcy* equation"	**21,381**
		a) "Darcy* law"	16,131
		b) "Darcy* model*"	3,603
		c) "Darcy* equation"	3,209
Richards (1931)	7,936 [4,484]	"Richard* model*" OR "Richard* equation*"	**8,763**
		a) "Richard* model*"	2,295
		b) "Richard* equation*"	6,584
van Genuchten (1980)	32,113 [19,904]	"van Genuchten model*" OR "van Genuchten equation" OR "van Genuchten parameter*"	**2,068**

2.10. Model parameterization

2.10.1. Evolution of the infiltration parameters

2.10.1.1. Hydraulic conductivity K

Saturated hydraulic conductivity, K_s (LT^{-1}), was originally defined by Darcy (1856) as a measure of the water infiltration through the soil porous medium, and later described as function of permeability k (L^2), density, ρ (ML^{-3}), and kinematic viscosity, η ($ML^{-1}T^{-1}$), of a fluid through an empirical equation developed by Kozeny (1927):

$$K_s = k\left(\frac{\rho g}{\eta}\right) \quad [2.23]$$

Unsaturated hydraulic conductivity, K (LT^{-1}), was introduced by Buckingham (1907), symbolized by $K(\theta)$ (LT^{-1}) as a function of the water content θ (L^3L^{-3}), and by $K(\psi)$ as function of the matric potential ψ (L). Accordingly, Wind (1955) proposed an empirical equation relating $K(\psi)$ (LT^{-1}) to the matric potential ψ (L) as follows:

$$K(\psi) = b^*\psi^{-a^*} \quad [2.24]$$

where: b^* (L^2T^{-1}) and a^* (dimensionless) are empirical parameters.

Although there exist numerous models in the literature, we only summarize several empirical and/or theoretical equations developed to illustrate the relationship between the unsaturated ($K(\theta)$ or $K(\psi)$) and the saturated (K_s) hydraulic conductivities, as summarized in **Error! Reference source not found.**.3.

Table 2.3: Empirical equations for the unsaturated hydraulic conductivities $K(\theta)$ and $K(\psi)$

Equation	Reference
Unsaturated hydraulic conductivity $K(\theta)$ or $K(S_e)$	
$K(\theta) = K_s {S_e}^n \quad \theta < \theta_s$ $K(\theta) = K_s \quad \theta = \theta_s$	Brooks and Corey (1964)
$K(\theta) = K_s e^{(\theta - \theta_s)}$	Davidson et al. (1969)
$K(\theta) = K_s \left(\frac{\theta}{\theta_s}\right)^n$	Campbell (1974)
$K(\theta) = K_s {S_e}^{0.5} \left[\int_0^{S_e} \frac{dS_e}{\psi} / \int_0^1 \frac{dS_e}{\psi}\right]^2$	Mualem (1976)
$K(\theta) = K_s {S_e}^2 \left[\int_0^{S_e} \frac{dS_e}{\psi^2} / \int_0^1 \frac{dS_e}{\psi^2}\right]^2$	Burdine (1953)
$K(\theta) = K_s {S_e}^{0.5} \left[1 - \left(1 - {S_e}^{1/m_{ssc}}\right)^{m_{ssc}}\right]^2$	Mualem's model applied on van Genuchten (1980) model for water retention curve (WRC)
$K(\theta) = K_s e^{\beta_l(\theta - \theta_s)}$	Libardi et al. (1980)
$K(\theta) = K_s \left(\frac{S_e}{S_{e_o}}\right)^{0.5} \left[\frac{1-\left(1-{S_e}^{1/m_{ssc}}\right)^{m_{ssc}}}{1-\left(1-{S_{e_o}}^{1/m_{ssc}}\right)^{m_{ssc}}}\right]^2$	van Genuchten et al. (1991)
$K(\theta) = K_s e^{-a_{sn}(\theta_s - \theta)^{b_{sn}}}$	Setiawan and Nakano (1993)
$K(\theta) = K_s {S_e}^{\alpha_k} \left\{\frac{1}{2} erfc\left[erfc^{-1}(2S_e) + \frac{\beta_k \sigma_k}{\sqrt{2}}\right]\right\}^{\gamma_k}$	Kosugi (1999)
$K(\theta) = K_s \left[\frac{\frac{\beta_g}{\phi} - 1 + \theta - \theta_c}{\frac{\beta_g}{\phi} - \theta_c}\right]^{\frac{\lambda_g}{3-D_g}} \quad \theta_x \leq \theta < \phi$ $K(\theta) = K_s \left[\frac{\frac{\beta_g}{\phi} - 1 + \theta_x - \theta_c}{\frac{\beta_g}{\phi} - \theta_c}\right]^{\frac{\lambda_g}{3-D_g}} \left(\frac{\theta - \theta_c}{\theta_x - \theta_c}\right)^2 \quad \theta_c \leq \theta < \theta_x$	Ghanbarian et al. (2016)
Unsaturated hydraulic conductivity $K(\psi)$	
$K(\psi) = K_s {S_e}^{3.5}$	Averjanov (1950)
$K(\psi) = K_s e^{\alpha\psi}$	Gardner (1958)
$K(\psi) = K_s e^{\alpha(\psi - \psi_{str})} \quad \psi < 0$ $K(\psi) = K_s \quad \psi \geq 0$	Rijtema (1965)
$K(\psi) = K_s \left\{\frac{1}{2} erfc\left[\frac{\ln(\psi/\beta_k) - {\gamma_k}^2}{\gamma_k\sqrt{2}}\right]\right\}^{\gamma_k} \left\{\frac{1}{2} erfc\left[\frac{\ln(\psi/\beta_k)}{\gamma_k\sqrt{2}}\right]\right\}^2$	Das and Kluitenberg (1995)
$S_e = \frac{\theta - \theta_r}{\theta_s - \theta_r}$; $S_{e_o} = \frac{\theta_o - \theta_r}{\theta_s - \theta_r}$ θ_o, θ_r, θ_s, θ_c and θ_x are arbitrary, residual, saturated, critical and the crossover water content at which fractal scaling from critical path analysis switches to universal percolation scaling from percolation theory, respectively. ψ_{str} (L) is the suction at the air-entry point. All other model parameters are fitted parameters.	

Using the exponential equation developed by Gardner (1958) in **Error! Reference source not found.**.3, Raats (1971) defined the saturated hydraulic conductivity K_s (LT^{-1}), in terms of the matric flux potential, φ (L^2T^{-1}), as:

$$K_s = \frac{\alpha\varphi}{1-e^{\alpha\psi_i}} \quad [2.25]$$

Considering that the matrix flux potential is defined by:

$$\varphi = \int_{h_i}^{0} K(h)\, dh \quad [2.26]$$

A well-known equation for estimating K_s (LT^{-1}) was derived from Equation 2.25 for soils initially at "field capacity" or drier (Raats 1971; Scotter et al., 1982; Reynolds et al., 1985; Yeh, 1989; Ankeny et al., 1991; Wu and Pan, 1997; Stewart and Abou Najm, 2018):

$$K_s = \alpha^{*}\varphi \quad [2.27]$$

Although the hydraulic conductivity improved our understanding of infiltration problem, researchers realized that solving this problem was still so far from complete. Thus, they recognized the need of an additional soil property that can improve the estimation of water infiltration. This major characteristic is the soil sorptivity, symbolized by S (LT^{-1}), that describes the water absorption by capillarity.

2.10.1.2. Sorptivity S

Philip (1957b) introduced the sorptivity S_0 ($LT^{-0.5}$), as the first term in his two-term equation of cumulative, one-dimensional, unsaturated infiltration I (L) with negative or zero head surface boundary condition ($h_0 \leq 0$ and $\theta_o \leq \theta_s$):

$$I = S_0 t^{0.5} + At \quad [2.28]$$

After he introduced the term sorptivity in 1957, Philip undertook a series of successive events to entrench soil sorptivity into literature. In 1969, he first developed an analytical equation describing sorptivity, S_0 ($LT^{-0.5}$), for an unsaturated soil with a constant diffusivity D (L^2T^{-1}) independent of θ (L^3L^{-3}):

$$S_0 = 2(\theta_o - \theta_i)\left(\frac{D}{\pi}\right)^{0.5} \quad [2.29]$$

Then, in 1973, he introduced the concept of flux concentration function $F(\theta)$ to describe the water absorption by capillary. He defined this concept as the ratio of water flux at any location in the profile $i(t) - K_i$, to the infiltration rate at surface, $i_0(t) - K_i$, where K_i (LT^{-1}) is the initial hydraulic conductivity. In 1974, Philip and Knight further used this concept to estimate the sorptivity S_0 ($LT^{-0.5}$):

$$S_0^2 = 2\int_{\theta_i}^{\theta_0} \frac{[\theta-\theta_i]D(\theta)}{F(\theta)} d\theta \quad [2.30]$$

where θ_i and θ_o (L^3L^{-3}) are the initial ($t = 0$) and specific ($t > 0$) water contents, respectively. Many estimates for sorptivity S_0 ($LT^{-0.5}$) have relied on the use of the flux concentration function $F(\theta)$ as shown in Table 2.4.

Table 2.4: Main approximations of the flux concentration function $F(\theta)$ and sorptivity S_0^2 (L^2T^{-1}) (Angulo-Jaramillo et al., 2016)

$F(\theta)$	S_0^2 (L^2T^{-1})	Reference
$\frac{\theta - \theta_i}{\theta_o - \theta_i}$	$2(\theta_o - \theta_i)\int_{\theta_i}^{\theta_0} D(\theta)d\theta$	Philip and Knight (1974)
$\frac{2(\theta - \theta_i)}{\theta_o + \theta - 2\theta_i}$	$\int_{\theta_i}^{\theta_0} (\theta_o + \theta - 2\theta_i)D(\theta)d\theta$	Parlange (1975)
$\left(\frac{\theta - \theta_i}{\theta_o - \theta_i}\right)^{0.5}$	$2(\theta_o - \theta_i)^{0.5}\int_{\theta_i}^{\theta_0} (\theta - \theta_i)^{0.5}D(\theta)d\theta$	Brutsaert (1976)
$exp\left\{-\left[inverfc\left(\frac{\theta - \theta_i}{\theta_o - \theta_i}\right)\right]^2\right\}$	$2D\int_{\theta_i}^{\theta_0} \frac{\theta - \theta_i}{exp\left\{-\left[inverfc\left(\frac{\theta - \theta_i}{\theta_o - \theta_i}\right)\right]^2\right\}} d\theta$	Crank (1979)

Another approximation for sorptivity, S_0 ($LT^{-0.5}$), was derived by equating the Green-Ampt equation (considering a surface pressure of zero i.e., $h_0 = 0$) to Philip's two-term infiltration equation (Collis-George, 1977):

$$S_0^2 = 2\psi_{wf}(\theta_o - \theta_i)K_s \quad [2.31]$$

Where ψ_{wf} (L) is the wetting front potential.

Later, Philip (1985) introduced the macroscopic capillary length, λ_c (L), typically equivalent to the wetting front potential, ψ_{wf} (L) as:

$$\lambda_c = \frac{1}{K_o - K_i}\int_{\theta_i}^{\theta_o} D(\theta)d\theta \quad [2.32]$$

Based on Philip's definition of λ_c,White and Sully (1987) reformulated the sorptivity, S_0 ($LT^{-0.5}$), by substituting Equation 2.29 into 2.32, with $F = 0$ for $\theta = \theta_i$ and $F = 1$ for $\theta = \theta_o$:

$$S_0^2 = \frac{\lambda_c(K_o - K_i)(\theta_o - \theta_i)}{b} \quad [2.33]$$

where: b is a dimensionless constant. White and Sully (1987) showed that $b = 0.5$ exactly for soils exhibiting a step-function infiltration front (Philip and Knight, 1974) and $b = \pi/4$ if soil diffusivity $D(\theta)$ is constant (Philip, 1969a). For general field soils, White and Sully (1987) suggested $b = 0.55$, since the actual infiltration fronts does not tend to be as sharp as a step function.

Using the matric flux potential term, φ (L^2T^{-1}), Reynolds and Elrick (1990) redefined the sorptivity S_0 ($LT^{-0.5}$) as:

$$S_0^2 = \frac{\varphi(\theta_o - \theta_i)}{b} \quad [2.34]$$

Now for the case of ponded head infiltration ($h_0 \geq 0$ and $\theta_o = \theta_s$), the sorptivity, here defined as S_H ($LT^{-0.5}$), was related to S_0 ($LT^{-0.5}$) (White and Sully, 1987, Haverkamp et al., 1990) by:

$$S_H^2 = S_0^2 + 2h_0K_s(\theta_s - \theta_i) \quad [2.35]$$

The Reynolds and Elrick (1990) expression in Equation 2.34 can also be applied to Equation 2.35 to define the sorptivity S_H ($LT^{-0.5}$) as:

$$S_H^2 = (\theta_s - \theta_i)(\frac{\varphi}{b} + h_0K_s) \quad [2.36]$$

Recently, Lassabatere et al. (2021) proposed a specific scaling procedure to simplify the computation of sorptivity. In addition, the same authors proposed a specific mixed formulation to ease the numerical computation of sorptivity, when the final state corresponds to water ponding and for very low initial water contents (Lassabatere et al., 2023). These authors demonstrated that the saturated part of sorptivity, $2h_0K_s(\theta_s - \theta_i)$ must not be forgotten and its omission may lead to erroneous modeling of water infiltration.

2.10.2. Methods and challenges behind K and S estimation in literature

There are many techniques to measure infiltration in the laboratory and in the field. Starting with characterization of the $K(\theta)$ or $K(\psi)$ functions, the commonly used methods are the instantaneous profile (Watson., 1966) and the plane of zero flux (Arya et al., 1975) methods. These methods are further divided between direct approaches, in which both θ (L^3L^{-3}) and ψ (L) are measured within the soil profile, and indirect approaches, in which one variable is measured while estimating the other variable is determined from a separate water retention curve $\theta(\psi)$. In principle, these methods are simple; however, complications often arise in practice leading to complex and time-consuming measurements. To simplify the field determination of $K(\theta)$ and $K(\psi)$ and therefore the extensive labor requirements, these two functions can be determined using the empirical equations illustrated in **Error! Reference source not found.**.3 once the water retention curve $\theta(\psi)$ is determined (Libardi et al., 1980; Zachmann et al., 1981; Dane and Hruska, 1983). However, this

simplification can show a disagreement between the $\theta(\psi)$ curves as determined in-situ and on undisturbed core samples – a common disadvantage among all described methods. In addition, applying the widely used equations of $K(\theta)$ and $K(\psi)$ (Table 2.3) involves the determination of the saturated hydraulic conductivity K_s (LT^{-1}), which gives rise to more efforts and challenges knowing the soil heterogeneity (Fodor et al., 2011), the spatial and seasonal variability of K_s (LT^{-1}) (Farkas et al., 2006; Gülser et al. 2016), as well as its scale dependency (Lai and Ren, 2007).

To determine the saturated hydraulic conductivity K_s (LT^{-1}) as well as soil sorptivity S_0 or S_H ($LT^{-0.5}$), (noted hereafter as $S_{0/H}$), different experimental tools were designed to measure one- or multi-dimensional flow that can include early, transient, and steady-state flow stages depending on the approach being applied. Starting with single and double ring-infiltrometers, these tools were built to determine the saturated hydraulic conductivity either under constant- (Schiff, 1953; Parr and Bertrand, 1960; Olson, 1960; Touma et al., 2007; Xu et al., 2012; Di Prima et al., 2016; Ronnqvist, 2018) or falling-head conditions (Elrick et al., 1995; Angulo-Jaramillo et al., 2003, Bagarello et al., 2004). In a series of papers, Bouwer (1960, 1963, 1986) introduced a simple field measurement cylinder which can be used to determine the two parameters, saturated hydraulic conductivity, K_s (LT^{-1}), and wetting front potential, ψ_{wf} (L), required to apply the Green-Ampt approach. Bouwer's cylinder infiltrometer is discussed in detail in Selker's vadose zone book (Selker et al., 1999). Moving to the disc infiltrometer developed by Perroux and White (1988), referred to also as a tension infiltrometer (Watson and Luxmoore, 1986), this tool involved supplying water to the soil surface under controlled suction (Smettem and Clothier 1989; Zhang 1997; Latorre et al., 2015). These techniques are all non-destructive and allow rapid flow measurements if steady flow can be quickly achieved depending on the ring size, soil texture, and soil structure. However, while driving discs, rings and cylinders into the soil, some disturbance, such as compaction, fracturing

or smearing, almost inevitably occurs (Bouma and Dekker 1981). In addition to soil disturbance, the large spatial variability of K_s (LT^{-1}) and $S_{0/H}$ ($LT^{-0.5}$) can affect the precision and accuracy of the measured parameters (Sharma et al., 1980; Logsdon and Jaynes, 1996). To overcome the challenges of soil heterogeneity and spatial variability of K_s (LT^{-1}), the rainfall simulator can be used as an alternative experimental tool (Bradford et al., 1987; Lassu et al. 2015; Di Prima et al., 2018). However, infiltrometers are still the most widely used devices for measuring field infiltration rates due to their simple application in the field (Rahmati et al., 2018). However, more complex parameter estimation models need to be developed to consider soil behavior such as swelling (Gérard-Marchant et al., 1997). Indeed, failure to take deviant behavior into account can lead to an underestimation, or even unrealistic values, of both sorptivity and hydraulic conductivity.

Different infiltration models are employed to determine K_s (LT^{-1}) and $S_{0/H}$ ($LT^{-0.5}$), from the multi-dimensional infiltration measured using ring, cylinder, and disc infiltrometers. Among these models, numerous conceptual equations relate the one-dimensional cumulative infiltration I_{1D} (L) to both parameters, K_s (LT^{-1}) and either S_0 ($LT^{-0.5}$) (Philip, 1957b, 1969a; Talsma and Parlange, 1972; Barry et al., 1993) or S_H ($LT^{-0.5}$) (Smith and Parlange, 1978; Parlange 1980; Barry et al., 1993; Swartzendruber, 2000; Valiantzas, 2010). These relationships reveal the relevance and applicability of estimating these two properties by fitting analytical equations numerically to infiltration data. In this context, the two-term equation derived by Philip (1957b) has been extensively used to determine K_s (LT^{-1}) and S_0 ($LT^{-0.5}$) due to its explicit numerical application (Equation 2.28). In one application, S_0 ($LT^{-0.5}$) is estimated by plotting I_{1D} (L), measured into a uniform unsaturated soil profile, against $t^{0.5}$ ($T^{0.5}$) during the very early stage of infiltration. The slope of the linear relationship (I_{1D} vs. $t^{0.5}$) allows the determination of S_0 ($LT^{-0.5}$). A (LT^{-1}), on

the other hand, can be estimated by plotting I_{1D} (L) against t (T) for larger times of infiltration. The slope of the linear relationship (I_{1D} vs. t) allows the determination of A (LT^{-1}), which is further used to estimate the saturated hydraulic conductivity K_s (LT^{-1}). Specifically, $A = mK_s$ with $1/3 \leq m \leq 2/3$ (Youngs, 1968; Philip, 1969a; Talsma, 1969, Talsma and Parlange, 1972). A value of $m = 0.363$ may be appropriate for soils with a relatively low initial water content (Philip, 1987), while a value of $m = 2/3$ is often used (Whisler and Bouwer, 1970, Fodor et al., 2011). In some studies, $m = 1$ and hence $A = K_s$ (Davidoff and Selim, 1986, Swartzendruber and Young, 1974, Ghorbani et al., 2009). It is crucial noting that Philip's equation is no longer valid for very large times reaching the steady state and should be restricted to the modeling of the transient state (Philip, 1957b).

A second set of models, based on three-parameter equations, are also fitted to infiltration data measured at any given time. In addition to K_s (LT^{-1}) and $S_{0/H}$ ($LT^{-0.5}$), each of these equations depend on a dimensionless constant symbolized by β_0 (Brutsaert, 1977), A_0 ($T^{-0.5}$) (Swartzendruber, 1987b; Swartzendruber and Hogarth, 1991), δ (Parlange et al., 1982, 1985, 2002; Haverkamp et al., 1990) or β (Haverkamp et al., 1994) that also needs to be estimated failing to be able to be calculated simply analytically. Brutsaert (1977) recommended the value $\beta_0 = 2/3$ for practical applications. Swartzendruber (1987b) showed that A_0 ($T^{-0.5}$) can be equal to $\frac{4K_s}{3S_H}$. Parlange et al. (1982, 1985) defined $\delta = \frac{1}{(\theta_s - \theta_i)(K_s - K_i)} \int_{\theta_i}^{\theta_s} (K_s - K) d\theta$ where K_i (LT^{-1}) is the initial soil hydraulic conductivity; δ can take values from 0 to 1, with an approximate used value of 0.8 or 0.85. Haverkamp et al. (1994) further replaced δ by a new dimensionless constant, β, which varies from 0.3 (sand) to 1.7 (silt), with an average value of 0.6 according to Lassabatere et

al. (2009) who fitted the analytical model to analytically generated data to quantify the best values of constants β and γ.

A third set of 1D infiltration equations, based on the approach of Green and Ampt (1911), also leads to the estimation of K_s (LT^{-1}) and $S_{0/H}$ ($LT^{-0.5}$) under constant- (Li et al., 1976; Salvucci and Entekhabi, 1994; Stone et al., 1994; Swamee et al., 2012; Almedeij and Esen, 2014; Vatankhah, 2015; Selker and Assouline, 2017) or falling-head ponding conditions (Philip 1992; Elrick et al., 2002). By fitting the equations to one-dimensional infiltration data, we can estimate the parameters, K_s (LT^{-1}) and wetting front potential, ψ_{wf} (L). Then, the parameter S_H ($LT^{-0.5}$) can be deduced from Equation 2.36, with h_0 (L), θ_s and θ_i (L^3L^{-3}) measured directly from the field.

In addition, the quasilinear analysis of steady state infiltration, Q_{inf} (L^3T^{-1}), using the 3D infiltration equations (Wooding, 1968; Scotter et al., 1982; Reynolds et al., 1983, 1985; Reynolds and Elrick, 1990; Ankeny et al., 1991) allows the determination of parameters K_s (LT^{-1}) and φ (L^2T), and thus leads to the estimation of S_0 ($LT^{-0.5}$) from Equation 2.34 or S_H ($LT^{-0.5}$) from Equation 2.35 or 2.36. Haverkamp et al. (1994) proposed an implicit formulation for the 1D infiltration model (Equation 2.37a) and Smettem et al. (1994) extended it to define the 3D cumulative infiltration, I_{3D} (L), from a surface disk infiltrometer, adding the term γ (average value $\gamma = 0.75$) to represent 3D geometrical effects as (Equation 2.37b):

$$\frac{2\,\Delta K^2}{S^2}\,t = \frac{1}{1-\beta}\frac{2\,\Delta K}{S^2}\left(I(t) - K_i\mathrm{t}\right) - \frac{1}{1-\beta}\,ln\left(\frac{exp\left(\frac{2\beta\,\Delta K}{S^2}\left(I(t)-K_i\mathrm{t}\right)\right)+\beta-1}{\beta}\right) \qquad [2.37a]$$

$$I_{3D} = I_{1D} + \frac{\gamma {S_0}^2 t}{r(\theta_s-\theta_i)} \qquad [2.37b]$$

Where $\Delta K = (K_s - K_i)$, r(L) stands for the disc radius. Equation (2.37a) defines an implicit formulation that does not ease the computation of the cumulative infiltration. Consequently, Haverkamp et al. (1994) have proposed two simplified expansions that are valid at transient and steady state, respectively (Haverkamp et al., 1994; Lassabatere et al., 2006):

$$I_{3D} = S_0 t^{0.5} + \left(\frac{2-\beta}{3}(K_s - K_i) + K_i + \frac{\gamma {S_0}^2}{r(\theta_s - \theta_i)}\right) t \quad [38]$$

$$I_{3D} = \left(K_s + \frac{\gamma {S_0}^2}{r(\theta_s - \theta_i)}\right) t + \frac{1}{2(1-\beta)} ln\left(\frac{1}{\beta}\right) \frac{{S_0}^2}{K_s - K_i} \quad [38]$$

Note that more precise approximate expansions may be defined for the transient state according to the number of terms considered (Lassabatere et al., 2009, Appendix 2.11).

Based on Haverkamp et al. approach (1994), BEST methods were designed to estimate the whole set of unsaturated hydraulic parameters, offering a complete hydraulic characterization of soils. The BEST-Slope method was pioneered by Lassabatere et al. (2006) and was followed by BEST-Intercept (Yilmaz et al., 2010) and BEST-Steady methods (Bagarello et al., 2014). The three methods consider the same hydraulic function for defining water retention and hydraulic conductivity functions, with the use of van Genuchten (1980) model along with the Burdine condition and Brook and Corey (1964) model for describing the hydraulic conductivity. The three methods consider the same pedo-transfer functions to relate soil texture (i.e., particle size distribution) to hydraulic shape parameters, but differ in the use of experimental infiltration data to estimate the scale hydraulic parameters. The infiltration data is obtained by a Beerkan infiltration run which consists of water infiltrating through a single ring under ponded conditions (Braud et al., 2005; Aiello et al., 2014; Di Prima et al., 2016, 2018; 2020; Lassabatere et al., 2019a)

BEST-Slope and BEST-Intercept use the last/steady part of the cumulative infiltration to fit the asymptotic model (Equation 2.39) to estimate either the slope $a = K_s + \frac{\gamma {S_0}^2}{r(\theta_s - \theta_i)}$ or the intercept $b = \frac{1}{2(1-\beta)} ln\left(\frac{1}{\beta}\right) \frac{{S_0}^2}{K_s - K_i}$ relating the hydraulic conductivity and the sorptivity. The two methods reduce the number of unknowns from two (K_s, S_0) to one (S_0), which strengthens the robustness of the inversion. Then, the two methods fit the two-term equation (Equation 2.38) to the first part of the cumulative infiltration (transient part) to derive the value of sorptivity S_0 ($LT^{-0.5}$). The part of the curves assigned to the transient state is defined by a specific iterative procedure that defines a validity time as a function of the estimated values of (K_s, S_0). BEST-Steady only considers the steady-state part and fits the asymptotic model (Equation 2.39) to the steady part of the cumulative infiltration data. The estimation of the intercept and of the slope leads to a system with two equations and two unknowns, leading to simultaneous estimations of the couple (K_s, S_0). Lastly, the scale parameter is estimated from the knowledge of sorptivity and saturated hydraulic conductivity (Lassabatere et al., 2006, Eq. 8).

Bagarello et al. (2013, 2014, 2017) used these explicit expansions to propose two simplified versions of the BEST methods, Transient (TSBI) and Steady (SSBI), to determine K_s (LT^{-1}) of an initially rather nonconductive soil ($K_i = 0$). The TSBI method (Bagarello et al., 2013, 2014) is based on the explicit transient relationship (Equation 2.38) which, divided by $t^{0.5}$, results in a linear relationship between $I_{3D}/t^{0.5}$ and $t^{0.5}$ with slope b_1 (LT^{-1}), defined by:

$$b_1 = \frac{\gamma {S_0}^2}{r(\theta_s - \theta_i)} + \frac{2-\beta}{3} K_s \qquad [2.40]$$

The slope b_1 (LT^{-1}) can be estimated by a linear regression analysis of the ($I_{3D}/t^{0.5}$, $t^{0.5}$) data collected during the transient phase of the infiltration run. The intercept of the regression line ($I_{3D}/t^{0.5}$, $t^{0.5}$) indicates the sorptivity S_0 ($LT^{-0.5}$). Then, solving for K_s (LT^{-1}) gives:

$$K_s = \frac{b_1}{\frac{b\gamma}{r\alpha}+\frac{2-\beta}{3}} \quad [2.41a]$$

$$K_s = \frac{b_1}{\frac{\gamma\gamma_w}{r\alpha^*}+\frac{2-\beta}{3}} \quad [2.41b]$$

where γ_w is a dimensionless constant (White and Sully, 1987) related to the shape of the wetting (or drainage) front and α^*(L^{-1}) corresponds to the ratio between the matrix flux potential and the saturated hydraulic conductivity, $\alpha^* = \frac{K_s}{\varphi}$ (Bagarello et al., 2017). Note that the two methods SSBI and TSBI make use of the relation between sorptivity and hydraulic conductivity $S_0^2 = \gamma_w\,(\theta_s - \theta_i)\,\varphi$ (Bagarello et al., 2017).

The SSBI method, on the other hand, is based on the explicit steady-state expansion (Equation 2.39). The slope, b_2 (LT^{-1}), of the linear relationship between I_{3D} (L) and t (T) collected during the steady-state phase of the infiltration run is defined as:

$$b_2 = K_s + \frac{\gamma {S_0}^2}{r(\theta_s-\theta_i)} \quad [2.42]$$

Solving for K_s gives:

$$K_s = \frac{b_2}{\frac{b\gamma}{r\alpha}+1} \quad [2.43a]$$

$$K_s = \frac{b_2}{\frac{\gamma\gamma_w}{r\alpha^*}+1} \quad [2.43b]$$

BEST methods have been used for many applications and in many contexts and encountered several difficulties with real soils for some types of situations (water repellency, preferential flows,

and self-sealing soils). Di Prima (2021) recently pioneered a new BEST method dedicated to water-repellent soil. Yilmaz et al. (2023) proposed an improvement of the same method by developing a three-term expansion to describe the transient state. Regarding preferential flows, Lassabatere et al. (2019b) developed BEST-2K for the hydraulic characterization of dual-permeability soils. This version allows the characterization of the soil as the combination of matrix and fast-flow regions, with the complete characterization of the unsaturated hydraulic parameters of the two regions .

Alternatively, further approaches were developed based on model variations that solve for K_s and include different parameters including Stewart and Abou Najm (2018b), Iovino et al. (2021) and Kargas et al. (2022).

2.11. Conclusion

A substantial challenge researcher encounters when analyzing infiltration data is choosing which model to use, and then which procedures to follow for extracting hydraulic properties. The proliferation of infiltration models has on one hand led to better understanding and quantification of these processes, but on the other hand may be creating confusion regarding the origins, assumptions, and limitations of different approaches. While many reviews have covered different aspects of infiltration processes and modeling, until now there has not been a comprehensive and objective examination of infiltration models in the literature. This gap motivated us to develop a comprehensive literature review that summarizes and organizes the many distinct conceptual and empirical infiltration models that have been developed over the past two centuries. Our literature search has identified 138 unique infiltration models. We categorized them based on characteristics such as conceptual versus empirical equations, application to rigid versus deformable swelling soils, one-dimensional versus multi-dimensional infiltration, unsaturated to completely saturated porous media, and so on. Most of the developed infiltration models clustered theoretically around major milestones that were achieved by six or seven major contributions. Our citation analysis determined that Darcy's law, the Richardson-Richards-Buckingham paradigm and the Green-Ampt models were very common sources for subsequent advancements, while models building on Stokes work and other earlier theories represent potential areas for further investigation and advancement.

We end our critical review by embracing how the evolution of infiltration models has led to incremental advancements along with limited improvements in characterizing the inherent variability of soil systems, preferential flows, water repellency and surface processes. With that being said, we should always aspire to develop practical and adaptive models to characterize the

infiltration behavior by treating all theories with the critical lens of a curious scientist, and step outside the comfort zone secured with some of our basic assumptions, theories, and boundary conditions.

2.12. Appendix

Table 2.5: Summary of model parameters

Symbol	Unit	Description
		Characteristics
A	L^2	Area
$\tilde{A}$	$L^2\ T^{-2}$	Specific Helmholtz free energy
b_R	$L\ T^{-1}$	Conductance of a rivulet (Germann et al., 2007)
C	$M\ L^{-3}$	Concentration
d	L	Depth
D	$L^2\ T^{-1}$	Diffusivity
D_b	Dimensionless	Backbone fractal dimension in three dimensions (Hunt et al., 2014, 2017)
e	$L^3\ L^{-3}$	Void ratio
E	$L^2\ T^{-2}\ T^{o-1}$	Entropy
E	$M\ L^{-1}\ T^{-2}$	Energy
g	$L\ T^{-2}$	Acceleration of gravity
h	L	Total head
i	$L\ T^{-1}$	Infiltration rate
I	L	Cumulative infiltration
$\overline{K}$	$L\ T^{-1}$	Averaged hydraulic conductivity
k_{rc}	Dimensionless	Relative water conductivity accounting for air-confining condition (Wang et al., 1997)
k	L^2	Permeability
K	$L\ T^{-1}$	Hydraulic conductivity
l	L	Thickness
L	L	Length
P	$M\ L^{-1}\ T^{-2}$	Pressure
q	$L\ T^{-1}$	Flux
q_0	$L\ T^{-1}$	Precipitation/rainfall rate
Q_0	$L^3\ T^{-1}$	Volumetric Precipitation/rainfall rate
Q	$L^3\ T^{-1}$	Volumetric flow rate
Q_{inf}	$L^3\ T^{-1}$	Volumetric infiltration rate
r	L	Radius
s	Dimensionless	Slope
s	T^{-1}	Sink-source term
S_0	$L\ T^{-0.5}$	Sorptivity of the soil alone (with $h_0 = 0$)
S_H	$L\ T^{-0.5}$	Sorptivity including the effect of the constant ponded head h_0
S_e	$L^3\ L^{-3}$	Saturation degree
t	T	Time
t_c	T	Critical time between transient and steady-state infiltration
T_c	T	Sorptive time
T_S	T	Duration of rainfall
T	T^o	Temperature
v	$L\ T^{-1}$	Velocity

V	L^3	Volume
$\bar{V}$	Dimensionless	Slope of the shrinkage curve
w	L	Width
w_f	Dimensionless	Ratio of the volume occupied by each fast-flow region to total pore volume (called β in Stewart 2019)
W	L	Perimeter
W^*	L	Adjusted wetted perimeter (Warrick et al., 2007; Bautista et al., 2014, 2016; Liu et al., 2020)
z	L	Vertical distance in the z-direction (+ downward)
ϑ	$L^2\ T^{-1}$	Volumetric infiltration rate per unit length
σ	$M\ T^{-1}\ T^{-2}$	Stress
μ	$M\ T^{-1}\ T^{-1}$	Dynamic viscosity of the fluid
γ_w	Dimensionless	Wet specific gravity
ρ_b	$M\ L^{-3}$	Soil bulk density
$\tilde{\mu}$	$L^4\ M^{-1}\ T^{-2}$	Chemical potential
ν	Dimensionless	Geometrical aspect ratio
ϕ	$L^3\ L^{-3}$	Volume fraction
θ	$L^3\ L^{-3}$	Volumetric water content
ω	$M\ M^{-1}$	Gravimetric water content
u^2	Dimensionless	Anisotropy
λ	Dimensionless	Pore size distribution index
$\emptyset$	$L^3\ L^{-3}$	Porosity
Γ	T^{-1}	Transfer of water between two pore systems
ψ	L	Matric head
ψ_{str}	L	Air entry value
ψ_{wf}	L	Wetting front potential
γ_0	Degrees	Slope angle of the infiltration surface
ε	Dimensionless	Surface roughness coefficient
λ_c	L	Macroscopic capillary length (called λ_s in Wu and Pan, 1997; Wu et al., 1999; Abou Najm and Stewart, 2019)
κ	$L^3\ T\ M^{-1}$	Second order positive semi-definite tensor (Bennethum and Cushman, 1996)
α_{wr}	L^{-1}	Rate of water repellency attenuation (Abou Najm et al., 2021)
Υ	Dimensionless	Ratio of volume occupied by border cracks to total crack volume (Stewart 2018)
		Model Constants
a	Dimensionless	Wu and Pan (1997); Wu et al. (1999); Stewart and Abou Najm (2018)
a_1	L^{-1}	originally called a (Beven and German, 1981; Germann, 1985)
a_2	Dimensionless	originally called a' (Beven and German, 1981; Germann, 1985)
a_3	Dimensionless	Lambe and Whitman (1979); Su et al. (2020)
a_4	Dimensionless	originally called a (Govindaraju et al., 2012)
a^*	Dimensionless	originally called a (Basha, 1994)
a'	Dimensionless	originally called a (Wind, 1995)
a_{sn}	Dimensionless	originally called a (Setiawan and Nakano, 1993)
A	$L\ T^{-1}$	Mezencev (1948); Philip (1957a, b)
A_0	Dimensionless	Swartzendruber (1987b); Swartzendruber and Hogarth (1991)
A_1	T^{-1}	originally called A (Holtan, 1961; Overton, 1964; Huggins and Monke; 1966)
A^*	Dimensionless	originally called A (Smith, 1972)
A'	Dimensionless	originally called A (Warrick et al., 1985)
A''	Dimensionless	originally called A (Lambe and Whitman, 1979; Su et al., 2020)
b	Dimensionless	White et al. (1992); Fallow et al. (1994); Wu and Pan (1997); Wu et al. (1999); Stewart and Abou Najm (2018)

b_0	Dimensionless	originally called b (Broadbridge and White, 1988)
b_1	Dimensionless	originally called b (Beven and German, 1981; Germann, 1985)
b_2	Dimensionless	originally called b (Swartzendruber, 1974)
b^*	Dimensionless	originally called b (Basha, 1994)
b'	T^{-1}	originally b (Wind, 1995)
b_{sn}	Dimensionless	originally called b (Setiawan and Nakano, 1993)
B	Dimensionless	Chu (1985)
B'	Dimensionless	originally B (Warrick et al., 1985)
B''	Dimensionless	originally called B (Lambe and Whitman, 1979; Su et al., 2020)
c	L	Wu et al., (1999)
c_0	Dimensionless	originally called c (Poulovassilis and Argyrokastritis, 2020)
c_1	Dimensionless	Corradini et al. (1997, 2011)
c_2	Dimensionless	Corradini et al. (1997, 2011)
c_3	Dimensionless	Corradini et al. (1997, 2011)
c_4	Dimensionless	originally called c (Swartzendruber, 1974)
C	Dimensionless	Reynolds et al. (1983,1985)
C'	Dimensionless	originally C(Warrick et al., 1985)
C_1	$L\ T^{-0.5}$	Kutilek and Krejca (1987)
C_2	$L\ T^{-1}$	Kutilek and Krejca (1987)
C_3	$L\ T^{-1.5}$	Kutilek and Krejca (1987)
d_1	Dimensionless	Corradini et al. (2011)
D_g	Dimensionless	originally called D (Ghanbarian et al., 2016)
f^*	L^{-1}	Beven (1984)
f_i	Dimensionless	Morel-Seytoux and Khanji (1976)
F_1	Dimensionless	Ali et al. (2013)
F_2	Dimensionless	Ali et al. (2013)
F_3	Dimensionless	Ali et al. (2013)
G	Dimensionless	Reynolds and Elrick (1990)
k_1	Dimensionless	originally called k (Overton, 1964)
k'	$L\ T^{-1}$	originally called k (Kostiakov, 1932; Mezencev, 1948)
K_F	Dimensionless	Horton (1941)
m_{ssc}	Dimensionless	originally called m (van Genuchten et al., 1980; Su et al., 2020)
m'	Dimensionless	Lambe and Whitman (1979); Su et al. (2020)
n	Dimensionless	Brooks and Corey (1964); Lassabetere et al. (2006); Essig et al. (2009)
n_1	Dimensionless	originally called n (Swartzendruber, 1974)
n_{ssc}	Dimensionless	originally called n (van Genuchten et al., 1980; Su et al., 2020)
n'	Dimensionless	originally n (Kostiakov, 1932; Mezencev, 1948)
n^*	Dimensionless	originally called n (Selker et al., 1999a)
p	Dimensionless	Philip et al. (1993); Corradini et al., (1994, 1997)
P	Dimensionless	Holtan, (1961); Huggins and Monke; (1966)
t_0	T	Smith (1972)
t_S	T	Srivastava et al. (1996); Chen and Young (2007)
α	L^{-1}	Gardner (1958); Philip (1968, 1972); Warrick et al. (1985); Ankeny et al. (1991)
α_1	Dimensionless	originally called α (Smith et al., 1999, Corradini et al., 2000; 2011)
α_3	Dimensionless	Lambe and Whitman (1979); Su et al. (2020)
α_{swell}	Dimensionless	originally called α (Smiles and Raats, 2005; Su, 2009; 2010)

α_k	Dimensionless	originally called α (Das and Kluitenberg, 1995; Kosugi, 1999)
α^*	Dimensionless	originally called α (Smith, 1972)
α'	Dimensionless	originally called α (Srivastava et al. 1996)
β_0	Dimensionless	Brutsaert (1977); Selker and Assouline (2017); called A and α in Stewart (2018, 2019) respectively
β	Dimensionless	Haverkamp et al. (1994); Lassabetere et al. (2006, 2014); Rahmati et al. (2019)
β_1	T^{-1}	originally called β (Novak and Soltesz, 1984)
β_2	Dimensionless	originally called β (Philip, 1972)
β_3	Dimensionless	originally called β (Morel-Seytoux and Khanji, 1974; 1976)
β_4	Dimensionless	originally called β (Su, 2010)
β^*	Dimensionless	originally called β (Selker et al., 1999a)
β'	Dimensionless	originally β (Srivastava et al. 1996)
β_{swell}	Dimensionless	originally called β (Smiles and Raats, 2005; Su, 2009; 2010)
β_l	Dimensionless	originally called β (Libardi et al., 1980)
β_g	Dimensionless	originally called β (Ghanbarian et al., 2016)
β_k	Dimensionless	originally called β (Das and Kluitenberg, 1995; Kosugi, 1999)
δ	Dimensionless	Parlange et al. (1982, 1985, 2002); Haverkamp et al. (1990); Smith et al. (1993); Corradini et al. (1994)
δ'	Dimensionless	originally called δ (Srivastava et al. 1996)
γ	Dimensionless	Haverkamp et al. (1994); Lassabetere et al. (2006, 2014); Warrick and Lazarovitch (2007); Warrick et al. (2007)
γ_k	Dimensionless	originally called γ (Das and Kluitenberg, 1995; Kosugi, 1999)
λ_g	Dimensionless	originally called λ (Ghanbarian et al., 2016)
$\mathcal{B}$	Dimensionless	originally called β (Smith et al., 1993; Corradini et al., 1994, 1997; Smith et al., 1999; Corradini et al., 2000; 2011)
σ_k	Dimensionless	originally called σ (Das and Kluitenberg, 1995; Kosugi, 1999)

Table 2.6: Detailed Summary of infiltration models (Subscripts: m, f and h denote the matrix, the fast-flow, and the interface between these two regions; p, w and d denote the ponding, wetting, and draining stage; i, s, r and ∞ denote the initial, saturated, relative, and final phase, respectively; 0 denote the soil surface (z=0)).

Model	Year	Equation(s)	Applied Concepts
Green and Ampt	1911	$t = \frac{I}{K_s} - \frac{(\psi_{wf}+h_0)(\theta_s-\theta_i)}{K_s}\ln\left(1+\frac{I}{(\theta_s-\theta_i)(\psi_{wf}+h_0)}\right)$	Green and Ampt equation is derived from the following expression of the infiltration rate, I (L T^{-1}), with respect to time: $i = K_s\left[\frac{\psi_{wf}+z_w+h_0}{z_w}\right] = \frac{d[z_w(\theta_s-\theta_i)]}{dt}$
Kostiakov	1932	$I = k't^{n'}$	Kostiakov proposed the empirical equation from field-measured data, which predicts physically a zero-infiltration capacity for prolonged rainfall events. $k' > 0$ and $0 < n' < 1$
Horton	1941	$i = i_\infty + (i_i - i_\infty)e^{-K_F t}$	Horton derived the empirical equation from field-measured data, assuming that the reduction in the infiltration capacity is directly proportional to the rate of infiltration and is applicable only when the effective rainfall intensity is greater than i_∞. $i_\infty = K_s$ and $K_F > 0$
Mezencev	1948	$I = k't^{n'} + At$	Mezencev modified the Kostiakov's model (1932) by including a linear term with a coefficient A (L T^{-1}) that is equal to the saturated hydraulic conductivity, K_s (LT^{-1}), at infinite times. $k' > 0$ and $0 < n' < 1$
Hansen	1955	$x_w = \left(\frac{2Kh}{\emptyset\Delta S}\right)^{0.5} t^{0.5}$ Horizontal $t = \frac{\emptyset\Delta S}{K}[h\{1-ln(h-z_w)\}-z_w]$ Upward $t = \frac{\emptyset\Delta S}{K}[h\{1-ln(h+z_w)\}+z_w]$ Downward	Hansen related the soil-water movement and one-dimensional infiltration in the horizontal, upward, and downward directions and noted that the nature of flow from a free water surface through unsaturated soil exhibited three distinct zones, namely, the transmission zone, the wetting zone, and the wetting front.
Philip	1957a	$I = \sum_{i=1}^{\infty} A_n(\theta)\, t^{n/2} + K_i t$	A time series solution for $x(\theta,t)$ is developed in powers of $t^{1/2}$ as: $x(\theta,t) = \varphi(\theta)t^{\frac{1}{2}} + \chi(\theta)t + \psi(\theta)t^{\frac{2}{3}} + \omega(\theta)t^2 + \cdots$ The first term, $X_1(\theta)$, reflects the influence of the capillary forces on the flow process, and the following terms, $X_2(\theta)$ and $X_3(\theta)$…, reflect the gravity effect on infiltration. The cumulative infiltration equation, I (L), was obtained by integrating the time series solution for $z(\emptyset,t)$, resulting in: $I = A_1(\theta)t^{1/2} + (A_2(\theta)+K_i)t + A_3(\theta)t^{\frac{2}{3}} + A_4(\theta)t^2 + \cdots$ (Implicit) One broad equation describes early and transient infiltration behaviors.

Philip	1957b	$I = S_0 t^{0.5} + At$ $\quad 0 \le t \le t_c$ $I = K_s t + \frac{{S_0}^2}{4(K_s - A)}$ $\quad t > t_c$ Where: $t_c = \frac{{S_0}^2}{4(K_s - A)^2}$	The Philip's time series solution for $x(\theta, t)$ is approximated by the two first terms for small times. The parameter A is an estimate of $(A_2 + K_i +$ the truncation error $\varepsilon)$ such that $A = mK_s$ where $1/3 \le m \le 2/3$ (Youngs, 1968; Philip, 1969a; Talsma, 1969, Talsma and Parlange, 1972). $m = 0.363$ may be appropriate for soils with a relatively low initial moisture content (Philip, 1987), while a value of $m = 2/3$ is often used (Whisler and Bouwer, 1970, Fodor et al., 2011). In some studies (Davidoff and Selim, 1986, Swartzentruber and Young (1974), Ghorbani et al., 2009), $m = 1$ and hence $A = K_s$. Then, for large times $(t > t_c)$, $I = K_s t$ which is nothing but the linear term in the equation valid for short times $(0 \le t \le t_c)$. (Explicit) Two specific equations were developed for each infiltration behavior, the first describing the early-state $(0 \le t \le t_c)$, while the second describing steady-state behavior $(t > t_c)$.
Holtan	1961	$i = i_\infty + A_1 (s_0 - I)^P$ Where $s_0 = \emptyset - \theta_i$	Holtan expressed the infiltration capacity as a function of the residual potential storage in the upper soil layers. The advantage of Holtan's approach is that it can compute the infiltration rate for both periods of rain intensity lower than infiltration capacity and periods of no rain.
Overton	1964	$I = k_1 s_0 - \sqrt{\frac{i_\infty}{A_1}} tan[\sqrt{A_1 i_\infty}(t_c - t)]$ Where: $t_c = \frac{1}{\sqrt{A_1 i_\infty}} tan^{-1}\left(\sqrt{\frac{A_1}{i_\infty}} k_1 s_0\right)$ and $s_0 = \emptyset - \theta_i$	Using the Holtan model with P = 2, Overton derived an infiltration equation which computes the infiltration rate at any time during a storm, even when rainfall does not exceed the infiltration capacity or when there is a temporary interruption in rainfall. k_1 is based on vegetation, varying between 0.3 for weeds to 1 for bluegrass.
Huggins and Monke	1966	$i = i_\infty + A_1 \left(\frac{s_0 - I}{\emptyset}\right)^P$	Huggins and Monke introduced porosity $\emptyset$ ($L^3\ L^{-3}$) in the Holtan model. As s_0 (L) takes the dimension of length, it cannot be equal to a non-dimensional quantity, i.e., $(\emptyset - \theta_i)$ as originally hypothesized, rather it is equal to $(\emptyset - \theta_i)$ times the depth of soil stratum above the impeding layer.
Fok and Hansen	1966	$\frac{I}{h\emptyset\Delta S} - ln\left(1 + \frac{I}{h\emptyset\Delta S}\right) = \frac{Kt}{h\emptyset\Delta S}$	Fok and Hansen derived an equation for one-dimensional downward infiltration from furrow irrigation based on Hansen (1955) who described soil-water movement through homogeneous unsaturated soils exhibiting three distinct zones, the transmission zone, the wetting zone, and the wetting front. Within the transmission zone (T), the hydraulic conductivity, K ($L\ T^{-1}$), is essentially constant. The moisture content, and thus the hydraulic conductivity within the wetting zone, decreases toward the wetting front; however, the energy consumed within this zone is approximately constant. The wetting front is, in effect, a capillary fringe; the moisture content of the foremost part is approximately the same.

Philip	1967	$I = S_0 t^{0.5} + A_2 t + A_3 t^{3/2} + A_4 t^2 + \cdots$	Philip developed the following one-dimensional infiltration equation for an unsaturated heterogeneous medium: $\frac{\partial \theta}{\partial t} = \frac{\partial}{\partial x}\left(K(\theta,x)\frac{\partial}{\partial x}\{\psi(\theta,x)\}\right) - \frac{\partial}{\partial x}\{K(\theta,x)\}$. To solve this equation, Philip (1967) applied a quasi-analytical method previously established in Philip (1957a) for small and moderate times: $x(\psi,t) = \phi_1(\psi)t^{1/2} + \chi_1(\psi)t + \cdots$ The expression for cumulative infiltration I(L) into this subclass of scale-heterogeneous media is formally like that for infiltration into homogeneous media (1957a, b).
Philip	1968	For buried point source, $i = \frac{\alpha^2 Q_0 i^*}{8\pi}$ Where: $i^* = \frac{1}{2T}e^{Z-R}\left[1 + \frac{Z}{T} + \frac{Z}{T^2}\right]$ direction of z $i^* = \frac{R}{2T^2}e^{Z-R}\left[1 + \frac{1}{T}\right]$ direction of r $R = 0.5\alpha r$; $Z = 0.5\alpha z$ and $T = \sqrt{R^2 + Z^2}$ For spherical cavity, $Q_{inf} = 4\pi r \varphi V^*$ $V^* = (1 - R)^{-1}$ (1) $V^* = 1$ (2) $V^* = R$ (3)	Philip treated 3D steady infiltration from buried point sources and spherical cavities of continuous supply Q_0 (L^3 T^{-1}). Hydraulic conductivity K (L T^{-1}) depends exponentially on moisture (capillary) potential ψ (L) ➔ $K(\psi) = K_s e^{\alpha\psi}$; For soils initially at "field capacity" or drier, $e^{\alpha\psi_i} \ll 1$, and thus $\varphi = \frac{K_s}{\alpha}$. The fundamental point source solution is first explored and then is used as the basis of an analysis of steady infiltration from spherical cavities. Philip (1968) analyzed steady infiltration from spherical cavities using the dimensionless infiltration V^* for small R (1), capillarity dominant ($R \to 0$) (2), and for gravity dominant ($R \to \infty$) (3).
Wooding	1968	$Q_{inf} = \pi r^2 \alpha\varphi + 4r\varphi$	Wooding approximated a steady-state infiltration of water from a circular ring of radius r (L) assuming no surface ponding and the ratio $K(\psi)/\varphi(\psi)$ is equal to the constant parameter α (Philip, 1968).
Philip	1969a	1D Absorption and Infiltration (1): For absorption (1.1): $i = \frac{1}{2}S_0 t^{-1/2}$ (1.1.A) $i = \sqrt{\frac{D^*}{\pi}}(\theta_s - \theta_i)t^{-1/2}$ (1.1.B) $i = \frac{1}{2}\sqrt{2K_s C(\theta_s - \theta_i)}t^{-1/2}$ (1.1.C) Where: $D^* = \frac{\pi {S_0}^2}{4(\theta_s - \theta_i)^2}$ and $C = \frac{S_0^2}{2K_s(\theta_s - \theta_i)}$ For Infiltration (1.2): (1.2.A) $i = \frac{1}{2}S_0 t^{-1/2} + (A_2 + K_i) + \frac{3}{2}A_3 t^{1/2} + \cdots$ $t < \infty$ $i = K_s$ $t \to \infty$ (1.2.B and C) $i = (K_s - K_i)i^* + K_s$ $i^* = \frac{1}{2}\left(\frac{1}{\sqrt{\pi T}} - 1 + \cdots\right)$ small T (B)	A. Philip expressed the dynamics of cumulative 1D surface absorption (1.1) and surface infiltration rate i (L T^{-1}) (1.2), as well as two- and three- dimensional subsurface infiltration (2.2) with non-linear exact series solutions. In two-dimensions, there is no steady-state (i.e., $t \to \infty$), unless diffusivity D (L^2 T^{-1}) takes particular values, e.g., for constant D or approaching delta function. B. Philip also expressed the dynamics of 1D surface absorption (1.1) and surface infiltration rate i (L T^{-1}) (1.2), as well as two- and three-dimensional subsurface absorption (2.1) and infiltration (2.2) in terms of dimensionless functions for constant diffusivity D (L^2 T^{-1}) with hydraulic conductivity K (L T^{-1}) depending exponentially on moisture (capillary) potential ➔ $K(\psi) = K_s e^{\alpha\psi}$; For soils initially at "field capacity" or drier, $e^{\alpha\psi_i} \ll 1$, and thus $\varphi = \frac{K_s}{\alpha}$. C. Philip also expressed the dynamics of 1D cumulative surface absorption (1.1) and surface infiltration i (L T^{-1}) (1.2), as well as two-

		$i^* = \frac{1}{4\sqrt{\pi}T^{\frac{3}{2}}}e^{-T}$ large T (B) $i^* = \frac{1}{2\pi}\left(\frac{1}{i^*} - \ln\left(1+\frac{1}{i^*}\right)\right)$ small (C) $i^* = \frac{1}{2\pi T}$ large T (C) Where: $T = \frac{(K_s - K_i)^2 t}{\pi {S_0}^2}$ 2D and 3D Absorption and Infiltration (2): For 2D and 3D absorption (2.1): $i = \frac{(\theta_s - \theta_i)D^* i^*}{r}$ Where: $D^* = \frac{\pi {S_0}^2}{4(\theta_s - \theta_i)^2}$ (2.1.B) For cylindrical cavity: $i^* = \frac{1}{\sqrt{\pi T}} + \frac{1}{2} - \frac{1}{4}\sqrt{\frac{T}{\pi}} + \frac{T}{8} - \cdots$ small T $i^* = \frac{2}{lnT}$ large T Where: $T = \frac{\pi t}{t_{geom}}$; $t_{geom} = \left(\frac{2r(\theta_s - \theta_i)}{S_0}\right)^2$ and $\gamma = 0.57722$ For spherical cavity: $i^* = \frac{1}{\sqrt{\pi T}} + 1$ large T Where: $T = \frac{\pi t}{4t_{geom}}$ and $t_{geom} = \left(\frac{r(\theta_s - \theta_i)}{S_0}\right)^2$ (2.1.C) For cylindrical cavity: $T = \frac{\pi}{8}\left[\left(\frac{4}{\pi i^*} - 1\right)e^{4/\pi i^*} + 1\right]$ small T $i^* = \frac{4}{\pi \ln(T)}$ large T Where: $T = \frac{\pi t}{t_{geom}}$ and $t_{geom} = \left(\frac{2r(\theta_s - \theta_i)}{S_0}\right)^2$ For spherical cavity: $T = \frac{\pi}{12}\left[2\left(1 - \frac{2}{\pi i^*}\right)^{-3} - 3\left(1 - \frac{2}{\pi i^*}\right)^{-2} + 1\right]$ small T $i^* = \frac{2}{\pi} + \left(\frac{4\pi^2}{3T}\right)^{1/3}$ large T Where $T = \frac{\pi t}{4t_{geom}}$ and $t_{geom} = \left(\frac{r(\theta_s - \theta_i)}{S_0}\right)^2$ For 2D and 3D infiltration (2.2): (2.2.A) $i = \frac{1}{2}S_0 t^{-1/2} + \frac{A_2^*}{r} + \frac{3A_3^*}{2r^2}t^{1/2} + \cdots$ $t < \infty$ $i_{3D} = \int_{\theta_i}^{\theta_s}\frac{D(\theta)}{r}d\theta$ $t \to \infty$ $i = k(\theta_s - \theta_i)i^*$ (2.2.B) For cylindrical cavity: $i^* = \frac{1}{4RK_0(2R)}$ $t \to \infty$ For spherical cavity:	and three- dimensional subsurface absorption i (L T^{-1}) (2.1) in terms of dimensionless function i^* for diffusivity D (L^2 T^{-1}) approaching delta function. K_0 *is the modified Bessel function of the second kind of order 0.*

		$i^* = 1/2\left[\sqrt{\pi T^*}e^{-T^*} + \frac{1}{2} + \sqrt{2R} + erf(\sqrt{T})\right]$ $t < \infty$ $i^* = \frac{1}{2} + \frac{1}{4R}$ $t \to \infty$ Where $k = \frac{(K_s - K_i)}{(\theta_s - \theta_i)}$; $R = \frac{kr}{4D^*}$; $T^* = \frac{k^2 t}{4D^*}$ and $D^* = \frac{\pi {S_0}^2}{4(\theta_s - \theta_i)^2}$	
Parlange	1971a	$I = \int_{\theta_i}^{\theta_s} z_w d\theta$ $z_w = \frac{\sqrt{2t}\int_{\theta}^{\theta_s} D(\theta)d\theta}{\sqrt{\int_{\theta_i}^{\theta_s} \theta D(\theta)d\theta}}$	An accurate, analytic representation of one-dimensional horizontal infiltration was developed by Parlange et al. where absorption is dominant and gravity effect is omitted.
Parlange	1971b	$I = \int_{\theta_i}^{\theta_s} z_w d\theta$ $z_w = K_s(t - t_i) + \int_{\theta}^{\theta_s - \Delta\theta} \frac{D(\theta)d\theta}{K_s\theta - K(\theta)}$ $t < t_\infty$ $z_w = -\int_{\theta}^{\theta_s} \frac{D(\theta)d\theta}{K(\theta) + K_s\theta}$ $t \to t_\infty$	The theory by (Parlange 1971a) was extended to develop an accurate, analytic representation of one-dimensional infiltration, valid for all times, where gravity plays a role. Diffusivity D ($L^2\ T^{-1}$) and hydraulic conductivity K ($L\ T^{-1}$) vary rapidly near saturation.
Parlange	1971c	2D Absorption: $I = \frac{r\sqrt{4D_i\tau}\int_{\theta}^{\theta_s} D(\theta)d\theta}{\sqrt{\int_{\theta_i}^{\theta_s} \theta D(\theta)d\theta}}$ 3D Absorption: $1 - \frac{r}{I} = g(\tau)\int_{\theta}^{\theta_s} D(\theta)d\theta$ Where: $\tau = \frac{t}{r^2}$ and $g(\tau)$ is given by Eq.20	An analytic solution for absorption (i.e., movement without gravity) in two and three dimensions is obtained, valid for all times, for arbitrary diffusivity D ($L^2\ T^{-1}$). For simplicity, the two- and three-dimensional problems are treated for the case of a cylinder and a sphere, respectively.
Philip	1971	2D Infiltration: $\vartheta = \frac{\alpha Q_0 \vartheta^*}{2\pi}$ For surface line source: $\vartheta^* = \frac{Z}{T}e^Z \mathrm{K}_1(T)$ direction of x $\vartheta^* = Xe^Z\left[\frac{\mathrm{K}_1(T)}{T} - e^Z\int_Z^\infty e^{-Z}\frac{\mathrm{K}_1(T)}{T}dZ\right]$ direction of z For buried line source: $\vartheta^* = \frac{1}{2}e^Z\left[\mathrm{K}_0(T) + \frac{Z}{T}\mathrm{K}_1(T)\right]$ direction of x $\vartheta^* = \frac{X}{2T}e^Z \mathrm{K}_1(T)$ direction of z Where: $X = 0.5\alpha x$; $Z = 0.5\alpha z$ and $T = \sqrt{X^2 + Z^2}$ 3D Infiltration:	Philip established the solution of the quasilinear steady infiltration equation for any distribution of surface and buried sources of continuous supply Q_0 ($L^3\ T^{-1}$). Hydraulic conductivity K ($L\ T^{-1}$) depends exponentially on moisture (capillary) potential ➔ $K(\psi) = K_s e^{\alpha\psi}$; For soils initially at "field capacity" or drier, $e^{\alpha\psi_i} \ll 1$, and thus $\varphi = \frac{K_s}{\alpha}$. K_0 *and* K_1 *are the modified Bessel function of the second kind of order 0 and 1.*

		$i = \frac{\alpha^2 Q_0 i^*}{8\pi}$ For surface point source: $i^* = \frac{Z(1+T)}{T^3} e^{Z-T}$ direction of z $i^* = \frac{R^2+ZT(T-Z)}{RT^3} e^{Z-T}$ direction of r For buried point source: $i^* = \frac{1}{2T} e^{Z-R}\left[1+\frac{Z}{T}+\frac{Z}{T^2}\right]$ direction of z $i^* = \frac{R}{2T^2} e^{Z-R}\left[1+\frac{1}{T}\right]$ direction of r Where: $R = 0.5\alpha r$, $Z = 0.5\alpha z$ and $T = \sqrt{R^2+Z^2}$	
Parlange	1972a	Spherical cavity: $Q_{inf} = 4\pi r\varphi V^*$ Where: $V^* = 1 + \alpha r/2$	The solution for the steady state infiltration from a cavity is obtained analytically in two and three dimensions by a singular perturbation technique i.e., a solution valid near the cavity is matched to a solution valid far from it. Details of the method are given for a spherical cavity. The form of the solution depends upon the product $\alpha r \leq 1$ where α (L^{-1}) is a soil property that characterizes the relative importance of gravity and capillarity, and r (L) characterizes the size of the cavity. When $\alpha r \to 0$, gravity effects become negligible in three dimensions.
Parlange	1972b	Spherical cavity: $Q_{inf} = 4\pi r\varphi V^*$ Where: $V^* = \frac{1}{g(t)\varphi} + \frac{r^3}{r_1^2\varphi}\int_{r/r_1}^{1} \gamma^{-4} K\, d\gamma$ $g(t)$ and $r_1(t)$ are given by Eq. (10) and (22) in Parlange's paper, respectively.	An analytical technique is presented to study unsteady infiltration from multidimensional cavities for moderate times. The solution reduces to known expressions for very short (Parlange, 1971c) and very long times (Parlnage, 1972b). Only the simplest geometry, i.e., a spherical cavity, is considered.
Smith	1972	$i = i_\infty + A^*(t-t_0)^{-\alpha^*}$	Richards' equation for unsaturated soil moisture flow is solved by extensive numerical simulation of infiltration for various patterns of rainfall to develop a single dimensionless formula that describes the infiltration decay curves for all soils, initial conditions, and rainfall rates.

Philip	1972	2D Infiltration: $\vartheta = \frac{\alpha Q_0 \vartheta^*}{2\pi}$ For surface line source: $\vartheta^* = (1+\beta_2)\frac{Z}{T}e^{(1+\beta_2)Z}\mathrm{K}_1[(1+\beta_2)T]$ direction of x $\vartheta^* = (1+\beta_2)Xe^{(1+\beta_2)Z}\left\{\frac{1}{T}\mathrm{K}_1[(1+\beta_2)T] - (1+\beta_2)e^{(1+\beta_2)Z}\int_Z^\infty \frac{1}{T}e^{-(1+\beta_2)Z}\mathrm{K}_1[(1+\beta_2)T]dZ\right\}$ direction of z For buried line source: $\vartheta^* = \frac{1}{2}(1+\beta_2)e^{(1+\beta_2)Z}\left\{\mathrm{K}_0[(1+\beta_2)T] + \frac{Z}{T}\mathrm{K}_1[(1+\beta_2)T]\right\}$ direction of x $\vartheta^* = \frac{1}{2}(1+\beta_2)\frac{X}{T}e^{(1+\beta_2)Z}\mathrm{K}_1[(1+\beta_2)T]$ direction of z Where: $X = 0.5\alpha x$; $Z = 0.5\alpha z$ and $T = \sqrt{X^2+Z^2}$ 3D Infiltration: $i = \frac{\alpha^2 Q_0 i^*}{8\pi}$ For buried point source: $i^* = \frac{1}{2T}e^{(1+\beta_2)(Z-T)}\left[\frac{(1+\beta_2)(Z+T)}{T} + \frac{Z}{T^2}\right]$ direction of z $i^* = \frac{R}{2T^2}e^{(1+\beta_2)(Z-T)}\left[1+\beta_2+\frac{1}{T}\right]$ direction of r For surface point source: $i^* = \frac{Z}{T^3}[1+(1+\beta_2)T]e^{(1+\beta_2)(Z-T)}$ direction of z $i^* = \frac{1}{RT^3}[R^2+(1+\beta_2)ZT(T-Z)]e^{(1+\beta_2)(Z-T)}$ direction of r Where: $R = 0.5\alpha r$; $Z = 0.5\alpha z$ and $T = \sqrt{R^2+Z^2}$	Philip developed a quasi-linearized steady infiltration equation for heterogeneous soils under buried and surface sources of continuous supply Q_0 ($L^3\ T^{-1}$). Hydraulic conductivity K ($L\ T^{-1}$) depends exponentially on both moisture (capillary) potential ψ (L) and depth z (L) ➔ $K(\psi) = K_s e^{[\alpha(\psi+\beta_2 z]}$. β_2 is the dimensionless coefficient of dependence of conductivity K ($L\ T^{-1}$) on depth z (L), $\beta_2 \geq 0$ K_0 *and* K_1 *are the modified Bessel function of the second kind of order 0 and 1.*
Talsma and Parlange	1972	$i^* = \frac{i-K_s}{K_s}$ $2\pi T = ln\left(\frac{1+i^*}{i^*}\right) + \frac{1}{i^*}$ (1) $2\pi T = ln\left(\frac{1+i^*}{i^*}\right) - \frac{1}{+i^*}$ (2) $2\pi T = 3\left\{(1+2i^*)ln\left(\frac{1+i^*}{i^*}\right) - 2\right\}$ (3) Where: $T = \frac{{K_s}^2 t}{\pi {S_0}^2}$	Taslma and Parlange used the linearized infiltration equations (Philip, 1969a) to develop 1D infiltration equation assuming the diffusivity D ($L^2\ T^{-1}$) is (1) a delta function, (2) proportional to the variation rate of the hydraulic conductivity in respect to the volumetric moisture content $\partial K/\partial\theta$ or (3) a constant.
Parlange	1972c	$D_0(t)\theta_0(t)\frac{d\theta_0}{dt} = i[i-K_0(t)]$ $t < t_\infty$ (1) $z_w = \int_\theta^{\theta_s}\frac{D(\theta)d\theta}{i-K(\theta)}$ $t \to t_\infty$ (2)	The one-dimensional infiltration was solved analytically. If $i > K_s$ ($t \to t_\infty$), the surface becomes saturated with water and ponding occurs, then equation (1) ceases to apply. Equation (2) (Parlange, 1971b) shows that the limiting profile is identical to the "profile at infinity" and therefore can be applied at infinite times.
Mein and Larson	1973	$t = \frac{I}{K_s} - \frac{(\theta_s-\theta_i)\psi_{wf}}{K_s}\ln\left(1+\frac{I}{(\theta_s-\theta_i)\psi_{wf}}\right)$ $0 \leq t < t_p$ $I_p = i_p t_p$ $t = t_p$ $t - t_p = \frac{I}{K_s} - \frac{i_p t_p}{K_s} - (\psi_{wf}+h_0)(\theta_s-\theta_i)\ln\left(\frac{(\psi_{wf}+h_0)(\theta_s-\theta_i)+I}{(\psi_{wf}+h_0)(\theta_s-\theta_i)+i_p t_p}\right)$ $t > t_p$ Where: $t_p = \frac{K_s\psi_{wf}(\theta_s-\theta_i)}{i_p(i_p-K_s)}$	Mein and Larson published an extension of the Green and Ampt (1911) model of ponded infiltration, which applied the same piston flow concept to the case of constant flux surface conditions. Prior to the ponding time $(0 \leq t < t_p)$, the rainfall intensity is less than the potential infiltration rate and the soil surface is unsaturated. Ponding $(t = t_p)$ begins when the rainfall intensity exceeds the potential infiltration rate; the soil

			surface becomes saturated. As rainfall continues $(t > t_p)$, the saturated zone extends deeper into the soil.
Smiles	1974	$I = S_0 t^{0.5} + 0.5\left[(1-\gamma_{w,i})K_i - (1-\gamma_{w,n})K_n\right]t$	Smiles approximated infiltration into swelling soils into a two-term infiltration equation in which S_0 (L T$^{-0.5}$) is the analogue of sorptivity in the swelling system and hydraulic conductivity K (L T^{-1}) reflects gravity. As for $(1-\gamma_w)$, this term may be interpreted as if it reduced the effect of gravity to $(1-\gamma_w)$ times its values in a rigid soil, and thus increases the time before which the effect of gravity is unimportant when compared with that of the moisture potential gradient.
Turner and Parlange	1974	$I = S_0 t^{1/2} + 1/3\left[K_s + \frac{0.72WS_0{}^2}{A(\theta_s-\theta_i)}\right]t$	An analytical solution for the lateral movement at the periphery of a one-dimensional flow of water is derived, valid for short times when water infiltrates through a region having an area A (L^2) and a perimeter W (L).
Swartzendruber	1974	$t = \frac{I}{K_s} - \frac{(\theta_s-\theta_i)\psi_{wf}}{K_s}\ln\left(1+\frac{I}{(\theta_s-\theta_i)\psi_{wf}}\right)$ $\quad 0 \le t < t_p$ $I_p = \frac{(\theta_s-\theta_i)\psi_{wf}K_s}{q_0-K_s}$ $\quad t = t_p$ $\quad t > t_p$ $I - I_p = \left[\frac{(q_0-K_s)t_p}{1-n_1}\right]\left[\left(\frac{t}{t_p}\right)^{1-n_1} - 1\right] + K_s(t-t_p)$ (1) $I - I_p = 2(q_0-K_s)(t_p-c_4)\left\{\left[(t-c_4)/(t_p-c_4)\right]^{0.5} - 1\right\} + K_s(t-t_p)$ (2)	Swartzendruber presented a theoretical study of one-dimensional infiltration under constant-flux rainfall q_0 (L T^{-1}) into a uniform soil by treating the soil-water profile as step function, as assumed in Green and Ampt (1911). The analysis is like that of Mein and Larson (1973) for $t \le t_p$. For describing the infiltration characteristics after the ponding time t_p (L), two explicit-form equations, (1) and (2), are proposed for i versus t, both equations being integrable into explicit forms of I versus t under constant-flux rainfall. Both equations are somewhat like that of Smith (1972) but contain one less characterizing constant. Equation (1) may be viewed as an altered Kostiakov (1932) form, modified to contain the feature of an asymptotically-approached the saturated hydraulic conductivity, K_s (L T^{-1}). In Equation (2), the exponent of $(t-c_4)$ is taken as $-1/2$ rather than the more general $-\alpha^*$ (Smith, 1972). (1) $i = at^{-n_1} + K_s$ where $a = (q_0-K_s)t_p^{n_1}$ (2) $i = b_2(t-c_4)^{-1/2} + K_s$
Morel-Seytoux and Khanji	1974	$t = \frac{\beta_3}{K_s}\left\{I - (\psi_{wf}+h_0)(\theta_s-\theta_i)ln\left[1+\frac{I}{(\psi_{wf}+h_0)(\theta_s-\theta_i)}\right]\right\}$	Morel-Seytoux and Khanji modified Green and Ampt equation to account for the effects of air viscous resistance to water flow where β_3 (originally called β, dimensionless) is a correction factor for viscosity.

Morel-Seytoux	1976	$I_p = i_p t_p$ $t = t_p$ $\frac{K_s}{\beta_3}(t - t_p) = I - I_p - \left[\frac{(\theta_s-\theta_i)(\psi_{wf}+h_0)}{1-f_i} + I_p\left(1 - \frac{1}{\beta_3}\right)\right] ln\left[\frac{1+(1-f_i)I/(\theta_s-\theta_i)(\psi_{wf}+h_0)}{1+(1-f_i)I_p/(\theta_s-\theta_i)(\psi_{wf}+h_0)}\right]$ $t > t_p$ Where: $t_p = \frac{\psi_{wf}(\theta_s-\theta_i)}{(1-f_i)i_p}\left(e^{\frac{1}{\beta_3 i_p/K_s - 1}} - 1\right)$ constant rainfall rate Check Eq. (55) in Morel-Seytoux's paper for t_p variable rainfall rate	Formulas were derived for prediction of ponding time and cumulative infiltration following ponding under the influence of rainfall. The derivations use a piston profile but with corrections for air flow and resistance effects i.e., do not assume immediate saturation at the surface nor a piston displacement of air by water.
Li et al.	1976	$I = \frac{1}{2}(\psi_{wf} + h_0)(\theta_s - \theta_i)\left(t^* + \sqrt{(t^*)^2 + 8t^*}\right)$ Where: $t^* = \frac{K_s}{(\psi_{wf}+h_0)(\theta_s-\theta_i)}t$	One of the simplest explicit solutions of the implicit Green and Ampt model was derived by Li et al. based on the approximation of the logarithmic term in GA equation using the first term of the power series expansion.
Brutsaert	1977	$I = K_s t + \frac{{S_0}^2}{\beta_0 K_s}\left[1 - \frac{1}{1 + \frac{\beta_0 K_s t^{0.5}}{S_0}}\right]$	Brutsaert presented a closed form solution for each of the functions $X_1(\theta), X_2(\theta), X_3(\theta)$ and $X_4(\theta)$ in Philip's time series solution for $z(\emptyset, t)$. The method of obtaining these solutions assumes that these functions are near-step functions. $0 \leq \beta_0 \leq 1$; $\beta_0 = 2/3$ is sufficiently accurate for most soils. However, for soils with a very wide distribution of pore sizes, a larger value such as $\beta_0 = 1$, may yield a better result. For most practical purposes, $\beta_0 = 1$ is recommended (Kutilek et al., 1991).
Collis-George	1977	$I = i_0(tanhT)^{0.5} + i_\infty t$ Where: $i_0 = S_0(t_c)^{0.5}$ and $T = t/t_c$	An empirical equation is proposed by Collis-George which satisfies the conditions that cumulative infiltration is proportional to (time)$^{1/2}$ at short times and reaches a steady state infiltration rate at long times.
Hachum and Alfaro	1977	$I = \int_0^t q_0(t)dt - K_i t$ $0 < t \leq t_p$ $I = I_p + \frac{(\psi_{wf}+h_0)K_s(\theta_s-\theta_i)}{(K_s-K_i)} ln\left\{\frac{K_s(\psi_{wf}+h_0)(\theta_s-\theta_i)+(K_s-K_i)[I-K_i t]}{K_s(\psi_{wf}+h_0)(\theta_s-\theta_i)+(K_s-K_i)[I_p-K_i t_p]}\right\} + K_s(t - t_p)$ $t > t_p$	By extending the analysis of Mein and Larson (1973), Hachum and Alfaro developed a physical model for studying one-dimensional infiltration under variable application rainfall rate patterns q_0 (L T^{-1}), subjected to the assumptions of an abrupt wetting front, constant saturated hydraulic conductivity in the wetted zone, K_s (L T^{-1}), and constant wetting front potential ψ_{wf} (L).

Smith and Parlange	1978	$i = K_s\left(\frac{C}{K_s I}+1\right)$ (1) $i = K_s\frac{e^{K_s I/C}}{e^{K_s I/C}-1}$ (2) Where $C = (\psi_{wf}+h_0)(\theta_s-\theta_i)$	By adopting two extreme assumptions concerning the behavior of unsaturated soil hydraulic conductivity K (L T^{-1}) near saturation, Smith and Parlange derived a two-branched model for infiltration rate i (L T^{-1}) for arbitrary rainfall rates. Assumption (1) was that diffusivity D (L^2 T^{-1}) is a step function (i.e., $D(\theta)$ varies rapidly with water content θ (L^3 L^{-3})). For initially ponded conditions, $t_p \to 0$, and with rainfall rate $q_0 \to \infty$, the familiar Green and Ampt (1911) expression results. Assumption (2) was that D and $dK/d\theta$ are closely proportional. This model also holds for both rainfall and ponded surface conditions.
Batu	1978	$i = \frac{q_0 \alpha L i^*}{2\pi}$ For single strip source: Check Eq. (25) and (26) in Batu's paper, for horizontal and vertical infiltration, respectively. For periodic strip sources equally spaced by 2D (L): Check Eq. (48) and (49) in Batu's paper, for horizontal and vertical infiltration, respectively. Where: F_{2N}, F_{2n}, F_{2n-1} and I_n from Eq. (20), (21), (22), and (47), in Batu's paper, respectively. $X_0 = \frac{\alpha L}{2}$; $X_1 = \frac{\alpha D}{2}$; $X = \frac{\alpha x}{2}$; $Z = \frac{\alpha z}{2}$; $L = \frac{w}{2}$	Batu presented analytical solutions for steady 2D infiltration from single and periodic strip sources of width w (L) and constant flux q_0 (L T^{-1}) using Fourier analysis techniques with no flow outside the strip. The theory assumes that the hydraulic conductivity K (L T^{-1}) is an exponential function of the soil water potential ψ (L).
Kutilek	1980	$i = \frac{1}{2}S_0 t^{-1/2}$ $0 \le t < t_p$ $i = i_p$ $t = t_p$ $i = \frac{1}{2}S_0\left[t-\frac{S_0^2}{4A^2 b(b-1)}\right]^{-1/2}+A$ $t > t_p$ Where: $b = \frac{q_0}{i_\infty}$	An approximate solution of the infiltration equation for rain of constant intensity q_0 (L T^{-1}) is developed. The solution of infiltration for $t > t_p$ is obtained for "delta function" soil.
Parlange	1980	$t = \frac{I}{(K_s-K_i)} - \frac{{S_H}^2}{2(K_s-K_i)^2}\ln\left(1+\frac{2(K_s-K_i)I}{{S_H}^2}\right)$ (1) $t = \frac{I}{(K_s-K_i)} + \frac{{S_H}^2}{2(K_s-K_i)^2}\left(e^{-\frac{2(K_s-K_i)I}{{S_H}^2}}-1\right)$ (2)	Using Darcy's law and the conservation of mass, Parlange solved the following partial differential equation governing water movement: $\frac{\partial\theta}{\partial t} = \frac{\partial}{\partial z}\left[D\frac{\partial\theta}{\partial z}\right]-\frac{\partial K}{\partial z}$ under ponding conditions ($h_0 \ge 0$), assuming that: (1) D (L^2 T^{-1}) increases rapidly with water content, θ (L^3 L^{-3}), while the conductivity, K (L T^{-1}), varies much less rapidly near saturation and (2) D and $\frac{\partial K}{\partial z}$ increase rapidly, and in similar fashion.
Parlange et al.	1982	$t = \frac{{S_0}^2}{2(K_s-K_i)^2(1-\delta)}\left[2\frac{(K_s-K_i)}{{S_0}^2}I - ln\frac{e^{2\delta\frac{(K_s-K_i)}{{S_0}^2}I}+\delta-1}{\delta}\right]$ $I = S_0 t^{0.5}+\frac{1}{3}(2-\delta)(K_s-K_i)t$ small t $I = (K_s-K_i)t+\frac{{S_0}^2}{2(K_s-K_i)(1-\delta)}\ln\left(\frac{1}{\delta}\right)$ large t	A new infiltration equation is obtained by introducing a new parameter δ to embrace different variations of the diffusivity term D (L^2 T^{-1}) and the hydraulic conductivity K (L T^{-1}) under zero ponding ($h_0 = 0$). D is considered as a delta function. δ takes values from 0 to 1, with an approximate used value of 0.85. Equations (1) and (2) in Parlange (1980) can be obtained by setting δ equal to 0 and equal to 1, respectively.

Scotter et al.	1982	$i = K_s + \frac{4\varphi}{\pi r}$	Wooding's equation is rewritten assuming the exponential relationship between $K(\psi)$ and ψ as defined by Gardner (1958): $K(\psi) = K_s e^{\alpha\psi}$; For soils initially at "field capacity" or drier, $e^{\alpha\psi_i} \ll 1$, and thus $\varphi = \frac{K_s}{\alpha}$.
Fok et al.	1982	$\mathrm{V} = \frac{\pi}{2} x_w z_w l \emptyset \Delta S_e$ Where: $x_w = \left(\frac{2Kh_x}{\emptyset \Delta S}\right)^{0.5} t^{0.5}$; $\frac{z_w}{h} - ln\left(1 + \frac{z_w}{h}\right) = \frac{Kt}{\emptyset h \Delta S_e}$	A physical two-dimensional infiltration equation is developed assuming that the loci of the wetting pattern for two-dimensional furrow infiltration are half-ellipses, and their vertical and horizontal flow components can be described as one-dimensional infiltration derived in an earlier study (Hansen, 1955; Fok and Hansen, 1966).
Brakensiek and Rawls	1983	$i = \frac{K_{prec}}{2}\left(\frac{z_w + \psi_{wf,prec}}{z_w}\right)$ $0 \le t < t_p$ $z_{w,p} = \frac{\psi_{wf,subc} - \left(\frac{2q_0}{K_{s,subc}}\right)\left(\frac{1-q_0}{q_0}\right) l_c}{\frac{2q_0}{K_{s,subc}} - 1}$ $t = t_p$ $i = \frac{K_e}{2}\left(\frac{z_w + \psi_{wf,subc} + h_0}{z_w}\right)$ $t > t_p$ Where $K_e = \frac{z_w}{\frac{z_w - l_c}{K_{s,subc}} + \frac{l_c}{K_{s,c}}}$; $r = \frac{K_{s,c}}{K_{s,subc}}$ and $t_p = z_{w,p}\emptyset / q_0$	Brakensiek and Rawls developed a two-layer Green-Ampt model with transient crust conductivity to describe infiltration on crusted soils during uniform rainfall intensity. Infiltration for soil crust modeling may proceed during two periods, pre-ponding, and post-ponding. Crusting of thickness l_c (L) is assumed to start at the time of surface ponding.
Reynolds et al.	1983	$Q_{inf} = \frac{2\pi h_0^2 K_s}{C} + \pi r^2 K_s$	The flow out of a well into the surrounding soil is a three-dimensional infiltration process that achieves steady state rapidly and is described in terms of pressure- and gravity-induced fluxes. The steady flow is affected by weak capillarity assuming semi-infinite, field-saturated flow (i.e., $\varphi_m = 0$). The water head inside the well remains constant. Analytical solutions are described for the estimation of the parameter *C*.
Novak and Soltesz	1984	$i_f = q_0$ $0 \le t \le t_p$ $i_f = K_{s,f} + (q_0 - K_{s,f}) e^{-\beta_1 (t - t_p)}$ $t > t_p$	An empirical method is presented to determine the rate of infiltration into heavy, swelling soils, assuming water infiltrates into heavy soils primarily through the cracks, infiltration through the soil matrix is relatively small, and the geometry of cracks is a function of the water content.
Fok and Chiang	1984	$\mathrm{V} = \left[2x_w d + w z_w + \left(\frac{\pi}{2}\right) x_w z_w\right] l \emptyset \Delta S_e$ Where: $x_w = \left(\frac{2Kh_x}{\emptyset \Delta S_e}\right)^{0.5} t^{0.5}$; $\frac{z_w}{h} - ln\left(1 + \frac{z_w}{h}\right) = \frac{Kt}{\emptyset h \Delta S_e}$	Fok and Chiang estimated the total volume of water infiltrated into the soil from irrigation furrow of depth d (L), width w (L) and thickness l (L), using developed 1-D and 2-D infiltration equations obtained from previous studies (Hansen, 1955; Fok et al., 1982).
Philip	1984a	$i = 0.5\alpha\varphi i^*$ $i^* = -[R(\gamma + \ln(0.5R))]^{-1}$ (1) $i^* = \frac{2}{\pi}(1 + R^{-2/3})$ (2) Where: $\gamma = 0.57722$ and $R = 0.5\alpha r$	Philip analyzed steady 2D infiltration from cylindrical cavities averaged over the whole cavity surface using the dimensionless infiltration rate i^* for very small R (1), and for gravity dominant ($R \to \infty$) (2).
Philip	1984b	$i = \frac{\varphi V^*}{r}$ $V^* = 1$ (1) $V^* = (1 - R)^{-1}$ (2) $V^* = 1 + R$ (3) $V^* = 0.5R + R^{1/3}$ (4) Where: $R = 0.5\alpha r$	Philip analyzed steady 3D infiltration from spherical cavities averaged over the whole cavity surface using the dimensionless infiltration V^* for capillarity dominant ($R \to 0$) (1), very small R (2), small R (3), and for gravity dominant ($R \to \infty$) (4).
Beven	1984	$i = \frac{-(\theta_s - \theta_i) f^* K_i \left(\psi_{wf} + \frac{I}{\theta_s - \theta_i}\right)}{1 - e^{f^* I}}$ $0 \le t \le t_p$	Beven developed an infiltration model based on the Green-Ampt assumptions on a class of non-uniform soils in which saturated hydraulic conductivity decreases as an exponential function of depth z ($K_s = K_i e^{-f^*(\theta_s - \theta_i) z}$).

		$t - t_p = \frac{1}{f^* K_i}\left[\ln(I+C) - \frac{1}{e^{f^* C}}\ln(I+C) + \sum_{m=1}^{\infty}\frac{\{f^*(I+C)\}^m}{m!m} - \lambda\right] \quad t > t_p$ Where: $t_p = \frac{I_p\left(1-e^{f^* I_p}\right)}{-(\theta_s-\theta_i)f^* K_i\left(\psi_{wf}+\frac{I_p}{\theta_s-\theta_i}\right)}$; $C = (\psi_{wf} + h_0)(\theta_s - \theta_i)$; $\lambda = \ln\left(I_p + C\right) - \frac{1}{e^{f^* C}}\left[\ln\left(I_p + C\right) + \sum_{m=1}^{\infty}\frac{\{f^*(I_p+C)\}^m}{m!m}\right]$	
Germann	1985	$i = 0 \quad t < 0$ $c = {b_1}^{1/a_1} i^{(1-1/a_1)} \quad 0 \le t \le T_s$ $i = 0 \quad t > T_s$	Kinematic wave theory [1] was applied to the infiltration of water in the non-capillary macropore system of a porous medium. Water sorbance from the macropores into the matrix was ignored, limiting the approach to nearly saturated porous media. [1]Kinematic wave theory: $\frac{\partial q}{\partial t} + c\frac{\partial q}{\partial z} = 0$ where c (L T^{-1}) is the kinematic wave velocity
Warrick et al.	1985	$I = \frac{(\theta_s - \theta_i)I^*}{\alpha}$ $I^* = A'T^{0.5} + B'T + C'T^{1.5} \quad 0 \le T \le T_g$ $I^* = I_g^* + T - {T_g}^2 \quad T > T_g$ $I_g^* = A'{T_g}^{0.5} + B'T_g + C'{T_g}^{1.5}$; Where: $T = \frac{\alpha K_s t}{\theta_s - \theta_i}$; $T_g = \left(\frac{A'}{1 - K_i/K_s}\right)^2$	A generalized solution to the moisture flow Richards' (1931) equation is developed for vertical infiltration using the solution of Philip (1957a) by applying reduced forms of time, depth, water moisture and infiltration.
Reynolds et al.	1985	$Q_{inf} = \frac{2\pi h_0}{C}(K_s h_0 + \varphi) + \pi r^2 K_s$	The original theory, as presented in Reynolds et al. (1983), is extended to account for the matric effects of the unsaturated soil (the initial suction head, ψ_i (L), and the capillarity of the outer unsaturated envelope, φ (L^2 T^{-1})). By assuming an exponential relationship between $K(\psi)$ and ψ as defined by Gardner (1958): $K(\psi) = K_s e^{\alpha\psi}$, then $\varphi = \int_{\psi_i}^{0} K(\psi)d\psi = \frac{K_s}{\alpha}[1 - e^{\alpha\psi_i}]$. For soils initially at "field capacity" or drier, $e^{\alpha\psi_i} \ll 1$, and thus $\varphi = \frac{K_s}{\alpha}$ (Scotter et al.,1982).
Parlange et al.	1985	$t = \frac{{S_0}^2}{2\delta(1-\delta)(K_s-K_i)^2} ln\left(1 + \delta\frac{(K_s-K_i)}{i-K_s}\right) + \frac{K_s h_0(\theta_s-\theta_i)}{(i-K_s)(K_s-K_i)} -$ $\frac{{S_0}^2+2\delta(1-\delta)K_s h_0(\theta_s-\theta_i)}{2(1-\delta)(K_s-K_i)^2} ln\left(\frac{i-K_i}{i-K_s}\right)$	Parlange et al. extended the work developed under zero surface head condition (Parlange (1982)) to positive head boundary condition for arbitrary diffusivity D (L^2 T^{-1}). δ takes values from 0 to 1, and changes slightly with the type of soil. For heavy clay soils, δ tends to be equal to 1, and for coarse-structured soils, the value of δ decreases below the value of $\delta = 0.8$ or 0.85. For the case of $\delta = 0$, the equation takes the Green and Ampt form.
Chu	1985	Constant rainfall: $I = \theta_c l_c + \theta_{till}(z_w - l_c)$ $\frac{dz_w}{dt} = \frac{K_e}{2\theta_{till}}\left(\frac{z_w+\psi_{wf,till}}{z_w}\right)$ Where: $K_e = \frac{z_w}{\frac{z_w-l_c}{K_{till}}+\frac{l_c}{K_c}}$; $K_c = K_{s,c} + (K_{i,c} - K_{s,c})e^{-CE}$; $C = ln\left(\frac{K_{s,c}}{K_{i,c}-K_{s,c}}\right) B\left(1 - \frac{\varepsilon}{4}\right) E_o$;	The layered Green-Ampt model proposed by Brakensiek and Rawls (1983) was extended to include the effect of non-uniform rainfall of intensity q_0 (L T^{-1}) and crusting energy E (M L^{-1} T^{-2}), as well as the water ponding on the interface between the tilled layer and the subsoil in the infiltration process. A tilled soil profile is assumed to consist of three layers - the surface crust, the tilled layer, and the subsoil, each characterized by specific thickness l (L), hydraulic conductivity K (L T^{-1}), wetting front potential ψ_{fp} (L), and water storage capacity θ (dimensionless). A ponded depth or zone of positive water pressure of thickness

		$E_o = [0.02062 + 0.00379\ln(q_0)]q_0 t_{1/2}$; Variable rainfall: $\frac{dz_w}{dt} = \frac{\frac{z_w + \psi_{wf,till}}{2\theta_{till}}}{\frac{l_c}{K_c} + \frac{z_w - l_c}{K_{till}}}$ $i = \min\left(q_0, \frac{\theta_{till} D_L}{T_s}\right)$ Where: D_L from Eq. (14) in Chu's paper; $K_c = K_{s,c} + (K_{i,c} - K_{s,c})e^{\ln\left(\frac{K_{s,c}}{K_{i,c} - K_{s,c}}\right)B\left(1 - \frac{\varepsilon}{4}\right)\frac{E(t)}{E_o}}$; $E(t) = E_i + [0.02062 + 0.00379\ln(q_0)]q_0 T_s$; Ponding on the interface: $i = \min\left(q_0, \frac{(l_c + l_{till} - l_{interpond})/2}{\frac{l_c}{K_c} + \frac{l_{till} - l_c}{K_{till}}}\right)$	$l_{interpond}$ (L) may exist in the tilled layer above the interface with the subsoil. The Runge-Kutta method was used to conduct the calculations.
Waechter and Philip	1985	$i = 0.5\alpha\varphi i^*$ $i^* = \frac{1}{s}\sum_{n=-\infty}^{\infty}(-1)^n \frac{\mathrm{I_n}}{\mathrm{K_n}}$ $i^* = \frac{2}{\pi}[1 + 0.996R^{-2/3} + 0.02235s^{-4/3} + O(s^{-2})]$; for large s Where: $s = 0.5\alpha r$	Waechter and Philip obtained the asymptotic expansion of the mean infiltration rate i (L T^{-1}) for large s (dominated by gravity, with capillary effects weak but nonzero) from buried circular cylindrical and spherical cavities using a scattering analog. $\mathrm{I_n}$ *and* $\mathrm{K_n}$ *are the modified Bessel functions of the first and second kinds of order* n.
Philip	1985	2D Infiltration: $\vartheta = s\varphi\vartheta^*$ Check Eq. (34) in Philip's paper for ϑ^* $\vartheta = 4\varphi\xi_0$ for large s 3D Infiltration: $Q_{inf} = \varphi s L V^*$ Check Eq. (53) in Philip's paper for V^* $Q_{inf} = \frac{8\pi\varphi}{\alpha}\xi_0$ for large s Where: $\xi_0 = \sum_{n=0}^{\infty} a_n$ and $s = 0.5\alpha L$	Philip analyzed 2D and 3D steady infiltration from cavities of arbitrary size and shape (characteristic length L (L)) using Van de Hulst theorem which connects 2D and 3D infiltration, ϑ (L^2 T^{-1}) and Q_{inf} (L^3 T^{-1}) respectively, to dimensionless "downward wetting function" ξ_0 at large R (i.e., $R \to \infty$).
Philip	1986a	$Q_{inf} = 8\pi\varphi\alpha^{-1}\xi_0(w, s)$ Where: $\xi_0(w, s) = s\sum_{n=0}^{5} a_n(w)s^n + O(s^7)$ for small s Check Eq. (31) to (33e) in Philip's paper for a_n $\xi_0(w, s) = \frac{1}{2}s^2[1 + 1.99230638w^{2/3}s^{-2/3}] + O(s^{-4/3})$ for large s $s = 0.5\alpha u r$ and $w = u * \nu$	Solutions are given for quasilinear 3D steady infiltration from spheroidal cavities of arbitrary aspect ratio ν and radius r (L) into isotropic and anisotropic homogeneous soils where anisotropy is defined by u^2. The isotropic case is simply that of $u^2 = 1$. For prolate spheroids $\nu > 1$, for spheres $\nu = 1$, and for oblate spheroids $\nu < 1$.
Philip	1986b	Buried disc, $Q_{inf} = 8\pi\varphi\alpha^{-1}\xi_0(s)$ Where: $\xi_0(s) = \frac{2s}{\pi}\left[\sum_{n=0}^{7} a_n\left(\frac{\pi}{2}\right)s^n + As^8\right]$ for small s Check Eq. (30) in Philip's paper for a_n with $\phi = \frac{\pi}{2}$ $\xi_0(s) = \frac{1}{2}s^2\left[1 + \frac{1}{s} + \frac{1}{4s^2} - \frac{1}{8s^3} + \frac{1}{16s^4} + \frac{B}{s^5}\right]$ for large s A and B are estimated by matching the two above expansions of $\xi_0(s)$ $s = 0.5\alpha r$	Philip studied steady quasilinear infiltration from buried discs and other sources of radius r (L) by expressing the volumetric infiltration rate Q_{inf} (L^3 T^{-1}) as function of the far-field wetting function ξ_0 and the dimensionless discharge function V^*.

		Circular cylinder, $Q_{inf} = \varphi V^*(s)$ Check Eq. (60) in Philip's paper for $V^*(s)$ Sphere, $Q_{inf} = 4\pi r \varphi V^*(s)$ Check Eq. (65) in Philip's paper for $V^*(s)$	
Kutilek and Krejca	1987	$I = C_1 t^{0.5} + C_2 t + C_3 t^{1.5}$	C_1 is an estimate of sorptivity S, C_2 is an estimate of $(A_2 + K_i)$, and C_3 is an estimate of (A_3 + the truncation error ε). The saturated hydraulic conductivity is: $K_s = (3C_1C_3)^{1/2} + C_2$
Swartzendruber	1987a	$I = K_s t + \frac{(\psi_{wf}+h_0)(\theta_s-\theta_i)K_s}{(K_s-K_i)} \ln\left(1 + \frac{(I-K_i t)(K_s-K_i)}{(\psi_{wf}+h_0)(\theta_s-\theta_i)}\right)$	Using the following expression of the infiltration rate i: $i = K_s\left[\frac{\psi_{wf} + z + h_0}{z}\right] = \frac{d[z(\theta_s - \theta_i)]}{dt} + K_i$ By setting K_i equal to 0, the equation becomes nothing but Green and Ampt equation.
Swartzendruber	1987b	$I = K_s t + \frac{S_H}{A_0}\left(1 - e^{-A_0 t^{0.5}}\right)$	Based on Swartzendruber, Philip's time series solution for $z(\emptyset, t)$ is unaffected by the pressure head condition at the soil surface h_0; each function $[X_1(\theta), X_2(\theta), X_3(\theta) \ldots]$ is still the solution of its own ordinary differential equation that can be solved by relatively numerical methods. A_0 is a fitting parameter depending on the initial water content θ_i. $A_0 = \frac{4K_s}{3S_H}$ (Stroosnijder, 1976). As $A_0 \rightarrow 0$, it reduces to a form of the Philip's model (1957b) with K_s as the coefficient of the linear term.
Broadbridge and White	1988	$I = q_0 t$ $\quad t < \infty$ $I = \lambda_c \Theta_e^{-1}\left[ln\left\{\frac{C(\Theta_e-\Theta)}{\Theta(C-\Theta_e)}\right\} - C^{-1} ln\left\{\frac{\Theta_e(C-\Theta)}{\Theta(C-\Theta_e)}\right\} + R^* t^*\right]$ $\quad t \rightarrow \infty$ Where: $\Theta_e = 2C\rho\left[(1+\rho^{-1})^{\frac{1}{2}} - 1\right]$; $\rho = R^*/m$; $m = 4C(C-1)$; $C = (b_0 - \theta_i)/(\theta_s - \theta_i)$; $\Theta = (\theta - \theta_i)/(\theta_s - \theta_i)$; $t^* = t/T_c$; $R^* = (q_0 - K_i)/K_s$	Broadbridge and White described constant rate rainfall infiltration q_0 (L T^{-1}) in uniform soils and other porous materials. The model is based on Darcy-Buckingham approach to unsaturated water flow and assumes simple functional forms for the soil water diffusivity $D(\theta)$ and hydraulic conductivity $K(\theta)$.
Yeh	1989	$\psi = \frac{1}{\alpha} ln\left\{e^{-\alpha(z_w - \psi_0)} + \frac{i}{K_s} e^{-\alpha z} - \frac{i}{K_s}\right\}$	Analytical solution to one-dimensional, steady state infiltration in heterogeneous soils is developed, only valid for $\psi \leq 0$. Yeh integrated Buckingham equation $q = -K(\psi)\left(\frac{\partial \psi}{\partial z} + 1\right)$ using the exponential model by Gardner (1958) which describes the unsaturated hydraulic conductivity by $K(\psi) = K_s e^{\alpha\psi}$.
Reynolds and Elrick	1990	$Q_{inf} = \frac{r}{G}(K_s h_0 + \varphi) + \pi r^2 K_s$	Reynolds and Elrick derived the steady-state infiltration by summing the steady flow out of the ring due to hydrostatic pressure of the ponded water in the ring and capillarity of the unsaturated flow, and the steady flow out of the ring due to gravity. The depth of the water ponding inside the ring remains constant. For ponding depths ranging from 5 to 25 cm, G factor in can be approximated by the average shape factor, Ge, of an infiltrometer, for different textured soils equal to: $Ge = 0.316(d/r) + 0.184$; Wooding's solution (1968) may be considered when H = 0 and G = 0.25.

Haverkamp et al.	1990	$t = \frac{{S_0}^2 - 2\psi_{str}K_s(\theta_s-\theta_i)}{2\delta(1-\delta)(K_s-K_i)^2} ln\left(1+\delta\frac{(K_s-K_i)}{i-K_s}\right) + \frac{K_s(h_0+\psi_{str})(\theta_s-\theta_i)}{(i-K_s)(K_s-K_i)} - \frac{[{S_0}^2 - 2\psi_{str}K_s(\theta_s-\theta_i)]+2\delta(1-\delta)K_s(h_0+\psi_{str})(\theta_s-\theta_i)}{2(1-\delta)\Delta K^2} ln\left(\frac{i-K_i}{i-K_s}\right)$	The infiltration equation of Parlange et al. (1985) is improved in such a way that it applies equally well for infiltration and capillary rise. This new equation considers the possibility of an infinite diffusivity near saturation. One can set $\delta = 1$ for all practical purposes (Barry et al., 1995).
Smith	1990	$i = \frac{K_s G}{I}$ $t < t_p$ $I_p = \int_{\theta_i}^{\theta_s}(\theta-\theta_i)\frac{D(\theta)}{q_0-K(\theta)}d\theta$ $t = t_p$ $i = K_s\left(\frac{G}{I}+1\right)$ $t > t_p$ (1) $i = K_s\frac{e^{I/G}}{e^{I/G}-1}$ $t > t_p$ (2) Where: $G = (\psi_{wf}+h_0)(\theta_s-\theta_i)$ (1) $G = \frac{S_H^2}{2K_s}$ (2)	The resulting analytic expressions relate the infiltration rate i (L T^{-1}) to infiltrated cumulative water I (L). This type of expression is uniquely general in describing the decay of i with I for either saturation or flux boundary conditions, and in describing the onset of ponding for flux boundary conditions (i.e., $t < t_p$, $t = t_p$ and $t > t_p$). Specific cases are for D (L^2 T^{-1}) following a step function (1) or D (L^2 T^{-1}) and $dK/d\theta$ (L T^{-1}) are closely proportional (2) (Smith and Parlange, 1978)). This study explored the applicability of this theory when the soil profile is composed of two layers. The behavior of the layered system exhibits the same unifying $i(I)$ response to flux boundary conditions as does a homogeneous profile, which lends unexpected generality to the I-based analytical infiltration mode.
Schmid	1990	$I = \int_0^{t_p} q_0(t)dt + q_{0,i}(t-t_p) + K_s(q_{o,p}-q_{0,i})\frac{(\psi_{wf}+h_0)(\theta_s-\theta_i)}{(q_{o,p}-K_s)^2}\left\{\left[1+2\frac{(q_{o,p}-K_s)^2}{K_s(\psi_{wf}+h_0)(\theta_s-\theta_i)}(t-t_p)\right]^{0.5}-1\right\}$ Where: $\int_0^{t_p}[q_0(t)-q_{0,i}]dt = K_s\frac{(\psi_{wf}+h_0)(\theta_s-\theta_i)}{(q_{o,p}-K_s)}$	Based on Mein and Larson (1973), an explicit equation for time-dependent cumulative infiltration following ponding was proposed in this paper considering time-varying rainfall intensity $q_0(t)$ (L T^{-1}).
Ankeny et al.	1991	$Q_{inf} = K_s e^{\alpha\psi}\left[\pi r^2 + \frac{4r}{\alpha}\right]$	Wooding's equation is rewritten assuming: • No water ponding occurs inside the ring • Exponential relationship between $K(\psi)$ and ψ as defined by Gardner (1958): $K(\psi) = K_s e^{\alpha\psi}$ • The ratio $K(\psi)/\varphi(\psi)$ is equal to the constant parameter α
Swartzendruber and Hogarth	1991	$I = \frac{I^* S_0^2}{K_s}$ $I^* = n^{-1}\left[1-e^{-\alpha t^{*0.5}}\right] + t^*$ Where: $n = \frac{\alpha}{(1+p)^{0.5}}$; $\alpha = \frac{A_0 S_0}{K_s}$; $p = \frac{S_H^2}{S_0^2}$ and $t^* = \frac{K_s^2 t}{S_0^2}$	Swartzendruber and Hogarth developed a new three-parameter infiltration equation based on Swartzendruber's equation (1987b) to describe the effect of soil-surface-ponded water head, h_0 (L), on the cumulative quantity of water infiltrated into the soil with time.

Philip	1992	$\frac{[1-(\theta_s-\theta_i)]\overline{K}}{(\theta_s-\theta_i)}t = \frac{I}{(\theta_s-\theta_i)} - \left(\frac{\psi_{wf}+h_0}{1-(\theta_s-\theta_i)}\right) ln\left(1+\frac{[1-(\theta_s-\theta_i)]I}{(\psi_{wf}+h_0)(\theta_s-\theta_i)}\right)$ $h_0 \neq cst$ $\frac{\overline{K}}{(\theta_s-\theta_i)}t = \frac{I}{(\theta_s-\theta_i)} - (\psi_{wf}+h_0) ln\left(1+\frac{I}{(\psi_{wf}+h_0)(\theta_s-\theta_i)}\right)$ $h_0 = cst$	Philip develops the solution for falling-head infiltration, which takes precisely the same functional form as that for constant ponded depth; only the values of the constants change.
White et al.	1992	$i = K_s + \frac{4bS_0^2}{(\theta_s-\theta_i)\pi r}$ $h_0 \leq 0$ $i = K_s + \frac{4bS_H^2}{(\theta_s-\theta_i)\pi r}$ $h_0 > 0$	White et al. combined the early-time transient and steady flow phases to estimate three-dimensional infiltration. The parameter b is constrained to $0.5 \leq b \leq \pi/4$. A typical "average" value for b is 0.55 (White and Sully, 1987).
Barry et al.	1993	$t = \frac{I}{K_s} - \alpha^* \ln\left(1+\frac{I}{\alpha^* K_s}\right)$ Where: $\alpha^* = \frac{{S_0}^2}{2K_s^2}$ no ponding ($h_0 \leq 0$) Or $\alpha^* = \frac{{S_H}^2}{2K_s^2}$ under ponding ($h_0 > 0$)	Barry et al. expressed the cumulative infiltration in terms of the Lambert *W*-function as $I = -\alpha^* K_s\left[1+W\left(-e^{-1-\frac{t}{\alpha^*}}\right)\right]$. As such, the new infiltration solution was derived, which has the general form of the Green and Ampt (1911) law without requiring a sharp wetting front. The saturated soil surface can be either ponded or not.
Fonteh and Podmore	1993	$V = \left[2x_w d + wz_w + \left(\frac{\pi}{2}\right)x_w z_w\right] l(\theta_s-\theta_i)$ (1) $V = \left[2(d+z_c)x_{w,max} + wz_w + \left(\frac{\pi}{2}\right)x_{w,max}(z_w-z_c)\right] l(\theta_s-\theta_i)$ (2) Where: $i_c = \frac{K_s(\psi_{wf}+h_0+z_c)}{z_c}$	Fonteh and Podmore developed a simple two-dimensional infiltration model for rectangular furrows for depth d (L), width w (L), and thickness l (L), based on the Green and Ampt equation and Fok and Chiang (1984) assuming the cumulative infiltrated volume is divided into two parts: before the wetting fronts meets (1) and after they meet (2). After the fronts meet, it is assumed that the region of two-dimensional flow shifts downwards due to vertical downward infiltration I_c (L) estimated using Green and Ampt (1911).
Smith et al.	1993	$0 < t \leq t_h$ (1) $i = q_0$ $t \leq t_p$ $K_s(t-t_p)(1-\delta) = (I-I_p) - \frac{(\theta_s-\theta_i)G(\theta_i,\theta_s)}{(K_s-K_i)} ln\left(\frac{e^{\delta I'/(\theta_s-\theta_i)G(\theta_i,\theta_s)}-1+\gamma}{e^{\delta I'_p/(\theta_s-\theta_i)G(\theta_i,\theta_s)}-1+\gamma}\right)$ $t > t_p$ Where: $I' = I - K_i t$, $G(\theta_i,\theta_s) = \frac{S(\theta_i,\theta_s)^2}{2K_s} = \frac{S_H^2}{2K_s}$ and $\gamma = \frac{\delta K_s}{(K_s-K_i)}$ $I = I_h + (q_0-K_i)(t-t_h)$ $t_h < t \leq t_n$ (2) $K_s(t-t_p)(1-\delta) = (I-I_p) - \frac{(\theta_s-\theta_n)G(\theta_i,\theta_n)K_s}{(K_s-K_n)} ln\left(\frac{F_G(I)-1+\gamma}{F_G(I_p)-1+\gamma}\right)$ $t > t_n$ (3) Where: $F_G(I) = e^{\frac{\delta(I-I_n)'}{G(\theta_s-\theta_n)}}$, $(I-I_n)' = I - I_n - K_n(t-t_n)$ and $\gamma = \frac{\delta K_s}{K_n-K_i}$	The main purpose of this paper is to propose a simple conceptual model of rainfall infiltration which continuously describes the infiltration/redistribution/infiltration cycle. Smith et al. considered three sequential periods of time, with the first (1), assuming an initial rainfall pattern having $q_0 > K_s$, lasting to a time t_h, which at some time $t_p < t_h$ causes ponding. The infiltration model (1) is based on the three-parameter analytic model of Parlange et al. (1982), extended to treat soils with very high initial water content θ_i. Then, during any significant interval within a storm in which q_0 (L T^{-1}) falls below i (L T^{-1}) at some time $t > t_h$ (t_h = time of hiatus) (2), $\theta_0 < \theta_s$. In this case, the redistribution model is based on profile extension with shape similarity defined by the scale factor $\mathcal{B}$, originally called β, and a shape factor, p. The similarity condition would be satisfied by a rectangle ($\mathcal{B} = 1$) which distorts in time, or the quadrant of an ellipse $\left(\mathcal{B} = \frac{\pi}{4}\right)$. After the rainfall hiatus (posthiatus period), q_0 (L T^{-1}) is assumed to increase at a time $t > t_n$ causing a second ponding (3). A secondary wetting profile of accumulated water $(I-I_n)' = I -$

			$I_n - K_n(t - t_n)$ advances alongside the earlier profile computed at $\theta_0 = \theta_n$ with $\mathcal{B} = 1$. A correction to $G(\theta_n, \theta_s)$ for $\beta < 1$ was also incorporated.
Philip	1993	Constant rainfall rate $q_0(t)$: $I = (\theta_s - \theta_i)[z(t) - z_0]$ $t < t_\infty$ To calculate $z(t)$, check Eq. (17), (20), and (26) in Philip's paper $i = 0.5\overline{K}[1 - (\theta_s - \theta_i)]\left[1 + \left\{1 + \frac{4q_0(\theta_s - \theta_i)}{\overline{K}[1-(\theta_s-\theta_i)]^2}\right\}^{0.5}\right]$ $t \to t_\infty$ Variable rainfall rate q_0(t): $I = (\theta_s - \theta_i)[z(t) - z_0]$ To calculate $z(t)$, differentiate with respect to time t: $q_0(t) = \frac{(\theta_s - \theta_i)}{\overline{K}}\frac{d}{dt}\left(z\frac{dz}{dt}\right) - [1 - (\theta_s - \theta_i)]\frac{dz}{dt}$	Philip established the study of the effect of excess rainfall, ponded without runoff, on the dynamics of infiltration into a deep homogeneous soil using Green and Ampt, or delta function, approximation under constant and variable rainfall rates.
Stone et al.	1994	$I = (\psi_{wf} + h_0)\Delta\theta\left(t^* + \sqrt{2t^*} - 0.2987t^{0.7913}\right)$ Where: $t^* = \frac{K_s}{(\psi_{wf}+h_0)\Delta\theta}t$	Stone et al. developed an explicit approximation of the Green-Ampt equation (one-stage infiltration) by rewriting it in the form of Philip's equation.
Mandal and Waechter	1994	$i = 0.5\alpha\varphi i^*$ $i^* = \frac{1}{s}\sum_{n=-\infty}^{\infty}(-1)^n\frac{\mathrm{I_n}}{\mathrm{K_n}}$ Top half: $i^* = \frac{2}{\pi}(0.69953s^{-2/3})$ Bottom half: $i^* = \frac{2}{\pi}(1 + 0.30066s^{-2/3})$ Semicircular trench: $i^* = \frac{4}{\pi}(1 + 0.69953s^{-2/3})$ Where: $s = 0.5\alpha r$	Mandal and Waechter obtained the separate contributions to the mean infiltration rate i (L T^{-1}) from the top and the bottom halves of the buried circular cylinders of radius r (L). I_n *and* K_n *are the modified Bessel functions of the first and second kinds of order* n.
Fallow et al.	1994	$I = \left[2(\theta_s - \theta_i)K_s h_0 + \frac{(\theta_s - \theta_i)\varphi}{b}\right]^{0.5} t^{0.5}$	Fallow et al. presented an analytical equation for determining early-time, transient, and one-dimensional infiltration under both, constant head, and falling-head conditions, in low-permeability soils, not significantly perturbed by gravitational effects. The parameter b is constrained to $0.5 \leq b \leq \pi/4$. A typical "average" value for b is 0.55 (White and Sully, 1987, White et al., 1992).

Basha	1994	$Q_{inf} = \frac{4K_s V^*}{\alpha^2}$ 2D shallow ditch: $V^* = \frac{2a^*}{1-b^*}$ 3D shallow pond: $V^* = \frac{2\pi a^* s}{(1-b^*)(2-b^*)}$ Where: $s = 0.5\alpha r$	The Green's function method was used to derive a general analytical model which can handle multidimensional steady infiltration problems in a semi-infinite medium with arbitrary boundary conditions and root uptake forcing functions and for various simple source geometries. Two special kinds of boundary conditions were considered in this work, 2D shallow ditch, and 3D shallow pond of radius r (L).
Salvucci and Entekhabi	1994	$I = K_s\left\{\left(1-\frac{\sqrt{2}}{3}\right)t + \left(\frac{\sqrt{2}}{3}\right)(\chi t + t^2)^{0.5} + \left(\frac{\sqrt{2}-1}{3}\right)\chi[ln(t+\chi) - ln(\chi)] + \left(\frac{\sqrt{2}}{3}\right)\chi\left[ln\left(t+\frac{\chi}{2}+(\chi t+t^2)^{0.5}\right) - ln\left(\frac{\chi}{2}\right)\right]\right\}$ Where $\chi = \frac{(\psi_{wf}+h_0)\Delta\theta}{K_s}$	An explicit expression for Green-Ampt cumulative infiltration is presented for any soil type definition and all times using Philip's time series solution (Philip,1957a).
Corradini et al.	1994	$I' = I - K_i t$ $I' - \frac{I'^2}{2(q_0-K_i)(\theta_0-\theta_i)}\frac{d\theta_0}{dt} = \frac{(\theta_0-\theta_i)G(\theta_i,\theta_0)K_s}{\delta K_0} ln\left(1+\frac{\delta K_0}{q_0-K_0}\right)$ (1) $(q_0 - K_i - K_{0*})I' = \mathcal{B}q_0 K_s(\theta_{0*}-\theta_i)G(\theta_i,\theta_{0*})$ (2) Where: $G(\theta_i,\theta_0) = \frac{1}{K_0}\int_{\theta_i}^{\theta_0} D(\theta)d\theta$	Corradini et al. extended the conceptual model earlier developed by Smith et al. (1993) towards further generality treating an arbitrary sequence of rainfall rates. They included the representation of a sequence of infiltration/redistribution cycles with situations of infiltration not leading to soil surface saturation (i.e., $t < t_p$) (1), and wetting profile reshaping under reduced rainfall rates (i.e., $q_0 < i$) (2). Corradini et al. used a slightly modified version of Parlange et al. (1985) model for description of increases in the surface water content (1) and the Smith et al. (1993) redistribution equation for decreases (2). Equation (1) gives the limited case of soil surface saturation (Smith et al., 1993) for $\theta_0 = \theta_s$ and $\frac{d\theta_0}{dt} = 0$. In Equation (2), the evolution of θ_{0*} will be estimated by Runge-Kutta integration of (1). p is a shape factor (Smith et al., 1993) approaching 1 for q_0 (L T^{-1}) near K_s (L T^{-1}). $\pi/4 \leq \mathcal{B} \leq 1$ (Smith et al., 1993).
Smettem et al.	1994	$I = I_{1D} + \frac{\sqrt{0.3}\pi r {S_0}^2 t}{(\theta_s-\theta_i)}$	Smetten et al. developed an analytical expression for three-dimensional unsteady, unconfined, gravity-free flow out of a disc infiltrometer from one-dimensional confined infiltration.
Haverkamp et al.	1994	1D Infiltration: $\frac{2(K_s-K_i)^2}{{S_0}^2}t = \frac{2}{1-\beta}\frac{(K_s-K_i)(I-K_i t)}{{S_0}^2} - \frac{1}{1-\beta} ln\left[\frac{1}{\beta}e^{2\beta\frac{(K_s-K_i)(I-K_i t)}{{S_0}^2}} + \frac{\beta-1}{\beta}\right]$ (1) $I = S_0 t^{0.5} + \frac{2-\beta}{3}K_s t$ (2) 3D Infiltration: $I = I_{1D} + \frac{\gamma {S_0}^2 t}{r\Delta\theta}$ $I = S_0 t^{0.5}$ very short t $I = S_0 t^{0.5} + \left[\frac{2-\beta}{3}(K_s-K_i) + K_i + \frac{\gamma {S_0}^2}{r(\theta_s-\theta_i)}\right]t$ short t $I = \left(K_s + \frac{\gamma {S_0}^2}{r(\theta_s-\theta_i)}\right)t + \frac{1}{2(1-\beta)} ln\left(\frac{1}{\beta}\right)\frac{{S_0}^2}{(K_s-K_i)}$ steady state	(1) Parlange's equation is redefined such that δ is replaced by new dimensionless constant β. (2) Haverkamp's equation (1) is simplified into two-term approximate expansion, for short infiltration times and K_i close to zero. β ranges between 0.3 and 1.7 for sand to silty soils (Lassabatere et al., 2009, Rahmati et al., 2019). $\beta = 0.6$ is an average value. A 3D cumulative infiltration, I_{3D}, from a disk source, is related to 1D cumulative infiltration, I_{1D}, particularly for water infiltration experiments that make use of disk or ring infiltrometers. An average value of 0.75 can be used for γ (Haverkamp et al., 1994, Lassabatere et al., 2006).

Barry et al.	1995	$I^* = (I - K_i t)\frac{2(K_s - K_i)}{{S_0}^2 + 2K_s h_0(\theta_s - \theta_i)}$ Where: $I^* = t^* + 1 - \gamma^* - exp\left(-\frac{\sqrt{2t^*}}{1+\frac{\sqrt{2t^*}}{6}} - \frac{2t^*}{3}\right) + \frac{\gamma}{1+t^*}\left\{exp\left(-\frac{2t^*}{3}\right)\left[1 - (1-\gamma)^8 {t^*}^{\frac{5}{2}}\right] + (2\gamma + t^*) ln\left(1 + \frac{t^*}{\gamma}\right)\right\}$; $t^* = \frac{2(K_s - K_i)^2}{{S_0}^2 + 2K_s h_0(\theta_s - \theta_i)} t$; $\gamma = \frac{2K_s(h_0 + \psi_{str})(\theta_s - \theta_i)}{{S_0}^2 + 2K_s h_0(\theta_s - \theta_i)}$	Barry et al. transformed the implicit infiltration formula presented by Haverkamp et al. (1990) into an explicit infiltration equation, which improved the applicability of the approach in both the short- and long-term limits.
Elrick et al.	1995	$I = \frac{\mathrm{A}_{pond}}{\mathrm{A}}[h_0 - h(t)]$	One-dimensional infiltration experiments conducted in the laboratory using undisturbed soil cores have been analyzed using numerical inversion procedures of a finite solution of Richards' equation. For falling-head conditions, the cumulative infiltration is a function of the ponded head $h(t)$, the cross-sectional area of the infiltrating surface, A (L^2), and that of the falling head tube, A_{pond} (L^2).
Sommer and Mortensen	1996	$I = [1 + s(0)]S_0 t^{0.5}$ $\theta'(\chi) = \frac{\theta \mu {S_0}^2}{2D(\theta)}[l(\chi) - s(\chi)]$ Where: $\chi = \frac{x - x_0}{S_0 t^{0.5}}$ $l'(\chi) = -\frac{\theta'(\chi)}{\theta}[l(\chi) - s(0) - \chi]$; $s'(\chi) = \frac{\theta'(\chi)}{(1-\theta)}[s(\chi) - s(0) - \chi]$ under pressure liquid Or $s'(\chi) = \frac{\theta'(\chi)}{3(1-\theta)}[s(\chi) - s(0) - \chi]$ under hydrostatic pressure	Using mixture theory, Sommer and Mortensen treated unidirectional infiltration of an initially dry deformable porous medium under constant liquid pressure, assuming the porous medium goes from completely dry to fully saturated (slug-flow assumption) and neglecting gravity and inertial forces. To solve for S_0 (L $T^{-0.5}$) and the dimensionless water content, liquid, and solid velocities, $\theta(\chi)$, $l(\chi)$, and $s(\chi)$ respectively, Sommer and Mortensen set the following boundary conditions: $\theta = \theta_i$ at $\chi = 0$ $\theta = \theta_s$ at $\chi = 1$ $l(1) = 1 + s(0)$ $s(1) = [1 + s(0)]\frac{\theta_s - \theta_c}{1 - \theta_s}$ Where θ_c (L^3 L^{-3}) the water content of the porous material immediately ahead of the infiltration front at time t. A simpler limiting case is obtained if there is no capillary pressure drop across the infiltration front, then, $\theta_c = \theta_s$ and therefore $s(1) = 0$.
Srivastava et al.	1996	$I = \alpha'(\theta_s - \theta_i)(\psi_{wf} + h_0)\emptyset^{[\beta' + \delta' \ln(\emptyset)]}$ Where: $\emptyset = \frac{K_s(t - t_p + t_S)}{(\theta_s - \theta_i)(\psi_{wf} + h_0)}$	Srivastava et al. developed an explicit equation to the modified Green-Ampt equation presented by Mein and Larson (1973) to represent cumulative infiltration at any time t greater than ponding time.
Preziosi et al.	1996	1D Infiltration: $\rho_{solid}\phi_{solid}\left(\frac{\partial v_{solid}}{\partial t} + v_{solid}\frac{\partial v}{s}\partial x\right) = -\frac{\mu}{k}[v_{solid} - C(t)] + \frac{\partial \sigma}{\partial x} - \phi_{solid}(\rho_{solid} - \rho_{liquid})g$ 3D Infiltration: Eqs. (1), (7) and (9) in Preziosi et al.'s paper	Preziosi et al. presented a mathematical model for unidirectional infiltration of an incompressible liquid into an initially deformable porous material assuming slug-flow in the absence of inertial forces. The quantity $C(t)$ depends on how the liquid constituent is pushed into the porous medium. The simplest case is when we are completely able to govern the inflow, for instance, we are able to steadily push liquid into the porous medium, which means *C(t)* = const. A more interesting situation for determining $C(t)$ arises in Eq. (23) in Preziosi et al.'s paper.
Corradini et al.	1997	$0 \le t < t_1$ $I = \int_0^t (q_0 - K_i)\, dt$ $t < t_p$ $I_p = \int_0^{t_p} (q_0 - K_i)\, dt = \frac{\Delta\theta G(\theta_i, \theta_s) B p K_s}{q_0 - K_s}$ $t = t_p$ $i = K_s + \frac{(\theta_s - \theta_i) G(\theta_i, \theta_s) B p K_s}{I - K_i t}$ $t > t_p$	A relatively simple conceptual model for infiltration during complex rainfall sequences is presented as a reformulation of an analytically derived model developed earlier by Smith et al. (1993) and Corradini et al. (1994) in a more homogeneous version suitable for hydrologic applications. During the first rainfall period ($0 \le t \le t_1$), infiltration and redistribution rates are described

		Where: $G(\theta_i,\theta_s)=\frac{1}{K_s}\int_{\theta_i}^{\theta_s}D(\theta)d\theta$ $i_1=\left(-\frac{1}{\mathcal{B}}\frac{d\mathcal{B}}{d\theta_0}-\frac{1}{\theta_0-\theta_i}\right)(I_1-K_it_1)\frac{d\theta_0}{dt}-K_i$ $t=t_1$ $\frac{d\theta_0}{dt}=\frac{(\theta_0-\theta_i)\mathcal{B}(\theta_0)}{[I-K_i(t-t_1)]\left[(\theta_0-\theta_i)\frac{d\mathcal{B}(\theta_0)}{d\theta_0}+\mathcal{B}(\theta_0)\right]}\left\{q_0-K_0-\frac{\mathcal{B}(\theta_0)pK_0(\theta_0-\theta_i)G(\theta_i,\theta_0)}{I-K_i(t-t_1)}\right\}$ $t>t_1$ if $q_0\le i_1$ $\frac{d\theta_0}{dt}=\frac{(\theta_0-\theta_1)\mathcal{B}(\theta_0)}{[I-I_1-K_1(t-t_1)]\left[(\theta_0-\theta_1)\frac{d\mathcal{B}(\theta_0)}{d\theta_0}+\mathcal{B}(\theta_0)\right]}\left\{q_0-K_0-\frac{\mathcal{B}(\theta_0)pK_0(\theta_0-\theta_1)G(\theta_1,\theta_0)}{I-I_1-K_1(t-t_1)}\right\}$ $t>t_1$ if $q_0>i_1$	prior to and during the rainfall hiatus, respectively. As for parameters, p approaches 1 near K_s (L T^{-1}) and $\pi/4\le\mathcal{B}\le 1$ (Smith et al., 1993; Corradini et al., 1994). Explicit relations for $\mathcal{B}$ and p were given as follows: $\mathcal{B}=c_1\frac{\theta_0-\theta_i}{\theta_s-\theta_r}+c_2$, $\mathcal{B}p=f(q_0/K_s)$, and $\mathcal{B}p=c_3$ (during redistribution), where c_1, c_2, and c_3 are constants to be determined, (q_0/K_s) is an implicit function through which the variation of the profile shape with q_0/K_s expressed in terms of values of p and $\mathcal{B}$ is invariant with time during redistribution. After a limited period of redistribution, a new rainfall period (post-hiatus, $t>t_1$) produces re-infiltration into the soil. If $q_0\le i_1$, the reinfiltrating water is approximately distributed through the whole dynamic profile. If $q_0>i_1$, re-infiltration creates a new $\theta(z,t)$ profile in a soil with fictitious initial water content $\theta(0,\ t_1)=\theta_1$ and initial hydraulic conductivity $K_i(t=t_1)=K_1$.
Parlange et al.	1997	For a linear soil, $I=2\sqrt{t/\pi}+\frac{t}{2}+O\left(t^{\frac{3}{2}}\right)$ short times $I=1+t-\left(1+\frac{t}{2}\right)erf\left(\frac{\sqrt{t}}{2}\right)+\sqrt{t/\pi}e^{-t/4}$ long times For a near- linear soil, $t=I-2/3\ln\left(1+\frac{3I}{2}\right)$ short times $I=2\sqrt{t/3}+\frac{2t}{3}+O\left(t^{\frac{3}{2}}\right)$ long times	A general approximation for the solution[2] to the one-dimensional Richards equation is presented for arbitrary soil properties and boundary conditions, exact for short times, in general, and for all times as D approaches a delta function. The approximation becomes increasingly accurate for "linear" and "near-linear" soils. [2] $2M=\frac{q_0}{\theta_0D_0}-\frac{d\theta_0}{dt}\frac{1}{q_0-K_s}$ Where: M (L^{-1}) is an unknown function of time.
Wu and Pan	1997	$i=i_c\left[a+b\left(\frac{t}{T_c}\right)^{-0.5}\right]$ Where: $i_c=fK_s$; $T_c=\frac{\Delta\theta\lambda_c}{K_s}$; $f=\frac{h_0+\lambda_c}{d+r/2}+1$	Wu and Pan developed a scaling method for axisymmetric, three-dimensional infiltration from a single ring infiltrometer, which resulted in a generalized solution to infiltration that can be applied to different soil conditions and ring geometry using two dimensionless parameters, a and b. The essential part of this method was to model the macroscopic capillary length, λ_c(L), the sorptive time, T_c(T) and the parameter i_c (L T^{-1}) used to scale the infiltration rate. λ_c(L) is defined as being equal to the matric flux potential, φ(L^2 T^{-1}), scaled by K_s (L T^{-1}): $\lambda_c=\varphi/K_s$. a and b were determined through curve-fitting to be approximately equal to 0.91 and 0.17, respectively.
Wang et al.	1997	Without air compression: $t=\frac{\emptyset(1-S_{e_i}-S_{e_{air}})}{K_s}\left[\frac{I}{\emptyset(1-S_{e_i}-S_{e_{air}})}-(\psi_{wf}+h_0)ln\left(1+\frac{I}{\emptyset(1-S_{e_i}-S_{e_{air}})(\psi_{wf}+h_0)}\right)\right]$ With air compression: $t=\frac{\emptyset(1-S_{e_i}-S_{e_{air}})}{k_{rc}K_s}\left[\frac{I}{\emptyset(1-S_{e_i}-S_{e_{air}})}-(\psi_{wf}+h_0+h_{af})ln\left(1+\frac{I}{\emptyset(1-S_{e_i}-S_{e_{air}})(\psi_{wf}+h_0+h_{af})}\right)\right]$	One-dimensional infiltration was derived on the basis of the Green and Ampt (1911) assumptions (infiltration process is isothermal, the porous medium is homogeneous, and the wetting front is sharp) by including the term h_{af} (L), air pressure immediately below the wetting front, to account for air entrapment effects. When soil air is not compressed during infiltration ➔ $h_{af}=0$.
Enciso-Medina et al.	1998	Zone (1): $i=\left(\frac{B+l_{seal}+(\psi_{wf}+h_0)}{\frac{l_{seal}}{K_{seal}}+\frac{B}{K_{till}}}\right)$ $z\le l_{seal}+l_{till}$ $i=\left(\frac{C+l_{seal}+l_{till}+(\psi_{wf}+h_0)}{\frac{l_{seal}}{K_{seal}}+\frac{l_{till}}{K_{till}}+\frac{C}{K_{seal}}}\right)$ $z>l_{seal}+l_{till}$ Where:	To simulate the effects of surface sealing, soil cracking, and initial soil water content, Enciso-Medina et al developed a model for a three-layered soil system consisting of a surface seal of thickness l_{seal} (L), a tillage layer of thickness l_{till} (L), and the subsoil. The portion of the soil profile that receives water during infiltration is represented by three zones. The first zone (1) is directly below the wetted furrow and only involves vertical one-dimensional infiltration predicted using Green-Ampt method for vertical flow. Enciso-Medina et al. assumed that the time required to wet the seal is

		$B = \frac{I - l_{seal}\Delta\theta}{\Delta\theta_{till}}$; $C = \frac{I - l_{seal}\Delta\theta_{seal} - l_{till}\Delta\theta_{till}}{\Delta\theta}$; Zone (2): $i = \frac{\psi_{wf} + h_0}{\frac{x_{seal}}{K_{seal}} + \frac{x_w - x_{seal}}{K_{till}}}$ Zone (3): $\vartheta = \left[2x_w d + wz_w + \left(\frac{\pi}{2}\right)x_w z_w\right]\Delta\theta t$	negligible; therefore, infiltration starts when the wetting front reaches the bottom of the seal, l_{seal} (L). Thus, the infiltration rate was predicted when the wetting front is withing the tillage layer *($l \le l_{seal} + l_{till}$)* or extends into the subsoil *($l > l_{seal} + l_{till}$)* The second zone (2) represents one-dimensional horizontal flow of water through the sides of the wetted furrow using Green-Ampt method for horizontal infiltration. The third zone (3) is represented by a semielliptical shape that connects the corners of the first two zones predicting quasi-two-dimensional infiltration ϑ (L^2 T^{-1}) for a rectangular furrow based on the model by Fok and Chiang (1984).
Philip	1998	$I = S_{0,c}t^{0.5}$ small t $I = \int_0^{l_c}(\theta_c - \theta_{c,i})dz + \int_{l_c}^{\infty}(\theta - \theta_i)dz$ intermediate t $I = K_s t$ large t	Quasi-analytic methods are used to analyze ponded infiltration into crusted soils for both small and large times and a good approximation for intermediate times is anchored at both ends by these results. Philip (1998) assumed a uniform soil of initial water content, θ_i (L^3 L^{-3}) and saturated hydraulic conductivity K_s (L T^{-1}) lying underneath the crusted soil of initial water content $\theta_{c,i}$ (L^3 L^{-3}).
Smith et al.	1999	$0 \le t < t_{crust}$ $q_0 = \frac{dI_1}{dt} + K_{1,i}$ $t \le t_p$ $0 = \frac{(\theta_{1,s} - \theta_{1,i})\mathcal{B}_1(\theta_s)[q_0 - K_{1,s} - (\theta_{1,s} - \theta_{1,i})\mathcal{B}_1(\theta_s)p_1 G_1(\psi_i, 0)K_{1,s}/I_1]}{I_1[(\theta_{1,s} - \theta_{1,i})\gamma_1 + \mathcal{B}_1(\theta_s)]}$ $t > t_p$ Where: $G_1(\psi_i, \psi_0) = \frac{1}{K_s}\int_{\psi_i}^{\psi_0} K(\psi)d\psi$ and $\gamma_1 = \frac{d\mathcal{B}_1}{d\theta_0}$ $t \ge t_{crust}$ $\frac{d\psi_c}{dt} = \frac{1}{P(\psi_0, \psi_c, t)}\left\{K_0 + \frac{G_1(\psi_c, \psi_0)K_{1,s}}{l_c} - K_{2,c} - \frac{\mathcal{B}_2(\theta_{2,c})p_2(\theta_{2,c} - \theta_{2,i})K_{2,s}G_2(\psi_i, \psi_c)}{I - l_c[\theta_{1,c} - \theta_{1,i} + \alpha_1(\theta_0 - \theta_{1,c})] - K_{2,i}t}\right\}$ Where: $P(\psi_0, \psi_c, t)$ from Eq. (22) in Smith et al.'s paper $G_2(\psi_i, \psi_c) = \frac{1}{K_s}\int_{\psi_i}^{\psi_c} K(\psi)d\psi$, $\theta_{1,c} = \theta_1(l_c)$, $\theta_{2,c} = \theta_2(l_c)$, $K_{2,c} = K_2(l_c)$, $\gamma_2 = \frac{d\mathcal{B}_2}{d\theta_{2,c}}$	Smith et al. proposed a relatively simple analytical/conceptual model for infiltration in crusted soils treating the crust (1) as a single layer of thickness l_c (L) overlaying the subsoil (2) where the upper layer is always the most restrictive, i.e., $K_{1,s} < K_{2,s}$. Cumulative dynamic infiltration comprises that in the crust layer I_1 (L) plus that in the subsoil I_2 (L). For $t < t_{crust}$, $\theta(z)$ evolves within the crust layer, and cumulative infiltration in the crust upper layer is described by the model for homogeneous soils developed earlier (Smith et al., 1993; Corradini et al., 1994, 1997). For $t \ge t_{crust}$, the dynamic water content in the crust is expressed as fraction α_1 associated with the surface and the remaining $(1 - \alpha_1)$ associated with the interface. Also, for $t \ge t_{crust}$, the previous model is extended in order to represent the effects of water flow in the subsoil, I_2 (L), but with the upper boundary at the crust-subsoil interface. The system of equations may be solved by a standard Runge-Kutta method. Explicit relations for $\mathcal{B}$ and p were given by Corradini et al. (1997): $\mathcal{B}_1(\theta_0) = 0.6\frac{\theta_0 - \theta_{1,i}}{\theta_{1,s} - \theta_{1,r}} + 0.4$, $\mathcal{B}_1 p_1 = 0.98 - 0.87e^{-q_0/K_{1,s}}$, and $\mathcal{B}_1 p_1 = 1.7$ (during redistribution). A constant value of 0.86 is assumed for α_1 (originally called α).
Selker et al.	1999a	$i = (\theta_s - \theta_i)\frac{dz_w}{dt}$ $i = \frac{-3K_i(\beta^*\psi_{wf} - 1)}{z_w^2\beta^{*2}}$ (1) $i = K_i\beta^*\left(\frac{2n^* - 1}{n^*}\right)\left[\frac{\psi_{wf}\left(1 - \frac{\beta^*}{n^*}z_w\right)^{-n^*} - z_w}{1 - \left(1 - \frac{\beta^*}{n^*}z_w\right)^{1-2n^*}}\right]$ (2) $i = \frac{2\beta^* K_i\left(\psi_{wf}e^{\beta^* z_w} - z_w\right)}{1 - e^{2\beta^* z_w}}$ (3)	Selker et al. developed three expressions for the time rate of infiltration using Green and Ampt approach for soils with hydraulic properties (K_s (L T^{-1}) and ψ_{wf} (L)) decreasing with depth following linear (1), power law (2), and exponential (3) relationships. (1) $K_s(z) = K_i\beta^{*-2}z^{-2}$; $\psi_{wf}(z) = \psi_{wf,0}\beta^* z$ (2) $K_s(z) = K_i\left(1 - \frac{\beta^* z}{n^*}\right)^{2n^*}$; $\psi_{wf}(z) = K_i\left(1 - \frac{\beta^* z}{n^*}\right)^{-n^*}$ (3) $K_s(z) = K_i e^{-2\beta^* z}$; $\psi_{wf}(z) = \psi_{wf,0}e^{\beta^* z}$
Wu et al.	1999	$I = afK_s t + 2bfK_s(T_c t)^{0.5}$ short t $I = afK_s t + c$ steady state Where: $T_c = \frac{(\theta_s - \theta_i)\lambda_c}{K_s}$;	Wu et al. integrates the generalized equation in Wu and Pan (1997) for early-, transient- and steady-state infiltration behavior.

		$f = \frac{h_0+\lambda_c}{d+r/2} + 1$	
Novak et al.	2000	$\frac{\partial\theta}{\partial t} = \frac{\partial}{\partial z}\left[K(\psi)\left(\frac{\partial\psi}{\partial z}+1\right)\right] - s_r + s_f$ where: $s_f = \left(K_{s,h}\frac{\psi_{wf,m}+h_0}{z_w}\right)\mathrm{A}_f$ and $z_w = \sqrt{2K_{s,h}\frac{\psi_{wf,m}+h_0}{(\theta_s-\theta_i)}T_s}$	Novek et al. developed an infiltration model for swelling, cracked fine-textured soils that permits changes in the dimensions of the cracks during the infiltration process. The extended Richards' equation by Feddes et al. (1988) was solved, subject to three upper boundary conditions were considered: (1) unsaturated soil surface, (2) soil surface is saturated and a sub-critical surface layer *($h \le h_{0,max}$)* is being formed, and (3) surface water layer reaches its maximum and water flows into cracks. $i_m = -K_m(\psi)(\partial\psi/\partial z + 1)$ $h < 0$ (1) $i_m = \partial\psi/\partial t - K_{s,m}(\partial\psi/\partial z + 1)$ $0 \le h \le h_{0,max}$ (2) $i_m = i_f - K_{s.m}(\partial\psi/\partial z + 1)$ $h > h_{0,max}$ (3)
Corradini et al.	2000	$0 \le t < t_{crust}$ $q_0 = \frac{dI_1}{dt} + K_{1,i}$ $t \le t_p$ $i = K_{1,s} + \frac{(\theta_{1,s}-\theta_{1,i})G_1(\psi_i,0)\mathcal{B}_1(\theta_s)p_1K_{1,s}}{I_1}$ $t > t_p$ Where: $G_1(\psi_i,0) = \frac{1}{K_s}\int_{\psi_i}^{0} K(\psi)d\psi$ $t \ge t_c$ $I = \left[\alpha_1(\theta_0-\theta_{1,i}) + (1-\alpha_1)(\theta_{1,c}-\theta_{1,i})\right]l_c + I_2 + K_{2,i}t$ Where: I_2 from Eq. (20) in Corradini et al.'s paper $P_L(\psi_c,t)$ from Eq. (19) in Corradini et al.'s paper $\theta_{1,c} = \theta_1(l_c)$, $\theta_{2,c} = \theta_2(l_c)$, $K_{1,c} = K_1(l_c)$ and $K_{2,c} = K_2(l_c)$	Corradini et al. proposed an analytical/conceptual model, which is formulated by an extension of the Smith et al. (1999) model, for the solution of the infiltration and reinfiltration problem into any horizontal two layered soil where either layer may be less permeable under any real rainfall pattern. The model represents both the infiltration rate i (L T^{-1}), cumulative infiltration I (L T^{-1}), and soil water potentials ψ_0 and ψ_c (L) at the surface and the interface, respectively. For $0 \le t < t_c$, the solution is that of the vertically homogeneous case described by Corradini et al. (1997). As to the parameters incorporated in the system, α_1 (originally called α) is considered to be a constant, while $\mathcal{B}_2$ and p_2 are given, by analogy with the relations by Corradini et al. (1997) and Smith et al., (1999): $\mathcal{B}_2(\theta_{2,c}) = 0.6\frac{\theta_{2,c}-\theta_{2,i}}{\theta_{2,s}-\theta_{2,r}} + 0.4$, $\mathcal{B}_2 p_2 = 0.98 - 0.87e^{-v_{12}/K_{2,s}}$, Where $v_{12} = \frac{G_1(\psi_c,\psi_0)K_{1,s}}{l_c} + K_{1,c}$ and $\mathcal{B}_2 p_2 = 1.7$ (during redistribution). In case of re-infiltration following redistribution from a rainfall hiatus, Corradini et al. (2000) adopted the same concept proposed by Corradini et al. (1997).
Swartzendruber	2000	$I = K_s t + E\ln\left(1 + \frac{(I-K_i t)}{E}\right)$ $E = \frac{{S_H}^2}{2(K_s-K_i)}$;	Using the following expression of the infiltration rate i: $i = K_s\left[\frac{\psi_{wf}+z_w+h}{z_w}\right] = \frac{d[z_w(\theta_s-\theta_i)]}{dt} + K_i$ where the head $h_0(t)$ at the soil surface increases with time *t* according to: $h_0(t) = h_0 + p(t)$ such that $p(t) = \frac{S_H(K_s-K_i)t^{1/2}}{2K_s(\theta_s-\theta_i)}$
Govindaraju et al.	2001	Constant rainfall: Local-scale Infiltration: $i = q_0$ $0 \le t \le t_p$ $i = \frac{(\psi_{wf}+h_0)(\theta_s-\theta_i)+I}{I}$ $t > t_p$ Field-scale Infiltration:	Govindaraju et al. studied the problem of field-scale infiltration over soils where spatial variability of saturated hydraulic conductivity K_s (L T^{-1}) is represented by a homogeneous correlated lognormal random field $Y = ln(K_s)$ with mean σ_Y and standard deviation μ_Y. The cumulative infiltration, I (L) (symbolized as F in the paper), was used as an independent variable to develop expressions for the averaged field-scale infiltration under both constant and time-dependent rainfall

		$I = q_0 t$ $\quad 0 \le t \le t_p$ $t > t_p$ $I = I_p + \sqrt{2K_s(\psi_{wf}+h_0)(\theta_s-\theta_i)}\left(t^{\frac{1}{2}} - t_p^{\frac{1}{2}}\right) + \frac{2}{3}K_s(t-t_p) +$ $\frac{1}{18}\left(\frac{2K_s^3}{(\psi_{wf}+h_0)(\theta_s-\theta_i)}\right)^{1/2}(t^{3/2} - t_p^{3/2})$ Where: $t_p = I_p/q_0$ and $I_p = \frac{K_s\psi_{wf}(\theta_s-\theta_i)}{q_0-K_s}$ Time-dependent rainfall: Local-scale Infiltration: $t = \frac{I-I_i}{q_0} + t_i$ $\quad 0 \le t < t_p$ $t > t_p$ $t = t_i - \left(\frac{(\psi_{wf}+h_0)(\theta_s-\theta_i)+I_i}{q_0}\right) + \frac{1}{K_s}\left[I - (\psi_{wf}+h_0)(\theta_s-\theta_i)\ln\left(I +\right.\right.$ $\left.\left.(\psi_{wf}+h_0)(\theta_s-\theta_i)\right)\right] + \frac{(\psi_{wf}+h_0)(\theta_s-\theta_i)}{K_s}\ln\left(I_p + (\psi_{wf}+h_0)(\theta_s-\theta_i)\right)$ Where: $t_p = \frac{K_s\psi_{wf}(\theta_s-\theta_i)}{q_0(q_0-K_s)} - \frac{I_i}{q_0} + t_i$ and $I_p = I_i + q_0(t_p - t_i)$ Field-scale Infiltration: $\bar{\imath} = q_0[1-\mu_\Omega] + \left\{1 + \frac{(\psi_{wf}+h_0)(\theta_s-\theta_i)}{I}\right\}G(K_c, 1)$ Where: $t = t_i - \frac{I}{q_0}(1-\mu_\Omega) - \frac{I_i}{q_0} + \left[I + (\psi_{wf}+h_0)(\theta_s -\right.$ $\left.\theta_i)\ln\left(\frac{(\psi_{wf}+h_0)(\theta_s-\theta_i)}{I+(\psi_{wf}+h_0)(\theta_s-\theta_i)}\right)\right]G(K_c,-1) + (\psi_{wf}+h_0)(\theta_s-\theta_i)\sum_{i=1}^{\infty}\frac{G(K_c,i)}{(1+i)q_0^{i+1}}$ $G(K_c, \xi)$ from Eq. (7), K_c from Eq. (14) and μ_Ω from Eq. (16) in Govindaraju et al.'s paper.	rates. However, Govindaraju et al. also developed an explicit expression for the field-scale infiltration rate at any given time t (T) under continuously ponded conditions of constant rainfall q_0 (L T^{-1}) (Green and Ampt, 1911).
Serrano	2001	$I = I_0(t) + a ln\left[\frac{I_0(t)+a}{I_p+a}\right]\left[\frac{I_0(t)+a}{I_0(t)}\right] - \frac{a}{2}ln^2\left[\frac{I_0(t)+a}{I_p+a}\right]\left[\frac{I_0(t)+a}{I_0^3(t)}\right] +$ $\frac{a}{3}ln^3\left[\frac{I_0(t)+a}{I_p+a}\right]\left\{\frac{[I_0(t)+a]^2}{I_0^5(t)}\right\} - \cdots$ Where: $a = (\psi + h_0)(\theta_s - \theta_i)$	Serrano developed an explicit solution of Green and Ampt infiltration equation by constructing a decomposition series, valid for deep homogeneous soils under ponding conditions resulting from intense rainfall events.
Corradini et al.	2002	$\bar{\imath} = q_0[1 - prob(K_s \le K_c)] + \sum_{j=1}^{3}\left(1 + \frac{(\psi_{wf}+h_0)(\theta_s-\theta_i)}{I^*}\right)\left[G\left(K_j\right) - G\left(K_{j-1}\right)\right]$ (1) Where: $I^* = \overline{K_J}\left(\frac{(\psi_{wf}+h_0)(\theta_s-\theta_i)}{q_0} + t\right) + 4\sqrt{\overline{K_J}}\left((\psi_{wf}+h_0)(\theta_s -\right.$ $\left.\theta_i)\right)^{0.00022\psi_{wf}}\left(t - \frac{(\psi_{wf}+h_0)(\theta_s-\theta_i)\overline{K_J}}{q_0(q_0-\overline{K_J})}\right)^{0.5}$; $G\left(K_j\right) = \int_0^{K_j} K f_{K_s}(K)dK$ and $K_c = \frac{q_0 I}{I+(\psi_{wf}+h_0)(\theta_s-\theta_i)}$ $\bar{I} = I_p\left(1 - \frac{K_{se}}{q_0}\right) + K_{se}T_s + \psi_{wf}(\theta_s-\theta_i)\ln\left(\frac{I-(\psi_{wf}+h_0)(\theta_s-\theta_i)}{I_p-(\psi_{wf}+h_0)(\theta_s-\theta_i)}\right)$ (2) Where: $I_p = \frac{K_{se}\psi_{wf}(\theta_s-\theta_i)}{q_0-K_{se}}$; $t_p = \frac{\overline{K_s}\psi_{wf}(\theta_s-\theta_i)}{q_0(q_0-\overline{K_s})}$; $K_{se} = \overline{K_s}\left\{0.89 - 0.0831 ln\mathrm{CV}(K_s) - 0.8e^{(0.429\mathrm{CV}(K_s)-1.629)\frac{T_s}{t_p}}\right\}$;	Two models for estimating expected areal-average infiltration rate, $\bar{\imath}$ (L T^{-1}), at the hillslope scale were presented, under the condition of a negligible infiltration of surface water running downslope (run-on process) into soils. The soil is vertically homogeneous but the saturated hydraulic conductivity K_s (L T^{-1}) is assumed as a lognormally distributed random variable with PDF, $f_{K_s}(K)$, characterized by its mean value $\overline{K_s}$ and coefficient of variation $\mathrm{CV}(K_s)$. The first model (1) assumes that the areal-average infiltration is partly rainfall-controlled, and partly soil-controlled. It was developed based on the formulation of the field-scale infiltration rate for a given realization of K_s and following Govindaraju et al. (2001). The second model (2) incorporates the run-on process and is based on an empirical approach that uses an effective saturated hydraulic conductivity K_{se} (L T^{-1}), derived for each specific rainfall event of duration T_s (T).

Elrick et al.	2002	$I = S_H t^{1/2} + 1/3 K_s t$ $\quad 0 \le t \le t_c$ $t = t_c - \frac{(\theta_s-\theta_i)}{CK_s}\left\{\frac{I-I_c}{(\theta_s-\theta_i)} - \frac{h_0+\psi_{wf}}{C} ln\left(\frac{(h_0+\psi_{wf})+CI(\theta_s-\theta_i)}{(h_0+\psi_{wf})+CI_C(\theta_s-\theta_i)}\right)\right\}$ $\quad t > t_c$ Where: $C = 1$ Constant head $C = 1 - \frac{(\theta_s-\theta_i)}{R};\ R = \frac{A_{pond}}{A}$ Falling head	Elrick et al. used the GA approach to deduce a new implicit equation for constant- and falling-head conditions by using the term R (Elrick et al., 1995) which is the ratio of the cross-sectional area of the falling head tube, A_{pond} (L^2), to the infiltrating surface, A (L^2).
Parlange et al.	2002	$I = \frac{S_0^{\ 2}}{2K_s}\left\{t^* + \frac{1}{1-\delta} ln\left[1 + \frac{1-\delta}{\delta}\sqrt{1-f}\right]\right\}$ Where: $t^* = \frac{S_0^{\ 2}}{K_s^2}$; $f = e^{\left\{-2\delta^2 t\left[\frac{1+A\sqrt{2t}+2Bt}{1+C\sqrt{2t}+2Bt\sqrt{2\delta}}\right]^2\right\}}$; $A = \frac{1}{2} + \frac{\lambda-2\delta}{3}$; $B = \frac{1+\sqrt{2\delta}}{12}\left(\frac{4\lambda-11\delta}{3}+1\right)$; $C = \frac{1}{6} + \frac{\lambda}{3}$; $\lambda = \frac{35}{17}\delta - \frac{3}{2}\delta^{1/4} e^{\left(\frac{-15}{4}\sqrt{\delta}\right)}$	Parlange et al. developed an explicit approximation to Parlange's equation (1982) assuming an initially dry, homogeneous soil where the surface of the soil is saturated, but not ponded. δ varies between 0 (Green and Ampt, 1911) and 1 (Talsma and Parlange, 1972). Average value $\delta = 0.8$ or 0.85 (Parlange et al., 1985, Haverkamp et al., 1990).
Warrick et al.	2005	$I = (\theta_s - \theta_i) z$ $\frac{K_s(t-t_i)}{(\theta_s-\theta_i)} = z - z_i - (\psi_{wf} + h_i) ln\left(\frac{z+\psi_{wf}+h_i}{z_i+\psi_{wf}+h_i}\right)$ $t_i \le t \le t_{i+1},\ i = 0,1, \ldots$	Cumulative infiltration was computed as a function of time-varying ponded water depths h_i (L) using a Green and Ampt analysis; the ponded depth h_i (L) changes stepwise with time.
Weiler	2005	$I_m = \frac{1}{2}\frac{b^{1/3}}{(\theta_s-\theta_i)} + \frac{1}{2}\frac{a}{b^{1/3}} + \frac{1}{2} r_f$ Horizontal I Where: $a = (\theta_s - \theta_i) r_f^2$; $b = r_f(\theta_s - \theta_i)^2\left[12c - a + 2\sqrt{6c(6c-a)}\right]$; $c = K_{s,m}(\psi_{wf,m} + h_0)$ $\frac{dI_m}{dt} = K_{s,m}\left(\frac{\psi_{wf,m}+h_0}{I_m}+1\right)$ Vertical I	Weiler developed an infiltration model which combines macropore flow variability to model dual- permeability soils using analytical solutions of the Green-Ampt equation which serve as the basis for the model.
Govindaraju et al.	2006	$\bar{\imath}$ from Eqs. (9) and (13) in Govindaraju et al.'s paper. Where: $F_c = \frac{I}{I+(\psi_{wf}+h_0)(\theta_s-\theta_i)}$ and $G_{K_s}(K_1, \xi) = \int_0^{K_1} K^{\xi} f_K(K) dK$	A semi-analytical model estimating the areal-average infiltration rate at hillslope scale was presented, which neglects the infiltration of surface water running downslope into pervious soils (run-on process). It accounts for spatial heterogeneity of the saturated hydraulic conductivity, K_s (L T^{-1}), and rainfall rate, q_0 (L T^{-1}). The K_s field is characterized by a lognormal probability density function with PDF, $f_{K_s}(K)$, characterized by its mean value $\overline{K_s}$ and coefficient of variation $CV(K_s)$, while the rainfall rate q_0 (symbolized as r in the paper) is represented by a uniform distribution between two extreme values, r_{min} and $r_{min} + R$. The model formulation relies upon the use of cumulative infiltration (symbolized as F in the paper) as the independent variable which is expressed as function of time for use in practical applications.
Morbidelli et al.	2006	$\bar{\imath} = \frac{1}{A}\int_{A_1}\int_t \left(q_0 - \frac{s^{1/2}}{\varepsilon_{Manning}}\frac{\partial h^{5/3}}{\partial x}\right) dA_1 + \int_{A_2}\int_t i\, dA_2$	Morbidelli et al. explored the role of spatial heterogeneity, in both the saturated hydraulic conductivity K_s (L T^{-1}) and rainfall intensity q_0 (L T^{-1}), on the integrated hydrological response of a natural slope. On this basis, Morbidelli et al.

		$i = K_s + \frac{K_s(\theta_s - \theta_i)(\psi_{wf} + h_0)}{I}$	(2006) developed a model which estimates the areal-average infiltration rate $\bar{\imath}$ (L T^{-1}) in the plane area A (L^2), partly controlled (over the unsaturated area A_1 (L^2)) by the rainfall and run-on, and partly controlled by the soil (saturated area A_2 (L^2)).
Lassabatere et al.	2006	$I = S_0 t^{0.5} + \left[A(1-B){S_0}^2 + Bi_\infty\right]t$ small t $I = (AS^2 + K_s)t + C\frac{S^2}{K_s}$ large t Where: $A = \frac{\gamma}{r(\theta_s - \theta_i)}$; $B = \frac{2-\beta}{3}\left[1 - \left(\frac{\theta_i}{\theta_s}\right)^n\right] + \left(\frac{\theta_i}{\theta_s}\right)^n$; $C = \frac{1}{2\left[1-\left(\frac{\theta_i}{\theta_s}\right)^n\right](1-\beta)} ln\left(\frac{1}{\beta}\right)$; $i_\infty = A{S_0}^2 + K_s$	Lassabatere et al. adopted the BEST approach; this latter uses the following equation developed in Haverkamp et al. (1994): $I = S_0 t^{0.5} + \left[A{S_0}^2 + BK_s\right]t$ for short times and expresses an equivalent equation by replacing the hydraulic conductivity K_s (L T^{-1}) by the formula of the steady-state infiltration rate i_∞. $\beta \approx 0.6$ and $\gamma \approx 0.75$, which applies for most soils when $\theta_i < 0.25\theta_s$ (Smettem et al., 1994, Haverkamp et al., 1994).
Chen and Young	2006	Steady rainfall $p(t)$: $i = q_0 cos(\gamma_0)$ $t \le t_p$ $K_s\left[t - \left(t_p - t_s\right)\right]cos(\gamma_0) = I - \frac{(\psi_{wf}+h_0)(\theta_s-\theta_i)}{cos(\gamma_0)} ln\left[1 + \frac{Icos(\gamma_0)}{(\psi_{wf}+h_0)(\theta_s-\theta_i)}\right]$ $t > t_p$ Unsteady rainfall $p(t)$: Detailed derivation is presented in the paper's appendix.	Chen and Young quantified and explained the effects of slope angle γ_0(degrees) on infiltration into homogeneous and isotropic soils by extending the Green-Ampt equation onto sloping surfaces. For the steady rainfall case, the infiltration rate is determined by the rainfall intensity q_0 (L T^{-1}) before ponding (i.e., $t \le t_p$) and is calculated using the GA model after ponding (i.e., $t > t_p$). For unsteady rainfall, detailed derivation is presented in the appendix.
Warrick and Lazarovitch	2007	$I = I_{1D} + \frac{\gamma S_0^2 t}{w(\theta_s - \theta_i)}$ $i = K_s + \frac{\gamma S_0^2}{w(\theta_s - \theta_i)}$ $t \to \infty$	Warrick and Lazarovitch addressed two-dimensional infiltration from water strip sources of width w (L) on the soil surface. The assumption is that when the cumulative infiltration is expressed per unit area of the wetted strip, the difference of that value and one-dimensional infiltration is linear with time.
Warrick et al.	2007	$\frac{I}{W^*} = I_{1D} + \frac{\gamma S_0^2 t}{W(\theta_s - \theta_i)}$ $i = W^* K_s + \frac{W^* \gamma S_0^2}{W(\theta_s - \theta_i)}$ $t \to \infty$	Warrick addressed infiltration from furrows or narrow channels of wetted perimeter W (L). The basic approach was to develop the two-dimensional infiltration I (L) as a combination of the corresponding one-dimensional vertical I_{1D} (L) and an edge effect. Also, a simplified expression was found for the limiting steady-state case, which is analogous to Wooding's equation for infiltration from a shallow pond. Haverkamp et al. rationalized that a reasonable bound on γ was 0.6–0.8, but the results of Warrick and Lazarovitch (2007) for the strip showed generally a wider range from 0.6 to 1.1.
Assouline et al.	2007	$i = q_0(t)$ $t \le t_p$ $i = i_{cap}(I_{cap})$ $t > t_p$	A simple accurate method was presented to study infiltration under variable intensity rainfall. Before ponding ($t \le t_p$), infiltration rate is equal to the rainfall rate. After ponding ($t > t_p$), the infiltration rate i_{cap} (L T^{-1}) is a unique function of cumulative infiltration I_{cap} (L). Many mathematical expressions can be readily adapted to represent available i_{cap} [e.g., Green and Ampt, 1911; Kostiakov, 1932; Horton, 1940; Philip, 1957a; Smith and Parlange, 1978; Parlange et al., 1999].
Germann et al.	2007	$i = 0$ $t < t_w(z)$ $i = b_R\theta_R^3$ $t_w(z) \le t \le t_d(z)$ $i = b_R\theta_R^3\left(\frac{t_d(z)-T_s}{t-T_s}\right)^{3/2}$ $t > t_d(z)$ Where: $t_w(z) = \frac{z}{b_R\theta_R^2}$; $t_d(z) = T_s + \frac{t_w(z)}{3}$	German et al. introduced a rivulet of conductance b_R (L T^{-1}) modeled as Stokes flow assuming steady and gravity-driven flow in which the effects of capillarity on infiltration are negligible, while viscous momentum dissipation impedes it.

Essig et al.	2009	$\bar{\imath}z_w = cos\gamma_0 \overline{K} z_w - \frac{\psi_{wf}}{(1-n)}\left(K_i S_i^{-1/\lambda} - \overline{KS}^{-1/\lambda}\right)$	Essig et al. developed a simplified 1-D sharp-front model for sloping surfaces of slope angle γ_0 (degrees) using the Brooks and Corey (1964) relationship in combination with Darcy's law (1856), applicable for different boundary conditions: concentration (constant water content at the soil surface), flux (constant rainfall rate at the soil surface), and constant pressure head.
Valiantzas	2010	$I = S_0 t^{1/2} + \frac{K_s}{2} t + \frac{K_s^2}{8S_0} t^{3/2}$ no ponding $I = S_H t^{1/2} + \frac{K_s}{2} t + \frac{K_s^2}{8S_H} t^{3/2}$ ponding	A simple mathematical form of an infiltration equation is developed using the two-algebraic equation (Philip, 1975b), which applies for the complete time range.
Su	2010	$I = S_0 t^{\beta_4/2} + At$	A new equation of 1D cumulative infiltration into swelling soils is derived from the fractional Fokker–Planck equation (fFPE) of flow in swelling porous media, following the form of Philip's two-parameter infiltration equation (Philip, 1957b).
Corradini et al.	2011	$K_{1,s} < K_{1,h}$ $q_0 = \frac{dI_1}{dt} + K_{1,i}$ $t \le t_p < t_{crust}$ $I_1 = I_{1,p} + \sqrt{2K_{1,s}G_1(\psi_i,\psi_0)}\left[t^{1/2} - t_p^{1/2}\right] + \frac{2}{3}K_{1,s}\left[t - t_p\right] +$ $\frac{1}{18}\left[\frac{2K_{1,s}^3}{(\theta_{1,s}-\theta_{1,i})G_1(\psi_i,\psi_0)}\right]^{1/2}\left[t^{3/2} - t_p^{3/2}\right]$ $t_p < t < t_{crust}$ $i = K_{1,s}\left[1 + \frac{G_1(\psi_c,0)}{l_c}\right]$ $t \ge t_{crust}$ Where: $I_{1,p} = \left[1 + \frac{\mathcal{B}_1 p_1 K_{1,s}(\theta_{1,s}-\theta_{1,i})G_1(\psi_i,0)}{q_0 - K_{1,s}}\right]$; $t_p = I_{1,p}/q_0$; $K_{1,h} = \frac{q_0}{\frac{p_1 G_1(\psi_i,0)}{l_c}+1}$; $G_1(\psi_i,0) = \frac{1}{K_{1,s}}\int_{\psi_i}^{\psi_0} K_1(\psi)d\psi$; $K_1(\psi) = K_{1,s}\left[1 + \left(\frac{\psi - d_1}{\psi_{1,str}}\right)^{c_1}\right]^{-\frac{(3n+2)}{c_1}}$ $K_{1,s} \ge K_{1,h}$ (i.e., $t_p > t_{crust}$) $i = q_0$ $t \le t_p$ $i = K_{1,s}\left[1 + \frac{G_1(\psi_c,0)}{l_c}\right]$ $t > t_p$ $t_p = (1.5 - S_{2i})^{0.7}\left(2.5K_{2,s}\right)^{0.12}(25 + 0.4l_c)q_0^{-(1+1.5/l_c{}^{0.5})}$ Where: $S_{2i} = \frac{\theta_{2,i}-\theta_{2,r}}{\theta_{2,s}-\theta_{2,r}}$; $G_1(\psi_c,0) = \left(\frac{4}{5}n - 1.7\right)\left(\psi_{1,str} + d_1\right)\left(1 - e^{-\frac{\psi_c}{\psi_{1,str}}}\right)$ for $\psi_c \le 0$ $G_1(\psi_c,0) = -\psi_c$ for $\psi_c > 0$	A simple conceptual model was proposed for local infiltration into a two-layered soil profile with the upper layer much more permeable than the subsoil under any rainfall pattern. It is a reformulation of a conceptual model of Corradini et al. (2000). First, the maximum value, $K_{1,h}$ (L T^{-1}), of the saturated hydraulic conductivity of the upper soil, $K_{1,s}$ (L T^{-1}) (i.e., $K_{1,s} < K_{1,h}$) yields the ponding time t_p (T) while the dynamic wetting front is entirely within the upper layer. Then, when the front extends into the lower layer ($t \ge t_{crust}$) and $\theta_{1,c}$ is rather close to $\theta_{1,s}$, it is assumed that $K_{1,c} \approx K_{1,s}$ and $d\psi_c/dt$ negligible because $d\psi_1/\theta_1 \to 0$ as $\theta_1 \to \theta_{1,s}$. Then, parameterized forms for the time when the wetting front reaches the interface, for time to ponding t_p (T) associated with ($K_{1,s} \ge K_{1,h}$) is determined.
Swamee et al.	2012	$I = (\psi_{wf} + h_0)(\theta_s - \theta_i)[1.94(t^*)^{0.74} + (t^*)^{1.429}]^{0.7}$ (1) $I = (\psi_{wf} + h_0)(\theta_s - \theta_i)[2.66(t^*)^{1.124} + (t^*)^{2.174}]^{0.46}$ (2) Where: $t^* = \frac{K_s}{(\psi_{wf}+h_0)(\theta_s-\theta_i)}t$	Based on Green-Ampt (1911) and Talsma-Parlange (1972) implicit equations, Swamee et al. proposed the respective explicit expressions (1) and (2) derived from the interpolation technique of the curve-fitting, for determining cumulative infiltration. The main difference between the Green–Ampt and Talsma–Parlange assumptions is that (1) considers a soil which has a rapidly varying diffusivity D (L^2 T^{-1}) and a near-constant hydraulic conductivity $K = K_s$ (L T^{-1}) while (2) assumes that D and $\partial K/\partial\theta$ are proportional.
Govindaraju et al.	2012	Local-scale Infiltration: $I = q_0 t$ $0 \le t \le t_p$ $A\left(I^3 - I_p^3\right) + B\left(I^2 - I_p^2\right) + C\left(I - I_p\right) + Dln\frac{I + \Delta\psi\Delta\theta}{I_p + \Delta\psi\Delta\theta} = P(t - t_p)$ $t > t_p$	Govindaraju et al. studied the problem of local- and field-scale infiltration over a particular class of heterogeneous soils with the dimensionless parameter a_3 (originally called a) governing the non-uniformity in the saturated hydraulic conductivity K_s (L T^{-1}). At the local scale, the theory for infiltration refers to vertically nonuniform soils (K_s (L T^{-1}) decreasing with depth according to a power law) and is developed using a sharp front (Green–Ampt) approach. To

		Where: $A = 1/3$; $B = \Delta\theta/2(3a_4 - \Delta\psi)$; $C = (\Delta\psi\Delta\theta)^2 - 3a_4\Delta\psi\Delta\theta^2 + 3(a_4\Delta\theta)^2$; $D = -(\Delta\psi\Delta\theta)^3 + 3a_4\Delta\psi^2\Delta\theta^3 - 3a_4^2\Delta\psi\Delta\theta^3$; $P = 3(a_4\Delta\theta)^2 K_{s,0}$ $t_p = I_p/p$ and $p = \frac{3(a_4\Delta\theta)^2 K_s(I_p + \Delta\psi\Delta\theta)}{I_p^3 + 3a_4\Delta\theta I_p^2 + 3(a_4\Delta\theta)^2 I_p}$ Field-scale Infiltration: $\bar{\imath} = q_0[1 - G(K_c, 0)] + \frac{3(a_4\Delta\theta)^2(I + \Delta\psi\Delta\theta)}{I^3 + 3a_4\Delta\theta I^2 + 3(a_4\Delta\theta)^2 I} G(K_c, 1)$ Where: I from Eqs. (12) and (13), $G(K_c, \xi)$ from Eq. (9) and K_c from Eq. (10) $\Delta\psi = \psi_{wf} + h_0$ and $\Delta\theta = \theta_s - \theta_i$	determine field-scale infiltration properties, the spatial variability in the surface saturated hydraulic conductivity is represented by a log-normal random field $Y = ln(K_{s,0})$ with mean μ_Y and standard deviation σ_Y.
Ali et al.	2013	$I = (\psi_{wf} + h_0)(\theta_s - \theta_i)\left[\sqrt{\frac{F_1 K_s}{(\psi_{wf} + h_0)(\theta_s - \theta_i)} t + F_2} + F_3\right]$	By replacing the logarithmic term of the GA model by sequential segmental second order polynomials, Ali et al. (2013) developed a generalized explicit model for estimation of cumulative infiltration, varying the length of wetting front, z_w(L). The universal values of the model's coefficients change with different ranges of $z_w/(\psi_{wf} + h_0)$.
Almedeij and Esen	2014	$I = \psi_{wf}(\theta_s - \theta_i)\left(0.65t^* + \sqrt{0.25{t^*}^2 + 2t^*}\right)$ $0 \le t \le t_p$ Where: $t^* = \frac{K_s}{\psi_{wf}(\theta_s - \theta_i)} t$ $I = (\psi_{wf} + h_0)(\theta_s - \theta_i)\left\{\frac{1}{2}\left(t^* + \sqrt{(t^*)^2 + 8t^*}\right) + 0.15t^*\right\}$ $t > t_p$ Where: $t^* = \frac{K_s}{(\psi_{wf} + h_0)(\theta_s - \theta_i)} t$; $t_p = \frac{K_s \psi_{wf}(\theta_s - \theta_i)}{i_p(i_p - K_s)}$	A proposed explicit modification for the infiltration model (Mein and Larson, 1973) is presented for the case when steady rainfall rate is less than the initial infiltration capacity of the soil until ponding time $(0 \le t \le t_p)$. After ponding $(t > t_p)$, the cumulative infiltration will follow the classical Green-Ampt model; the designated equation and that suggested by Li et al. (1976) are similar, but the equation here imposes an additional term of $0.15t^*$. This additional term accounts for the remaining components of the first order approximation of the power series expansion of the natural log in GA equation.
Bautista et al.	2014	$I(t_i) = I(t_{i-1}) + \Delta Z_2(t_i) + \Delta E(t_i)$ Eqs. (5)-(9) for $\Delta Z_2(t_i)$ in Bautista et al.'s paper. Eq. (11) for $\Delta E(t_i)$ in Bautista et al.'s paper.	This article discussed a methodology, derived from the two-dimensional Richards equation, for estimating two-dimensional furrow infiltration for time-variable surface flow depth h_0(t). The method was originally derived assuming a constant pressure head at the infiltrating surface by Warrick et al. (2007).

Lassabetere et al.	2014	$I = w_f I_f + (1 - w_f) I_m$ $\frac{2\Delta K_m}{{S_{0,m}}^2} t = \frac{1}{1-\beta_m}\left[\frac{2\Delta K_m}{{S_{0,m}}^2}\left(I_m - K_{i,m}t\right) - ln\left(\frac{e^{\frac{\beta_m 2\Delta K_m}{{S_{0,m}}^2}\left(I_m - K_{i,m}t\right)} + \beta_m - 1}{\beta_m}\right)\right]$ and $\frac{2\Delta K_f}{{S_{0,f}}^2} t = \frac{1}{1-\beta_f}\left[\frac{2\Delta K_f}{{S_{0,f}}^2}\left(I_f - K_{i,f}t\right) - ln\left(\frac{e^{\frac{\beta_f 2\Delta K_f}{{S_{0,f}}^2}\left(I_f - K_{i,f}t\right)} + \beta_f - 1}{\beta_f}\right)\right]$ $I_{3D} = w_f\left(I_{1D,f} + \frac{\gamma_f {S_{0,f}}^2}{r\Delta\theta_f}t\right) + (1 - w_f)\left(I_{1D,m} + \frac{\gamma_m {S_{0,m}}^2}{r\Delta\theta_m}t\right)$ Where: $\Delta K = K_s - K_i$ and $\Delta\theta = \theta_s - \theta_i$	Lassabetere et al. assumed that infiltration into the dual-permeability medium may be derived from infiltration into individual single-permeability domains, i.e., the matrix and the fast-flow region, while assuming that there is no water transfer between the two pore regions. As such, infiltration fluxes into the dual-permeability medium are simply a linear combination of fluxes into individual regions, with the proportionality coefficients corresponding to the fractions of surface occupied by each region. Lassabetere et al. further developed a three-dimensional water infiltration equation from a circular disk source into dual-permeability media assuming surface pressure head $h_0 \leq 0$.
Vatankhah	2015	$I = (\psi_{wf} + h_0)(\theta_s - \theta_i)\left(t^* + 2.693ln\left[1 + 0.527\sqrt{t^*}\right]\right)$ Where: $t^* = \frac{K_s}{(\psi_{wf}+h_0)(\theta_s-\theta_i)}t$	Vatankhah developed an explicit expression by further modifying Almedeij and Esen (2014) model using the nonlinear technique to reduce the maximum absolute relative error; this model is developed for any rainfall rate whether greater or less than the initial infiltration capacity and without requiring the determination of the ponding time, t_p(T).
Bautista et al.	2016	$I_{2D}^i = Z_k^i + E_k^i$ Computational method 1: Eq. (10) and (11) for Z_1^i and E_1^i, respectively. Computational method 2: Eqs. (14)-(16) for Z_2^i Eqs. (18)-(20), and (21) for E_2^i Computational method 3: Eq. (23) for Z_3^i Eqs. (24) and (25) for E_3^i (constant γ) Eqs. (25) and (26) for E_3^i (depth dependent γ) Find the above equations in Bautista et al.'s paper.	Bautista et al. proposed a methodology for estimating furrow infiltration under time-variable ponding depth. Bautista et al. (2014a) previously proposed a modification to the infiltration equation developed by Warrick et al. (2007) to account for time-variable ponding depth h_0 (t). This study further examined this problem, proposed an alternative formulation, and examined the problem of calibrating the parameter γ under variable depth conditions.
Nie et al.	2017a	$z_w(\theta_s - \theta_i) = 0.5K_s t + \sqrt{2K_s(h_0 + \psi)(\theta_s - \theta_i)t\left[1 + \frac{K_s t}{8(h_0+\psi)(\theta_s-\theta_i)}\right]}$	Nie et al. present an approximate explicit solution to the Green-Ampt (GA) infiltration model for estimating the wetting front depth of 1D infiltration based on Valiantzas (2010).
Selker and Assouline	2017	$i = K_s + \frac{\beta_0 K_s + \sqrt{\frac{(\theta_s-\theta_i)K_s\psi_{wf}}{2t}}}{1+\beta_0\frac{K_s t}{(\theta_s-\theta_i)\psi_{wf}} + \sqrt{\frac{2K_s t}{(\theta_s-\theta_i)\psi_{wf}}}}$	Selker and Assouline presented a simple explicit solution for ponded infiltration into soils using the Green and Ampt approach by describing early infiltration behavior in terms of the sum of gravitational flow and the exact solution for capillary imbibition. β_0 can be approximated by 2/3 (Brutsaert, 1977, Selker and Assouline, 2017, Stewart, 2019).
Stewart and Abou Najm	2018	$I = S_0 t^{0.5} + aK_s t + \frac{{S_0}^2 ab}{(\theta_s-\theta_i)\left(a+\frac{r}{2}\right)}t$ $0 \leq t \leq t_c$ $I = fK_s t + f(1-a)K_s t_c$ $t > t_c$	Based on two-term Philip type solutions for short and long times, the proposed model accounts for different ring sizes and depths of insertion, initial water

		Where: $t_c = \frac{(\theta_s-\theta_i)(h_0+\lambda_c)}{4bK_s f^2(1-a)^2}$; $f = \frac{h_0+\lambda_c}{d+r/2} + 1$	content and matric pressure head, transient and steady-state infiltration behaviors, and non-zero water supply pressures. For real soils, $0.4 < a < 0.5$ (Philip, 1990); a was determined through curve-fitting to be approximately equal to 0.91 (Wu and Pan, 1997). In most cases, $a = 0.45$ is recommended. b varies between 1/2 and $\pi/4$ depending on the shape of the soil water diffusivity function (White and Sully, 1987). $b = 0.17$ (Wu and Pan, 1997). A value of $b = 0.55$ is often assumed (Haverkamp et al., 1994, White and Sully, 1987, Reynolds and Elrick, 1990;). λ_c(L) is defined as being equal to the matric flux potential, φ(L^2 T^{-1}), scaled by K_s (L T^{-1}): $\lambda_c = \varphi/K_s$. According to Iovino et al. (2021), a could be fixed in advance.
Stewart	2018	$I = I_m + I_f$ $I_m = q_{0,m}t \quad t \le t_{p,m}$ $I_f = \min\left(q_{0,f}t, K_f t, \frac{V_f}{A_f}\right) \quad t > t_{p,m}$ $I_m = q_{0,m}t_{p,m} + K_m(t - t_{p,m}) + (\theta_s - \theta_i)\psi_{wf,m} ln\left[\frac{1+\beta_0\frac{K_m t}{(\theta_s-\theta_i)\psi_{wf,m}} + \sqrt{\frac{2K_m t}{(\theta_s-\theta_i)\psi_{wf,m}}}}{1+\beta_0\frac{K_m t_{p,m}}{(\theta_s-\theta_i)\psi_{wf,m}} + \sqrt{\frac{2K_m t_{p,m}}{(\theta_s-\theta_i)\psi_{wf,m}}}}\right]$ $I_f = \min\left(q_{0,f}t_{p,m} + q_0(t - t_{p,m}) - (I_m - I_{p,m}), K_{crack}t, \frac{V_f}{A_f}\right)$ Where: $q_{0,m} = \left(1 - \frac{\Upsilon\emptyset_f}{1-\emptyset_{sub}}\right)q_0$ and $q_{0,f} = \left(\frac{\Upsilon\emptyset_f}{1-\emptyset_{sub}}\right)q_0$	A multidomain infiltration model was proposed based on Green and Ampt (1991) to estimate infiltration in shrink-swell soils mediated by the matrix, which may include small-scale interaggregate shrinkage cracks, from those associated with inter-block cracks that surround the matrix. The two domains are related to the total crack porosity via a proportionality factor Υ ($0 \le \Upsilon \le 1$). To apply the Green-Ampt model in a multidomain formulation, Stewart divided the rainfall (precipitation) rate, q_0 (L T^{-1}), between the soil matrix and border crack domains.
Rahmati et al.	2019	$I = S_0 t^{0.5} + \frac{2-\beta}{3}K_s t + \frac{1}{9}(\beta^2 - \beta + 1)\frac{K_s^2}{S_0}t^{\frac{3}{2}}$	Rahmati et al. applied the Taylor series (Philip 1957a) up to third order in powers of 0.5 to the quasi-exact implicit analytical expansion presented by Haverkamp et al. (1994) to introduce a three-term infiltration model. β can take the value of 0.6 over the whole range of θ (Haverkamp et al., 1990). It ranges between 0.3 and 1.7 for sand to silty soils (Lassabatere et al., 2009, Rahmati et al., 2019).
Stewart	2019	$I_f = q_0 t - I_m \quad t < t_{p,f}$(1) $t < t_{p,m}$(2) $I_m = (1 - w_f)q_0 t$ $I_f = w_f q_0 t$ $I_m = (1 - w_f)K_{s,m}t\left[\left(\frac{q_0}{K_{s,m}} - 1\right)\frac{t_{p,m}}{t} + 1 + \frac{1}{\tau}ln\left(\frac{1+\beta_0\,\tau+\sqrt{2\tau}}{1+\beta_0\,\tau_{p,m}+\sqrt{2\tau_{p,m}}}\right)\right]$ $t \ge t_{p,m}$ (3) $I_f = K_{s,m}t\left[\left(\frac{q_0}{K_{s,m}}\right)\frac{t_{p,f}}{t} + w_f\frac{K_{s,f}}{K_{s,m}}\left(1 - \frac{t_{p,f}}{t}\right) - I_{mp,f}\right] \quad t \ge t_{p,f}$ (4) Where: $I_{mp,f} = (1 - w_f)K_{s,m}t\left[\left(\frac{q_0}{K_{s,m}} - 1\right)\tau_{p,m} + \tau_{p,f} + \frac{1}{\tau}ln\left(\frac{1+\beta_0\,\tau_{p,f}+\sqrt{2\tau_{p,f}}}{1+\beta_0\,\tau_{p,m}+\sqrt{2\tau_{p,m}}}\right)\right]$; $\tau = \frac{K_{s,m}t}{\Delta\theta_m\psi_{wf,m}}$; $\tau_{p,m} = \frac{K_{s,m}t_{p,m}}{\Delta\theta_m\psi_{wf,m}}$; $\tau_{p,f} = \frac{K_{s,m}t_{p,f}}{\Delta\theta_m\psi_{wf,m}}$	Stewart applied the Green–Ampt infiltration model within a dual-domain framework to distinguish water movement through the soil matrix vs. through macropores. For all time prior to ponding in the macropore domain ($t < t_{p,f}$), the cumulative infiltration as preferential flow is determined as the cumulative precipitation minus cumulative infiltration into the soil matrix (1). Before the soil matrix experiences ponding ($t < t_{p,m}$), both domains absorb rainfall in proportion to their surface-connected areas (2). After the soil matrix ponds ($t \ge t_{p,m}$), its cumulative infiltration is determined by equation (3). Assuming that water is moving through the macropores as plug flow under a unit hydraulic gradient, cumulative infiltration into the preferential flow domain after ponding ($t \ge t_{p,f}$) is found by equation (4). β_0 (Called α in Stewart, 2019) can be approximated by 2/3 (Brutsaert, 1977, Selker and Assouline, 2017, Stewart, 2019).
Baiamonte	2020	$I = I^* K_s t_c$ Where: (1):	An exact analytical solution of Richards' equation under gravity-driven infiltration and constant rainfall intensity is derived. In (1), the solution is presented under Torricelli's law, which simulates the soil hydraulic conductivity

		$I^* = 2\rho^2 \ln\left(\frac{\rho-\sqrt{\Theta_i}}{\rho-\sqrt{\Theta}}\right) - 2\rho\left(\sqrt{\Theta} - \sqrt{\Theta_i}\right) - (\Theta - \Theta_0)$; $0 < \tau \leq T_s$ $I^* = 2\rho^2 \ln\left(\frac{\rho-\sqrt{\Theta_i}}{\rho-\sqrt{\Theta_s}}\right) - 2\rho\left(\sqrt{\Theta_s} - \sqrt{\Theta_i}\right) - (\Theta - \Theta_0)$; $\tau > T_s$ (2): I^* from Eq. (29a) and (29b) for $0 < \tau \leq T_s$ and $\tau > T_s$, respectively. $\rho = q_0/K_s; \Theta = (\theta - \theta_i)/\Delta\theta; \tau = t/t_c$	function and describes the emptying or filling process of a nonlinear water reservoir. In (2), the solution is extended to the Brooks and Corey soil hydraulic conductivity function.
Su et al.	2020	$i = -K_e(\partial\psi/\partial z + 1)$ $h \leq 0$ (1) $i = -\partial\psi/\partial t - K_e(\partial\psi/\partial z + 1)$ $0 < h \leq h_{max}$ (2) Where: $K_e = K_{sh} S_e^{0.5}\left[1 - \left(1 - S_e^{1/m_1}\right)^{m_1}\right]^2$; $K_{sh} = K_s 10^{m'(\theta_{sh}-\theta_s)}$; $\theta_{sh} = 2 - \emptyset_i - \frac{1}{\rho_b(a_3+\alpha_3\omega)} - \frac{A''+B''\ln(\rho_{bw}z)}{\rho_b}$; $S_e = \left[\frac{1}{1+(\alpha\psi)^{n_{SSC}}}\right]^{m_{SSC}}$ and $m_{SSC} = 1 - 1/n_{SSC}$	A modified Richards model (RMSD)[3] was developed to simulate soil water movement into deformable soils subject to the following upper boundary conditions: (1) when rainfall intensity does not exceed the infiltration capacity of the soil, and (2) when rainfall intensity exceeds the infiltration capacity of the soil. Su et al. introduced the unsaturated hydraulic conductivity of deformable soils, K_e (L T^{-1}) and related it to physical properties using Lambe and Whitman (1979) and van Genuchten (1980, 1991) models. [3]RMSD: $\frac{\partial\theta}{\partial t} + \frac{\theta_i}{1+\emptyset_i}\frac{\partial\emptyset}{\partial t} = \frac{\partial}{\partial z}\left[K_e(\psi)\frac{\partial\psi}{\partial z}\right] + \frac{\partial K_e(\psi)}{\partial z} + W_r$ Where: $W_r = -S_r\Delta x\Delta y\Delta z\Delta t$ S_r (T^{-1}) is the water absorption strength of plant roots.
Poulovassilis and Argyrokastritis	2020	$I = (S_0 t^{0.5} - a_t) + K_s t$ Where: $a_t = S_0 t^{0.5}\left(1 - e^{-c_0\left(\frac{K_s}{S}\right)t^{0.5}}\right)$	A new two-term analytical equation, which takes the form of Philip's two-term equation, was derived for estimating vertical cumulative infiltration occurring in homogeneous porous media under zero ponding, including a factor a_t (L), characteristic of each porous body, valid for all t.
Abou Najm et al.	2021	$i_{WR} = i(1 - e^{-\alpha_{wr}t})$	Abou Najm et al. (2021) proposed a simple correction term $(1 - e^{-\alpha_{wr}t})$ that can be applied to any infiltration model to simulate infiltration behaviors of water-repellent soils. The correction term starts with a value of zero at the beginning of the infiltration experiment (t = 0) and asymptotically approaches 1 as time increases, thus simulating decreasing soil water repellency through time. To demonstrate the effectiveness of this method, Abou Najm et al. (2021) used a simple two-term infiltration model similar to two-term Philip type solution (Check Eq. 9 in the paper).
Di Prima et al.	2021	$I = S_0\sqrt{t} - \frac{S_0\sqrt{\pi}}{2\sqrt{\alpha_{wr}}}\text{erf}\left(\sqrt{\alpha_{wr}t}\right) + \left[A(1-B){S_0}^2 + Bi_\infty\right]t - \frac{\left[A(1-B){S_0}^2 + Bi_\infty\right]\left(1-e^{-\alpha_{wr}t}\right)}{\alpha_{wr}}$ small t $I = (AS^2 + K_s)t + C\frac{S^2}{K_s}$ large t Where: $A = \frac{\gamma}{r\Delta\theta}$; $B = \frac{2-\beta}{3}\left[1 - \left(\frac{\theta_i}{\theta_s}\right)^n\right] + \left(\frac{\theta_i}{\theta_s}\right)^n$; $C = \frac{1}{2\left[1-\left(\frac{\theta_i}{\theta_s}\right)^n\right](1-\beta)} ln\left(\frac{1}{\beta}\right)$ and $i_\infty = A{S_0}^2 + K_s$	Di Prima et al. presented an adaptation of the BEST method, namely BEST-WR, to characterize soils at any stage of water-repellency. They modified the Haverkamp explicit transient infiltration model, included in BEST for modeling infiltration data, by embedding the scaling factor $(1 - e^{-\alpha_{wr}t})$ introduced by Abou Najm et al. (2021) that describes the rate of attenuation of infiltration rate due to water repellency.
All parameters are algebraically positive values, unless otherwise specified.			

2.13. References

Abou Najm, M., Lassabatere, L., & Stewart, R. D. (2019). Current Insights into Nonuniform Flow across Scales, Processes, and Applications. *Vadose Zone Journal*. https://doi.org/10.2136/vzj2019.10.0113

Abou Najm, M. R., Stewart, R. D., Di Prima, S., & Lassabatere, L. (2021). A Simple Correction Term to Model Infiltration in Water-Repellent Soils. *Water Resources Research*. https://doi.org/10.1029/2020WR028539

Abou Najm, Majdi R., & Atallah, N. M. (2016). Non-Newtonian Fluids in Action: Revisiting Hydraulic Conductivity and Pore Size Distribution of Porous Media. *Vadose Zone Journal*. https://doi.org/10.2136/vzj2015.06.0092

Aiello, R., Bagarello, V., Barbagallo, S., Consoli, S., Di Prima, S., Giordano, G., & Iovino, M. (2014). An assessment of the Beerkan method for determining the hydraulic properties of a sandy loam soil. *Geoderma*, *235*, 300–307.

Ali, S., Ghosh, N. C., Singh, R., & Sethy, B. K. (2013). Generalized Explicit Models for Estimation of Wetting Front Length and Potential Recharge. *Water Resources Management*. https://doi.org/10.1007/s11269-013-0295-2

Almedeij, J., & Esen, I. I. (2014). Modified Green-Ampt Infiltration Model for Steady Rainfall. *Journal of Hydrologic Engineering*. https://doi.org/10.1061/(ASCE)HE.1943-5584.0000944

Angulo-Jaramillo, Rafaël, Bagarello, V., Di Prima, S., Gosset, A., Iovino, M., & Lassabatere, L. (2019). Beerkan Estimation of Soil Transfer parameters (BEST) across soils and scales. *Journal of Hydrology*, *576*, 239–261.

Angulo-Jaramillo, Rafael, Bagarello, V., Iovino, M., & Lassabatere, L. (2016). An Introduction to Soil and Water Infiltration. In *Infiltration Measurements for Soil Hydraulic Characterization* (pp. 1–42). Springer.

Angulo-Jaramillo, Rafael, Elrick, D., Parlange, J.-Y., Gérard-Marchant, P., & Haverkamp, R. (2003). Analysis of short-time single-ring infiltration under falling-head conditions with gravitational effects. *Hydrology Days Proceedings*.

Ankeny, M. D., Ahmed, M., Kaspar, T. C., & Horton, R. (1991). Simple Field Method for Determining Unsaturated Hydraulic Conductivity. *Soil Science Society of America Journal*. https://doi.org/10.2136/sssaj1991.03615995005500020028x

Arya, L. M., Farrell, D. A., & Blake, G. R. (1975). Field study of soil water depletion patterns in presence of growing soybean roots: I. Determination of hydraulic properties of the soil. *Proc Soil Sci Soc Am*. https://doi.org/10.2136/sssaj1975.03615995003900030021x

Assouline, S., Selker, J. S., & Parlange, J. Y. (2007). A simple accurate method to predict time of ponding under variable intensity rainfall. *Water Resources Research*. https://doi.org/10.1029/2006WR005138

Assouline, Shmuel. (2013). Infiltration into soils: Conceptual approaches and solutions. In *Water Resources Research*. https://doi.org/10.1002/wrcr.20155

Atallah, N. M., & Abou Najm, M. R. (2019). Characterization of synthetic porous media using non-Newtonian fluids: experimental evidence. *European Journal of Soil Science*. https://doi.org/10.1111/ejss.12746

Averjanov, S. F. (1950). About permeability of subsurface soils in case of incomplete saturation. *English Collection*.

Bagarello, V., Castellini, M., Di Prima, S., Giordano, G., & Iovino, M. (2013). Testing a Simplified Approach to Determine Field Saturated Soil Hydraulic Conductivity. *Procedia*

Environmental Sciences. https://doi.org/10.1016/j.proenv.2013.06.068
Bagarello, V., Di Prima, S., & Iovino, M. (2017). Estimating saturated soil hydraulic conductivity by the near steady-state phase of a Beerkan infiltration test. *Geoderma*. https://doi.org/10.1016/j.geoderma.2017.04.030
Bagarello, V., Di Prima, S., Iovino, M., & Provenzano, G. (2014). Estimating field-saturated soil hydraulic conductivity by a simplified Beerkan infiltration experiment. *Hydrological Processes*. https://doi.org/10.1002/hyp.9649
Bagarello, V., Iovino, M., & Elrick, D. (2004). A Simplified Falling-Head Technique for Rapid Determination of Field-Saturated Hydraulic Conductivity. *Soil Science Society of America Journal*. https://doi.org/10.2136/sssaj2004.6600
Baiamonte, G. (2020). Analytical Solution of the Richards Equation under Gravity-Driven Infiltration and Constant Rainfall Intensity. *Journal of Hydrologic Engineering*. https://doi.org/10.1061/(asce)he.1943-5584.0001933
Barry, D.A., J.-Y. Parlange, M.-C . Lju, G.C. Sander, M.B. Parlange, D.A. Lockington, et al. (2007). Infiltration and ponding. In *Life support systems: Mathematical sciences. Mathematical modeling*. EOLSS.
Barry, D. A., Parlange, J. Y., Haverkamp, R., & Ross, P. J. (1995). Infiltration under ponded conditions: 4. An explicit predictive infiltration formula. *Soil Science*. https://doi.org/10.1097/00010694-199507000-00002
Barry, D. A., Parlange, J. Y., Sander, G. C., & Sivaplan, M. (1993). A class of exact solutions for Richards' equation. *Journal of Hydrology*. https://doi.org/10.1016/0022-1694(93)90003-R
Basha, H. A. (1994). Multidimensional steady infiltration with prescribed boundary conditions at the soil surface. *Water Resources Research*. https://doi.org/10.1029/94WR00484
Basset, C. N., Abou Najm, M. R., Ammar, A., Stewart, R. D., Hauswirth, S. C., & Saad, G. (2019). Physically Based Model for Extracting Dual-Permeability Parameters Using Non-Newtonian Fluids. *Vadose Zone Journal*. https://doi.org/10.2136/vzj2018.09.0172
Batu, V. (1978). Steady Infiltration from Single and Periodic Strip Sources. *Soil Science Society of America Journal*. https://doi.org/10.2136/sssaj1978.03615995004200040033x
Bautista, E., Warrick, A. W., & Schlegel, J. L. (2014). Wetted-Perimeter-Dependent Furrow Infiltration and Its Implication for the Hydraulic Analysis of Furrow Irrigation Systems. *World Environmental and Water Resources Congress 2014: Water Without Borders - Proceedings of the 2014 World Environmental and Water Resources Congress*. https://doi.org/10.1061/9780784413548.171
Bautista, E., Warrick, A. W., Schlegel, J. L., Thorp, K. R., & Hunsaker, D. J. (2016). Approximate Furrow Infiltration Model for Time-Variable Ponding Depth. *Journal of Irrigation and Drainage Engineering*. https://doi.org/10.1061/(asce)ir.1943-4774.0001057
Bayabil, H. K., Dile, Y. T., Tebebu, T. Y., Engda, T. A., & Steenhuis, T. S. (2019). Evaluating infiltration models and pedotransfer functions: Implications for hydrologic modeling. *Geoderma*. https://doi.org/10.1016/j.geoderma.2018.11.028
Bennethum, L. S., & Cushman, J. H. (1996). Multiscale, hybrid mixture theory for swelling systems - II: Constitutive theory. *International Journal of Engineering Science*. https://doi.org/10.1016/0020-7225(95)00090-9
Beven, K. (1984). Infiltration into a class of vertically non-uniform soils. *Hydrological Sciences Journal*. https://doi.org/10.1080/02626668409490960
Beven, K. (2018). A Century of Denial: Preferential and Nonequilibrium Water Flow in Soils, 1864-1984. *Vadose Zone Journal*. https://doi.org/10.2136/vzj2018.08.0153

Beven, K., & Germann, P. (1982). Macropores and water flow in soils. *Water Resources Research*. https://doi.org/10.1029/WR018i005p01311

Beven, K., & Germann, P. (2013). Macropores and water flow in soils revisited. *Water Resources Research*. https://doi.org/10.1002/wrcr.20156

Beven, K., Germann, P., Seven, K., Germann, P., Beven, K., Germann, P., Seven, K., & Germann, P. (1981). Water flow in soil macropores II. A combined flow model. *Journal of Soil Science*. https://doi.org/10.1111/j.1365-2389.1981.tb01682.x

Beven, K. J. (2010). Preferential flows and travel time distributions: defining adequate hypothesis tests for hydrological process models. *Hydrological Processes*, *24*(12), 1537–1547.

Biot, M. A. (1955). Theory of elasticity and consolidation for a porous anisotropic solid. *Journal of Applied Physics*. https://doi.org/10.1063/1.1721956

Blunt, M. J. (2001). Flow in porous media - Pore-network models and multiphase flow. In *Current Opinion in Colloid and Interface Science*. https://doi.org/10.1016/S1359-0294(01)00084-X

Blunt, M. J. (2017). Multiphase flow in permeable media: A pore-scale perspective. Cambridge university press.

Blunt, M. J., Bijeljic, B., Dong, H., Gharbi, O., Iglauer, S., Mostaghimi, P., Paluszny, A., & Pentland, C. (2013). Pore-scale imaging and modelling. *Advances in Water Resources*. https://doi.org/10.1016/j.advwatres.2012.03.003

Blunt, M. J., Jackson, M. D., Piri, M., & Valvatne, P. H. (2002). Detailed physics, predictive capabilities and macroscopic consequences for pore-network models of multiphase flow. *Advances in Water Resources*. https://doi.org/10.1016/S0309-1708(02)00049-0

Blunt, M. J., & Scher, H. (1995). Pore-level modeling of wetting. *Physical Review E*. https://doi.org/10.1103/PhysRevE.52.6387

Blunt, M., King, M. J., & Scher, H. (1992). Simulation and theory of two-phase flow in porous media. *Physical Review A*. https://doi.org/10.1103/PhysRevA.46.7680

Blunt, M., & King, P. (1991). Relative permeabilities from two- and three-dimensional pore-scale network modelling. *Transport in Porous Media*. https://doi.org/10.1007/BF00136349

Bouma, J., & Dekker, L. W. (1981). A Method for Measuring the Vertical and Horizontal Ksat of Clay Soils with Macropores. *Soil Science Society of America Journal*. https://doi.org/10.2136/sssaj1981.03615995004500030046x

Bouwer, H. (1960). A study of final infiltration rates from cylinder infiltrometers and irrigation furrows with an electrical resistance network. *Transactions 7th Int. Congr. Soil Sci.*, *1*, 448–456.

Bouwer, H. (1963). Theoretical effect of unequal water levels on the infiltration rate determined with buffered cylinder infiltrometers. *Journal of Hydrology*, *1*(1), 29–34.

Bouwer, H. (1986). Intake rate: cylinder infiltrometer. *Methods of Soil Analysis: Part 1 Physical and Mineralogical Methods*, *5*, 825–844.

Bowen, R. M. (1980). Incompressible porous media models by use of the theory of mixtures. *International Journal of Engineering Science*. https://doi.org/10.1016/0020-7225(80)90114-7

Bradford, J. M., Ferris, J. E., & Remley, P. A. (1987). Interrill Soil Erosion Processes: I. Effect of Surface Sealing on Infiltration, Runoff, and Soil Splash Detachment. *Soil Science Society of America Journal*. https://doi.org/10.2136/sssaj1987.03615995005100060029x

Brakensiek, D. L., & Rawls, W. J. (1983). Agricultural management effects on soil water processes, part II: Green and Ampt parameters for crusting soils. In *Transactions - American Society of Agricultural Engineers*. https://doi.org/10.13031/2013.33838

Braud, I., De Condappa, D., Soria, J. M., Haverkamp, R., Angulo-Jaramillo, R., Galle, S., & Vauclin, M. (2005). Use of scaled forms of the infiltration equation for the estimation of unsaturated soil hydraulic properties (the Beerkan method). *European Journal of Soil Science*, *56*(3), 361–374. https://doi.org/10.1111/j.1365-2389.2004.00660.x

Briggs, L. J. (1897). *Mechanics of soil moisture*.

Broadbridge, P., & White, I. (1988). Constant rate rainfall infiltration: A versatile nonlinear model: 1. Analytic solution. *Water Resources Research*. https://doi.org/10.1029/WR024i001p00145

Brooks, R., & Corey, A. (1964). Hydraulic properties of porous media. *Hydrology Papers, Colorado State University*.

Brutsaert, W. (1976). The concise formulation of diffusive sorption of water in a dry soil. *Water Resources Research*. https://doi.org/10.1029/WR012i006p01118

Brutsaert, W. (1977). Vertical infiltration in dry soil. *Water Resources Research*. https://doi.org/10.1029/WR013i002p00363

Buckingham, E. (1907). Studies on the Movement of Soil Moisture. *Bureau of Soils---Bulletin No. 38*.

Bultreys, T., Van Hoorebeke, L., & Cnudde, V. (2015). Multi-scale, micro-computed tomography-based pore network models to simulate drainage in heterogeneous rocks. *Advances in Water Resources*. https://doi.org/10.1016/j.advwatres.2015.02.003

Burdine, N. (1953). Relative permeability calculations from pore size distribution data. *Journal of Petroleum Technology*, *5*(03), 71–78.

Campbell, G. S. (1974). A simple method for determining unsaturated conductivity from moisture retention data. *Soil Science*, *117*(6), 311–314.

Campbell, G. S. (1985). *Soil physics with BASIC: transport models for soil-plant systems*. Elsevier.

Chandler, R., Koplik, J., Lerman, K., & Willemsen, J. F. (1982). Capillary displacement and percolation in porous media. *Journal of Fluid Mechanics*. https://doi.org/10.1017/S0022112082001335

Chen, L., & Young, M. H. (2006). Green-Ampt infiltration model for sloping surfaces. *Water Resources Research*. https://doi.org/10.1029/2005WR004468

Childs, E C. (1936). The transport of water through heavy clay soils. I. *The Journal of Agricultural Science*, *26*(1), 114–127.

Childs, Eo C, & Collis-George, N. (1950). The permeability of porous materials. *Proceedings of the Royal Society of London. Series A. Mathematical and Physical Sciences*, *201*(1066), 392–405.

Chu, S T. (1994). Capillary-tube infiltration model with Brooks-Corey parameters. *Transactions of the ASAE*, *37*(4), 1205–1208.

Chu, Shu Tung. (1985). Modeling infiltration into tilled soil during non-uniform rainfall. *Transactions of the American Society of Agricultural Engineers*. https://doi.org/10.13031/2013.32415

Chu, Shu Tung. (1993). Capillary-tube infiltration model. *Journal of Irrigation and Drainage Engineering*, *119*(3), 514–521.

Clothier, B. E. (2001). Infiltration. *Soil and Environmental Analysis, Physical Methods*, 239–280.

Collis-George, N. (1977). Infiltration equations for simple soil systems. *Water Resources Research*. https://doi.org/10.1029/WR013i002p00395

Corradini, C., Melone, F., & Smith, R. E. (2000). Modeling local infiltration for a two-layered soil under complex rainfall patterns. *Journal of Hydrology*. https://doi.org/10.1016/S0022-1694(00)00298-5

Corradini, Corrado, Govindaraju, R. S., & Morbidelli, R. (2002). Simplified modelling of areal average infiltration at the hillslope scale. *Hydrological Processes*. https://doi.org/10.1002/hyp.394

Corradini, Corrado, Melone, F., & Smith, R. E. (1994). Modeling infiltration during complex rainfall sequences. *Water Resources Research*. https://doi.org/10.1029/94WR00951

Corradini, Corrado, Melone, F., & Smith, R. E. (1997). A unified model for infiltration and redistribution during complex rainfall patterns. *Journal of Hydrology*. https://doi.org/10.1016/S0022-1694(96)03110-1

Corradini, Corrado, Morbidelli, R., Flammini, A., & Govindaraju, R. S. (2011). A parameterized model for local infiltration in two-layered soils with a more permeable upper layer. *Journal of Hydrology*. https://doi.org/10.1016/j.jhydrol.2010.11.010

Crank, J. (1979). The mathematics of diffusion. 2nd Edn. https://doi.org/10.1088/0031-9112/26/11/044

Dane, J. H., & Hruska, S. (1983). In-Situ Determination of Soil Hydraulic Properties during Drainage. *Soil Science Society of America Journal*. https://doi.org/10.2136/sssaj1983.03615995004700040001x

Darcy, H. (1856). Les fontaines publiques de la ville de Dijon. *Recherche*.

Das, B. S., & Kluitenberg, G. J. (1995). Using pore size distribution to model the unsaturated hydraulic conductivity of soil. *Vadose Zone Hydrology: Cutting Across Disciplines. Proc. Kearney Foundation, Univ. California, Davis, CA*, 31–32.

Davidoff, B., & Selim, H. M. (1986). Goodness of Fit for Eight Water Infiltration Models. *Soil Science Society of America Journal*. https://doi.org/10.2136/sssaj1986.03615995005000030039x

Davidson, M. R. (1984). A Green-Ampt Model of infiltration in a cracked soil. *Water Resources Research*, *20*(11), 1685–1690.

Delleur, J. W. (2006). *The handbook of groundwater engineering*. CRC press.

Di Prima, S., Concialdi, P., Lassabatere, L., Angulo-Jaramillo, R., Pirastru, M., Cerdà, A., & Keesstra, S. (2018). Laboratory testing of Beerkan infiltration experiments for assessing the role of soil sealing on water infiltration. *Catena*. https://doi.org/10.1016/j.catena.2018.05.013

Di Prima, S., Lassabatere, L., Bagarello, V., Iovino, M., & Angulo-Jaramillo, R. (2016). Testing a new automated single ring infiltrometer for Beerkan infiltration experiments. *Geoderma*. https://doi.org/10.1016/j.geoderma.2015.08.006

Di Prima, Simone, Stewart, R. D., Abou Najm, M. R., Ribeiro Roder, L., Giadrossich, F., Campus, S., Angulo-Jaramillo, R., Yilmaz, D., Roggero, P. P., Pirastru, M., & Lassabatere, L. (2021). BEST-WR: An adapted algorithm for the hydraulic characterization of hydrophilic and water-repellent soils. *Journal of Hydrology*. https://doi.org/10.1016/j.jhydrol.2021.126936

Di Prima, Simone, Stewart, R. D., Castellini, M., Bagarello, V., Abou Najm, M. R., Pirastru, M., Giadrossich, F., Iovino, M., Angulo-Jaramillo, R., & Lassabatere, L. (2020). Estimating the macroscopic capillary length from Beerkan infiltration experiments and its impact on saturated soil hydraulic conductivity predictions. *Journal of Hydrology*, *589*, 125159.

Dong, H., & Blunt, M. J. (2009). Pore-network extraction from micro-computerized-tomography images. *Physical Review E - Statistical, Nonlinear, and Soft Matter Physics*. https://doi.org/10.1103/PhysRevE.80.036307

Elrick, D. E., Angulo-Jaramillo, R., Fallow, D. J., Reynolds, W. D., & Parkin, G. W. (2002). Infiltration under constant head and falling head conditions. In *Geophysical Monograph Series*. https://doi.org/10.1029/129GM04

Elrick, D. E., & Reynolds, W. D. (1992). Methods for Analyzing Constant-Head Well Permeameter Data. *Soil Science Society of America Journal*. https://doi.org/10.2136/sssaj1992.03615995005600010052x

Elrick, David E., Parkin, G. W., Reynolds, W. D., & Fallow, D. J. (1995). Analysis of Early-Time and Steady State Single-Ring Infiltration Under Falling Head Conditions. *Water Resources Research*. https://doi.org/10.1029/95WR01139

Enciso-Medina, J., Martin, D., & Eisenhauer, D. (1998). Infiltration Model for Furrow Irrigation. *Journal of Irrigation and Drainage Engineering*. https://doi.org/10.1061/(asce)0733-9437(1998)124:2(73)

Essig, E. T., Corradini, C., Morbidelli, R., & Govindaraju, R. S. (2009). Infiltration and deep flow over sloping surfaces: Comparison of numerical and experimental results. *Journal of Hydrology*. https://doi.org/10.1016/j.jhydrol.2009.05.017

Fallow, D. J., Elrick, D. E., Reynolds, W. D., Baumgartner, N., & Parkin, G. W. (1994). Field measurement of hydraulic conductivity in slowly permeable materials using early-time infiltration measurements in unsaturated media. *ASTM Special Technical Publication*. https://doi.org/10.1520/stp23898s

Farkas, C., Gyuricza, C., & Birkás, M. (2006). Seasonal changes of hydraulic properties of a Chromic Luvisol under different soil management. *Biologia (Poland)*. https://doi.org/10.2478/s11756-006-0186-6

Fatt, I. (1956a). The network model of porous media. II. Dynamic properties of a single size tube network. *Petroleum Transactions AIME*, *207*(7), 160–163.

Fatt, I. (1956b). The Network Model of Porous Media - I. Capillary Pressure Characteristics. In *Petroleum Transactions AIME*.

Fatt, I. (1956c). The network model of porous media III. Dynamic properties of networks with tube radius distribution. *Petroleum Transactions AIME*.

Feddes, R. A., Kabat, P., Van Bakel, P. J. T., Bronswijk, J. J. B., & Halbertsma, J. (1988). Modelling soil water dynamics in the unsaturated zone - State of the art. *Journal of Hydrology*. https://doi.org/10.1016/0022-1694(88)90182-5

Fodor, N., Sándor, R., Orfanus, T., Lichner, L., & Rajkai, K. (2011). Evaluation method dependency of measured saturated hydraulic conductivity. *Geoderma*. https://doi.org/10.1016/j.geoderma.2011.07.004

Fok, Y.-S., & Hansen, V. E. (1966). One-Dimensional Infiltration into Homogeneous Soil. *Journal of the Irrigation and Drainage Division*. https://doi.org/10.1061/jrcea4.0000432

Fok, Y., & Chiang, S. (1984). 2-D Infiltration Equations for Furrow Irrigation. *Journal of Irrigation and Drainage Engineering*. https://doi.org/10.1061/(asce)0733-9437(1984)110:2(208)

Fok, Y. S., Chung, S. K., & Liu, C. C. K. (1982). Two-dimensional exponential infiltration equations. *Journal of the Irrigation & Drainage Division - ASCE*. https://doi.org/10.1061/jrcea4.0001391

Fonteh, M. F., & Podmore, T. (1993). A physically based infiltration model for furrow irrigation. *Agricultural Water Management*. https://doi.org/10.1016/0378-3774(93)90040-H

Gardner, W. R. (1958). Some steady-state solutions of the unsaturated moisture flow equation with application to evaporation from a water table. *Soil Science*. https://doi.org/10.1097/00010694-195804000-00006

Geistlinger, H., & Ataei-Dadavi, I. (2015). Influence of the heterogeneous wettability on capillary trapping in glass-beads monolayers: comparison between experiments and the invasion

percolation theory. *Journal of Colloid and Interface Science*, *459*, 230–240.
Gérard-Marchant, P., Angulo-Jaramillo, R., Haverkamp, R., Vauclin, M., Groenevelt, P., & Elrick, D. E. (1997). Estimating the hydraulic conductivity of slowly permeable and swelling materials from single-ring experiments. *Water Resources Research*, *33*(6), 1375–1382.
Gerke, H. H., & van Genuchten, M. T. (1993). A dual-porosity model for simulating the preferential movement of water and solutes in structured porous media. *Water Resources Research*. https://doi.org/10.1029/92WR02339
Germann, P. F. (1985). KINEMATIC WAVE APPROACH TO INFILTRATION AND DRAINAGE INTO AND FROM SOIL MACROPORES. *Transactions of the American Society of Agricultural Engineers*. https://doi.org/10.13031/2013.32331
Germann, P. F. (2021). HESS Opinions: Unsaturated infiltration–the need for a reconsideration of historical misconceptions. *Hydrology and Earth System Sciences*, *25*(2), 1097–1101.
Germann, P., Helbling, A., & Vadilonga, T. (2007). Rivulet Approach to Rates of Preferential Infiltration. *Vadose Zone Journal*. https://doi.org/10.2136/vzj2006.0115
Ghanbarian, B., Hunt, A. G., & Daigle, H. (2016). Fluid flow in porous media with rough pore-solid interface. *Water Resources Research*, *52*(3), 2045–2058.
Ghorbani Dashtaki, S., Homaee, M., Mahdian, M. H., & Kouchakzadeh, M. (2009). Site-dependence performance of infiltration models. *Water Resources Management*. https://doi.org/10.1007/s11269-009-9408-3
Giraldez, J. V., & Sposito, G. (1985). Infiltration in Swelling Soils. *Water Resources Research*. https://doi.org/10.1029/WR021i001p00033
Glass, R J, & Yarrington, L. (1996). Simulation of gravity fingering in porous media using a modified invasion percolation model. *Geoderma*, *70*(2–4), 231–252.
Glass, Robert J, Conrad, S. H., & Peplinski, W. (2000). Gravity-destabilized nonwetting phase invasion in macroheterogeneous porous media: Experimental observations of invasion dynamics and scale analysis. *Water Resources Research*, *36*(11), 3121–3137.
Glass, Robert J, Conrad, S. H., & Yarrington, L. (2001). Gravity-destabilized nonwetting phase invasion in macroheterogeneous porous media: Near-pore-scale macro modified invasion percolation simulation of experiments. *Water Resources Research*, *37*(5), 1197–1207.
Govindaraju, R. S., Corradini, C., & Morbidelli, R. (2006). A semi-analytical model of expected areal-average infiltration under spatial heterogeneity of rainfall and soil saturated hydraulic conductivity. *Journal of Hydrology*. https://doi.org/10.1016/j.jhydrol.2005.04.019
Govindaraju, R. S., Corradini, C., & Morbidelli, R. (2012). Local- and field-scale infiltration into vertically non-uniform soils with spatially-variable surface hydraulic conductivities. *Hydrological Processes*. https://doi.org/10.1002/hyp.8454
Green, H. W., & Ampt, G. A. (1911). Studies on soil physics: Flow of air and water through soils. *J. Aric. Sci.*
Gülser, C., Ekberli, I., & Candemir, F. (2016). Spatial variability of soil physical properties in a cultivated field. *EURASIAN JOURNAL OF SOIL SCIENCE (EJSS)*. https://doi.org/10.18393/ejss.2016.3.192-200
Hachum, A. Y., & Alfaro, J. F. (1977). Water Infiltration and Runoff under Rain Applications. *Soil Science Society of America Journal*. https://doi.org/10.2136/sssaj1977.03615995004100050031x
Hammecker, C., Siltecho, S., Angulo Jaramillo, R., & Lassabatere, L. (2022). Modelling of water infiltration into water repellent soils. *Hydrology and Earth System Sciences Discussions*, 1–24.

Hansen, V. E. (1955). Infiltration and soil water movement during irrigation. *Soil Science*. https://doi.org/10.1097/00010694-195502000-00002

Hauswirth, S. C., Abou Najm, M. R., & Miller, C. T. (2019). Characterization of the Pore Structure of Porous Media Using non-Newtonian Fluids. *Water Resources Research*. https://doi.org/10.1029/2019WR025044

Haverkamp, R., Parlange, J. Y., Starr, J. L., Schmitz, G., & Fuentes, C. (1990). Infiltration under ponded conditions: 3. A predictive equation based on physical parameters. *Soil Science*. https://doi.org/10.1097/00010694-199005000-00006

Haverkamp, R., Ross, P. J., Smettem, K. R. J., & Parlange, J. Y. (1994). Three-dimensional analysis of infiltration from the disc infiltrometer: 2. Physically based infiltration equation. *Water Resources Research*. https://doi.org/10.1029/94WR01788

Heiba, A. A., Davis, H. T., & Scriven, L. E. (1984). Statistical network theory of three-phase relative permeabilities. *Society of Petroleum Engineers of AIME, (Paper) SPE*. https://doi.org/10.2523/12690-ms

Holtan, H. N. (1961). Concept for infiltration estimates in watershed engineering.

Horton, R. E. (1940). The infiltration-theory of surface-runoff. *Eos, Transactions American Geophysical Union*. https://doi.org/10.1029/TR021i002p00541-1

Huggins, L. F., & Monke, E. J. (1966). The mathematical simulation of the hydrology of small watersheds.

Hunt, A., Ewing, R., & Ghanbarian, B. (2014). Percolation theory for flow in porous media (Vol. 880). Springer.

Hunt, A. G. (1997). Dependence of the hydraulic conductivity on space and time scales. *In the Proceedings of the International Workshop on Characterization and Measurement of the Hydraulic Properties of Unsaturated Porous Media*, 1403–1414.

Hunt, A. G., Ewing, R. P., & Horton, R. (2013). What's Wrong with Soil Physics? *Soil Science Society of America Journal*. https://doi.org/10.2136/sssaj2013.01.0020

Hunt, Allen G, Holtzman, R., & Ghanbarian, B. (2017). A percolation-based approach to scaling infiltration and evapotranspiration. *Water*, *9*(2), 104.

Hunt, Allen G, & Sahimi, M. (2017). Flow, transport, and reaction in porous media: Percolation scaling, critical-path analysis, and effective medium approximation. *Reviews of Geophysics*, *55*(4), 993–1078.

Iovino, M., Abou Najm, M. R., Angulo-Jaramillo, R., Bagarello, V., Castellini, M., Concialdi, P., Di Prima, S., Lassabatere, L., & Stewart, R. D. (2021). Parameterization of a comprehensive explicit model for single-ring infiltration. *Journal of Hydrology*, *601*, 126801.

Jačka, L., Pavlásek, J., Pech, P., & Kuráž, V. (2016). Assessment of evaluation methods using infiltration data measured in heterogeneous mountain soils. *Geoderma*. https://doi.org/10.1016/j.geoderma.2016.04.023

James, A. L., McDonnell, J. J., Tromp-van Meerveld, I., & Peters, N. E. (2010). Gypsies in the palace: Experimentalist's view on the use of 3-D physics-based simulation of hillslope hydrological response. *Hydrological Processes*, *24*(26), 3878–3893.

Jarvis, N. (1994). The MACRO Model (version 3.1). Technical description and sample simulations.

Jarvis, N. J. (2007). A review of non-equilibrium water flow and solute transport in soil macropores: Principles, controlling factors and consequences for water quality. *European Journal of Soil Science*, *58*(3), 523–546.

Jarvis, N. J., & Larsson, M. H. (1998). The MACRO model (version 4.3): Technical description.

Reports and Dissertations, *19*.
Joekar-Niasar, V., Hassanizadeh, S. M., & Leijnse, A. (2008). Insights into the relationships among capillary pressure, saturation, interfacial area and relative permeability using pore-network modeling. *Transport in Porous Media*. https://doi.org/10.1007/s11242-007-9191-7
Kargas, G., Koka, D., & Londra, P. A. (2022). Evaluation of Soil Hydraulic Parameters Calculation Methods Using a Tension Infiltrometer. *Soil Systems*, *6*(3), 63.
Koplik, J., & Lasseter, T. J. (1985). Two-phase flow in random network models of porous media. *Society of Petroleum Engineers Journal*. https://doi.org/10.2118/11014-PA
Koplik, Joel. (1982). Creeping flow in two-dimensional networks. *Journal of Fluid Mechanics*. https://doi.org/10.1017/S0022112082001323
Kostiakov, A. N. (1932). On the dynamics of the coefficient of water percolation in soils and the necessity of studying it from the dynamic point of view for the purposes of amelioration. *Trans. Sixth Comm. Int. Soc. Soil Sci.*, *1*, 7–21.
Kosugi, K. (1999). General model for unsaturated hydraulic conductivity for soils with lognormal pore-size distribution. *Soil Science Society of America Journal*, *63*(2), 270–277.
Kozeny, J. (1927). Uber kapillare leitung der wasser in boden. *Royal Academy of Science, Vienna, Proc. Class I, 136*, 271–306.
Krummel, A. T., Datta, S. S., Münster, S., & Weitz, D. A. (2013). Visualizing multiphase flow and trapped fluid configurations in a model three-dimensional porous medium. *AIChE Journal*, *59*(3), 1022–1029.
Kutílek, M. (1980). Constant-rainfall infiltration. *Journal of Hydrology*. https://doi.org/10.1016/0022-1694(80)90025-6
Kutilek, M., Zayani, K., Haverkamp, R., Parlance, J. Y., & Vachaud, G. (1991). Scaling of the Richards Equation Under Invariant Flux Boundary Conditions. *Water Resources Research*. https://doi.org/10.1029/91WR01550
Kutílek, M, & Krejca, M. (1987). Three-parameter infiltration equation of Philip type. *Vodohosp. ˇCas*, *35*, 52–61.
Kutílek, Miroslav, & Nielsen, D. R. (1994). Soil hydrology: texbook for students of soil science, agriculture, forestry, geoecology, hydrology, geomorphology and other related disciplines. Catena Verlag.
Larsbo, M., & Jarvis, N. (2003). MACRO 5.0: a model of water flow and solute transport in macroporous soil: technical description (Vol. 1). Department of Soil Sciences, Swedish University of Agricultural Sciences Uppsala.
Larson, R. G., Scriven, L. E., & Davis, H. T. (1981). Percolation theory of two phase flow in porous media. *Chemical Engineering Science*. https://doi.org/10.1016/0009-2509(81)80048-6
Lassabatère, L., Angulo-Jaramillo, R., Soria Ugalde, J. M., Cuenca, R., Braud, I., & Haverkamp, R. (2006). Beerkan Estimation of Soil Transfer Parameters through Infiltration Experiments-BEST. *Soil Science Society of America Journal*. https://doi.org/10.2136/sssaj2005.0026
Lassabatere, L, Angulo-Jaramillo, R., Soria-Ugalde, J. M., Šimůnek, J., & Haverkamp, R. (2009). Numerical evaluation of a set of analytical infiltration equations. *Water Resources Research*. https://doi.org/10.1029/2009WR007941
Lassabatere, Laurent, Di Prima, S., Angulo-Jaramillo, R., Keesstra, S., & Salesa, D. (2019a). Beerkan multi-runs for characterizing water infiltration and spatial variability of soil hydraulic properties across scales. *Hydrological Sciences Journal*, *64*(2), 165–178.
Lassabatere, Laurent, Di Prima, S., Bouarafa, S., Iovino, M., Bagarello, V., & Angulo-Jaramillo,

R. (2019b). BEST-2K method for characterizing dual-permeability unsaturated soils with ponded and tension infiltrometers. *Vadose Zone Journal*, *18*(1), 1–20.

Lassabatere, Laurent, Peyneau, P.-E., Yilmaz, D., Pollacco, J., Fernández-Gálvez, J., Latorre, B., Moret-Fernández, D., Di Prima, S., Rahmati, M., & Stewart, R. D. (2021). A scaling procedure for straightforward computation of sorptivity. *Hydrology and Earth System Sciences*, *25*(9), 5083–5104.

Lassabatere, Laurent, Peyneau, P.-E., Yilmaz, D., Pollacco, J., Fernández-Gálvez, J., Latorre, B., Moret-Fernández, D., Di Prima, S., Rahmati, M., & Stewart, R. D. (2023). Mixed formulation for an easy and robust numerical computation of sorptivity. *Hydrology and Earth System Sciences*, *27*(4), 895–915.

Lassabatere, Laurent, Yilmaz, D., Peyrard, X., Peyneau, P. E., Lenoir, T., Šimůnek, J., & Angulo-Jaramillo, R. (2014). New Analytical Model for Cumulative Infiltration into Dual-Permeability Soils. *Vadose Zone Journal*. https://doi.org/10.2136/vzj2013.10.0181

Lassu, T., Seeger, M., Peters, P., & Keesstra, S. D. (2015). The Wageningen Rainfall Simulator: Set-up and Calibration of an Indoor Nozzle-Type Rainfall Simulator for Soil Erosion Studies. *Land Degradation and Development*. https://doi.org/10.1002/ldr.2360

Latorre, B., Peña, C., Lassabatere, L., Angulo-Jaramillo, R., & Moret-Fernández, D. (2015). Estimate of soil hydraulic properties from disc infiltrometer three-dimensional infiltration curve: Numerical analysis and field application. In *Journal of Hydrology*. https://doi.org/10.1016/j.jhydrol.2015.04.015

Lewandowska, J., Szymkiewicz, A., Burzyński, K., & Vauclin, M. (2004). Modeling of unsaturated water flow in double-porosity soils by the homogenization approach. *Advances in Water Resources*, *27*(3), 283–296.

Li, R. M., Stevens, M. A., & Simons. (1976). Solutions to Green-Ampt infiltration equation. *ASCE J Irrig Drain Div*.

Libardi, P. L., Reichardt, K., Nielsen, D. R., & Biggar, J. W. (1980). Simple Field Methods for Estimating Soil Hydraulic Conductivity. *Soil Science Society of America Journal*. https://doi.org/10.2136/sssaj1980.03615995004400010001x

Liu, J., & Song, R. (2015). Investigation of water and CO2 flooding using pore-scale reconstructed model based on micro-CT images of Berea sandstone core. *Progress in Computational Fluid Dynamics, An International Journal*, *15*(5), 317–326.

Liu, M., Meakin, P., & Huang, H. (2006). Dissipative particle dynamics with attractive and repulsive particle-particle interactions. *Physics of Fluids*. https://doi.org/10.1063/1.2163366

Logsdon, S. D., & Jaynes, D. B. (1996). Spatial Variability of Hydraulic Conductivity in a Cultivated Field at Different Times. *Soil Science Society of America Journal*. https://doi.org/10.2136/sssaj1996.03615995006000030003x

Mandal, A. C., & Waechter, R. T. (1994). Steady infiltration in unsaturated soil from a buried circular cylinder: The separate contributions from top and bottom halves. *Water Resources Research*. https://doi.org/10.1029/93WR02468

Martys, N. S., & Hagedorn, J. G. (2002). Multiscale modeling of fluid transport in heterogeneous materials using discrete Boltzmann methods. *Materials and Structures/Materiaux et Constructions*. https://doi.org/10.1617/13973

Mein, R. G., & Larson, C. L. (1973). Modeling infiltration during a steady rain. *Water Resources Research*. https://doi.org/10.1029/WR009i002p00384

Mezencev, V. J. (1948). Theory of formation of the surface runoff. *Meteorol. Gidrol*, *3*, 33–40.

Mogensen, K., & Stenby, E. H. (1998). A Dynamic Two-Phase Pore-Scale Model of Imbibition.

Transport in Porous Media. https://doi.org/10.1023/a:1006578721129
Morbidelli, R., Corradini, C., & Govindaraju, R. S. (2006). A field-scale infiltration model accounting for spatial heterogeneity of rainfall and soil saturated hydraulic conductivity. *Hydrological Processes*. https://doi.org/10.1002/hyp.5943
Morel-Seytoux, H. J. (1976). Derivation of equations for rainfall infiltration. *Journal of Hydrology*. https://doi.org/10.1016/0022-1694(76)90125-6
Morel-Seytoux, H. J., & Khanji, J. (1974). Derivation of an equation of infiltration. *Water Resources Research*. https://doi.org/10.1029/WR010i004p00795
Mualem, Y. (1976). A new model for predicting the hydraulic conductivity of unsaturated porous media. *Water Resources Research*. https://doi.org/10.1029/WR012i003p00513
Navier, C. L. (1823). Mémoire sur les lois du mouvement des fluides. *Mémoires de l'Académie Des Sciences de l'Institut de France*.
Niasar, V. J., Hassanizadeh, S. M., Pyrak-Nolte, L. J., & Berentsen, C. (2009). Simulating drainage and imbibition experiments in a high-porosity micromodel using an unstructured pore network model. *Water Resources Research*. https://doi.org/10.1029/2007WR006641
Nicholson, D. (1968). Capillary models for porous media. Part 2. - Sorption desorption hysteresis in three dimensional networks. *Transactions of the Faraday Society*. https://doi.org/10.1039/TF9686403416
Nie, W.-B., Li, Y.-B., Fei, L.-J., & Ma, X.-Y. (2017a). Approximate explicit solution to the Green-Ampt infiltration model for estimating wetting front depth. *Water*, *9*(8), 609.
Nie, W., Ma, X., & Fei, L. (2017b). Evaluation of Infiltration Models and Variability of Soil Infiltration Properties at Multiple Scales. *Irrigation and Drainage*. https://doi.org/10.1002/ird.2126
Nimmo, J. R., Perkins, K. S., Plampin, M. R., Walvoord, M. A., Ebel, B. A., & Mirus, B. B. (2021). Rapid-response unsaturated zone hydrology: Small-scale data, small-scale theory, big problems. *Frontiers in Earth Science*, 123.
Novák, V., Šimůnek, J., & Genuchten, M. T. van. (2000). Infiltration of Water into Soil with Cracks. *Journal of Irrigation and Drainage Engineering*. https://doi.org/10.1061/(asce)0733-9437(2000)126:1(41)
Novák, V., & Soltesz, A. (1984). Infiltration of water into cracked soil.
Olson, T. C. (1960). Model study of the double-ring infiltrometer in layered systems. *Int. Congr. Soil Sci. Trans. 7th*, 441–447.
Overton, D. (1964). Mathematical refinement of an infiltration equation for watershed engineering. *Department of Agricultural Services, Wasington*.
Pachepsky, Y., & Karahan, G. (2022). On shapes of cumulative infiltration curves. *Geoderma*, *412*, 115715.
Parlange, J. Y. (1980). Water transport in soils. *Annu. Rev. Fluid Mech.;(United States)*, *12*.
Parlange, J. Y., Barry, D. A., & Haverkamp, R. (2002). Explicit infiltration equations and the Lambert W-function. *Advances in Water Resources*. https://doi.org/10.1016/S0309-1708(02)00051-9
Parlange, J. Y., Haverkamp, R., & Touma, J. (1985). Infiltration under ponded conditions: 1. Optimal analytical solution and comparison with experimental observations. *Soil Science*. https://doi.org/10.1097/00010694-198504000-00003
Parlange, J. Y., Lisle, I., Braddock, R. D., & Smith, R. E. (1982). The three-parameter infiltration equation. *Soil Science*. https://doi.org/10.1097/00010694-198206000-00001
Parlange, Jean Yves. (1971a). Theory of water-movement in soils: 1. one-dimensional absorption.

Soil Science. https://doi.org/10.1097/00010694-197103000-00004
Parlange, Jean Yves. (1971b). Theory of water movement in soils: 3. two and three dimensional absorption. *Soil Science*. https://doi.org/10.1097/00010694-197202000-00004
Parlange, Jean Yves. (1972a). Theory of water movement in soils: 5. unsteady infiltration from spherical cavities. *Soil Science*. https://doi.org/10.1097/00010694-197203000-00002
Parlange, Jean Yves. (1972b). Theory of water movement in soils: 8.: One-dimensional infiltration with constant flux at the surface. *Soil Science*. https://doi.org/10.1097/00010694-197207000-00001
Parr, J. F., & Bertrand, A. R. (1960). Water infiltration into soils. *Advances in Agronomy*, *12*, 311–363.
Peng, X., & Horn, R. (2005). Modeling Soil Shrinkage Curve across a Wide Range of Soil Types. *Soil Science Society of America Journal*. https://doi.org/10.2136/sssaj2004.0146
Perroux, K. M., & White, I. (1988). Designs for Disc Permeameters. *Soil Science Society of America Journal*. https://doi.org/10.2136/sssaj1988.03615995005200050001x
Philip. (1971). *General theorem on steady infiltration from surface sources, with application to point and line sources*. https://doi.org/10.2136/sssaj1971.03615995003500060010x
Philip, J. R. (1957a). The theory of infiltration: 1. The infiltration equation and its solution. *Soil Science*. https://doi.org/10.1097/00010694-195705000-00002
Philip, J. R. (1957b). The theory of infiltration: 4. Sorptivity and algebraic infiltration equations. *Soil Science*. https://doi.org/10.1097/00010694-195709000-00010
Philip, J. R. (1967). Sorption and infiltration in heterogeneous media. *Australian Journal of Soil Research*. https://doi.org/10.1071/SR9670001
Philip, J. R. (1968). Steady Infiltration From Buried Point Sources and Spherical Cavities. *Water Resources Research*. https://doi.org/10.1029/WR004i005p01039
Philip, J. R. (1969). Hydrostatics and hydrodynamics in swelling soils. *Water Resources Research*. https://doi.org/10.1029/WR005i005p01070
Philip, J. R. (1972). Steady Infiltration from Buried, Surface, and Perched Point and Line Sources in Heterogeneous Soils: I. Analysis. *Soil Science Society of America Journal*. https://doi.org/10.2136/sssaj1972.03615995003600020020x
Philip, J. R. (1973). On solving the unsaturated flow equation: 1. the flux-concentration relation. *Soil Science*. https://doi.org/10.1097/00010694-197311000-00002
Philip, J. R. (1984). Steady Infiltration from Circular Cylindrical Cavities. *Soil Science Society of America Journal*. https://doi.org/10.2136/sssaj1984.03615995004800020008x
Philip, J. R. (1985a). Reply To "Comments on Steady Infiltration from Spherical Cavities. *Soil Science Society of America Journal*. https://doi.org/10.2136/sssaj1985.03615995004900060064x
Philip, J. R. (1985b). Scattering Functions and Infiltration. *Water Resources Research*. https://doi.org/10.1029/WR021i012p01889
Philip, J. R. (1986). Steady Infiltration From Buried Discs and Other Sources. *Water Resources Research*. https://doi.org/10.1029/WR022i007p01058
Philip, J. R. (1987). The infiltration joining problem. *Water Resources Research*. https://doi.org/10.1029/WR023i012p02239
Philip, J. R. (1992). Falling head ponded infiltration. *Water Resources Research*. https://doi.org/10.1029/92WR00704
Philip, J. R. (1993). Variable-head ponded infiltration under constant or variable rainfall. *Water Resources Research*. https://doi.org/10.1029/93WR00748

Philip, J. R. (1998). Infiltration into crusted soils. *Water Resources Research*. https://doi.org/10.1029/98WR01207

Philip, J. R. (1969). Theory of Infiltration. https://doi.org/10.1016/b978-1-4831-9936-8.50010-6

Philip, J. R., & Knight, J. H. (1974). On solving the unsaturated flow equation: 3. new quasi-analytical technique. *Soil Science*. https://doi.org/10.1097/00010694-197401000-00001

Poiseuille, J. L. (1844). *Recherches expérimentales sur le mouvement des liquides dans les tubes de très-petits diamètres*. Imprimerie Royale.

Pomchaitaward, C., Manas-Zloczower, I., & Feke, D. L. (2003). Lattice Boltzmann simulation of capillary infiltration in agglomerates and beds of fine particles. *Advanced Powder Technology*, *14*(3), 295–311.

Poulovassilis, A., & Argyrokastritis, I. (2020). A new approach for studying vertical infiltration. *Soil Research*. https://doi.org/10.1071/SR19266

Preziosi, L., Joseph, D. D., & Beavers, G. S. (1996). Infiltration of initially dry, deformable porous media. *International Journal of Multiphase Flow*. https://doi.org/10.1016/0301-9322(96)00035-3

Prodanović, M., & Bryant, S. L. (2006). A level set method for determining critical curvatures for drainage and imbibition. *Journal of Colloid and Interface Science*. https://doi.org/10.1016/j.jcis.2006.08.048

Raats, P. A. C. (1971). Steady Infiltration from Point Sources, Cavities, and Basins. *Soil Science Society of America Journal*. https://doi.org/10.2136/sssaj1971.03615995003500050020x

Raats, Peter A.C., & Knight, J. H. (2018). The contributions of Lewis Fry Richardson to drainage theory, soil physics, and the soil-plant-atmosphere continuum. *Frontiers in Environmental Science*. https://doi.org/10.3389/fenvs.2018.00013

Raats, Peter A C, Smiles, D., & Warrick, A. W. (2002). Environmental mechanics: water, mass and energy transfer in the biosphere. *American Geophysical Union.*

Rahmati, M., Latorre, B., Lassabatere, L., Angulo-Jaramillo, R., & Moret-Fernández, D. (2019). The relevance of Philip theory to Haverkamp quasi-exact implicit analytical formulation and its uses to predict soil hydraulic properties. *Journal of Hydrology*. https://doi.org/10.1016/j.jhydrol.2019.01.038

Rahmati, M., Weihermüller, L., Vanderborght, J., Pachepsky, Y. A., Mao, L., Sadeghi, S. H., Moosavi, N., Kheirfam, H., Montzka, C., Van Looy, K., Toth, B., Hazbavi, Z., Al Yamani, W., Albalasmeh, A. A., Alghzawi, M. Z., Angulo-Jaramillo, R., Antonino, A. C. D., Arampatzis, G., Armindo, R. A., … Vereecken, H. (2018). Development and analysis of the Soil Water Infiltration Global database. *Earth System Science Data*. https://doi.org/10.5194/essd-10-1237-2018

Raoof, A., & Majid Hassanizadeh, S. (2010). A new method for generating pore-network models of porous media. *Transport in Porous Media*. https://doi.org/10.1007/s11242-009-9412-3

Redinger, G. J., Campbell, G. S., Saxton, K. E., & Papendick, R. I. (1984). Infiltration rate of slot mulches: Measurement and numerical simulation. *Soil Science Society of America Journal*, *48*(5), 982–986.

Reichenberger, S., Amelung, W., Laabs, V., Pinto, A., Totsche, K. U., & Zech, W. (2002). Pesticide displacement along preferential flow pathways in a Brazilian Oxisol. *Geoderma*, *110*(1–2), 63–86.

Reynolds, W. D., & Elrick, D. E. (1990). Ponded Infiltration From a Single Ring: I. Analysis of Steady Flow. *Soil Science Society of America Journal*. https://doi.org/10.2136/sssaj1990.03615995005400050006x

Reynolds, W. D., Elrick, D. E., & Clothier, B. E. (1985). The constant head well permeameter: Effect of unsaturated flow. *Soil Science*. https://doi.org/10.1097/00010694-198502000-00011

Reynolds, W. D., Elrick, D. E., & Topp, G. C. (1983). A reexamination of the constant head well permeameter method for measuring saturated hydraulic conductivity above the water table. *Soil Science*. https://doi.org/10.1097/00010694-198310000-00008

Richards, L. A. (1931). Capillary conduction of liquids through porous mediums. *Journal of Applied Physics*. https://doi.org/10.1063/1.1745010

Richardson, L. F. (1922). Weather prediction by numerical process Cambridge University Press. *Monthly Weather Review*.

Rijtema, P. E. (1965). An analysis of actual evapotranspiration. Pudoc.

Rönnqvist, H. (2018). Double-Ring Infiltrometer for In-Situ Permeability Determination of Dam Material. *Engineering*, *10*(06), 320.

Rose, W. (1957). Studies of waterflood performance:[pt.] III. Use of network models. *Circular No. 237*.

Ross, Peter J, & Bristow, K. L. (1990). Simulating water movement in layered and gradational soils using the Kirchhoff transform. *Soil Science Society of America Journal*, *54*(6), 1519–1524.

Ross, Po Jo. (1990). Efficient numerical methods for infiltration using Richards' equation. *Water Resources Research*, *26*(2), 279–290.

Sahimi, M. (2011). *Flow and transport in porous media and fractured rock: from classical methods to modern approaches*. John Wiley & Sons.

Salvucci, G. D., & Entekhabi, D. (1994). Explicit expressions for Green-Ampt (delta function diffusivity) infiltration rate and cumulative storage. *Water Resources Research*. https://doi.org/10.1029/94WR01494

Schiff, L. (1953). The effect of surface head on infiltration rates based on the performance of ring infiltrometers and ponds. *Eos, Transactions American Geophysical Union*, *34*(2), 257–266.

Schmid, B. H. (1990). Derivation of an explicit equation for infiltration on the basis of the mein-larson model. *Hydrological Sciences Journal*. https://doi.org/10.1080/02626669009492418

Scotter, D. R., Clothier, B. E., & Harper, E. R. (1982). Measuring saturated hydraulic conductivity and sorptivity using twin rings. *Australian Journal of Soil Research*. https://doi.org/10.1071/SR9820295

Selker, J. S., & Assouline, S. (2017). An explicit, parsimonious, and accurate estimate for ponded infiltration into soils using the Green and Ampt approach. *Water Resources Research*. https://doi.org/10.1002/2017WR021020

Selker, J. S., Duan, J., & Parlange, J. Y. (1999). Green and Ampt infiltration into soils of variable pore size with depth. *Water Resources Research*. https://doi.org/10.1029/1999WR900008

Selker, J. S., McCord, J. T., & Keller, C. K. (1999). *Vadose zone processes*. CRC Press.

Serrano, S. E. (2001). Explicit solution to Green and Ampt infiltration equation. *Journal of Hydrologic Engineering*, *6*(4), 336–340.

Setiawan, B. I., & Nakano, M. (1993). On the determination of unsaturated hydraulic conductivity from soil moisture profiles and from water retention curves. *Soil Science*, *156*(6), 389–395.

Sharma, M. L., Gander, G. A., & Hunt, C. G. (1980). Spatial variability of infiltration in a watershed. *Journal of Hydrology*. https://doi.org/10.1016/0022-1694(80)90008-6

Shillito, R. M., Berli, M., & Ghezzehei, T. A. (2020). Quantifying the effect of subcritical water repellency on sorptivity: A physically based model. *Water Resources Research*, *56*(11),

e2020WR027942.
Simon, R., & Kelsey, F. J. (1971). The Use of Capillary Tube Networks in Reservoir Performance Studies: I. Equal-Viscosity Miscible Displacements. *Society of Petroleum Engineers Journal*. https://doi.org/10.2118/3068-pa
Simon, R., & Kelsey, F. J. (1972). The Use of Capillary Tube Networks in Reservoir Performance Studies: II. Effect of Heterogeneity and Mobility on Miscible Displacement Efficiency. *Society of Petroleum Engineers Journal*. https://doi.org/10.2118/3482-pa
Šimunek, J., Šejna, M., & Van Genuchten, M. T. (1998). The HYDRUS-1D software package for simulating the one-dimensional movement of water, heat, and multiple solutes in variably-saturated media, Version 2.0, 202 pp. *Rep. IGWMC-TPS*, *70*.
Simunek, J., Van Genuchten, M. T., & Sejna, M. (2005). The HYDRUS-1D software package for simulating the one-dimensional movement of water, heat, and multiple solutes in variably-saturated media. *University of California-Riverside Research Reports*, *3*, 1–240.
Šimůnek, J, Šejna, M., & Van Genuchten, M. T. (1999). The HYDRUS-2D software package for simulating the two-dimensional movement of water, heat, and multiple solutes in variably-saturated media: Version 2.0. US Salinity Laboratory, Agricultural Research Service, US Department of ….
Šimůnek, J, Van Genuchten, M. T., & Šejna, M. (2006). The HYDRUS software package for simulating two-and three-dimensional movement of water, heat, and multiple solutes in variably-saturated media. *Technical Manual, Version*, *1*, 241.
Šimůnek, Jirí, Genuchten, M. T., & Šejna, M. (2008). Development and Applications of the HYDRUS and STANMOD Software Packages and Related Codes. *Vadose Zone Journal*. https://doi.org/10.2136/vzj2007.0077
Šimůnek, Jiří, Genuchten, M. T., & Šejna, M. (2016). Recent Developments and Applications of the HYDRUS Computer Software Packages. *Vadose Zone Journal*. https://doi.org/10.2136/vzj2016.04.0033
Šimůnek, Jirka, Jarvis, N. J., Van Genuchten, M. T., & Gärdenäs, A. (2003). Review and comparison of models for describing non-equilibrium and preferential flow and transport in the vadose zone. *Journal of Hydrology*, *272*(1–4), 14–35.
Šimůnek, Jirka, & van Genuchten, M. T. (2008). Modeling nonequilibrium flow and transport processes using HYDRUS. *Vadose Zone Journal*, *7*(2), 782–797.
Singh, V. P. (2010). Entropy theory for derivation of infiltration equations. *Water Resources Research*. https://doi.org/10.1029/2009WR008193
Smettem, K. R. J., & Clothier, B. E. (1989). Measuring unsaturated sorptivity and hydraulic conductivity using multiple disc permeameters. *Journal of Soil Science*. https://doi.org/10.1111/j.1365-2389.1989.tb01297.x
Smettem, K. R. J., Parlange, J. Y., Ross, P. J., & Haverkamp, R. (1994). Three-dimensional analysis of infiltration from the disc infiltrometer: 1. A capillary-based theory. *Water Resources Research*. https://doi.org/10.1029/94WR01787
Smiles, D. E. (1974). Iltration into a swelling material. *Soil Science*. https://doi.org/10.1097/00010694-197403000-00002
Smiles, D., & Raats, P. A. C. (2005). Hydrology of Swelling Clay Soils. In *Encyclopedia of Hydrological Sciences*. https://doi.org/10.1002/0470848944.hsa071
Smith, R. E. (1990). Analysis of Infiltration through a Two-Layer Soil Profile. *Soil Science Society of America Journal*. https://doi.org/10.2136/sssaj1990.03615995005400050004x
Smith, R. E., Corradini, C., & Melone, F. (1999). A conceptual model for infiltration and

redistribution in crusted soils. *Water Resources Research*. https://doi.org/10.1029/1998WR900046
Smith, R. E., & Parlange, J. -Y. (1978). A parameter-efficient hydrologic infiltration model. *Water Resources Research*. https://doi.org/10.1029/WR014i003p00533
Smith, Roger E. (1972). The infiltration envelope: Results from a theoretical infiltrometer. *Journal of Hydrology*. https://doi.org/10.1016/0022-1694(72)90063-7
Smith, Roger E., Corradini, C., & Melone, F. (1993). Modeling infiltration for multistorm runoff events. *Water Resources Research*. https://doi.org/10.1029/92WR02093
Sommer, J. L., & Mortensen, A. (1996). Forced unidirectional infiltration of deformable porous media. *Journal of Fluid Mechanics*. https://doi.org/10.1017/S002211209600256X
Song, R., Peng, J., Sun, S., Wang, Y., Cui, M., & Liu, J. (2020). Visualized experiments on residual oil classification and its influencing factors in waterflooding using micro-computed tomography. *Journal of Energy Resources Technology*, *142*(8), 83003.
Srivastava, P., Costello, T. A., & Edwards, D. R. (1996). A direct, approximate solution to the modified Green-Ampt infiltration equation. *Transactions of the American Society of Agricultural Engineers*. https://doi.org/10.13031/2013.27633
Stewart, R. D. (2018). A Dynamic Multidomain Green-Ampt Infiltration Model. *Water Resources Research*. https://doi.org/10.1029/2018WR023297
Stewart, R. D. (2019). A generalized analytical solution for preferential infiltration and wetting. *Vadose Zone Journal*, *18*(1), 1–10. https://doi.org/10.2136/vzj2018.08.0148
Stewart, R. D., & Abou Najm, M. R. (2018a). A Comprehensive Model for Single Ring Infiltration I: Initial Water Content and Soil Hydraulic Properties. *Soil Science Society of America Journal*. https://doi.org/10.2136/sssaj2017.09.0313
Stewart, R. D., & Abou Najm, M. R. (2018b). A Comprehensive Model for Single Ring Infiltration II: Estimating Field-Saturated Hydraulic Conductivity. *Soil Science Society of America Journal*, *82*(3), 558–567.
Stewart, R. D., Abou Najm, M. R., Rupp, D. E., & Selker, J. S. (2016). Modeling multidomain hydraulic properties of shrink-swell soils. *Water Resources Research*, *52*(10), 7911–7930.
Stokes, G. G. (1850). On the effect of the Internal friction of fluids on the motion of pendulums - Section III. *Transactions of the Cambridge Philosophical Society*.
Stone, J. J., Hawkins, R. H., & Shirley, E. D. (1994). Approximate form of Green-Ampt infiltration equation. *Journal of Irrigation and Drainage Engineering*. https://doi.org/10.1061/(ASCE)0733-9437(1994)120:1(128)
Stroosnijder, L. (1976). Infiltratie en herverdeling van water in grond, Versl. *Landbouwkd. Onderz*, *847*.
Su, H., Jia, Y., Gan, Y., Ni, G., Niu, C., Liu, H., Jin, T., & Yao, Y. (2020). Soil water movement model for deformable soils. *Journal of Water and Climate Change*. https://doi.org/10.2166/wcc.2019.262
Su, N. (2009). Equations of anomalous absorption onto swelling porous media. *Materials Letters*. https://doi.org/10.1016/j.matlet.2009.08.039
Su, N. (2010). Theory of infiltration: Infiltration into swelling soils in a material coordinate. *Journal of Hydrology*. https://doi.org/10.1016/j.jhydrol.2010.10.019
Swamee, P. K., Rathie, P. N., & Ozelim, L. C. de S. M. (2012). Explicit equations for infiltration. *Journal of Hydrology*. https://doi.org/10.1016/j.jhydrol.2012.01.020
Swartzendruber, D. (1974). Infiltration of constant-flux rainfall into soil as analyzed by the approach of green and ampt. *Soil Science*. https://doi.org/10.1097/00010694-197405000-

00006
Swartzendruber, D. (2000). Derivation of a two-term infiltration equation from the Green-Ampt model. *Journal of Hydrology*. https://doi.org/10.1016/S0022-1694(00)00297-3
Swartzendruber, D., & Hogarth, W. L. (1991). Water Infiltration into Soil in Response to Ponded-Water Head. *Soil Science Society of America Journal*. https://doi.org/10.2136/sssaj1991.03615995005500060001x
Swartzendruber, D. (1987). Rigorous derivation and interpretation of the Green and Ampt equation. *Infiltration Development and Application. Water Resour. Res. Ctr., Univ. of Hawaii, Honolulu*.
Swartzendruber, D, & Youngs, E. G. (1974). A comparison of physically-based infiltration equations. *Soil Science*, *117*(3), 165–167.
Swartzendruber, Dale. (1987). A quasi-solution of Richards' Equation for the downward infiltration of water into soil. *Water Resources Research*. https://doi.org/10.1029/WR023i005p00809
Talsma, T. (1969). In situ measurement of sorptivity. *Soil Research*. https://doi.org/10.1071/sr9690269
Talsma, T., & Parlange, J. Y. (1972). One-dimensional vertical infiltration. *Australian Journal of Soil Research*. https://doi.org/10.1071/SR9720143
Toledo, P. G., Scriven, L. E., & Davis, H. T. (1994). Pore-space statistics and capillary pressure curves from volume- controlled porosimetry. *SPE Formation Evaluation*. https://doi.org/10.2118/19618-PA
Torelli, L., & Scheidegger, A. E. (1971). Random maze models of flow through porous media. *Pure and Applied Geophysics PAGEOPH*. https://doi.org/10.1007/BF00875202
Touma, J., Voltz, M., & Albergel, J. (2007). Determining soil saturated hydraulic conductivity and sorptivity from single ring infiltration tests. *European Journal of Soil Science*. https://doi.org/10.1111/j.1365-2389.2006.00830.x
Tzavaras, J., Köhne, M., & Vogel, H.-J. (2017). From pore scale to continuum scale modeling of infiltration. *Advances in Water Resources*, *103*, 108–118.
Valiantzas, J. D. (2010). New linearized two-parameter infiltration equation for direct determination of conductivity and sorptivity. *Journal of Hydrology*. https://doi.org/10.1016/j.jhydrol.2009.12.049
Valvatne, P. H., & Blunt, M. J. (2004). Predictive pore-scale modeling of two-phase flow in mixed wet media. *Water Resources Research*. https://doi.org/10.1029/2003WR002627
Van De Hulst, H. C. (1949). On the attenuation of plane waves by obstacles of arbitrary size and form. *Physica*. https://doi.org/10.1016/0031-8914(49)90079-8
van Genuchten, M. Th. (1980). A Closed-form Equation for Predicting the Hydraulic Conductivity of Unsaturated Soils. *Soil Science Society of America Journal*. https://doi.org/10.2136/sssaj1980.03615995004400050002x
Van Genuchten, M T van, Leij, F. J., & Yates, S. R. (1991). The RETC code for quantifying the hydraulic functions of unsaturated soils.
Van Schaik, N., Schnabel, S., & Jetten, V. G. (2008). The influence of preferential flow on hillslope hydrology in a semi-arid watershed (in the Spanish Dehesas). *Hydrological Processes: An International Journal*, *22*(18), 3844–3855.
Vatankhah, A. R. (2015a). Discussion of "Modified green-ampt infiltration model for steady rainfall" by J. Almedeij and I. I. Esen. In *Journal of Hydrologic Engineering*. https://doi.org/10.1061/(ASCE)HE.1943-5584.0001110

Vatankhah, A. R. (2015b). Discussion of "Modified Green-Ampt Infiltration Model for Steady Rainfall" by J. Almedeij and I. I. Esen. *Journal of Hydrologic Engineering*. https://doi.org/10.1061/(asce)he.1943-5584.0001110

Waechter, R. T., & Philip, J. R. (1985). Steady Two- and Three-Dimensional Flows in Unsaturated Soil: The Scattering Analog. *Water Resources Research*. https://doi.org/10.1029/WR021i012p01875

Warrick, A. W., & Lazarovitch, N. (2007). Infiltration from a strip source. *Water Resources Research*. https://doi.org/10.1029/2006WR004975

Warrick, A. W., Lazarovitch, N., Furman, A., & Zerihun, D. (2007). Explicit Infiltration Function for Furrows. *Journal of Irrigation and Drainage Engineering*. https://doi.org/10.1061/(asce)0733-9437(2007)133:4(307)

Warrick, A. W., Lomen, D. O., & Yates, S. R. (1985). A Generalized Solution to Infiltration. *Soil Science Society of America Journal*. https://doi.org/10.2136/sssaj1985.03615995004900010006x

Watson, K. K. (1966). An instantaneous profile method for determining the hydraulic conductivity of unsaturated porous materials. *Water Resources Research*. https://doi.org/10.1029/WR002i004p00709

Watson, K. W., & Luxmoore, R. J. (1986). Estimating Macroporosity in a Forest Watershed by use of a Tension Infiltrometer. *Soil Science Society of America Journal*. https://doi.org/10.2136/sssaj1986.03615995005000030007x

Weiler, M. (2005). An infiltration model based on flow variability in macropores: Development, sensitivity analysis and applications. *Journal of Hydrology*. https://doi.org/10.1016/j.jhydrol.2005.01.010

Whisler, F. D., & Bouwer, H. (1970). Comparison of methods for calculating vertical drainage and infiltration for soils. *Journal of Hydrology*. https://doi.org/10.1016/0022-1694(70)90051-X

White, I., & Sully, M. J. (1987). Macroscopic and microscopic capillary length and time scales from field infiltration. *Water Resources Research*. https://doi.org/10.1029/WR023i008p01514

White, Ian, Sully, M. J., & Perroux, K. M. (1992). Measurement of surface-soil hydraulic properties: Disk permeameters, tension infiltrometers, and other techniques. *Advances in Measurement of Soil Physical Properties: Bringing Theory into Practice*, *30*, 69–103.

Wilkinson, D., & Willemsen, J. F. (1983). Invasion percolation: A new form of percolation theory. *Journal of Physics A: Mathematical and General*. https://doi.org/10.1088/0305-4470/16/14/028

Wilkinson, David. (1984). Percolation model of immiscible displacement in the presence of buoyancy forces. *Physical Review A*. https://doi.org/10.1103/PhysRevA.30.520

Wind, G. P. (1955). A field experiment concerning capillary rise of moisture in a heavy clay soil. *Netherlands Journal of Agricultural Science*. https://doi.org/10.18174/njas.v3i1.17827

Wooding, R. A. (1968). Steady Infiltration from a Shallow Circular Pond. *Water Resources Research*. https://doi.org/10.1029/WR004i006p01259

Wu, L., & Pan, L. (1997). A Generalized Solution to Infiltration from Single-Ring Infiltrometers by Scaling. *Soil Science Society of America Journal*. https://doi.org/10.2136/sssaj1997.03615995006100050005x

Wu, L., Pan, L., Mitchell, J., & Sanden, B. (1999). Measuring Saturated Hydraulic Conductivity using a Generalized Solution for Single-Ring Infiltrometers. *Soil Science Society of America Journal*. https://doi.org/10.2136/sssaj1999.634788x

Xu, X., Lewis, C., Liu, W., Albertson, J. D., & Kiely, G. (2012). Analysis of single-ring infiltrometer data for soil hydraulic properties estimation: Comparison of BEST and Wu methods. *Agricultural Water Management*. https://doi.org/10.1016/j.agwat.2012.01.004

Yeh, T. -C J. (1989). One-dimensional steady state infiltration in heterogeneous soils. *Water Resources Research*. https://doi.org/10.1029/WR025i010p02149

Yilmaz, D., Di Prima, S., Stewart, R. D., Abou Najm, M. R., Fernandez-Moret, D., Latorre, B., & Lassabatere, L. (2022). Three-term formulation to describe infiltration in water-repellent soils. *Geoderma*, *427*, 116127.

Youngs, E. G. (1968). An estimation of sorptivity for infiltration studies from moisture moment considerations. *Soil Science*. https://doi.org/10.1097/00010694-196809000-00001

Youngs, E. G. (1995). Developments in the Physics of Infiltration. *Soil Science Society of America Journal*. https://doi.org/10.2136/sssaj1995.03615995005900020005x

Zachmann, D. W., DuChateau, P. C., & Klute, A. (1981). The Calibration of the Richards Flow Equation for a Draining Column by Parameter Identification. *Soil Science Society of America Journal*. https://doi.org/10.2136/sssaj1981.03615995004500060002x

Zadeh, K. S., Shirmohammadi, A., Montas, H. J., & Felton, G. (2007). Evaluation of infiltration models in contaminated landscape. *Journal of Environmental Science and Health - Part A Toxic/Hazardous Substances and Environmental Engineering*. https://doi.org/10.1080/10934520701373000

Zehe, E., & Flühler, H. (2001). Preferential transport of isoproturon at a plot scale and a field scale tile-drained site. *Journal of Hydrology*, *247*(1–2), 100–115.

Zhang, R. (1997). Determination of Soil Sorptivity and Hydraulic Conductivity from the Disk Infiltrometer. *Soil Science Society of America Journal*. https://doi.org/10.2136/sssaj1997.03615995006100040005x

Zheng, C., & Gorelick, S. M. (2003). Analysis of solute transport in flow fields influenced by preferential flowpaths at the decimeter scale. *Groundwater*, *41*(2), 142–155.

CHAPTER 3: The Problem of Too Many Infiltration Models: How Can We Maintain the Physical Meaning of Soil Hydraulic Parameters?

3.1. Abstract

The crucial impact of infiltration process on many related physical and biogeochemical processes has motivated researchers to develop numerous models for assessing infiltration over the past two centuries, resulting in 138 identified infiltration models. The proliferation of infiltration models, in one respect, has enhanced understanding and assessment of these processes. However, this proliferation has potentially challenged researchers to decide which model to utilize when analyzing experimental infiltration data, and subsequently determine the appropriate procedures for extracting soil hydraulic properties, such as saturated hydraulic conductivity K_s (LT^{-1}) and sorptivity S ($LT^{-0.5}$). At this level, an accurate estimation of hydraulic properties requires a complete investigation of soil hydraulic models and data extraction techniques. Although several studies have touched upon the various concepts of infiltration modeling and evaluated model performance, a comprehensive and unbiased evaluation of the variability among the estimated infiltration characteristics from different models has been lacking till now. This gap exists not only among different models but also extends to various extraction techniques. Addressing this gap is essential for determining the consistency and uniqueness of the estimated infiltration parameters across different models and for exploring suitable procedures for extracting saturated hydraulic conductivity K_s (LT^{-1}) and sorptivity S ($LT^{-0.5}$). At this end, an uncertainty meta-analysis was carried out using a global infiltration database of 5,023 cumulative infiltration curves. This analysis focused on assessing the variability of the estimated infiltration characteristics, K_s (LT^{-1}) and S ($LT^{-0.5}$) from eleven one-dimensional (1D) infiltration models and different extraction techniques applied to estimate those characteristics. Our results distinctly demonstrated the notable variations

in saturated hydraulic conductivity K_s (LT^{-1}) and sorptivity S ($LT^{-0.5}$) derived from various models under varying extraction techniques. The observed changes in K_s (LT^{-1}) and S ($LT^{-0.5}$) indicate that the characteristics related to the models and extraction methods have a significant impact on the predictions of soil hydraulic parameters. Ultimately, our study has demonstrated an appropriate practice to evaluate the performance of 1D infiltration models under different extraction methods and assess the variability of the predictions of soil hydraulic parameters including K_s (LT^{-1}) and S ($LT^{-0.5}$). These insights are crucial for practical applications in fields such as agriculture and hydrology, guiding the selection of both models and extraction techniques based on project-specific requirements. Additionally, our findings suggested avenues for future research and improvements in existing models and techniques.

3.2. Introduction

The infiltration process describes entry of water into soil, and its subsequent movement or retention within soil. Water retention due to capillarity, namely sorptivity S ($LT^{-0.5}$) according to Philip (1957b), controls water movement at the early state of infiltration; then at transient state, hydraulic conductivity comes into play and eventually governs the infiltration process at steady state which is mainly driven by gravity. Building upon Philip's theory which has been widely adopted and expanded by many researchers, saturated hydraulic conductivity K_s (LT^{-1}) can be determined as the steady-state slope of the cumulative infiltration curve. This curve is a graphical representation that shows the cumulative amount of water that has infiltrated into soil over time during a rainfall or irrigation event.

Because of the fundamental role of infiltration in soil hydrology and biogeochemistry, numerous models ranging from empirical to physically based have been developed to determine hydraulic parameters such as K_s (LT^{-1}) and S ($LT^{-0.5}$), and therefore estimate the infiltration capacity of soils. Basset et al. (2023), presented a comprehensive critical review that traced the development of conceptual and empirical models over the past two centuries through a historical and theoretical evolution assessment. Based on their review, 138 unique infiltration models were compiled and examined based on underlying infiltration philosophies and characteristics.

Commonly used models among the 138 infiltration models developed through the past century, specifically Green and Ampt (1911), Kostiakov (1932), Horton (1940), Mezencev (1948), Philip (1957b), Parlange et al. (1982), Swartzendruber (1987), and Haverkamp et al. (1990, 1994) were examined by several review studies to evaluate and determine which of these models are most suitable for field applications (Mishra et al., 2003; Fodor et al., 2011; Mirzaee et al., 2014; Jacka et al., 2016; Sihag et al., 2017; Nie at al., 2017; Vand et al., 2018; Bayabil et al., 2019). Such

studies identified best-fit models by curve-fitting infiltration equations using measured infiltration data.

Typically, infiltration data is measured by means of different experimental tools including ring, cylinder, and disc infiltrometers designed to measure one- or multi-dimensional flow that can include early, transient, and steady-state flow stages depending on the approach being applied (Schiff, 1953; Parr and Bertrand, 1960; Olson, 1960; Bouwer, 1960, 1963, 1986; Watson and Luxmoore, 1986; Perroux and White, 1988; Elrick et al., 1995; Angulo-Jaramillo et al., 2003, Bagarello et al., 2004; Touma et al., 2007; Xu et al., 2012; Di Prima et al., 2016; Ronnqvist, 2018). Once experimental data is collected, soil hydraulic properties such as saturated hydraulic conductivity K_s (LT^{-1}) and sorptivity S ($LT^{-0.5}$) which are key characteristics for many conceptual infiltration models can be determined by incorporating infiltration data into multi-dimensional infiltration equation, eventually obtaining solutions of K_s (LT^{-1}) and S ($LT^{-0.5}$) using approximate analytical or numerical techniques.

Accuracy of K_s (LT^{-1}) and S ($LT^{-0.5}$) estimates depends upon the degree to which steady flow is attained within the system, and upon the ability of each experimental method to account for various theoretical and practical constraints associated with representing the physical system using selected infiltration equations. Additionally, the evolving landscape of statistical and numerical data analysis techniques underscores the need to evaluate accuracy of the extraction techniques. Given these aspects, it has become imperative to determine the accuracy of K_s (LT^{-1}) and S ($LT^{-0.5}$) estimated from soil hydraulic models, as well as variability and uniqueness of these parameters across various models and different extraction techniques. By examining differences in predictions of K_s (LT^{-1}) and S ($LT^{-0.5}$) among infiltration models using diverse data analysis methods, we can

gain insight into the robustness of the available applied practices in estimating soil hydraulic parameter through infiltration modeling and data analysis.

Realizing the need for a thorough and impartial evaluation of the variability in estimated infiltration characteristics among infiltration models and extraction methods, we carried out an uncertainty metadata analysis to achieve two-folded objectives: 1) assess the variability of estimated infiltration characteristics, saturated hydraulic conductivity K_s (LT^{-1}) and sorptivity S ($LT^{-0.5}$) from different infiltration models, and 2) evaluate the robustness of these models across various extraction analysis techniques applied to estimate K_s (LT^{-1}) and S ($LT^{-0.5}$). Our meta-analysis is performed in R software using 5023 infiltration data curves extracted from SWIG, the global infiltration database developed by Rahmati et al. (2018).

3.3. Materials and Methods

3.3.1. Infiltration models

Basset et al. (2023) identified and compiled 138 unique infiltration models, among which 102 were one-dimensional (1D) infiltration models. Drawing from their review, we selected eleven one-dimensional (1D) infiltration models spanning from the 1900s to present, which represents a comprehensive spectrum of mathematical and physical concepts in infiltration modeling theory, while covering both widely utilized and recently developed approaches for estimating infiltration characteristics. Following is a summary of the specific characteristics of the selected infiltration models, along with their corresponding equations.

3.3.1.1.Green and Ampt (1911)

Green and Ampt (1911) is one of the earliest developed infiltration models recognized as a pioneering effort in understanding and quantifying one-dimensional water infiltration into soils during rainfall events with ponding conditions. The single equation proposed by Green and Ampt, commonly known as GA, was developed assuming a constant wetting front that moves at constant water content θ (L^3L^{-3}) and, thus, constant matric potential ψ_{wf} (L), as well as constant hydraulic conductivity K_s (LT^{-1}), since water always moves within a saturated soil. Despite the main assumption of a sharp wetting front throughout the infiltration process, Green and Ampt model had laid the foundation for many subsequent advancements in infiltration modeling.

$$t = \frac{I_{1D}}{K_s} - \frac{(\psi_{wf}+h_0)(\theta_s-\theta_i)}{K_s} ln\left(1 + \frac{I_{1D}}{(\theta_s-\theta_i)(\psi_{wf}+h_0)}\right) \quad [3.39]$$

where I_{1D} (L) is the cumulative one-dimensional infiltration, t (T) is time, h_0 (L) is the ponding head at the surface, θ_s and θ_i (L^3L^{-3}) are the saturated and initial water contents, respectively.

3.3.1.2. Philip (1957b)

Philip (1957b) is one of the most widely known and applied infiltration models and has been instrumental in advancing our understanding of the infiltration process. Philip (1957b) is credited with deriving an explicit two-term equation of cumulative, one-dimensional infiltration I_{1D} (L) with negative or zero head surface boundary condition ($h_0 \leq 0$ and $\theta_o \leq \theta_s$) for early and transient infiltration times based on his classical time series solution (Philip, 1957a). The two-term derived equation (hereafter called 2TR-Philip) has been extensively used to determine the saturated hydraulic conductivity K_s (LT^{-1}) and sorptivity S ($LT^{-0.5}$).

For small times,

$$I_{1D} = St^{0.5} + At \qquad [3.40TR]$$

where A (LT^{-1}) is the parameter describing water movement due to gravity. $A = mK_s$ with $1/3 \leq m \leq 2/3$ (Youngs, 1968; Philip, 1969; Talsma, 1969, Talsma and Parlange, 1972). $m = 0.363$ may be appropriate for soils with a relatively low initial moisture content (Philip, 1987), while a value of $m = 2/3$ is often used (Whisler and Bouwer, 1970, Fodor et al., 2011). Simultaneously, Philip (1957b) defined saturated hydraulic conductivity K_s (LT^{-1}) as the steady-state slope of the cumulative infiltration curve and accordingly expressed this asymptote through a linear regression equation in terms of K_s (LT^{-1}) and S ($LT^{-0.5}$) (hereafter called 2ST-Philip)

For large times,

$$I_{1D} = K_s t + \frac{S^2}{4(K_s - A)} \qquad [3.2ST]$$

3.3.1.3. Li et al. (1976)

Li et al. (1976) developed the first explicit solution for GA model to estimate cumulative one-dimensional infiltration I_{1D} (L) while eliminating the need for iterative computations. Their approach involved using the first term of a power-series expansion of the natural logarithmic term included in the original implicit equation of Green and Ampt (1911).

$$I_{1D} = \frac{1}{2}(\psi_{wf} + h_0)(\theta_s - \theta_i)\left(t^* + \sqrt{(t^*)^2 + 8t^*}\right) \quad [3.3]$$

where: $t^* = \frac{K_s}{(\psi_{wf}+h_0)(\theta_s-\theta_i)}t$

3.3.1.4. Brutsaert (1977)

Brutsaert (1977) proposed an approximate method that integrates the ordinary differential equations of each of the functions $X_1(\theta), X_2(\theta), X_3(\theta)$ and $X_4(\theta)$ in Philip's time series solution for $z(\theta, t)$ (Philip, 1957a) assuming these functions behave as near-step functions. His approach determines cumulative one-dimensional infiltration I_{1D} (L) with negative or zero head surface boundary condition ($h_0 \leq 0$ and $\theta_o \leq \theta_s$) for short but also, for large time of infiltration.

$$I_{1D} = K_s t + \frac{S^2}{\beta_0 K_s}\left[1 - \frac{1}{1+\frac{\beta_0 K_s t^{0.5}}{S}}\right] \quad [3.4]$$

where β_0 is a fitting parameter, $0 \leq \beta_0 \leq 1$; $\beta_0 = 2/3$ is sufficiently accurate for most soils.

3.3.1.5. Parlange (1980)

Using Darcy's law and the conservation of mass, Parlange (1980) formulated two equations to express cumulative one-dimensional infiltration I_{1D} (L) under ponding conditions $(h_0 \geq 0)$. Equation [5a] assumes that soil diffusivity D (L^2T^{-1}) increases rapidly with water content θ (L^3L^{-}

^{3}) while conductivity, K (LT^{-1}), varies much less rapidly near saturation; Equation [5b] assumes that D (L^2T^{-1}) and $\frac{\partial K}{\partial z}$ (T^{-1}) increase rapidly, and in similar fashion.

$$t = \frac{I_{1D}}{(K_s - K_i)} - \frac{S^2}{2(K_s - K_i)^2} ln \left(1 + \frac{2(K_s - K_i)I_{1D}}{S^2}\right) \quad [3.5a]$$

$$t = \frac{I_{1D}}{(K_s - K_i)} + \frac{S^2}{2(K_s - K_i)^2} \left(e^{-\frac{2(K_s - K_i)I_{1D}}{S^2}} - 1\right) \quad [3.5b]$$

Equation 3.5a can be expressed as GA equation 3.1 with $S = \sqrt{2(h_0 + \psi_{wf})K_s(\theta_s - \theta_i)}$ (Collis-George, 1977) and initial hydraulic conductivity $K_i = 0$, and therefore disregarded to avoid replicability.

3.3.1.6. Parlange et al. (1982)

As an attempt to embrace different variations of the diffusivity term D (L^2T^{-1}) and hydraulic conductivity K (LT^{-1}), Parlange et al. (1982) developed a three-parameter one-dimensional infiltration model for negative or zero head surface boundary condition ($h_0 \leq 0$ and $\theta_o \leq \theta_s$) by introducing a new dimensionless parameter δ.

For small times,

$$I_{1D} = St^{0.5} + \frac{1}{3}(2 - \delta)(K_s - K_i)t \quad [3.6TR]$$

For large times,

$$I_{1D} = (K_s - K_i)t + \frac{S^2}{2(K_s - K_i)(1 - \delta)} ln \left(\frac{1}{\delta}\right) \quad [3.6ST]$$

where δ takes values from 0 to 1, with an approximate used value of 0.85.

3.3.1.7. Swartzendruber (1987)

Swartzendruber (1987) derived a quasi-solution of Richards' equation for one-dimensional water infiltration into soils. His solution aligns with the classical Philip's time series solution $z(\theta, t)$ for early and transient times (Philip, 1957a). Furthermore, Swartzendruber's solution extends Philip's solution to cover asymptotically large times (Philip, 1957b).

$$I_{1D} = K_s t + \frac{S}{A_0}\left(1 - e^{-A_0 t^{0.5}}\right) \quad [3.7]$$

where A_0 is a fitting parameter depending on the initial water content θ_i. $A_0 = \frac{4K_s}{3S}$ (Stroosnijder, 1976). As $A_0 \rightarrow 0$, Swartzentruber's equation reduces to the steady-state form of Philip's model (1957b) with K_s (LT^{-1}) being the coefficient of the linear term.

3.3.1.8. Stone et al. (1994)

Stone et al. (1994) developed an explicit approximation of GA equation by using a Taylor-series expansion. The resulting one-dimensional infiltration equation takes the following form:

$$I_{1D} = (\psi_{wf} + h_0)\Delta\theta\left(t^* + \sqrt{2t^*} - 0.2987{t^*}^{0.7913}\right) \quad [3.8]$$

3.3.1.9. Valiantzas (2010)

Valiantzas (2010) proposed a three-parameter approximate equation as a direct method for determining saturated hydraulic conductivity K_s (LT^{-1}) and sorptivity S ($LT^{-0.5}$) of soils. The equation was derived to approach Philip's infinite time series solution at small and moderate times (Philip 1957a), while characterizing the constant K_s (LT^{-1}) at large times. Through his one-dimensional infiltration equation, Valiantzas aimed to provide a practical approach to estimating K_s (LT^{-1}) and S ($LT^{-0.5}$) without the need for extensive time-consuming measurements or complex modeling techniques.

$$I_{1D} = St^{0.5} + \frac{1}{2}K_s t + \frac{1}{8}\frac{K_s^2}{S}t^{1.5} \quad [3.9]$$

3.3.1.10. Rahmati et al. (2019)

Recognizing the complex resolution of the quasi-exact implicit (QEI) analytical formulation of Haverkamp's equation (Haverkamp et al., 1994), Rahmati et al. (2019) applied Taylor series up to third order in powers 0.5 to (QEI) to develop the following three-term one-dimensional infiltration model for early and transient time of infiltration:

$$I_{1D} = St^{0.5} + \frac{2-\beta}{3}K_s t + \frac{1}{9}(\beta^2 - \beta + 1)\frac{K_s^2}{S}t^{1.5} \quad [3.10]$$

3.3.1.11. Abou Najm et al. (2021)

In an effort to depict infiltration patterns across diverse structural interactions such as soil water-repellency, Abou Najm et al. (2021) presented a macroscopic approach by proposing a simple correction term $(1 - e^{-\alpha_{wr}t})$ that can be applied to any infiltration model estimating one- or three-dimensional infiltration rate i (LT^{-1}) while simulating infiltration behaviors of water-repellent soils, where α_{wr} (T^{-1}) is the soil water-repellency parameter.

To demonstrate the effectiveness of their method, Abou Najm et al. (2021) applied the correction term $(1 - e^{-\alpha_{wr}t})$ to a simple two-term infiltration model (Stewart and Abou Najm, 2018a) similar to the two-term type solution by Philip (1957b), leading to the following equation of cumulative one-dimensional infiltration I_{1D} (L) for small times:

$$I_{1D} = c_1\sqrt{t} + c_2 t - \frac{c_1\sqrt{\pi}}{2\sqrt{\alpha_{wr}}}\left(1 - e^{-\alpha_{wr}t}\left(\frac{1+\sqrt{\pi\alpha_{wr}t}-2\sqrt{\frac{\alpha_{wr}t}{\pi}}}{1+\sqrt{\pi\alpha_{wr}t}+(\pi-2)\alpha_{wr}t}\right)\right) - \frac{c_2\left(1-e^{-\alpha_{wr}t}\right)}{\alpha_{wr}} \quad [3.11]$$

where c_1 ($LT^{-1/2}$) and c_2 (LT^{-1}) are constants specific to the soil type and initial and boundary conditions (e.g., ponding depth, ring geometry, initial water content). In the one-dimensional infiltration model developed by Philip (1957b), c_1 is sorptivity S ($LT^{-1/2}$), and c_2 is A (LT^{-1}).

At this stage, we compiled the eleven selected models mentioned earlier, along with their corresponding parameters, as presented in Table 3.1. Additionally, we outlined the mathematical relationships relating hydraulic parameters defined by each model to both, sorptivity S ($LT^{-1/2}$) and saturated hydraulic conductivity K_s (LT^{-1}). These relationships are used to substitute model's parameters by S ($LT^{-1/2}$) and K_s (LT^{-1}), ultimately deriving infiltration equations with two unknowns (S, K_s). This substitution is a key aspect of our analysis since our study revolves around the estimation of two fundamental infiltration parameters, S ($LT^{-1/2}$) and K_s (LT^{-1}), while assessing the extent of variability in estimating these parameters across the eleven different models when subjected to different extraction techniques. Exceptionally, in Abou Najm et al.'s (2021) model, an additional new parameter, the soil water-repellency parameter α_{wr} (T^{-1}), is introduced and needs to be optimized as well. Any assumed values of the models' fitting-type parameters are included in Table 3.1.

Table 3.1: Compilation of the eleven selected infiltration models

Models	Parameters	Relationship between models' parameters and S and/or K_s	Fitting parameters
Green and Ampt (1911) - GA Li et al. (1976) Stone et al. (1994)	K_s, ψ_{wf}, h_0, θ_s and θ_i	$S = \sqrt{2(h_0+\psi_{wf})K_s(\theta_s - \theta_i)}$ (Collis-George, 1977)	
Philip (1957b)	S and A	$A = mK_s$	$1/3 \leq m \leq 2/3$ (Philip, 1969a; Talsma, 1969, Talsma and Parlange, 1972). $m = 0.363$ may be appropriate for soils with a relatively low initial moisture content (Philip, 1987), while a value of $m = 2/3$ is often used (Whisler and Bouwer, 1970, Fodor et al., 2011).
Abou Najm et al. (2021) - WR	c_1, c_2, and α_{wr}	$c_1 = S$ $c_2 = A = mK_s$ (Philip, 1957b)	
Brutsaert (1977)	K_s, S and β_0		$0 \leq \beta_0 \leq 1$; $\beta_0 = 2/3$ is sufficiently accurate for most soils (Brutsaert, 1977; Selker and Assouline, 2017; Stewart, 2019).
Parlange (1980)	K_s, K_i and S		$K_i = 0$
Parlange e al. (1982)	K_s, K_i, S and δ		$0 \leq \delta \leq 1$, and changes slightly with the type of soil. A value of $\delta = 0.85$ is representative for many types of soil (Parlange et al., 1985; Haverkamp et al., 1990). $K_i = 0$
Swartzendruber (1987)	K_s, S and A_0	$A_0 = \frac{4K_s}{3S_H}$ (Stroosnijder, 1976)	
Valiantzas (2010)	K_s and S		
Rahmati et al. (2019)	K_s, S and β		$0.3 \leq \beta \leq 1.7$ for sand to silty soils, respectively (Lassabatere et al., 2009, Rahmati et al., 2019). β is interpolated within this range depending on the specified soil textural class. In case where soil texture is unspecifief, an average value of $\beta = 0.6$ can be used.

3.3.2. R software

Our metadata analysis was conducted in R - a powerful programming language and open-source software environment that is widely used for statistical computing, data analysis, and graphical visualization. Using R software, we aimed to:

- Clean, transform, and restructure the collected infiltration data used for analysis.
- Build and statistically evaluate the eleven infiltration models.
- Estimate the two fundamental parameters, sorptivity S ($LT^{-0.5}$), and saturated hydraulic conductivity K_s (LT^{-1}) from the eleven models using different extraction techniques.
- Create high-quality visual graphs representing the performance of models and extraction techniques, as well as the variability of the estimated parameters, S ($LT^{-0.5}$) and K_s (LT^{-1}).

3.3.3. Data collection and preprocessing

We obtained infiltration data from the Soil Water Infiltration Global Database (SWIG), which was developed by Rahmati et al. (2018). SWIG stands out as the largest and most up-to-date infiltration database compiling 5023 experimental plots that depict cumulative infiltration curves (cumulative infiltration I (cm) vs. time T (hr)). These curves were digitized by collecting experimental data from available literature, as well as obtaining published or unpublished data from various researchers worldwide. SWIG also provides additional information about the location of infiltration measurements, soil characteristics, and the land management practices involved. Due to its vast amount of information on soil water infiltration characteristics, this comprehensive database can be instrumental in advancing our understanding of soil-water interactions and further supporting our analysis.

Then we thoroughly examined the actual dataset obtained from SWIG to identify any discrepancies or inconsistencies among the 5023 cumulative infiltration curves that can potentially disrupt the analysis. A quality check on any dataset prior to the analysis ensures the consistency of the dataset and prevents potential inaccuracies in the analysis. Following is step-by-step exclusion approach we followed to clean our infiltration dataset used in the analysis (Figure 3.1):

1) The dataset has been inspected for missing data and any inconsistencies, including typographical errors and NA values.
2) The dataset has been inspected for negative or decreasing data points within each experimental plot of the dataset. Since it is not physically possible for cumulative infiltration to decrease as infiltration time increases, such negative or decreasing values could be indicative of errors in measurement, data recording, or other experimental inconsistencies.
3) Infiltration plots consisting of fewer than five recorded observations were excluded. An infiltration test with fewer than five measurements might not adequately depict the whole infiltration behavior or capture the variability within the tested area.
4) Outliers have been detected and addressed to avoid inaccuracies or abnormalities in the data which could skew the analysis. We assumed that experimental plots with a final infiltration rate exceeding 100 cm/hr were suspicious or unusual for typical soil textures ranging from sand to clay (Table 1 in Ku, 2013). These outliers could be attributed to errors in unit conversion, data reporting, or experimental errors stemming from the experiment itself.
5) Infiltration plots where the initial measurement didn't start at t=0 and/or had not reached steady state were excluded from the analysis. Steady state refers to a condition where the

system's behavior does not change over time, and in the context of infiltration, it typically implies that the infiltration rate has stabilized. Plots that haven't reached steady state might exhibit varying and unpredictable infiltration rates, which can introduce noise and uncertainty into our results. By focusing on infiltration experiments that start the measurements from t=0 and have achieved steady state, we ensured that our analysis captured the complete and consistent evolution of the infiltration process from its initial state to its steady state. Now to determine whether steady state has been reached, we ran a regression analysis on the last three points of each cumulative infiltration curve. Then we calculated the error difference between predicted infiltration (cm), estimated from our regression analysis, and actual infiltration (cm). Eventually, we identified the segment of the curve where the estimated error difference is below 2% asymptotic, indicating a consistent trend and implying that the system has reached a steady state.

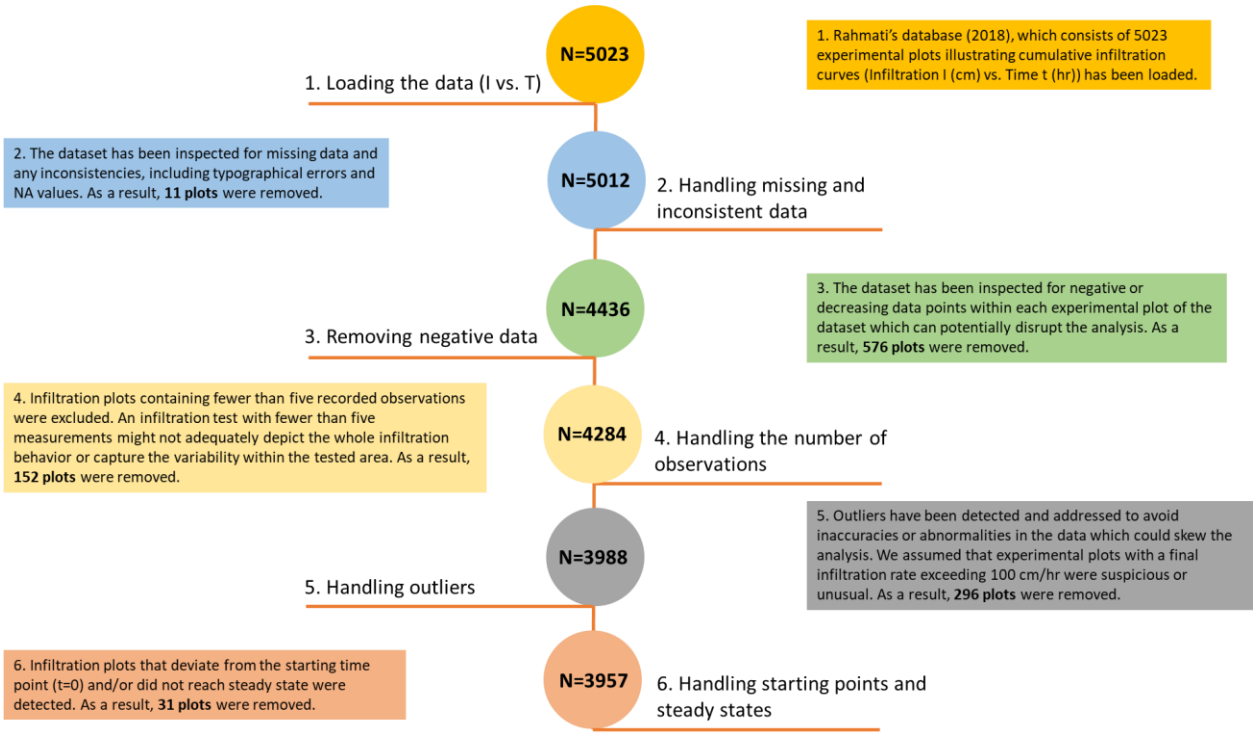

Figure 3.1: Step-by-step exclusion approach for data cleaning and preprocessing

3.3.4. Data visualization

Once the exclusion criteria were applied, we visualized the screened dataset by plotting cumulative infiltration I (cm) as function of the infiltration time T (hr). Examining the shapes of cumulative infiltration curves provided valuable insights into soil-water dynamics. As such, different features in the curve, such as inflection points, plateauing, or variations in slope can offer information about phenomena like water-repellency, preferential flow paths, and interactions related to soil structure.

To further assess soil-water interactions, we visualized data indicative of soil textural classes within the dataset using USDA soil texture triangle which categorizes soils based on the proportion of sand, silt, and clay particles. This visual representation allowed for a clear depiction of the soil texture distribution within the dataset. In addition, water content data, including initial and saturated water contents, θ_i and θ_s (cm^3cm^{-3}) respectively, for each experimental plot were incorporated into the visualization, offering a comprehensive view of the soil characteristics associated with water dynamics. In cases where direct measurements of θ_i and θ_s (cm^3cm^{-3}) were unavailable, a reasonable approximation was followed for further analysis:

- Saturated Water Content θ_s (cm^3cm^{-3})

Saturated water content θ_s (cm^3cm^{-3}) was assumed equal to soil porosity and accordingly estimated using the following formula: $\theta_s = 1 - \frac{\rho_b}{\rho_s}$ where ρ_b (gcm^{-3}) is the soil bulk density and ρ_s (gcm^{-3}) is the specific gravity of the soil particles.

- Initial Water Content θ_i (cm^3cm^{-3})

When the initial water content θ_i (cm^3cm^{-3}) was not reported in the dataset, θ_i (cm^3cm^{-3}) was estimated as 20% of the saturated water content θ_s (cm^3cm^{-3}): $\theta_i = 0.2\theta_s$

It's important to note that these assumptions provide reliable estimation of initial and saturated water contents θ_i and θ_s (cm^3cm^{-3}) when direct measurements are unavailable. However, whenever possible, direct measurements of initial and saturated water contents would always provide more accurate and reliable data based on the characteristics of the soils being studied. Relying on actual measurements of water content allows researchers to better capture the variability and trends in the soil's behavior, which might not be fully captured by estimations.

3.3.5. Extraction techniques for K_s and S estimation

Once data was obtained, cleaned, and visualized, we proceeded to extract two fundamental parameters, sorptivity S ($cmhr^{-0.5}$) and saturated hydraulic conductivity K_s ($cmhr^{-1}$), from the eleven selected infiltration models. To perform this extraction, three distinct scenarios were considered, each describing a different extraction technique (Figure 3.2 and Table 3.2):

The first scenario (denoted as Scenario 1) outlined a conventional optimization approach where optimal values of the two positive unknowns (S, K_s) were derived by curve fitting the infiltration dataset (i.e., actual cumulative infiltration I vs. time of infiltration t) into the equation of each model using the least square technique. This technique aimed to minimize the sum of the squared differences between the actual infiltration data y_j^i obtained from SWIG and the corresponding infiltration values predicted by each of the infiltration models $\hat{y}_j^i$, where j represents a single observation within the i^{th} experimental plot of total m observations, and N is the total number of experimental plots.

$$\min_{i=1 to N} \sum_{j=1}^{m} \left(\hat{y}_j^i - y_j^i\right)^2 \quad [3.12]$$

The second scenario (denoted as Scenario 2) expressed saturated hydraulic conductivity K_s (cmhr^{-1}) as the steady-state slope of the cumulative infiltration curve. At the final stage of infiltration, gravity dominates, and water infiltration achieves a steady state. During this stage, the slope of the cumulative infiltration curve is equal to the saturated hydraulic conductivity K_s (cmhr^{-1}), as described in a one-dimensional infiltration system by Philip (1957b). Therefore, a linear regression analysis of slope b (cmhr^{-1}) and intercept c (cm) of the data collected during the steady/final phase of the infiltration run (I_∞ vs. t_∞) was performed to estimate K_s (cmhr^{-1}).

$$I_{\infty,i} = b_i t_i + c_i \quad [3.13]$$

where:

$$K_{s,i} = b_i \quad [3.14]$$

This extraction technique reduced the number of unknowns from two (K_s, S) to one variable (S) which strengthens the robustness of the inversion.

To identify the steady/final phase of the infiltration run (I_∞ vs. t_∞), we started first by running a regression analysis on the last three points of each cumulative infiltration curve. This analysis involved fitting a linear mathematical model to these points to estimate the behavior of the infiltration process at end times. Following the regression analysis, we calculated the error difference between the predicted infiltration (cm), estimated from our regression analysis, and the actual infiltration (cm), for each point of the cumulative infiltration curve. To this end, we identified the section of the curve where the estimated error difference falls below 2% as asymptotic, thus representing the steady phase of the infiltration run (I_∞ vs. t_∞); The remaining observations where the error difference is above 2%, were designated as the transient phase of the infiltration run (I_{tr} vs. t_{tr}) (Di Prima et al., 2019).

To estimate sorptivity S (cmhr$^{-0.5}$) (K_s (cmhr^{-1}) being already estimated as described above), Scenario 2 was translated into two sub-scenarios with distinct extraction approaches:

- Scenario 2 – Transient (denoted as Scenario 2 – TR) estimated S (cmhr$^{-0.5}$) by fitting either the general equation of each model or exclusively its transient-state expression (if derived for short infiltration times) to the transient infiltration data (I_{tr} vs. t_{tr}).
- Scenario 2 – Steady (denoted as Scenario 2 – SS) only considered the steady phase of the infiltration dataset, and thus, estimated S (cmhr$^{-0.5}$) by fitting either the general equation of each model or exclusively its steady-state expression (if derived for long infiltration times) to the final infiltration data (I_∞ vs. t_∞). Notably, models that have derived asymptotic equations for cumulative infiltration under steady-state (Equation 3.13) have defined an expression for the intercept term c (L) in terms of K_s (cmhr^{-1}) and S (cmhr$^{-0.5}$). Consequently, solving the equation $c = f\ (S, K_s)$ led to the estimation of S (cmhr$^{-0.5}$) given that K_s (cmhr^{-1}) is known. Such models included Philip (1957b) and Parlange et al. (1982).

The third scenario (denoted as Scenario 3) replicated the same extraction technique used in Scenario 1, which involved curve fitting the infiltration dataset into the equation of each model using the least square technique. However, what differed in Scenario 3 vs Scenario 1 is that, in addition to minimizing the sum of the squared differences between the actual infiltration data y_j^i and the predicted values $\hat{y}_j^i$, Scenario 3 alternatively minimized the sum of the squared differences between the saturated hydraulic conductivity K_s (cmhr^{-1}) to be estimated and the steady-state slope b (cmhr^{-1}) of the cumulative infiltration curve.

$$\min_{i=1 to N} \left[\sum_{j=1}^{m} \frac{1}{m} \left(\hat{y}_j^i - y_j^i\right)^2 + (K_{s,i} - b_i)^2\right] \quad [3.15]$$

As a result, Scenario 3 served as a midway point between scenarios 1 and 2, highlighting an extraction technique that conventionally optimized for soil hydraulic parameters using the least square technique while anchoring the estimated value of K_s (cmhr^{-1}) to the steady-state slope b (cmhr^{-1}) of the cumulative infiltration curve. At this level, Scenario 3 illustrates a dual optimization approach combining analytical rigor with a focus on the underlying physical processes of infiltration.

Under the three scenarios (1, 2, and 3), saturated hydraulic conductivity K_s (cmhr^{-1}) and sorptivity S (cmhr$^{-0.5}$) require values greater than zero since it is physically impossible for these parameters to be negative. Negative values for these parameters would have no physical interpretation in the context of water flow and soil characteristics. As such, $K_{s,i} \geq 1e^{-06} cmhr^{-1}$ and $S_i \geq 1e^{-06}\ cmhr^{-0.5}$.

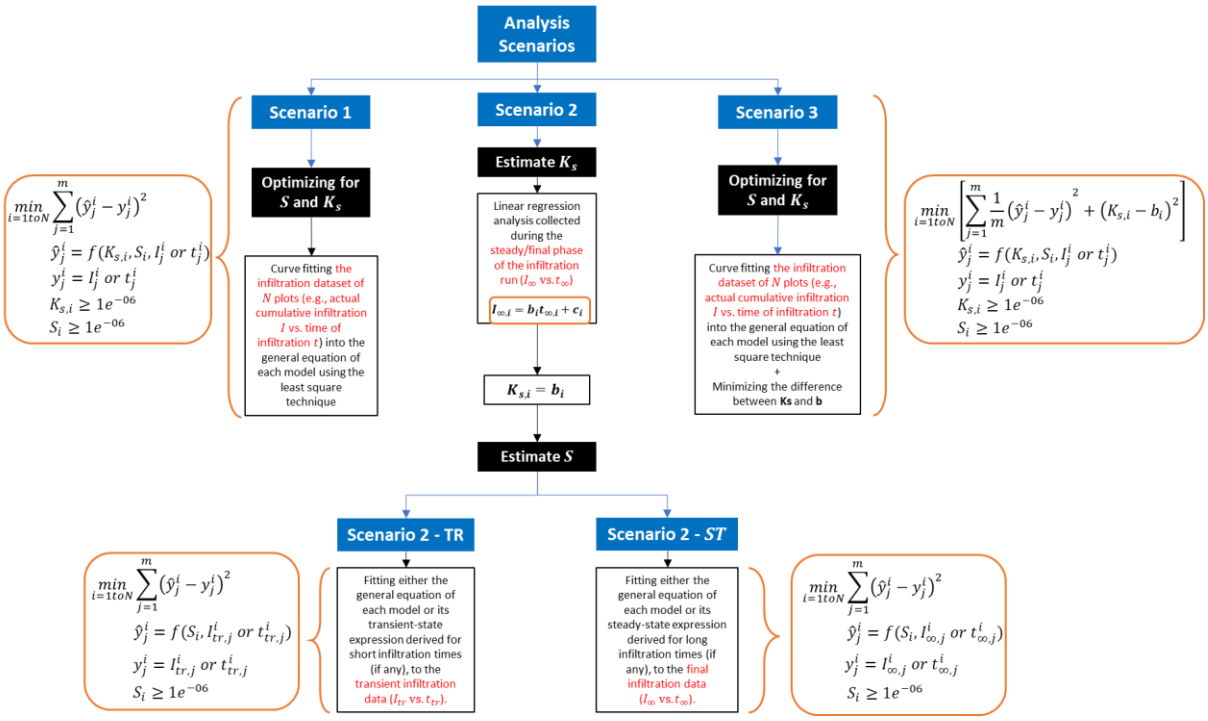

Figure 3.2: Diagram summarizing the methodology followed to estimate sorptivity S ($cmhr^{-05}$) and saturated hydraulic conductivity K_s ($cmhr^{-1}$) using three extraction techniques represented by three distinct scenarios.

Table 3.2: Summary of the eleven selected infiltration models subjected to the three extraction techniques represented by three distinct scenarios.

				Extraction technique			
				$\min_{i=1 to N} \sum_{j=1}^{m} (\hat{y}_j^i - y_j^i)^2$	$\min_{i=1 to N} \left[\sum_{j=1}^{m} \frac{1}{m} (\hat{y}_j^i - y_j^i)^2 + (K_{s,i} - b_i)^2 \right]$	$I_\infty = bt_\infty + c$ $\min_{i=1 to N} \sum_{j=1}^{m} (\hat{y}_j^i - y_j^i)^2$	
Models	Infiltration Behavior	I (t) curve	Analytical Equation	Scenario 1	Scenario 3	Scenario 2 - TR	Scenario 2 - ST
Green and Ampt (1911)	Early and Steady-State	Concave	$\hat{y}_i = \frac{I_i}{K_{s,i}} - \frac{{S_i}^2}{2{K_{s,i}}^2} ln\left(1 + \frac{2K_{s,i}}{{S_i}^2} I_i\right)$	$I_i = I_{t,i}$ $y_i = t_{t,i}$ $K_{s,i} \geq 0$ $S_i \geq 0$		$I_i = I_{tr,i}$ $y_i = t_{tr,i}$ $K_{s,i} = b_i$ $S_i \geq 0$	$I_i = I_{\infty,i}$ $y_i = t_{\infty,i}$ $K_{s,i} = b_i$ $S_i \geq 0$
Parlange (1980)	Early, Transient and Steady - State		$\hat{y}_i = \frac{I_i}{K_{s,i}} + \frac{{S_i}^2}{2{K_{s,i}}^2} \left(e^{-\frac{2K_{s,i}}{{S_i}^2} I_i} - 1\right)$				
Philip (1957b)	Early, Transient and Steady-State		$\hat{y}_i = S_i {t_i}^{0.5} + mK_{s,i} t_i$ small t (TR) $\hat{y}_i = K_{s,i} t_i + \frac{{S_i}^2}{4(K_{s,i} - mK_{s,i})}$ large t (ST) $m = 2/3$	(TR) $t_i = t_{tr,i}$ $y_i = I_{tr,i}$ (ST) $t_i = t_{st,i}$ $y_i = I_{st,i}$ $K_{s,i} \geq 0$ $S_i \geq 0$		$t_i = t_{tr,i}$ $y_i = I_{tr,i}$ $K_{s,i} = b_i$ $S_i \geq 0$	$K_{s,i} = b_i$ $S_i = \sqrt{4c_i(K_{s,i} - mK_{s,i})}$
Parlange et al. (1982)	Early and Steady -State		$\hat{y}_i = S_i {t_i}^{0.5} + \frac{1}{3}(2 - \delta) K_{s,i} t_i$ small t (TR) $\hat{y}_i = K_{s,i} t_i + \frac{{S_i}^2}{2K_{s,i}(1-\delta)} ln\left(\frac{1}{\delta}\right)$ large t (ST) $\delta = 0.85$				$K_{s,i} = b_i$ $S_i = \sqrt{\frac{2c_i K_{s,i}(1-\delta)}{\ln(1/\delta)}}$
Li et al. (1976)	Early and Steady -State		$\hat{y}_i = \frac{{S_i}^2}{4K_{s,i}} \left(t_i^* + \sqrt{(t_i^*)^2 + 8t_i^*}\right)$ $t_i^* = \frac{2{K_{s,i}}^2}{{S_i}^2} t_i$	$t_i = t_{t,i}$ $y_i = I_{t,i}$ $K_{s,i} \geq 0$ $S_i \geq 0$		$t_i = t_{tr,i}$ $y_i = I_{tr,i}$ $K_{s,i} = b_i$ $S_i \geq 0$	$t_i = t_{\infty,i}$ $y_i = I_{\infty,i}$ $K_{s,i} = b_i$ $S_i \geq 0$
Brutsaert (1977)	Early and Steady -State		$\hat{y}_i = K_{s,i} t_i + \frac{{S_i}^2}{\beta_0 K_{s,i}} \left[1 - \frac{1}{1 + \frac{\beta_0 K_{s,i}}{{S_i}^2} {t_i}^{0.5}}\right]$ $\beta_0 = 2/3$				
Swartzendruber (1987)	Early, Transient and Steady - State		$\hat{y}_i = K_{s,i} t_i + \frac{3{S_i}^2}{4K_{s,i}} \left(1 - e^{-\frac{4K_{s,i}}{3S_i} {t_i}^{0.5}}\right)$				
Stone et al. (1994)	Early and Steady -State		$\hat{y}_i = \frac{{S_i}^2}{2K_{s,i}} \left(t_i^* + \sqrt{2t_i^*} - 0.2987 {t_i^*}^{0.7913}\right)$ $t_i^* = \frac{2{K_{s,i}}^2}{{S_i}^2} t_i$				
Valiantzas (2010)	Early, Transient and Steady - State		$\hat{y}_i = S_i {t_i}^{0.5} + \frac{1}{2} K_{s,i} t_i + \frac{1}{8} \frac{{K_{s,i}}^2}{S_i} {t_i}^{1.5}$				
Rahmati (2019)	Early and Transient State		$\hat{y}_i = S_i {t_i}^{0.5} + \frac{2-\beta}{3} K_{s,i} t_i + \frac{1}{9}(\beta^2 - \beta + 1) \frac{{K_{s,i}}^2}{S_i} {t_i}^{1.5}$	$t_i = t_{tr,i}$ $y_i = I_{tr,i}$ $K_{s,i} \geq 0$ $S_i \geq 0$			
Abou Najm et al. (2021) - WR	Early and Transient	Non-uniform I(t)	$\hat{y}_i = S_i {t_i}^{0.5} + mK_{s,i} t_i - \frac{S_i\sqrt{\pi}}{2\sqrt{\alpha_{wr,i}}} \left(1 - e^{-\alpha_{wr,i} t_i} \left(\frac{1 + \sqrt{\pi \alpha_{wr,i} t_i} - 2\sqrt{\frac{\alpha_{wr,i} t_i}{\pi}}}{1 + \sqrt{\pi \alpha_{wr,i} t_i} + (\pi - 2)\alpha_{wr,i} t_i}\right)\right) - \frac{mK_{s,i}\left(1 - e^{-\alpha_{wr,i} t_i}\right)}{\alpha_{wr,i}}$	$t_i = t_{tr,i}$ $y_i = I_{tr,i}$ $K_{s,i} \geq 0$ $S_i \geq 0$ $\alpha_{wr,i} \geq 0$		$t_i = t_{tr,i}$ $y_i = I_{tr,i}$ $K_{s,i} = b_i$ $S_i \geq 0$ $\alpha_{wr,i} \geq 0$	$t_i = t_{\infty,i}$ $y_i = I_{\infty,i}$ $K_{s,i} = b_i$ $S_i \geq 0$ $\alpha_{wr,i} \geq 0$

3.3.6. Model performance parameters

To assess the deviation between model's predictions and actual dataset of cumulative infiltration *I* (cm), and comprehensively evaluate performance of infiltration models under each scenario, the following statistical parameters were used:

- Normalized Root Mean Square Error (NRMSE)

NRMSE is the normalized version of RMSE - one of the most used statistical parameters to quantify the accuracy of model's predictions. NRMSE scales the difference between predicted $\hat{y}_j$ and observed values y_j at the j^{th} data point within the experimental plot (i.e., RMSE) by the mean $\bar{\hat{y}}$ of actual values $\hat{y}_j$:

$$NRMSE = \frac{RMSE}{\bar{\hat{y}}} = \frac{\sum_{j=1}^{m} \frac{1}{m} \left(\hat{y}_j - y_j\right)^2}{\bar{\hat{y}}} \quad [3.16]$$

Since we aim to compare the performance of models across different experimental plots, using the normalized RMSE in our analysis allows for more meaningful comparisons and insights into the relative performance of models across different experimental plots within the dataset. NRMSE values typically range from 0% to 100%. Lower NRMSE, ideally approaching 0%, indicates better predictive performance as they signify smaller overall discrepancies between predictions and actual observations. Values closer to 100% signify larger discrepancies between the predicted and actual values, indicating poorer model's performance. A 100% NRMSE would indicate that the model's predictions have no correspondence with the actual data.

- Coefficient of Determination (R^2)

R^2 is a statistical parameter that quantifies the goodness of fit of a regression model to the actual data points. In other words, R^2 assesses how well the independent variable ($\hat{y}$) explains the variability in the dependent variable (y) in a predicted regression model, and therefore can determine the model performance.

$$R^2 = 1 - \frac{\sum_{j=1}^{m} \left(\hat{y}_j - y_j\right)^2}{\sum_{j=1}^{m} \left(\hat{y}_j - \bar{\hat{y}}\right)^2} \quad [3.17]$$

R^2 ranges from 0 to 1. Lower R^2 closer to 0 indicates that the model fails to explain the variability in the dependent variable. In other words, the independent variable in the model does not provide any information about the variability observed in the dependent variable. Higher R^2, ideally approaching 1, represents better predictive performance, indicating that the model significantly accounts for the variability in the dependent variable. However, it is important to note that a high R^2 (i.e., close to 1) does not necessarily indicate an appropriate or accurate model. It might be possible for a model with a high R^2 to overfit the data or have other issues, which justifies the need for at least one or two statistical measures of models' performance in addition to R^2. Moreover, it is possible for R^2 to be negative, which typically indicates that the model is a poor fit for the data and performs worse than a horizontal line.

- Coefficient of correlation (CC)

CC is a statistical measure that quantifies the strength and direction of the linear relationship between two variables. It is commonly used to assess how closely two variables are correlated to each other, and therefore can determine the success of numeric predictions. The coefficient of correlation ranges between -1 and 1, and is calculated using the following formula:

$$CC = \frac{m\sum_{j=1}^{m}\hat{y}_j y_j - \sum_{j=1}^{m}\hat{y}_j \sum_{j=1}^{m} y_j}{\sqrt{m\sum_{j=1}^{m}\hat{y}_j{}^2 - \left(\sum_{j=1}^{m}\hat{y}_j\right)^2}\sqrt{m\sum_{j=1}^{m} y_j{}^2 - \left(\sum_{j=1}^{m} y_j\right)^2}} \quad [3.18]$$

A positive value of CC ($0 < CC \leq 1$) indicates a positive linear relationship between the variables x and y, while a negative value of CC ($-1 \leq CC < 0$) indicates a negative linear relationship between the two variables. A value of CC near 0 ($CC \approx 0$) indicates that changes in one variable are not systematically associated with changes in the other.

3.4. Results and discussion

Here, we present a condensed overview of the insights learned from our metadata analysis applied on 3957 infiltration curves derived through the data cleaning process of 5023 cumulative infiltration curves extracted from SWIG database.

3.4.1. Cumulative Infiltration Curves

First, we visualized 3957 cumulative infiltration curves by plotting cumulative infiltration I (cm) as function of infiltration time T (hr). Observing the shape and slope of the cumulative infiltration curve offered insights into different components of soil-water interactions. Nine random simulations of 50 random actual cumulative infiltration curves $I(t)$ were plotted as illustrated in Figure 3.3. We observed that most curves exhibited a typical concave shape, where they steeply rose initially, reaching a constant slope over time. However, some curves showed non-classic shapes, deviating from the classic concave trend (Figure 3.3).

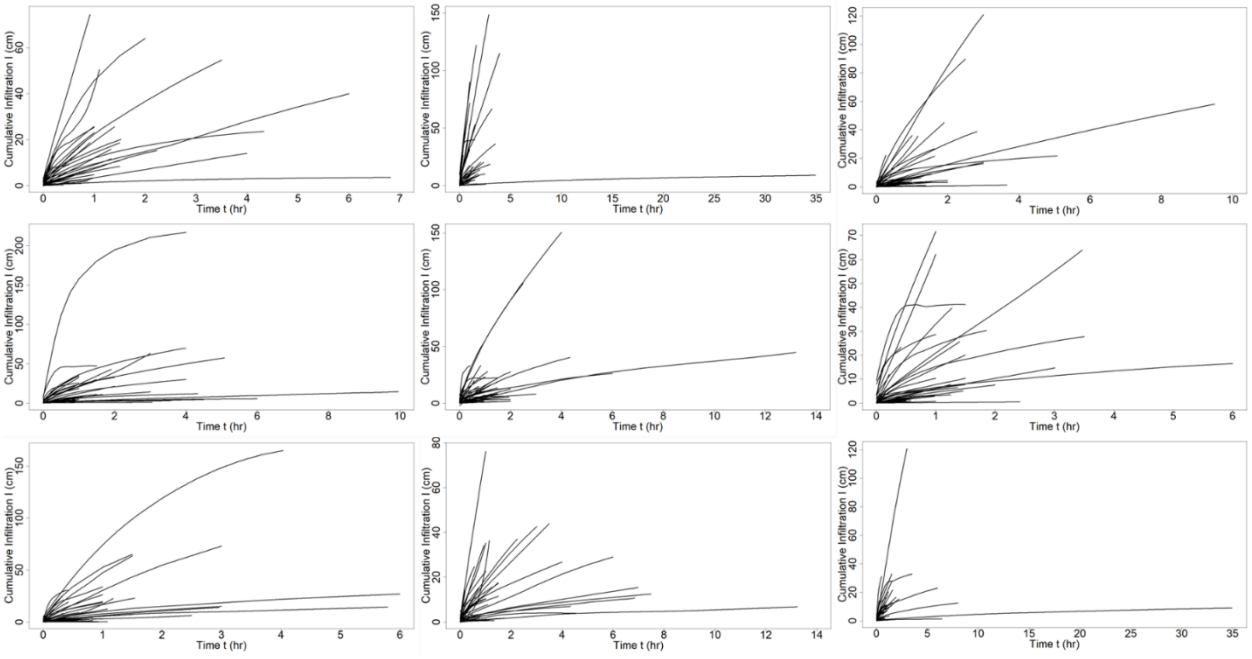

Figure 3.3: Nine random simulations of 50 random actual cumulative infiltration curves $I(t)$

To further analyze the shapes observed in Figure 3.3, we ran a function in R to identify convexity and concavity of cumulative infiltration curves by calculating the convex hull for both upward and downward directions, considering the "inside" of the curve, and taking the ratio of path lengths. A value < 1 indicates “convex” (concave up), while a value > 1 indicates “concave” (concave down). A value exactly equal to 1 indicates a line or a combination of both convex and concave shapes, hereafter called “non-uniform”. As a result, 79% of screened cumulative infiltration curves in SWIG exhibited a typical concave shape, representing what is considered "perfect" infiltration conditions with no water-repellency, preferential flow, or any other key components of soil-water interactions. However, about 21% of curves appeared to have shapes different from the commonly assumed concave classic shape; 6% were convex, and 15% showed non-uniform shapes (Figure 3.4). Our findings aligned with a study conducted by Pachepsky and Karahan (2022) who analyzed the 5023 infiltration curves extracted from SWIG and found that one third of the curves showed non-classic shape. The different shapes of cumulative infiltration curves indicate how different land use, field conditions, and soil properties significantly affect water infiltration, emphasizing the importance of assessing soil phenomena such as water-repellency, hydrophobicity, and preferential flow paths to understand soil-water interactions (Angulo-Jaramillo et al., 2019; Abou Najm et al., 2021; Di Prima et al., 2021; Pachepsky and Karahan, 2022; Basset et al., 2023).

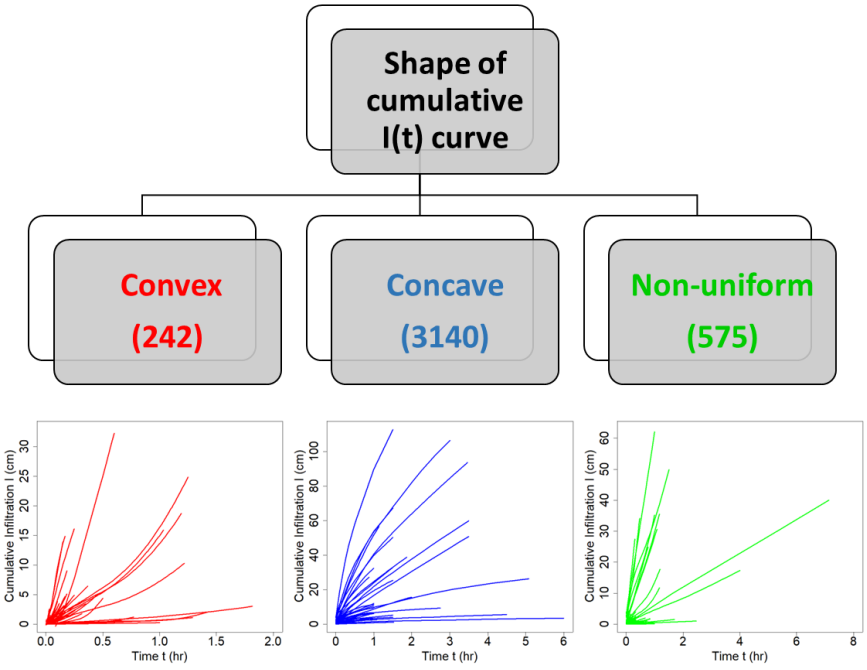

Figure 3.4: Classification of three different shapes (convex, concave, and non-uniform) observed in 3957 cumulative infiltration curves $I(t)$

3.4.2. Soil Characteristics

We conducted a detailed analysis of data indicative of soil textural classes, as well as physical attributes including initial and saturated water contents, θ_i and θ_s (cm^3cm^{-3}). This visual representation offered a comprehensive view of the soil characteristics associated with each infiltration curve.

Figure 3.5 covered the full range of soil texture across our dataset, as identified by the USDA soil texture triangle from coarse to fine particles. While 28% of the 3957 plots lacked soil texture information, our analysis indicated a diverse and representative dataset of 2857 experimental plots covering various soil textural classes, which is crucial for capturing the broad spectrum of soil-water interactions.

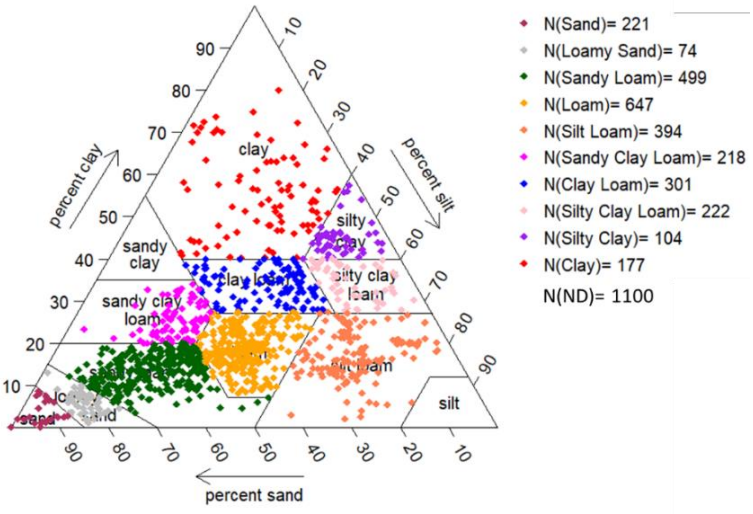

Figure 3.5: USDA soil texture triangle of soils under 3957 experimental infiltration plots (ND=Not Determined)

We plotted the data descriptive of initial and saturated water contents, θ_i and θ_s (cm^3cm^{-3}) as function of soil texture to determine the initial moisture condition of soils being investigated, and further understand soil-water interactions (Figure 3.6). Clearly, the difference between θ_i and θ_s (cm^3cm^{-3}) is relatively high, indicating that most of infiltration tests were performed under dry conditions. Another clear observation is that coarser soils, such as sandy and sandy loam soils, exhibit lower water retention capacity compared to finer soils, such as clay loam and clayey soils. This difference is attributed to the larger pores in coarser soils, facilitating rapid drainage and reducing water retention, whereas finer soils, with smaller pores, hold onto water more effectively through capillary action. We also observed noticeable variability in water retention capacity within the same textural class. This variability suggests that factors beyond soil texture alone contribute to the ability of soils to retain water. From a meta-data systematic review, Basset et al. (2023) revealed that studying soil texture alone, without considering soil structure, is not enough for an effective assessment of soil-water characteristics. Soil structure, with both its inherent and induced variations due to natural factors and management practices (tillage, cover crops, soil amendments, and others), have significantly shaped soil-water interactions (Lipiec et al., 2006; Hao et al., 2022; Vedere et al., 2022). Moreover, the variability in water contents within the same textural class was significantly higher in finer soils. This trend can be attributed to the inherent heterogeneity of finer soils in terms of particle arrangement, organic matter content, and mineralogy (Krull et al., 2003; Kogel-Knabner et al., 2008; Kooistra and van Noordwijk, 2020). This inherent heterogeneity contributes to a wider and more dynamic range of soil responses across finer soils to management practices like tillage, cover crops, and soil amendments, as well as responses to climate variations and seasonal changes (Ramesh et al., 2019).

It is worth noting that saturated water content values θ_s (cm^3cm^{-3}) equal to or greater than 0.7 are considered significantly high and uncommon (Figure 3.6). A value of $\theta_s \geq 0.7$ suggests that the soil may have a lower percentage of mineral components or a unique composition that allows it to retain more water than usual. Soil textures naturally have lower water-holding capacities, making it less common for them to reach such high saturation levels.

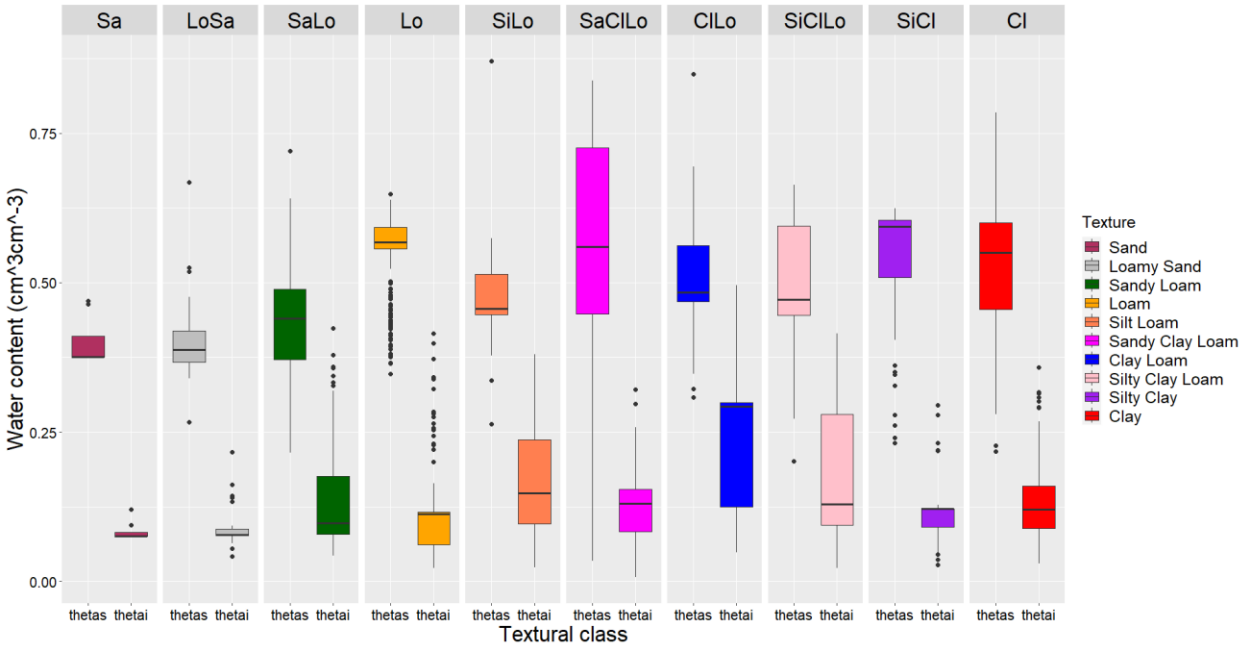

Figure 3.6: Water content distribution per soil textural class under 1428 experimental plots where both water content and textural class information are available. Soils are plotted from coarsest to the finest soil textural class (θ_s and θ_i = saturated and initial water contents, respectively).

3.4.3. Variability in K_s and S estimated values across 1D models

Here we present our findings on the variability in the estimated infiltration characteristics, K_s ($cmhr^{-1}$) and S ($cmhr^{-0.5}$) across eleven one-dimensional (1D) infiltration models using the three extraction techniques/scenarios.

First, we plotted boxplots that demonstrated the overall statistical variation of the saturated hydraulic conductivity K_s ($cmhr^{-1}$) and sorptivity S ($cmhr^{-0.5}$), estimated per each 1D infiltration

model among three scenarios, as illustrated in Figures 3.7 and 3.8, respectively. From Figure 3.7, notable patterns and trends can be observed among both 1D models and extraction techniques. The second extraction technique illustrated through Scenario 2 (2TR/2ST) showed no variance in K_s observations since K_s was estimated independently of each model as the steady-state slope b of the cumulative infiltration curve at end times. Scenario 3 behaved like Scenario 2 with the overall median and variance of each model being moderately constant. This similarity suggests that a dual optimization which optimizes for soil hydraulic parameters using each model's equation, while minimizing the difference between K_s and the steady-state slope b standardizes the estimation of K_s across different infiltration models. This resulted in a close alignment of aligning K_s with the steady-state slope b of the cumulative infiltration curve.

In Scenario 1 which found optimal values of K_s within each individual model, a greater variability emerged in the estimated K_s values, reflecting the diverse characteristics and behaviors of the models in predicting K_s. However, the overall median demonstrated a slight degree of consistency, potentially pointing to common trends or patterns across the models in Scenario 1. Notably, Abou Najm et al. (2021) stood out as distinct from other models in Scenario 1. The unique feature of Abou Najm et al. (2021) incorporating water repellency and hydrophobicity into infiltration modeling (i.e., integrating a third parameter α_{wr}, in addition to K_s and S) could be a significant factor contributing to its distinct behavior compared to the other models. Abou Najm et al. (2021) described the convex shape in cumulative infiltration curves induced by water repellency, unlike the other ten models that only depict the classic concave shape. Considering both effects led to a different representation of K_s under Scenario 1 since different shapes of cumulative infiltration curves existed in the dataset. We suggest that the addition of α_{wr} introduced by Abou Najm et al. (2021) is only warranted when dealing with convex shape complexity (Figure 3.9). Otherwise, we

are introducing a new parameter into infiltration modeling that may be a redundant addition when comparing K_s estimates between non-hydrophobic and hydrophobic soil hydraulic models. In addition, the similarity in K_s predictions across all models including Abou Najm et al. (2021) under scenarios 2 and 3 emphasized that, based on the physical definition of K_s, the shape of the cumulative infiltration curve, whether concave or convex, does not affect the estimation of K_s. This is because any cumulative infiltration curve, irrespective of its shape, reaches a steady state, showing a linear curve of slope representing K_s.

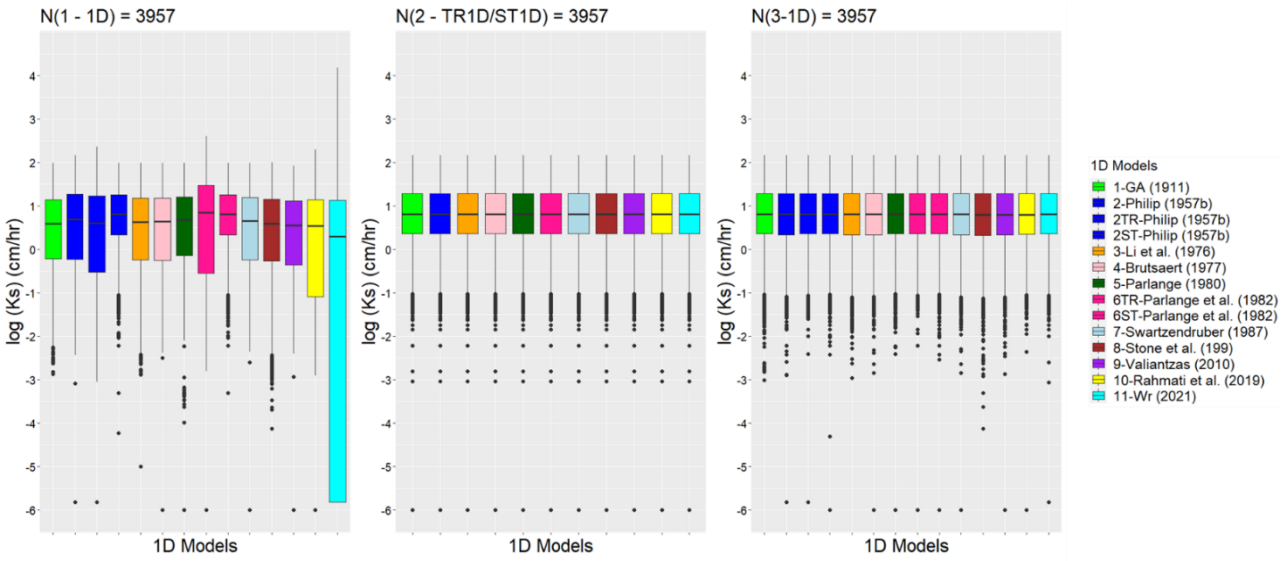

Figure 3.7: Boxplots illustrating the statistical variation of saturated hydraulic conductivity Ks ($cmhr^{-1}$) estimated across the experimental plots (N=3957) per each 1D infiltration model. Models are ordered by the historical evolution of infiltration modeling attempts from the oldest (left) to the most recent (right). Each model within each scenario contains the same number of observations (N= 3957 estimated values of K_s).

Significant variability in estimated S values resulted from the second extraction technique illustrated through Scenario 2. This variability was particularly striking given that K_s values were fixed while S estimates significantly fluctuated across all models. Despite this uniformity in K_s across models, the observed fluctuations in S values suggest that factors specific to each model,

including their mathematical expressions, play a significant role in influencing the estimated sorptivity within the framework of Scenario 2. In scientific terms, sorptivity describes the ability of soil to absorb water. Sorptivity, as introduced by Philip (1957b), is a measure of the initial rate at which water infiltrates into a soil under the influence of capillary forces. The concept of sorptivity itself is therefore rooted in the physical properties and behaviors of soils in response to water infiltration. However, Scenario 2 introduced the idea that sorptivity may behave as a mathematical parameter unique to each infiltration model. This expansion of the sorptivity concept in Scenario 2 underscores the influence of model-specific characteristics on the observed variability in S estimates.

This variability in S became much less apparent under scenarios 1 and 3 where no parameters were fixed for the optimizer, but rather both values K_s and S were subjected to optimization. In these scenarios, the overall median highlighted a level of consistency among the different models. This suggests that the optimization process, when applied to both K_s and S simultaneously, tends to align the estimated sorptivity values across various infiltration models. The contrast in variability between Scenario 2, where only K_s was fixed, and scenarios 1 and 3, where both K_s and S were optimized, emphasized the impact of extraction techniques on the predicted outcomes of soil water parameter estimation. This insight provided valuable information about the interplay between the concept of sorptivity as either a scientific concept rooted in physical properties or a mathematical parameter subject to optimization.

It is worth noting that Rahmati (2019) and Abou Najm et al. (2021) equations were specifically developed for transient infiltration times. Therefore, including them under Scenario 2-ST, where we estimated S by fitting models' equations to steady-state infiltration data (I_∞ vs. t_∞), would be conceptually inaccurate. Given this consideration, we have opted to exclude these models from

Scenario 2-ST to maintain the integrity of our analysis. We believe that this approach ensures a more accurate assessment of the models' performance within the context of steady-state infiltration.

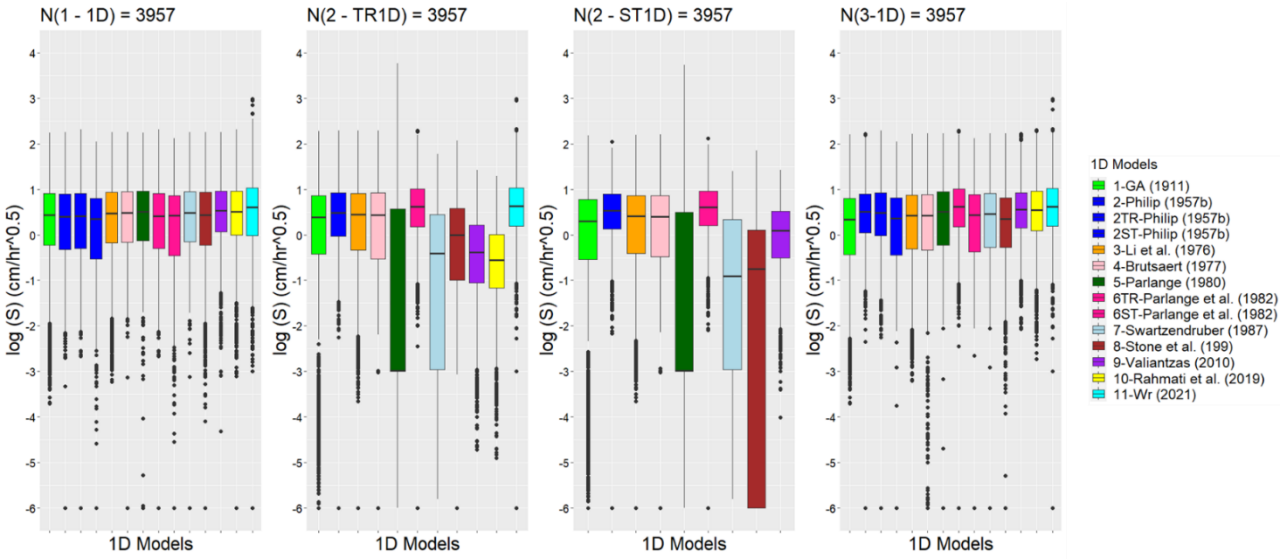

Figure 3.8: Boxplots illustrating the statistical variation of sorptivity S (cmhr$^{-0.5}$) estimated across the experimental plots of total N=3957 per each 1D infiltration model. Models are ordered by the historical evolution of infiltration modeling attempts from the oldest (left) to the most recent (right). Each model within each scenario contains the same number of observations (specifically 3957 estimated values of S).

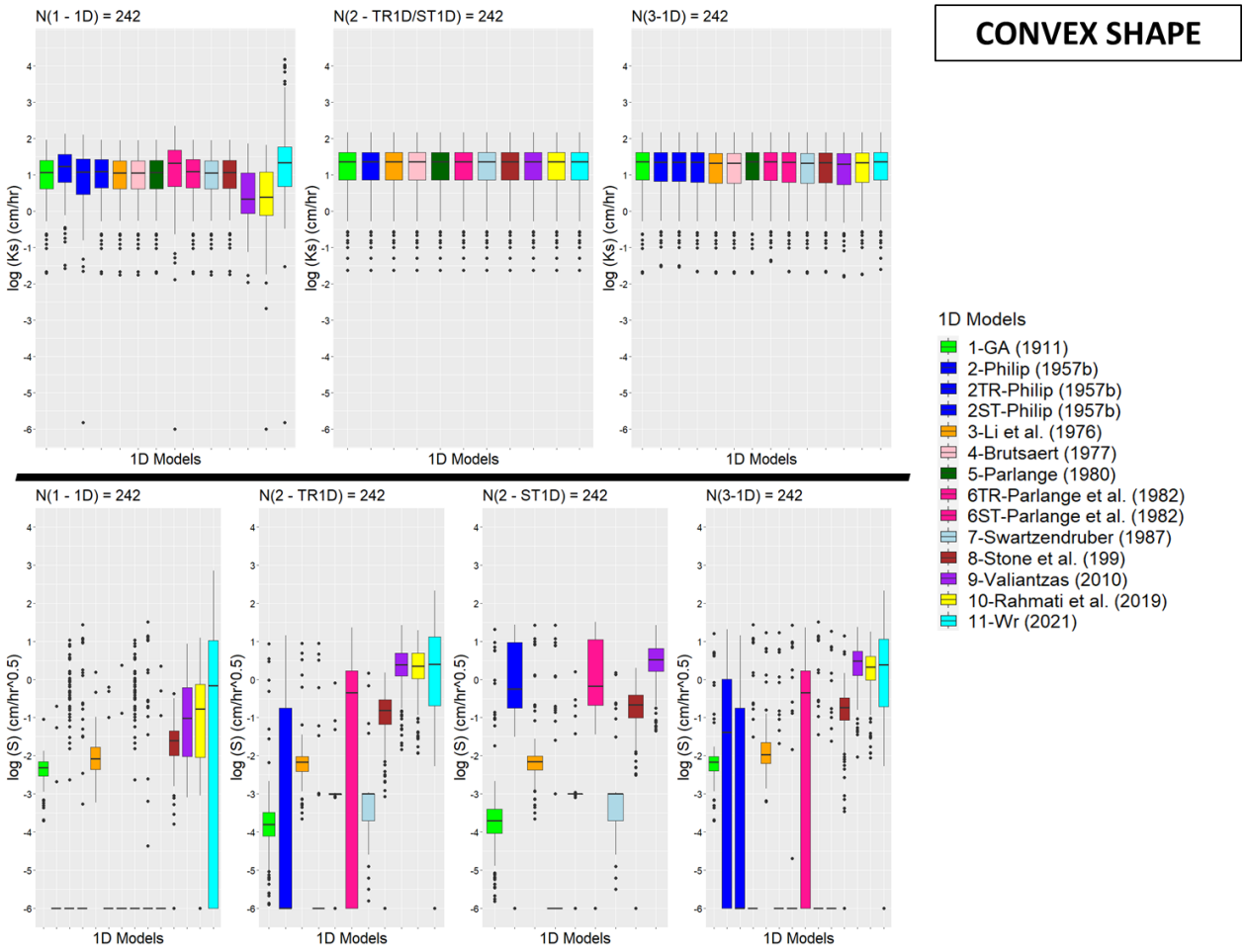

Figure 3.9: Boxplots illustrating the statistical variation of saturated hydraulic conductivity K_s ($cmhr^{-1}$) and sorptivity S ($cmhr^{-0.5}$) estimated across the experimental plots of total N=242 cumulative infiltration curves exhibiting convex shapes per each 1D infiltration model. Models are ordered by the historical evolution of infiltration modeling attempts from the oldest (left) to the most recent (right). Each model within each scenario contains the same number of observations (specifically 242 estimated values of K_s and S).

Although boxplots illustrated in Figures 3.7 and 3.8 effectively portrayed the degree of variability in the estimated infiltration characteristics, K_s and S, they may not capture every aspect of the underlying data descriptive of K_s and S estimates. This limitation highlighted the potential for generalizations or misinterpretations. For instance, underlying patterns of data specific to each experimental plot of the dataset were not evident in these visualizations. Moreover, with so many estimates (3957 observations of K_s and S per each model), the number of labeled outliers in Figures

3.7 and 3.8 is huge, far too many to investigate each one individually and discern whether they represent expected extreme values within the dataset or true outliers unique to each model.

3.4.4. Variability in K_s and S estimated values across 1D models and extraction methods per each infiltration experiment

To delve deeper into the analysis, we further explored K_s and S estimates across the eleven 1D infiltration models for each individual plot within the dataset (Figures 3.10 and 3.11). As such, our analysis offered a multifaceted view of the K_s and S estimates in each scenario, providing insights into the distributional characteristics, statistical variations, and outlier counts associated with each of the 1D infiltration models at the plot level. In both figures (i.e., Figures 3.10 and 3.11), the density plots on the left depicted the distribution of z-scores. Each z-score explains per infiltration plot how much of standard deviation is each 1D infiltration model away from the mean across eleven (1D) infiltration models and a total of N=3957 infiltration plots. The graphical plots in the middle segment provided a detailed examination of statistical variations within each experimental plot, with key statistical indicators including means (μ) highlighted in red, model-specific outliers highlighted in colors designated to each model, and +- standard deviation (σ) indicated by black horizontal lines. The barplots on the right summarized the total number of outliers observed in estimates for each of the 1D infiltration models. An outlier is defined as a data point (x) that deviates significantly from most other data points in the dataset. This deviation is determined based on a z-score falling outside the range of -2 to +2 where z is estimated using the following formula $z = \frac{x-\mu}{\sigma}$.

As seen from Figure 3.10, the dispersion of K_s estimates per individual plots was notably clear across the eleven models, particularly under scenarios 1 and 3. This observation provided a more

detailed understanding of the underlying variability of K_s predictions across different infiltration models and extraction techniques. This was not clearly demonstrated in Figure 3.8, which showed some general trends and patterns in estimates, but did not provide a detailed view of K_s variability across individual plots. Under Scenario 3, variability of K_s decreased significantly compared to Scenario 1, with estimates appearing clustered around the mean. This suggests a more uniform behavior of the models in terms of K_s estimates under Scenario 3. Obviously, under Scenario 2, all estimates of K_s were identical as Scenario 2 fixed K_s values across all models, expressed as the steady-state slopes of cumulative infiltration curves. Another observation in Figure 3.10 was the low K_s estimates ($K_s = 1e^{-06}\ cmhr^{-1}$ – minimum value set for the optimizer) within a significant number of plots under Scenario 1 compared to scenarios 2 and 3. To further investigate this observation, we generated histograms representing each model to depict the frequency of these minimal (approximately zero) values of K_s (Figure 3.12). A spike around $K_s = 1e^{-06}\ cmhr^{-1}$ across various models under Scenario 1, suggests that the optimizer in Scenario 1 was consistently converging to this minimum value across different models, indicating potential numerical convergence issues. To assess the physical validity of these minimal K_s estimates, we generated the USDA soil texture triangle covering the soil textural classes within these specific plots (Figure 3.12) which showed a diverse distribution of various soil textural classes, rather than representing only a finer texture commonly associated with very low values of K_s. While we ascertained the fact that soil texture alone may not be the sole indicator of soil-water characteristics, it became challenging to attribute physical meaning to all these minimal K_s values in the context of soils and water infiltration. Nevertheless, this finding underscored the importance of addressing the potential of numerical artifacts before considering the adoption of Scenario 1.

The total number of outliers observed in K_s estimates for each of the 1D infiltration models shed light on the divergent behaviors exhibited by different models (Figure 3.10). However, the presence of outliers does not always indicate that the corresponding models deviate significantly from the overall trend of the data. This point was emphasized under Scenario 3 where K_s data were clustered around the mean; however, model 9 (Valiantzas, 2010) exhibited a significant number of outliers. In situations where the standard deviation is very low, even a slight deviation from the mean might be considered an outlier statistically, but this deviation may not necessarily have a significant physical meaning. Therefore, based on our results, we suggest coupling the investigation of outliers with the visualization of the distribution of data around the mean and the standard deviation, as illustrated in Figures 3.10 and 3.11. Identifying outliers alone may not always reflect meaningful physical distinctions, and a thorough examination of the data distribution can provide a more accurate understanding of the observed patterns and behaviors in the context of characterizing soil hydraulic properties.

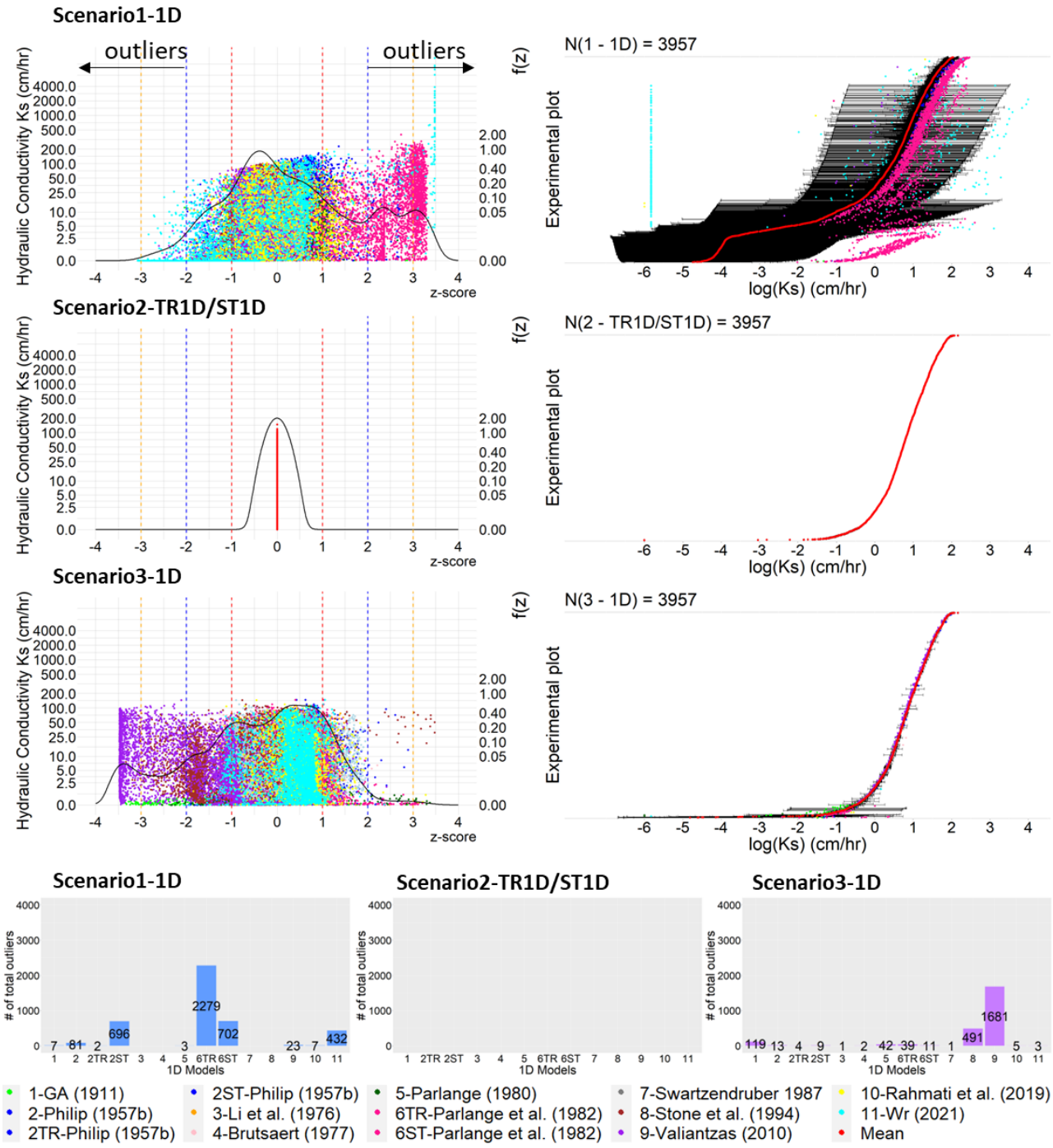

Figure 3.10: Graphical representation of the variability, skewness, and outliers in estimates of K_s (cmhr^{-1}) at the plot level per each 1D infiltration model.

Figure 3.11 clearly showed the significant dispersion of sorptivity S (cmhr$^{-0.5}$) estimated from the different models across the experimental plots under different scenarios. The observed fluctuations

in S values suggest that specifics related to each model and each extraction technique significantly impact predictions of sorptivity. The optimization process, when applied to both K_s and S as in scenarios 1 and 3, demonstrated smaller fluctuations in sorptivity estimates across various infiltration models compared to Scenario 2, particularly in Scenario 3 where less dispersion and lower number of outliers were depicted. A higher variability in S estimates was observed under Scenario 2 where K_s was fixed. While the concept of sorptivity itself is rooted in the physical properties and behaviors of soils in response to water infiltration, our analysis reconfirmed the idea that sorptivity may behave as a mathematical parameter unique to each infiltration model.

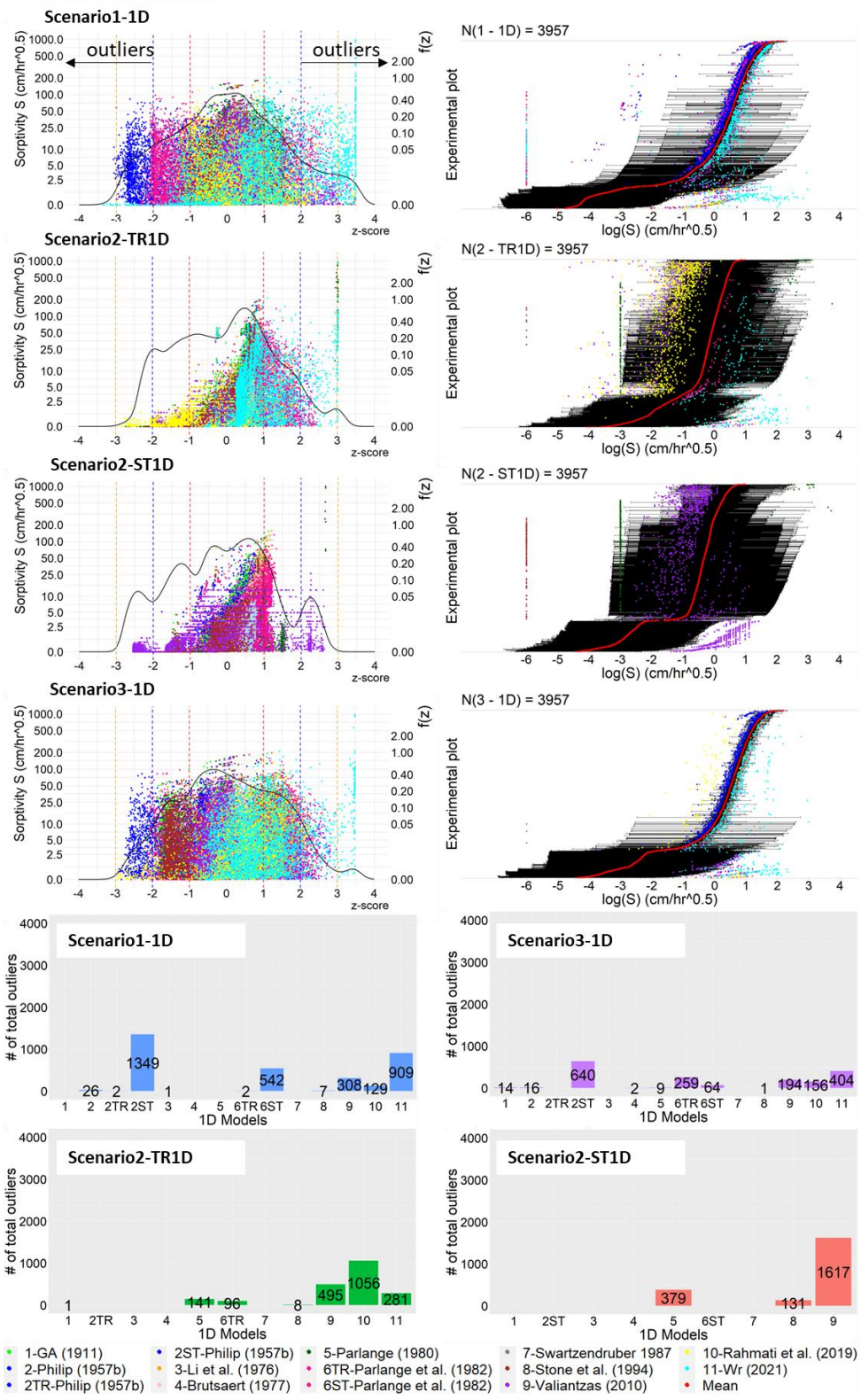

Figure 3.11: Graphical representing of the variability, skewness, and outliers in the estimates of S (cmhr$^{-0.5}$) at the plot level per each 1D infiltration model.

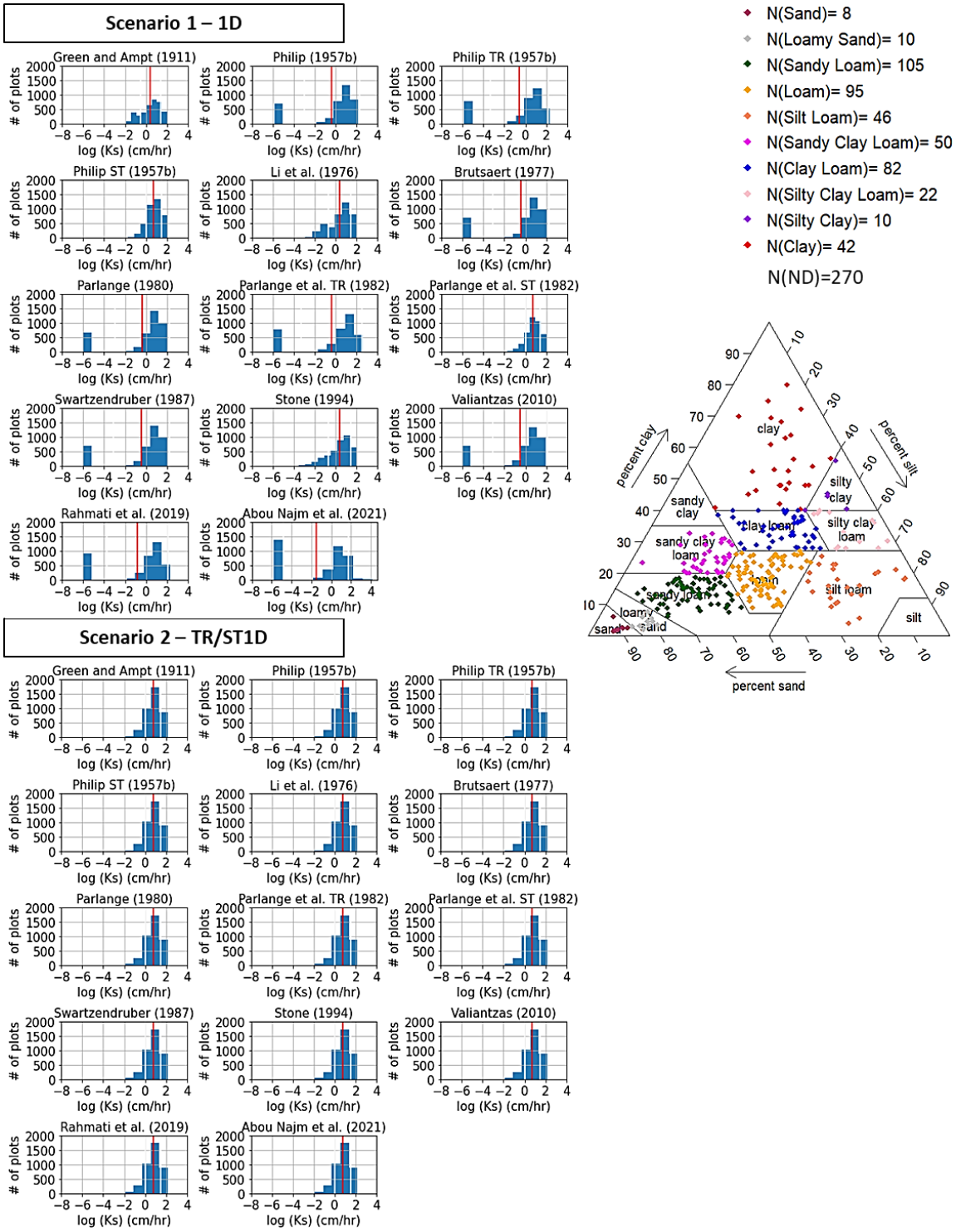

Figure 3.12: Histograms representing the statistical variation of saturated hydraulic conductivity K_s ($cmhr^{-1}$) per each 1D infiltration model across Scenarios 1 and 2 associated with USDA soil texture triangle of N=740 plots out of the 3957 plots *that had at least one minimal value of K_s (10^{-6} $cmhr^{-1}$) by any of the 11 models across Scenario 1.*

3.4.5. How far are K_s and S estimates from each other per plot?

Figure 3.13 highlighted the influence of both, infiltration models and extraction techniques on the predictions of K_s and S, contributing to a broader understanding of the complexities involved in soil-water parameter estimation. Table 3.3 further illustrates the percentages of experiments plots exhibiting a normalized magnitude (max-min)/mean greater to or equal to 0.1, 1 and 10 for K_s and S across all scenarios.

To recap on the extraction techniques followed in our analysis:

- Scenario 1: The first extraction technique was a conventional optimization exercise which optimized simultaneously for the two parameters, K_s and S, using each model's equation.
- Scenario 2: The second extraction technique estimated K_s independently of each model, as the steady-state slope of the cumulative infiltration curve at end times, and further optimized for S using each model's equation.
- Scenario 3: The third extraction technique was a dual optimization which optimized for soil hydraulic parameters, K_s and S, using each model's equation while minimizing the difference between K_s and the steady-state slope of the cumulative infiltration curve.

Once again, our analysis revealed significant variability in estimates of soil hydraulic parameters, K_s and S, across different 1D infiltration models, which varies under varying extraction techniques. Scenario 1 showed a greater disparity between the maximum and minimum values of K_s compared to scenarios 2 and 3. Specifically, 87% of the experimental plots under Scenario 1 showed a magnitude (max-min) exceeding the mean value, with 1.3% of plots showing a magnitude (max-min) exceeding 10 times the mean value (Table 3.3). This substantial difference indicated a wider

range of K_s estimates and therefore a greater variability in the predictions among models under Scenario 1.

Sorptivity generally showed to be highly influenced by models' expressions. However, for S estimates, Scenario 1 had a lower range compared to Scenario 2 although K_s values were all the same under Scenario 2 (i.e., min = max of K_s). This finding suggests that, despite having a wider range for K_s in Scenario 1, the simultaneous optimization process may result in a more constrained range for S. As of Scenario 3, this extraction technique demonstrated a relatively lower range for both K_s and S where the corresponding histograms emphasized a high frequency of values within low ranges. Specifically, for K_s, 84% of the experimental plots in Scenario 3 showed a very small, normalized difference between their maximum and minimum values, equal to at least 10^{-1}. In contrast, for S, 0% of the plots exhibited this small difference. Our results suggested that Scenario 3 could be an effective extraction technique for accurate estimation of both K_s and S. This suggestion aligns with the notion that considering the interplay between optimization analytics and the physical definition of K_s leads to a more robust parameter estimation. Sorptivity remained highly variable under all scenarios but clearly better also under Scenario 3. While sorptivity was originally introduced by Philip (1957b) as a soil-water characteristic describing the soil's capacity to sorb water due to capillary action, our findings emphasized that model-specific expressions play a significant role in shaping sorptivity estimates.

Table 3.3: Percentages of experiments plots exhibiting a normalized magnitude (max-min)/mean greater to or equal 0.1, 1 and 10 for K_s and S across all scenarios.

(max-min)/mean	**>0.1**	**>1**	**>10**
Scenario 1			
K_s	100%	87%	1.3%
S	100%	44%	4%
Scenario 2-TR			
K_s	0%	0%	0%
S	100%	99%	0.98%
Scenario 2-ST			
K_s	0%	0%	0%
S	100%	93%	0%
Scenario 3			
K_s	16%	2%	0%
S	100%	34%	1.5%

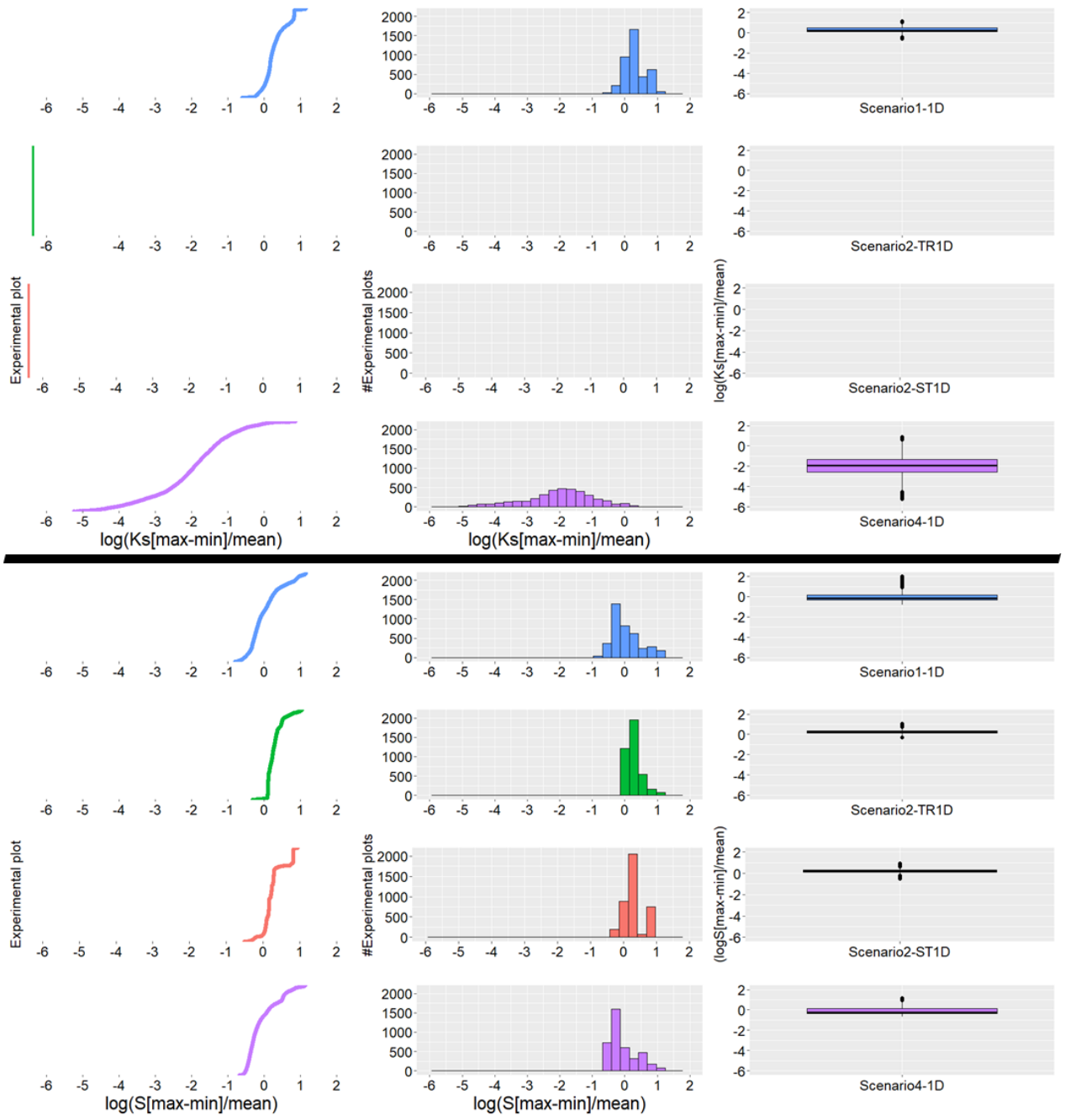

Figure 3.13: Graphical visualization of the statistical variation of the magnitude (max-min)/mean estimated from the saturated hydraulic conductivity K_s ($cmhr^{-1}$) and sorptivity S ($cmhr^{-0.5}$) values per each experimental plot of total N=3957 among 1D infiltration models

The physical significance of K_s predictions, specifically how much K_s is anchored to the steady-state slope b, was illustrated in heatmaps showing the statistical variation of the absolute difference

$(K_s - b)/\ b$ per each 1D infiltration model and classified per each textural class under scenarios 1 and 3 (Figure 3.14). Both scenarios 1 and 3 which predicted K_s by optimizing each model's equation resulted in some deviation from the true physical value of K_s which is equal to the steady-state slope b of the cumulative infiltration curve. However, Scenario 3 aligned K_s closely with b across major plots and textural classes, emphasizing the capability of the corresponding extraction technique to capture the physical dynamics of infiltration accurately and showcasing a robust parameter estimation that reflects the behavior of soil-water system. Notably, the steady-state expressions developed under Philip (1957b) and Parlange et al. (1982) expressed K_s as equal to steady-state slope under both scenarios. These expressions were formulated as linear equations for estimating infiltration at steady state where the slope represents K_s, providing a clear link between the mathematical representation of soil-water dynamics and the physical processes occurring in the soil-water system.

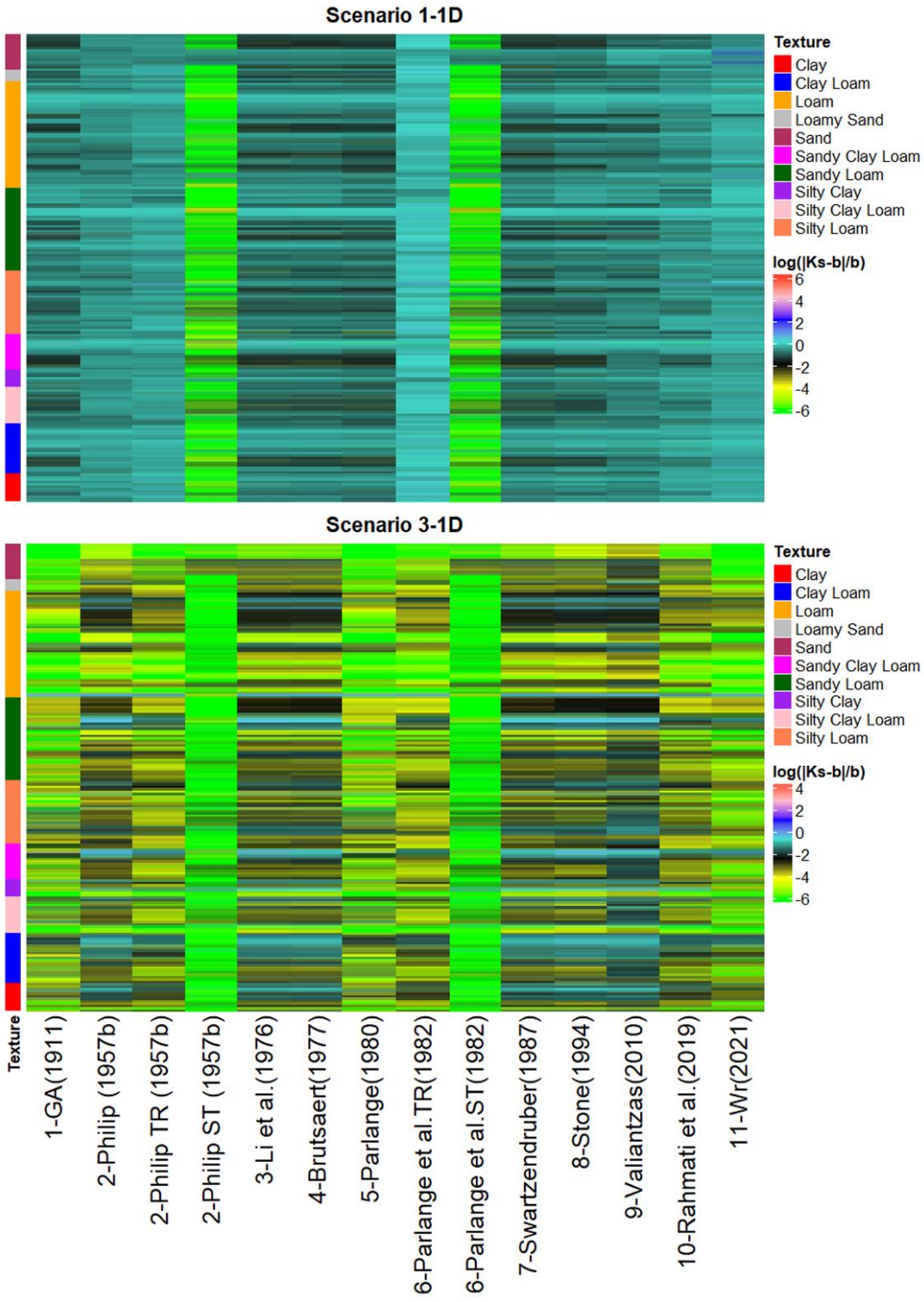

Figure 3.14: Heatmaps illustrating the statistical variation of the absolute difference (Ks – b)/b between the saturated hydraulic conductivity Ks at steady state minus the steady-slope b estimated across the experimental plots of total N =2857 per each 1D infiltration model and classified per each textural class

3.4.6. Performance of 1D infiltration models

We proceeded to evaluate the performance of infiltration models under each scenario (Figure 3.15). Our analysis demonstrated the relatively good performance of three extraction techniques (i.e., scenarios 1, 2 and 3) in predicting infiltration I (cm) considering low NRMSE, and high R^2 and CC values across major experimental plots. Comparing the three scenarios, Scenario 1 had the lowest NRMSE, the highest mean value of R^2 and the highest CC to estimate infiltration across models compared to scenarios 2 and 3. Scenario 2 was the least accurate extraction technique to predict infiltration according to the three key evaluation parameters. Scenario 3 was reasonably accurate, and its performance was more satisfactory than Scenario 2.

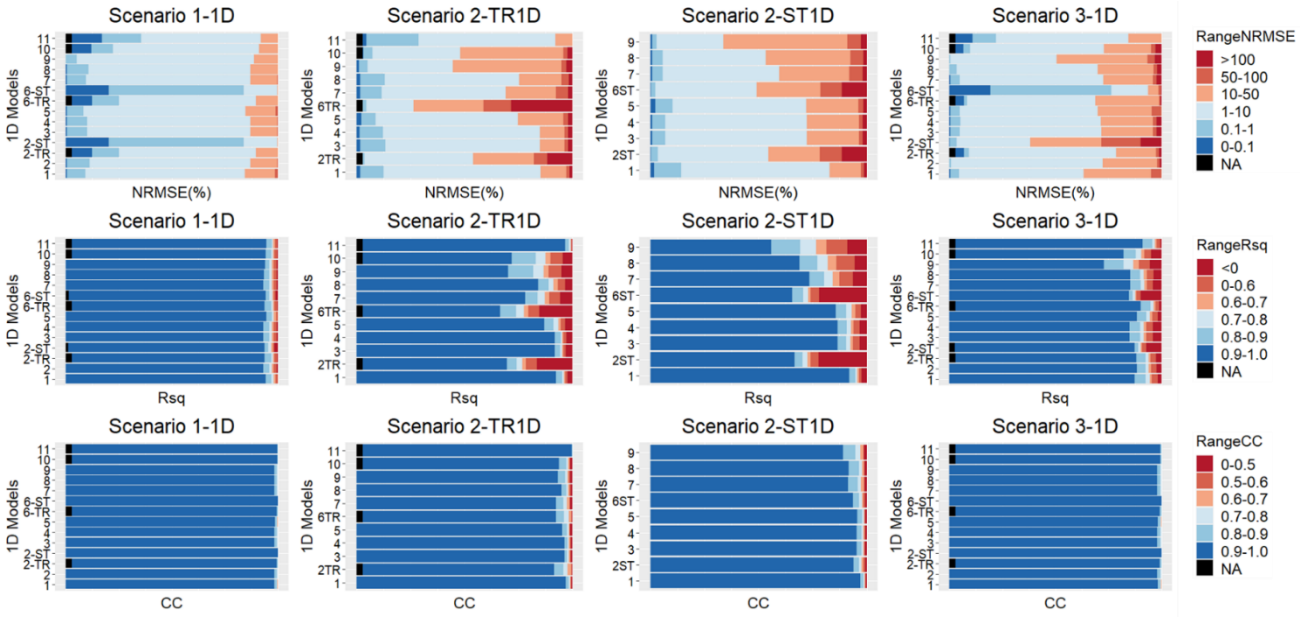

Figure 3.15: Range plots illustrating the performance of 1D infiltration models across 3957 experimental plots using three key model performance parameters: Normalized Root Mean Squared Error (NRMSE), R-squared value (R^2), and Coefficient of Correlation (CC).

While key evaluation parameters such as NRMSE, R-squared value (R^2), and Coefficient of Correlation (CC) provide valuable insights into the overall performance of infiltration models under our analysis scenarios, they do not capture all aspects of infiltration models and extraction

techniques. For instance, Scenario 1 might exhibit the lowest NRMSE, indicating good overall model performance, but it's essential to recognize that this might not necessarily reflect the accuracy of estimated parameters, K_s and S. High variability in these parameters, as observed in previous analyses, could indicate potential issues with the physical realism of models' predictions, despite favorable NRMSE values. While NRMSE provides a measure of error between actual and predicted infiltration, it does not reveal whether K_s and S adhere to physical principles of infiltration theory. Also, evaluation parameters do not capture the full range of behaviors exhibited by different models subject to a certain extraction technique. To avoid any misconceptions and fully understand the effectiveness of infiltration models, it is therefore crucial to, besides computing model performance parameters, perform quantitative assessments of soil parameter predictions, and consideration of specific study objectives to provide a comprehensive evaluation of infiltration models under varying extraction techniques.

It is worth noting that in Figure 3.15, NA estimates are shown across the transient-state expressions of 1D models, which are applicable to transient data comprising N=3871 experiment plots, compared to the total or steady-state data comprising N=3957 plots. This discrepancy is due to 86 infiltration tests in our dataset that did not undergo a transition phase and were already under saturation conditions. However, since this number represents only a negligible 2% of the total dataset, it will not affect the statistical comparison across all models.

3.5. Conclusion

Our analysis studied the complex relationships between soil properties, infiltration models, and parameter estimations, shedding light on the variability and uniqueness associated with estimated saturated hydraulic conductivity and sorptivity in the context of eleven different 1D infiltration models and three different extraction techniques. Scenario 1 optimized simultaneously for the two parameters, K_s and S, using each model's equation. Scenario 2 unified K_s across all models, as the steady-state slope of the cumulative infiltration curve at end times, and further optimized for S using each model's equation. Scenario 3 represented a dual optimization which optimized for K_s and S using each models' equation while minimizing the infiltration error and the difference between K_s and the steady-state slope of the cumulative infiltration curve. Our detailed analysis of the different scenarios and their impact on infiltration characteristics, K_s and S, provided valuable insights into the trade-offs and considerations involved in selecting extraction techniques for soil-water parameter estimation.

Overall, our results highlighted the divergent behaviors exhibited by different infiltration models in predicting K_s and S, both within the same and across different extraction methods, pointing out how different models can capture and represent soil-water interactions differently. More precisely, our analysis showed that adopting the physical significance of K_s as the steady-state slope of the cumulative infiltration curve (Scenario 3) reduced the dispersion of K_s predictions across models. Moreover, sorptivity behaved best also under Scenario 3, but continues to remain highly sensitive to model selection and extraction method. This emphasized the model-specific nature of sorptivity estimates and reinforced the notion that variations in infiltration models can lead to diverse estimations of such a key parameter.

Here, we recommend that the reporting of K_s and S should always be associated with details of the model used as well as the extraction technique being applied. We also recognize the need to standardize a reporting method to allow for generalizations to be realistic, particularly in the context of systematic reviews. Our results demonstrate that given the wide range of variability in estimates of K_s and S for the same experimental plot (just as a result of model or extraction method selection), it is really hard to extract any meaningful conclusions from a systematic review of the literature involving the values of K_s and S. Perhaps global and local values should be reported, where global values are based on their original definitions where K_s is the steady-state slope of the cumulative infiltration curve at end times, and S is Philip's introduced parameter estimated using Philip's equation (Equation 2a). Local values are values used in each specific study and can follow any model selection by researchers. For that, we offered Scenario 3 as a good common ground allowing for model-specific formulation to be anchored with the physically accepted definition of K_s.

By incorporating evaluation metrics of model behavior across the dataset used in the extraction, and adherence of estimated parameters to physical meanings, researchers can gain a more comprehensive understanding whether the applied extraction technique is suitable or not. This holistic approach ensures that the strengths and limitations of different extraction techniques are properly assessed, leading to more informed decision-making in the field of infiltration modeling. Furthermore, as the future of data analysis is closely tied to artificial intelligence (AI), researchers face significant challenges in determining the most appropriate approach to adopt as AI continues to progress. Unifying the physical meanings of K_s and S based on their real origins is a paramount practice to standardizing soil-water parameter estimation. Accordingly, researchers can ensure consistency, clarity, and transparency in infiltration modeling research.

3.6. References

Abou Najm, M. R., Stewart, R. D., Di Prima, S., & Lassabatere, L. (2021). A Simple Correction Term to Model Infiltration in Water-Repellent Soils. *Water Resources Research*. https://doi.org/10.1029/2020WR028539

Angulo-Jaramillo, R., Bagarello, V., Di Prima, S., Gosset, A., Iovino, M., & Lassabatere, L. (2019). Beerkan Estimation of Soil Transfer parameters (BEST) across soils and scales. *Journal of Hydrology*, *576*, 239–261.

Bagarello, V., Iovino, M., & Elrick, D. (2004). A Simplified Falling-Head Technique for Rapid Determination of Field-Saturated Hydraulic Conductivity. *Soil Science Society of America Journal*. https://doi.org/10.2136/sssaj2004.6600

Basset, Christelle; Abou Najm, Majdi; Angulo-Jaramillo, Rafael; Bagarello, Vincenzo; Ghanbarian, Behzad; Di Prima, Simone; Iovino, Massimo; Lassabatere, Laurent; Stewart, R. (2023). Conceptual and empirical approaches to characterize infiltration: A literature review (under review). *Vadose Zone Journal*.

Basset, C., Abou Najm, M., Ghezzehei, T., Hao, X., & Daccache, A. (2023). How does soil structure affect water infiltration? A meta-data systematic review. *Soil and Tillage Research*, *226*, 105577.

Bayabil, H. K., Dile, Y. T., Tebebu, T. Y., Engda, T. A., & Steenhuis, T. S. (2019). Evaluating infiltration models and pedotransfer functions: Implications for hydrologic modeling. *Geoderma*. https://doi.org/10.1016/j.geoderma.2018.11.028

Bouwer, H. (1960). A study of final infiltration rates from cylinder infiltrometers and irrigation furrows with an electrical resistance network. *Transactions 7th Int. Congr. Soil Sci.*, *1*, 448–456.

Bouwer, H. (1963). Theoretical effect of unequal water levels on the infiltration rate determined with buffered cylinder infiltrometers. *Journal of Hydrology*, *1*(1), 29–34.

Bouwer, H. (1986). Intake rate: cylinder infiltrometer. *Methods of Soil Analysis: Part 1 Physical and Mineralogical Methods*, *5*, 825–844.

Brutsaert, W. (1976). The concise formulation of diffusive sorption of water in a dry soil. *Water Resources Research*. https://doi.org/10.1029/WR012i006p01118

Di Prima, S., Lassabatere, L., Bagarello, V., Iovino, M., & Angulo-Jaramillo, R. (2016). Testing a new automated single ring infiltrometer for Beerkan infiltration experiments. *Geoderma*. https://doi.org/10.1016/j.geoderma.2015.08.006

Di Prima, Simone, Castellini, M., Abou Najm, M. R., Stewart, R. D., Angulo-Jaramillo, R., Winiarski, T., & Lassabatere, L. (2019). Experimental assessment of a new comprehensive model for single ring infiltration data. *Journal of Hydrology*, *573*, 937–951.

Di Prima, Simone, Stewart, R. D., Abou Najm, M. R., Ribeiro Roder, L., Giadrossich, F., Campus, S., Angulo-Jaramillo, R., Yilmaz, D., Roggero, P. P., Pirastru, M., & Lassabatere, L. (2021). BEST-WR: An adapted algorithm for the hydraulic characterization of hydrophilic and water-

repellent soils. *Journal of Hydrology*. https://doi.org/10.1016/j.jhydrol.2021.126936

Elrick, D. E., Parkin, G. W., Reynolds, W. D., & Fallow, D. J. (1995). Analysis of Early-Time and Steady State Single-Ring Infiltration Under Falling Head Conditions. *Water Resources Research*. https://doi.org/10.1029/95WR01139

Fodor, N., Sándor, R., Orfanus, T., Lichner, L., & Rajkai, K. (2011). Evaluation method dependency of measured saturated hydraulic conductivity. *Geoderma*. https://doi.org/10.1016/j.geoderma.2011.07.004

Green, H. W., & Ampt, G. A. (1911). Studies on soil physics: Flow of air and water through soils. *J. Aric. Sci.*

Hao, X., Abou Najm, M., Steenwerth, K. L., Nocco, M. A., Basset, C., & Daccache, A. (2023). Are there universal soil responses to cover cropping? A systematic review. *Science of the Total Environment*, *861*, 160600.

Haverkamp, R., Parlange, J. Y., Starr, J. L., Schmitz, G., & Fuentes, C. (1990). Infiltration under ponded conditions: 3. A predictive equation based on physical parameters. *Soil Science*. https://doi.org/10.1097/00010694-199005000-00006

Haverkamp, R., Ross, P. J., Smettem, K. R. J., & Parlange, J. Y. (1994). Three-dimensional analysis of infiltration from the disc infiltrometer: 2. Physically based infiltration equation. *Water Resources Research*. https://doi.org/10.1029/94WR01788

Jačka, L., Pavlásek, J., Pech, P., & Kuráž, V. (2016). Assessment of evaluation methods using infiltration data measured in heterogeneous mountain soils. *Geoderma*. https://doi.org/10.1016/j.geoderma.2016.04.023

Kögel-Knabner, I., Guggenberger, G., Kleber, M., Kandeler, E., Kalbitz, K., Scheu, S., Eusterhues, K., & Leinweber, P. (2008). Organo-mineral associations in temperate soils: Integrating biology, mineralogy, and organic matter chemistry. *Journal of Plant Nutrition and Soil Science*, *171*(1), 61–82.

Kooistra, M. J., & Van Noordwijk, M. (2020). Soil architecture and distribution of organic matter. In *Structure and organic matter storage in agricultural soils* (pp. 15–56). CRC Press.

Krull, E. S., Baldock, J. A., & Skjemstad, J. O. (2003). Importance of mechanisms and processes of the stabilisation of soil organic matter for modelling carbon turnover. *Functional Plant Biology*, *30*(2), 207–222.

Ku, C.-Y. (2013). *A novel method for solving ill-conditioned systems of linear equations with extreme physical property contrasts*.

Li, R. M., Stevens, M. A., & Simons. (1976). SOLUTIONS TO GREEN-AMPT INFILTRATION EQUATION. *ASCE J Irrig Drain Div*.

Lipiec, J., Kuś, J., Słowińska-Jurkiewicz, A., & Nosalewicz, A. (2006). Soil porosity and water infiltration as influenced by tillage methods. *Soil and Tillage Research*, *89*(2), 210–220.

Mezencev, V. J. (1948). Theory of formation of the surface runoff. *Meteorol. Gidrol*, *3*, 33–40.

Mirzaee, S., Zolfaghari, A. A., Gorji, M., Dyck, M., & Ghorbani Dashtaki, S. (2014). Evaluation

of infiltration models with different numbers of fitting parameters in different soil texture classes. *Archives of Agronomy and Soil Science*, *60*(5), 681–693.

Mishra, S. K., Tyagi, J. V, & Singh, V. P. (2003). Comparison of infiltration models. *Hydrological Processes*, *17*(13), 2629–2652.

Nie, W., Ma, X., & Fei, L. (2017). Evaluation of Infiltration Models and Variability of Soil Infiltration Properties at Multiple Scales. *Irrigation and Drainage*. https://doi.org/10.1002/ird.2126

Olson, T. C. (1960). Model study of the double-ring infiltrometer in layered systems. *Int. Congr. Soil Sci. Trans. 7th*, 441–447.

Pachepsky, Y., & Karahan, G. (2022). On shapes of cumulative infiltration curves. *Geoderma*, *412*, 115715.

Parlange, J. Y. (1980). Water transport in soils. *Annu. Rev. Fluid Mech.;(United States)*, *12*.

Parlange, J. Y., Lisle, I., Braddock, R. D., & Smith, R. E. (1982). The three-parameter infiltration equation. *Soil Science*. https://doi.org/10.1097/00010694-198206000-00001

Perroux, K. M., & White, I. (1988). Designs for Disc Permeameters. *Soil Science Society of America Journal*. https://doi.org/10.2136/sssaj1988.03615995005200050001x

Philip, J. R. (1957a). The theory of infiltration: 1. The infiltration equation and its solution. *Soil Science*. https://doi.org/10.1097/00010694-195705000-00002

Philip, J. R. (1957b). The theory of infiltration: 4. Sorptivity and algebraic infiltration equations. *Soil Science*. https://doi.org/10.1097/00010694-195709000-00010

PHILIP, J. R. (1969). *Theory of Infiltration*. https://doi.org/10.1016/b978-1-4831-9936-8.50010-6

Rahmati, M., Latorre, B., Lassabatere, L., Angulo-Jaramillo, R., & Moret-Fernández, D. (2019). The relevance of Philip theory to Haverkamp quasi-exact implicit analytical formulation and its uses to predict soil hydraulic properties. *Journal of Hydrology*. https://doi.org/10.1016/j.jhydrol.2019.01.038

Rahmati, M., Weihermüller, L., Vanderborght, J., Pachepsky, Y. A., Mao, L., Sadeghi, S. H., Moosavi, N., Kheirfam, H., Montzka, C., Van Looy, K., Toth, B., Hazbavi, Z., Al Yamani, W., Albalasmeh, A. A., Alghzawi, M. Z., Angulo-Jaramillo, R., Antonino, A. C. D., Arampatzis, G., Armindo, R. A., … Vereecken, H. (2018). Development and analysis of the Soil Water Infiltration Global database. *Earth System Science Data*. https://doi.org/10.5194/essd-10-1237-2018

Ramesh, T., Bolan, N. S., Kirkham, M. B., Wijesekara, H., Kanchikerimath, M., Rao, C. S., Sandeep, S., Rinklebe, J., Ok, Y. S., & Choudhury, B. U. (2019). Soil organic carbon dynamics: Impact of land use changes and management practices: A review. *Advances in Agronomy*, *156*, 1–107.

Rönnqvist, H. (2018). Double-Ring Infiltrometer for In-Situ Permeability Determination of Dam Material. *Engineering*, *10*(06), 320.

Schiff, L. (1953). The effect of surface head on infiltration rates based on the performance of ring infiltrometers and ponds. *Eos, Transactions American Geophysical Union*, *34*(2), 257–266.

Sihag, P., Tiwari, N. K., & Ranjan, S. (2017). Estimation and inter-comparison of infiltration models. *Water Science*, *31*(1), 34–43.

Stewart, R. D., & Abou Najm, M. R. (2018). A Comprehensive Model for Single Ring Infiltration I: Initial Water Content and Soil Hydraulic Properties. *Soil Science Society of America Journal*. https://doi.org/10.2136/sssaj2017.09.0313

Stone, J. J., Hawkins, R. H., & Shirley, E. D. (1994). Approximate form of Green-Ampt infiltration equation. *Journal of Irrigation and Drainage Engineering*. https://doi.org/10.1061/(ASCE)0733-9437(1994)120:1(128)

Stroosnijder, L. (1976). Infiltratie en herverdeling van water in grond, Versl. *Landbouwkd. Onderz*, *847*.

Swartzendruber, D. (1987). A quasi-solution of Richards' Equation for the downward infiltration of water into soil. *Water Resources Research*. https://doi.org/10.1029/WR023i005p00809

Talsma, T. (1969). In situ measurement of sorptivity. *Soil Research*. https://doi.org/10.1071/sr9690269

Talsma, T., & Parlange, J. Y. (1972). One-dimensional vertical infiltration. *Australian Journal of Soil Research*. https://doi.org/10.1071/SR9720143

Valiantzas, J. D. (2010). New linearized two-parameter infiltration equation for direct determination of conductivity and sorptivity. *Journal of Hydrology*. https://doi.org/10.1016/j.jhydrol.2009.12.049

Vand, A. S., Sihag, P., Singh, B., & Zand, M. (2018). Comparative evaluation of infiltration models. *KSCE Journal of Civil Engineering*, *22*, 4173–4184.

Védère, C., Lebrun, M., Honvault, N., Aubertin, M.-L., Girardin, C., Garnier, P., Dignac, M.-F., Houben, D., & Rumpel, C. (2022). How does soil water status influence the fate of soil organic matter? A review of processes across scales. *Earth-Science Reviews*, *234*, 104214.

Watson, K. W., & Luxmoore, R. J. (1986). Estimating Macroporosity in a Forest Watershed by use of a Tension Infiltrometer. *Soil Science Society of America Journal*. https://doi.org/10.2136/sssaj1986.03615995005000030007x

Whisler, F. D., & Bouwer, H. (1970). Comparison of methods for calculating vertical drainage and infiltration for soils. *Journal of Hydrology*. https://doi.org/10.1016/0022-1694(70)90051-X

Youngs, E. G. (1968). An estimation of sorptivity for infiltration studies from moisture moment considerations. *Soil Science*. https://doi.org/10.1097/00010694-196809000-00001

CHAPTER 4: Uncharted Territory: Evaluating 3D Infiltration Modeling for Enhanced Predictions of Soil Hydraulic Parameters

4.1. Abstract

Expanding upon our previous metadata analysis, which focused on the variability of infiltration predictions in one-dimensional (1D) models, we have now extended our investigation to three-dimensional (3D) infiltration modeling. This area, though critically important for more precise hydrological modeling and for scenarios where infiltration is not strictly vertical such as in heterogeneous soils, has been rarely evaluated. Our objective here is to provide comprehensive insights into the capabilities and limitations of different 3D infiltration models, thereby shedding light on the uniqueness and accuracy of saturated hydraulic conductivity K_s (LT^{-1}) and sorptivity S ($LT^{-0.5}$) predictions. Leveraging the same extensive dataset from the Soil Water Infiltration Global (SWIG) database comprised of 5,023 cumulative infiltration curves, we applied four different 3D infiltration equations and estimated the corresponding K_s (LT^{-1}) and S ($LT^{-0.5}$) using three different applied extraction techniques. Our results distinctly demonstrated notable similarities in K_s and S derived from models sharing similar algorithms and underlying assumptions, while also showing significant variabilities in these parameters within the same models under different infiltration conditions (transient- vs. steady-state) or across different models with varying theoretical foundations and extraction methods. These findings underscored the significant impact that model characteristics and extraction methods have on the estimation of K_s and S in 3D infiltration modeling. By identifying the conditions under which different models and methods perform best, we provide valuable guidance for practitioners aiming to achieve accurate and reliable infiltration predictions for specific applications, such as irrigation planning, hydrological studies, or soil conservation efforts.

4.2. Introduction

Given the fundamental role of infiltration in soil hydrology and biogeochemistry, numerous models have been developed to characterize infiltration and estimate key hydraulic parameters such as K_s (LT^{-1}) and S ($LT^{-0.5}$). At the early time of infiltration, sorptivity S ($LT^{-0.5}$) which was described by Philip (1957b) was water retention due to capillarity influences water movement. As infiltration progresses, hydraulic conductivity K_s (LT^{-1}) becomes significant, governing water movement at steady-state conditions, primarily driven by gravity.

Traditionally, infiltration models have predominantly focused on one-dimensional (1D) water movement, particularly in vertical infiltration scenarios, rather than fully accounting for three-dimensional (3D) infiltration processes. In a theoretical and historical review on infiltration theory, Basset et al. (2023) collected and identified 102 one-dimensional (1D) infiltration models, while only 28 three-dimensional (3D) models have been identified, indicating a significant gap in 3D representation compared to the more established 1D approaches.

This gap has resulted in numerous studies examining and comparing the performance of different 1D infiltration models (Mishra et al., 2003; Shukla et al., 2003; Fodor et al., 2011; Mirzaee et al., 2014; Jacka et al., 2016; Sihag et al., 2017; Nie at al., 2017; Vand et al., 2018; Bayabil et al., 2019) while comparatively less attention has been given to three-dimensional (3D) models (Lassabetere et al., 2009). The significant disparity in efforts dedicated to the development and evaluation of 1D infiltration models compared to 3D modeling is primarily attributed to greater complexity, computational demands, and data requirements associated with 3D modeling efforts. The need to account for spatial variability in soil properties, moisture content, and infiltration dynamics across multi dimensions has presented a real challenge to researchers to model 3D infiltration.

Additionally, there may be fewer benchmark datasets available for testing and validating 3D models compared to 1D models, making it more challenging to assess their performance.

Smettem et al. (1994) were the first to recognize the importance of capturing spatial variability of infiltration characteristics for a comprehensive understanding of water movement through the soil profile. Based on their research, Haverkamp et al. (1994) pioneered the development of a simple mathematical model describing water infiltration in three dimensions within the soil profile. Their work has been instrumental in driving the development of different three-dimensional infiltration models across the years (Wu and Pan, 1997; Wu et al., 1999; Lassabetere et al., 2006, 2014, Stewart and Abou Najm, 2018; Di Prima et al., 2021).

Building on these efforts, we aimed to gauge the capabilities and limitations of 3D infiltration models in predicting soil hydraulic parameters such as K_s (LT^{-1}) and S ($LT^{-0.5}$) across different extraction techniques. Different 3D infiltration models may produce varying predictions of soil hydraulic parameters due to differences in assumptions, parameterizations, and numerical techniques. Understanding the variability of estimated parameters among these models is essential for assessing their robustness and uncertainty, which has not been explored until now. Building upon our previous work on 1D modeling, we attempt to establish connections and identify similarities or differences between 1D and 3D modeling approaches. This comparative analysis can reveal whether insights and conclusions drawn from 1D models hold true in the context of 3D modeling, or if there are unique factors and considerations specific to 3D infiltration modeling.

To this end, we carried out a metadata analysis to evaluate different 3D infiltration models and assess the variability in estimated infiltration characteristics among these models and applied extraction methods. The key infiltration parameters that were assessed are saturated hydraulic conductivity K_s (LT^{-1}) and sorptivity S ($LT^{-0.5}$) due to their governing role in characterizing

infiltration processes. Our meta-analysis was performed in R software using 5023 infiltration data curves extracted from SWIG, the global infiltration database developed by Rahmati et al. (2018).

4.3. Methods

4.3.1. Infiltration models

Basset et al. (2023) conducted an in-depth review where they identified a total of 138 unique infiltration models, including 28 that were three-dimensional (3D) models. Based on their findings, we selected four three-dimensional (3D) infiltration models that span from historical to present times. These models represent comprehensive mathematical and physical concepts in infiltration modeling theory, encompassing both commonly used and recently developed methods for predicting infiltration properties. Moreover, these models were specifically selected because they incorporate soil water parameters relevant to our investigation, saturated hydraulic conductivity K_s (LT^{-1}) and sorptivity S ($LT^{-1/2}$). The following is a summary of distinctive features of the selected infiltration models, along with their corresponding equations.

4.3.1.1.Haverkamp et al. (1994)

Haverkamp et al. (1994) are well-known for developing the most practical analytical equation for three-dimensional infiltration from a disc or ring infiltrometer of radius r (L) for all infiltration times based on easily measurable soil and hydraulic properties.

$$I_{3D} = I_{1D} + \frac{\gamma S^2 t}{r\Delta\theta} \quad [41]$$

For small times,

$$I_{3D} = St^{0.5} + \left[\frac{2-\beta}{3}(K_s - K_i) + K_i + \frac{\gamma S^2}{r(\theta_s-\theta_i)}\right]t \quad [1TR]$$

For large times,

$$I_{3D} = \left(K_s + \frac{\gamma S^2}{r(\theta_s-\theta_i)}\right)t + \frac{1}{2(1-\beta)} ln\left(\frac{1}{\beta}\right)\frac{S^2}{(K_s-K_i)} \quad [1ST]$$

where β and γ are fitting parameters; $\gamma = 0.75$ and $0.3 \leq \beta \leq 1.7$ for sand to silty soils, respectively (Lassabatere et al., 2009, Rahmati et al., 2019).

4.3.1.2.Lassabatere et al. (2006)

Lassabatere et al. (2006) developed a simple and practical infiltration equation, commonly known as BEST equation, which gained popularity due to its influential contribution to estimating three-dimensional water infiltration for transient and steady state based on Haverkamp et al. (1994) model.

For small times,

$$I_{3D} = St^{0.5} + [A(1-B)S^2 + Bi_{3D.\infty}]t \qquad [2TR]$$

For large times,

$$I_{3D} = (AS^2 + K_s)t + C\frac{S^2}{K_s} \qquad [2ST]$$

where:

$$A = \frac{\gamma}{r(\theta_s - \theta_i)}$$

$$B = \frac{2-\beta}{3}\left[1 - \left(\frac{\theta_i}{\theta_s}\right)^n\right] + \left(\frac{\theta_i}{\theta_s}\right)^n$$

$$C = \frac{1}{2\left[1 - \left(\frac{\theta_i}{\theta_s}\right)^n\right](1-\beta)} ln\left(\frac{1}{\beta}\right)$$

$$i_{3D.\infty} = AS^2 + K_s$$

4.3.1.3.Stewart and Abou Najm (2018)

Stewart and Abou Najm (2018) proposed an approach for estimating three-dimensional (3D) infiltration by building upon the two-term Philip type solutions established by Philip (1957). Their

approach takes into consideration various factors such as different sizes of infiltration rings of radii r (L), depths of insertion d (L), saturated θ_s (L^3L^{-3}) and initial θ_i (L^3L^{-3}) water contents, matric flux potential, φ(L^2 T^{-1}), water supply pressure head h_0 (L), as well as transient and steady-state infiltration behaviors, ensuring a comprehensive analysis of infiltration processes across different conditions.

For small times,

$$I = St^{0.5} + aK_s t + \frac{S^2 ab}{(\theta_s - \theta_i)\left(d + \frac{r}{2}\right)} t \qquad [3TR]$$

For large times,

$$I = fK_s t + f(1-a)K_s t_c \qquad [3ST]$$

where:

$$t_c = \frac{(\theta_s - \theta_i)(h_0 + \lambda)}{4bK_s f^2 (1-a)^2}$$

$$f = \frac{h_0 + \lambda}{d + r/2} + 1$$

λ (L) is the capillary length equal to the inverse of a parameter α (L^{-1}) introduced by Gardner (1958) as a general description of soil textural and structural characteristics, thus $\lambda = \frac{1}{\alpha}$

For real soils, $0.4 < a < 0.5$ (Philip, 1990) and $0.5 < b < \pi/4$ (White and Sully, 1987). $a = 0.45$ and $b = 0.55$ are often assumed (Haverkamp et al., 1994, White and Sully, 1987, Reynolds and Elrick, 1990).

4.3.1.4.Di Prima et al. (2021)

Di Prima et al. (2021) expanded upon the existing BEST method by incorporating the scaling factor $(1 - e^{-\alpha_{wr}t})$ initially proposed by Abou Najm et al. (2021) as an attempt to mimic infiltration behaviors of water-repellent soils.

For small times,

$$I_{3D} = S\sqrt{t} - \frac{S\sqrt{\pi}}{2\sqrt{\alpha_{wr}}} erf\left(\sqrt{\alpha_{wr}t} + [A(1-B)S^2 + Bi_{3D.\infty}]t - \frac{[A(1-B)S^2 + Bi_{3D.\infty}](1-e^{-\alpha_{wr}t})}{\alpha_{wr}}\right) [4]$$

We compiled the four selected models mentioned earlier, along with their corresponding parameters, as presented in Table 4.1. Exceptionally, in Di Prima et al.'s (2021) model, an additional new parameter, the soil water-repellency parameter α_{wr} (T^{-1}), is introduced and needs to be optimized as well. Any assumed values of the models' fitting-type parameters are included in Table 4.1.

Table 4.1: Compilation of the four selected (3D) infiltration models

Models	Parameters	Fitting parameters
Haverkamp et al. (1994)	$K_s, K_i, S, r, \beta, \gamma, \theta_s$ and θ_i	$0.3 \leq \beta \leq 1.7$ for sand to silty soils, respectively. An average value of $\beta = 0.6$ was used when soil textural data was not determined. (Lassabatere et al., 2009, Rahmati et al., 2019). An average value of $\gamma = 0.75$ was used (Smettem et al., 1994; Haverkamp et al., 1994). n was estimated based on soil textural class using Table 4 (Minasny and McBratney, 2007). An average value of n derived from Table 4 was used when soil textural data was not determined. $K_i = 0$
Lassabatere et al. (2006) - BEST	$K_s, S, r, \beta, \gamma, n, \theta_s$ and θ_i	
Di Prima et al. (2021) - BESTWR	$K_s, S, \alpha_{wr}, r, \beta, \gamma, n, \theta_s$ and θ_i	
Stewart and Abou Najm (2018)	$K_s, S, r, d, \lambda, a, b, \theta_s$ and θ_i	$d = 5cm =$ ring insertion depth (Stewart and Abou Najm, 2018) $\lambda = 1/\alpha$ where α (cm^{-1}) is suggested by Elrick et al. (1988) as function of soil textural class (See Table 2 in Wu et al., 1999) $0.4 < a < 0.5$ (Philip, 1990) and $0.5 < b < \pi/4$ (White and Sully, 1987). $a = 0.45$ and $b = 0.55$ were used (Haverkamp et al., 1994, White and Sully, 1987, Reynolds and Elrick, 1990)
r, θ_s and θ_i were extracted from our infiltration database by Rahmati et al. (2018).		

4.3.2. Data collection and preprocessing

The methodology followed in Chapter 3 for collecting and preprocessing infiltration data was followed in this analysis. To elaborate, we first obtained infiltration data from the Soil Water Infiltration Global Database (SWIG) by Rahmati et al. (2018), which compiles 5023 experimental plots depicting cumulative infiltration curves (i.e., cumulative infiltration I (cm) vs. time T (hr)).

Then, we thoroughly examined this dataset to identify any discrepancies or inconsistencies that can potentially disrupt the analysis. Any such discrepancies were excluded from the analysis based on a step-by-step exclusion criterion outlined in Chapter 3, as illustrated in Figure 4.1. The last exclusion criteria (i.e., #7 in Figure 4.1) was specifically considered in this analysis since 3D infiltration modeling requires information about water contents and size of infiltration rings; therefore, any infiltration tests that did not measure the initial and saturated water contents, θ_i and θ_s (cm^3cm^{-3}) respectively, as well as the ring radius r (cm) were removed.

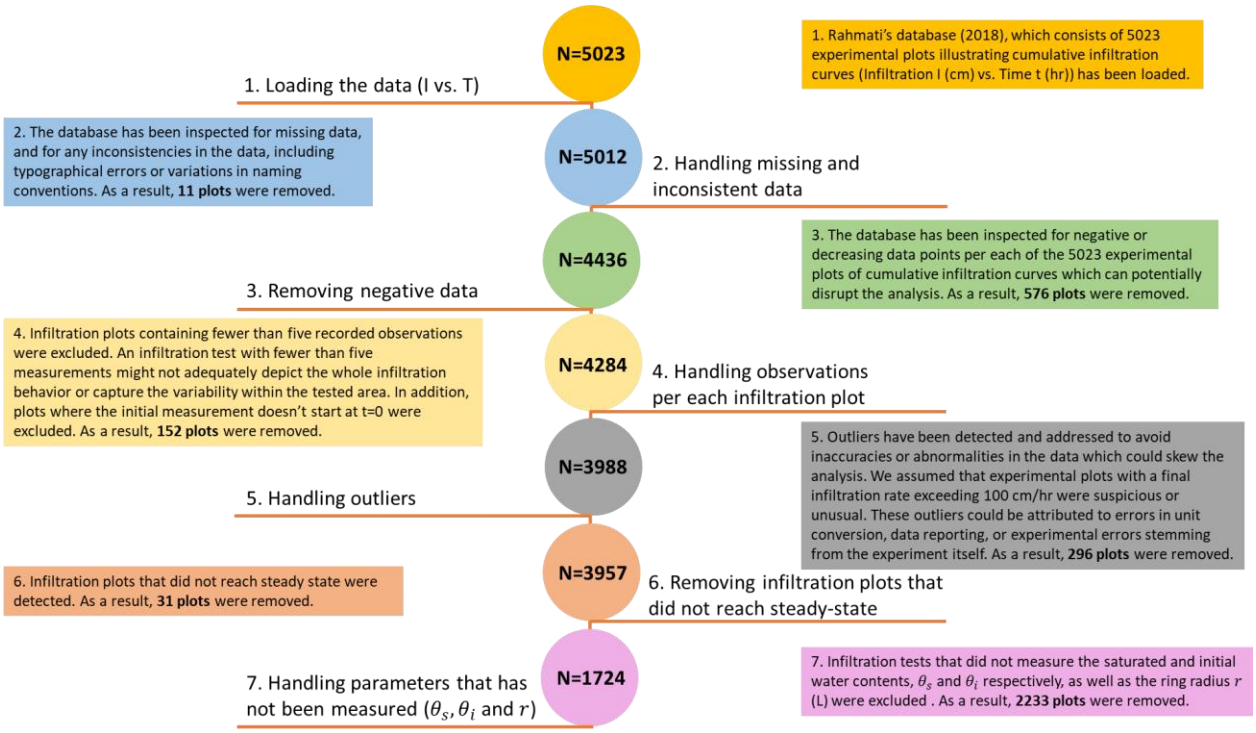

Figure 4.1: Step-by-step exclusion approach for 3D infiltration data cleaning and preprocessing

4.3.3. Extraction techniques for K_s and S estimation

To extract the two fundamental parameters, sorptivity S (cmhr$^{-0.5}$) and saturated hydraulic conductivity K_s (cmhr^{-1}), from the four selected infiltration models, we considered three distinct scenarios, each representing a different extraction technique (Figure 4.2 and Table 4.2):

The first scenario (denoted as Scenario 1) outlined a conventional optimization approach where optimal values for the two positive unknowns (S, K_s) were derived by curve fitting the infiltration dataset (i.e., actual cumulative infiltration I vs. time of infiltration t) into the equation of each model using the least square technique. This technique aimed to minimize the sum of squared differences between the actual infiltration data y_j^i obtained from SWIG and corresponding infiltration values predicted by each of infiltration model $\hat{y}_j^i$, where j represents a single observation within the i^{th} experimental plot of total m observations, and N is the total number of experimental plots.

$$\min_{i=1 to N} \sum_{j=1}^{m} \left(\hat{y}_j^i - y_j^i\right)^2 \quad [5]$$

The second scenario (denoted as Scenario 2) outlined a linear regression analysis of slope b (cmhr^{-1}) and intercept c (cm) of the data collected during the steady/final phase of the infiltration run (I_∞ vs. t_∞) to describe K_s (cmhr^{-1}).

$$I_{\infty,i} = b_i t_i + c_i \quad [6]$$

Unlike 1D modeling which directly expresses K_s (cmhr^{-1}) as the steady-state slope b (cmhr^{-1}), 3D models relate K_s (cmhr^{-1}) to b (cmhr^{-1}) based on more complex interactions and geometric considerations.

Following Haverkamp et al. (1994), Lassabatere et al. (2006), and Di Prima et al. (2021),

$$K_{s,i} = b_i - \frac{\gamma {S_i}^2}{r_i(\theta_{s,i} - \theta_{i,i})} \quad [7]$$

Following Stewart and Abou Najm (2018),

$$K_{s,i} = b_i / f_i \quad [8]$$

Where $f_i = \frac{h_{0,i} + \lambda_i}{d_i + r_i/2} + 1$

This extraction technique reduced the number of unknowns from two (K_s, S) to one variable (S) which strengthens the robustness of the inversion.

To identify the steady/final phase of the infiltration run (I_∞ vs. t_∞), we started by running a regression analysis on the last three points of each cumulative infiltration curve. This analysis involved fitting a linear mathematical model to these points to estimate the behavior of the infiltration process at end times. Following the regression analysis, we calculated the error difference between predicted infiltration (cm), estimated from our regression analysis, and actual infiltration (cm), for each point of the cumulative infiltration curve. To this end, we identified the section of the curve where the estimated error difference falls below 2% as asymptotic, thus representing the steady phase of the infiltration run (I_∞ vs. t_∞); The remaining observations where the error difference is above 2%, were designated as the transient phase of the infiltration run (I_{tr} vs. t_{tr}) (Di Prima et al., 2019).

To estimate sorptivity S (cmhr$^{-0.5}$), Scenario 2 was translated into two sub-scenarios with distinct extraction approaches:

- Scenario 2 – Transient (denoted as Scenario 2 – TR) estimated S (cmhr$^{-0.5}$) by fitting the transient-state expression derived for short infiltration times to the transient infiltration data (I_{tr} vs. t_{tr}).
- Scenario 2 – Steady (denoted as Scenario 2 – SS) only considered the steady phase of the infiltration dataset and thus estimated S (cmhr$^{-0.5}$) by fitting the steady-state expression derived for long infiltration times to the final infiltration data (I_{∞} vs. t_{∞}). Notably, models including Haverkamp et al. (1994), Lassabatere et al. (2006), and Di Prima et al. (2021) have derived asymptotic equations for cumulative infiltration under steady-state describing the intercept term c (L) in terms of K_s (cmhr^{-1}) and S (cmhr$^{-0.5}$). Consequently, solving the equation $c = f\ (S, K_s)$ led to estimation of S (cmhr$^{-0.5}$). It is worth noting that Di Prima et al. (2021) equation was specifically developed for transient infiltration times. Therefore, we have opted to exclude this model from Scenario 2-ST to maintain the integrity of our analysis.

The third scenario (denoted as Scenario 3) replicated the same extraction technique used in Scenario 1, which involved curve fitting the infiltration dataset into the equation of each model using the least square technique. However, what differed Scenario 3 from Scenario 1 is that, in addition to minimizing the sum of the squared differences between the actual infiltration data y_j^i and the predicted values $\hat{y}_j^i$, Scenario 3 alternatively minimized the sum of the squared differences between the estimated and the actual steady-state slopes of the cumulative infiltration curve, $\hat{b}$ and b (cmhr^{-1}) respectively.

$$\underset{i=1 to N}{min}\left[\sum_{j=1}^{m}\frac{1}{m}\left(\hat{y}_j^i - y_j^i\right)^2 + (\hat{b}_i - b_i)^2\right] \quad [9]$$

Consequently, Scenario 3 acted as an intermediate approach between scenarios 1 and 2. It showcased an extraction technique that conventionally optimized for soil hydraulic parameters using the least square technique, while also anchoring the steady-slope $\hat{b}$ (cmhr^{-1}) (calculated as function of the estimated S (cmhr$^{-0.5}$) and K_s (cmhr^{-1})) to the actual steady-state slope b (cmhr^{-1}) of the cumulative infiltration curve.

Under the three scenarios (1, 2, and 3), saturated hydraulic conductivity K_s (cmhr^{-1}) and sorptivity S (cmhr$^{-0.5}$) require values greater than zero since it is physically impossible for these parameters to be negative. Negative values for these parameters would have no physical interpretation in the context of water flow and soil characteristics. As such, $K_{s,i} \geq 1e^{-06} cmhr^{-1}$ and $S_i \geq 1e^{-06}\ cmhr^{-0.5}$.

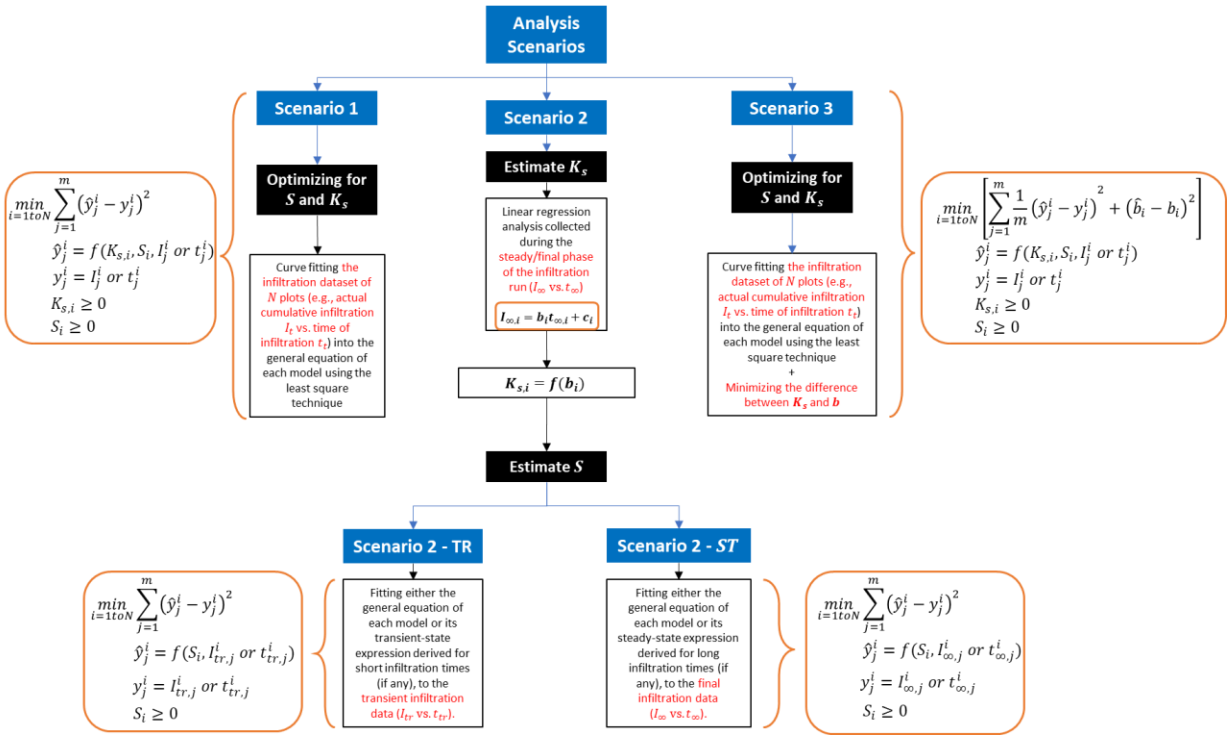

Figure 4.2: Diagram summarizing the methodology followed to estimate sorptivity S (cmhr^{-05}) and saturated hydraulic conductivity K_s (cmhr^{-1}) across 3D infiltration models using three extraction techniques represented by three distinct scenario

Table 4.2: Summary of the four selected (3D) infiltration models subjected to the three extraction techniques represented by three distinct scenarios

Models	Infiltration Behavior	I(t) curve	Analytical Equation	**Extraction technique**			
				$\min_{i=1toN} \sum_{j=1}^{m} (\hat{y}_j^i - y_j^i)^2$	$\min_{i=1toN} \left[\sum_{j=1}^{m} \frac{1}{m} (\hat{y}_j^i - y_j^i)^2 + (\hat{b}_i - b_i)^2 \right]$	$I_{\infty,i} = b_i t_i + c_i$ $\min_{i=1toN} \sum_{j=1}^{m} (\hat{y}_j^i - y_j^i)^2$	
				Scenario 1	Scenario 3	Scenario 2-TR	Scenario 2-ST
Haverkamp et al. (1994)	Early, Transient and Steady - State	Concave	$\hat{y}_i = S_i t_i^{0.5} + \left[\frac{2-\beta}{3} K_{s,i} + \frac{\gamma {S_i}^2}{r_i \Delta\theta_i}\right] t_i$ small t (TR) $\hat{y}_i = \left(K_{s,i} + \frac{\gamma {S_i}^2}{r_i \Delta\theta_i}\right) t_i + \frac{1}{2(1-\beta)} ln\left(\frac{1}{\beta}\right) \frac{{S_i}^2}{K_{s,i}}$ large t (ST) $0.3 \leq \beta \leq 1.7$ and $\gamma = 0.75$	(TR) $t_i = t_{tr,i}$ $y_i = I_{tr,i}$ (ST) $t_i = t_{st,i}$ $y_i = I_{st,i}$ $K_{s,i} \geq 0$ $S_i \geq 0$		$t_i = t_{tr,i}$ $y_i = I_{tr,i}$ $K_{s,i} = b_i - \frac{\gamma {S_i}^2}{r_i \Delta\theta_i}$ $0 \leq S_i \leq \sqrt{\frac{b_i r_i \Delta\theta_i}{\gamma}}$	$K_{s,i} = b_i - \frac{\gamma {S_i}^2}{r_i \Delta\theta_i}$ $S_i = \sqrt{\frac{2 c_i K_{s,i} (1-\beta)}{\ln(1/\beta)}}$
Lassabatere et al. (2006) - BEST	Early, Transient and Steady - State		$\hat{y}_i = S_i t_i^{0.5} + \left[A_i {S_i}^2 + B_i K_{s,i}\right] t_i$ small t (TR) $\hat{y}_i = \left(A_i {S_i}^2 + K_{s,i}\right) t_i + C_i \frac{{S_i}^2}{K_{s,i}}$ large t (ST) $A_i = \frac{\gamma}{r_i \Delta\theta_i}$; $B_i = \frac{2-\beta}{3}\left[1 - \left(\frac{\theta_{i,i}}{\theta_{s,i}}\right)^{n_i}\right] + \left(\frac{\theta_{i,i}}{\theta_{s,i}}\right)^{n_i}$; $C_i = \frac{1}{2\left[1-\left(\frac{\theta_{i,i}}{\theta_{s,i}}\right)^{n_i}\right](1-\beta)} ln\left(\frac{1}{\beta}\right)$; $0.3 \leq \beta \leq 1.7$ and $\gamma = 0.75$				$K_{s,i} = b_i - \frac{\gamma {S_i}^2}{r_i \Delta\theta_i}$ $S_i = \sqrt{\frac{c_i K_{s,i}}{C_i}}$
Stewart and Abou Najm (2018)	Early, Transient and Steady - State		$\hat{y}_i = S_i t_i^{0.5} + a K_{s,i} t_i + \frac{{S_i}^2 ab}{(\theta_{s,i} - \theta_{i,i})\left(d + \frac{r_i}{2}\right)} t_i$ small t (TR) $\hat{y}_i = f_i K_{s,i} t_i + f_i (1-a) K_{s,i} t_{c,i}$ large t (ST) $t_{c,i} = \frac{(\theta_{s,i} - \theta_{i,i})(h_{0,i} + \lambda_i)}{4 b_i K_{s,i} {f_i}^2 (1-a)^2}$ $f_i = \frac{h_{0,i} + \lambda_i}{d + r_i/2} + 1$ $\lambda_i = \frac{1}{\alpha_i}$, $d = 5cm$, $a = 0.45$, $b = 0.55$	(TR) $t_i = t_{tr,i}$ $y_i = I_{tr,i}$ (ST) $t_i = t_{st,i}$ $y_i = I_{st,i}$ $K_{s,i} \geq 0$ $S_i \geq 0$		$t_i = t_{tr,i}$ $y_i = I_{tr,i}$ $K_{s,i} = b_i / f_i$ $S_i \geq 0$	$t_i = t_{\infty,i}$ $y_i = I_{\infty,i}$ $K_{s,i} = b_i / f_i$ $S_i \geq 0$
Di Prima et al. (2021) - BESTWR	Transient	Non-uniform	$\hat{y}_i = S_i t_i^{0.5} - \frac{S_i \sqrt{\pi}}{2\sqrt{\alpha_{wr,i}}} erf\left(\sqrt{\alpha_{wr,i} t_i} + \left(A_i {S_i}^2 + B_i K_{s,i}\right) t_i - \frac{\left(A_i {S_i}^2 + B_i K_{s,i}\right)\left(1 - e^{-\alpha_{wr,i} t_i}\right)}{\alpha_{wr,i}}\right.$ $A_i = \frac{\gamma}{r_i \Delta\theta_i}$; $B_i = \frac{2-\beta}{3}\left[1 - \left(\frac{\theta_{i,i}}{\theta_{s,i}}\right)^{n_i}\right] + \left(\frac{\theta_{i,i}}{\theta_{s,i}}\right)^{n_i}$; $0.3 \leq \beta \leq 1.7$ and $\gamma = 0.75$	$t_i = t_{tr,i}$ $y_i = I_{tr,i}$ $K_{s,i} \geq 0$ $S_i \geq 0$ $\alpha_{wr,i} \geq 0$		$t_i = t_{tr,i}$ $y_i = I_{tr,i}$ $K_{s,i} = b_i - \frac{\gamma {S_i}^2}{r_i \Delta\theta_i}$ $0 \leq S_i \leq \sqrt{\frac{b_i r_i \Delta\theta_i}{\gamma}}$ $\alpha_{wr,i} \geq 0$	$t_i = t_{\infty,i}$ $y_i = I_{\infty,i}$ $K_{s,i} = b_i - \frac{\gamma {S_i}^2}{r_i \Delta\theta_i}$ $0 \leq S_i \leq \sqrt{\frac{b_i r_i \Delta\theta_i}{\gamma}}$ $\alpha_{wr,i} \geq 0$

4.3.4. Model performance parameters

To evaluate how accurately infiltration models predict cumulative infiltration I (cm) compared to actual data across various scenarios, we estimated several statistical parameters:

- Normalized Root Mean Square Error (NRMSE)

NRMSE is the normalized version of RMSE, which scales the difference between predicted $\hat{y}_j$ and observed values y_j at the j^{th} data point within the experimental plot (i.e., RMSE) by the mean $\bar{y}$ of actual values y_j:

$$NRMSE = \frac{RMSE}{\bar{y}} = \frac{\sum_{j=1}^{m} \frac{1}{m} \left(\hat{y}_j - y_j\right)^2}{\bar{y}} \quad [10]$$

Lower NRMSE values, ideally approaching 0%, signify better predictive performance, indicating smaller discrepancies between predictions and observations. Higher values, closer to 100%, suggest larger discrepancies and poorer model performance. A 100% NRMSE would mean no correspondence between predictions and actual infiltration data.

- Coefficient of Determination (R^2)

R^2 quantifies how well a regression model fits the actual data points by measuring how much the independent variable ($\hat{y}$) explains the variability in the dependent variable (y) in a predicted regression model.

$$R^2 = 1 - \frac{\sum_{j=1}^{m} \left(\hat{y}_j - y_j\right)^2}{\sum_{j=1}^{m} \left(\hat{y}_j - \bar{y}\right)^2} \quad [11]$$

R^2 ranges from 0 to 1, with higher values indicating better predictive performance. However, a high R^2 doesn't necessarily mean a perfect model; it could still overfit or have other issues, which

justifies the need for at least one or two statistical measures of models' performance in addition to R^2. Negative R^2 values typically indicate a poor fit for the data.

- Coefficient of correlation (CC)

CC measures the strength and direction of the linear relationship between two variables and is calculated as follows:

$$CC = \frac{m\sum_{j=1}^{m}\hat{y}_j y_j - \sum_{j=1}^{m}\hat{y}_j \sum_{j=1}^{m} y_j}{\sqrt{m\sum_{j=1}^{m}\hat{y}_j{}^2 - \left(\sum_{j=1}^{m}\hat{y}_j\right)^2}\sqrt{m\sum_{j=1}^{m} y_j{}^2 - \left(\sum_{j=1}^{m} y_j\right)^2}} \quad [12]$$

CC ranges from -1 to 1, with positive values($0 < CC \leq 1$) indicating a positive linear relationship, negative values ($-1 \leq CC < 0$) indicating a negative linear relationship, and values near 0 suggesting no systematic association between the variables.

4.4. Results and discussion

4.3.1. Variability in K_s and S estimates across 3D models

Here, we present insights learned from our metadata analysis applied on the 1724 out of 5023 infiltration curves to investigate the variability in infiltration characteristics, K_s (cmhr^{-1}) and S (cmhr$^{-0.5}$) across four one-dimensional (3D) infiltration models using the three extraction techniques/scenarios.

The first exploration of the overall statistical variation of saturated hydraulic conductivity K_s (cmhr^{-1}) and sorptivity S (cmhr$^{-0.5}$) estimates was illustrated in Figures 4.3 and 4.4, respectively. A notable observation was the significant similarity in K_s and S estimates across the models proposed by Haverkamp et al. (1994) and Lassabatere et al. (2006) (also known as BEST). This similarity was consistent under both transient- and steady-state expressions (between 1TR and 2TR from one end, and 1ST and 2ST from another end), and across different extraction techniques. This finding aligns with our expectations since BEST model is derived from Haverkamp et al. (1994) model, sharing similar algorithms and underlying assumptions, thereby leading to similar infiltration characteristic estimates.

Despite the overall similarity between Haverkamp et al. (1994) and BEST models, a significant variability emerged in the estimated K_s values when comparing transient- and steady-state expressions across each individual model (Figure 4.3). This variability suggests that the equations derived for specific behaviors of infiltration (either transient or steady state) within the same model can lead to different predictions of K_s. This is likely due to the distinct nature of transient and steady-state infiltration processes, each influenced by different soil and boundary conditions. Additionally, in 3D infiltration models, the estimation of K_s is complicated by the radial flow

component and the three-dimensional geometry of the wetting front, which differentiates between how water moves during transient and steady state within the soil profile. Unlike K_s, the estimates for sorptivity S under models proposed by Haverkmap et al. (1994) and BEST showed less sensitivity to whether they were derived using transient or steady-state equation (Figure 4.4). As well, the overall median of S estimates across different models demonstrated a slight degree of consistency, potentially pointing to common trends or patterns across the models in different scenarios. The relative stability of S estimates across different phases of infiltration or conditions implies that sorptivity, which reflects the initial infiltration rate, is less affected by variations in transient and steady-state 3D infiltration behaviors compared to K_s. In other words, as sorptivity is primarily driven by the soil's capacity to absorb water initially, S can tend to be a more consistent property across different phases of 3D infiltration compared to K_s.

The three extraction techniques employed, referred to as Scenario 1, Scenario 2-TR/ST, and Scenario 3, demonstrate relatively small varying degrees of impact on the estimated values of K_s when Haverkamp et al. (1994) and BEST were applied (Figure 4.3). Starting first with the transient-state equations (i.e., 1TR and 2TR), Scenario 1 exhibited a similar overall spread of K_s estimates compared to Scenarios 2-TR and 3 but with a slightly lower median, suggesting that these equations might slightly underestimate K_s under scenario 1. Under this scenario, Haverkamp et al. (1994) and BEST (i.e., 1TR and 2TR) optimized K_s directly from transient-state data focusing primarily on the early/transient infiltration phase, without any anchor to steady-state conditions (as used in Scenario 2-TR and 3), possibly leading to a more conservative estimate of K_s. Moving to the steady-state expressions (i.e., 1ST and 2ST), predictions of K_s across all scenarios align closely. This is expected as Haverkamp et al. (1994) and BEST developed steady-state expressions

as linear equations that inherently converge to the steady-state slope b incorporating K_s, S, and geometric considerations as defined in Equation [7] under Scenario 2.

Stewart and Abou Najm (2018) showed trends that are relatively like those observed in the models by Haverkamp et al. (1994) and BEST, under different extraction techniques. Under scenario 1, the three models (1TR, 2TR, and 3TR) exhibited a moderately similar spread in K_s estimates, with Stewart and Abou Najm (2018) showing a slightly higher median. Now under scenarios 2 and 3, Stewart and Abou Najm (2018) behave similarly to the steady-state expressions developed by Haverkamp et al. (1994) and BEST, which highlights a very interesting finding for K_s predictions. The close alignment in predictions suggests a high level of consistency in how K_s is defined as function of the steady-state slope b, soil's sorptive capacity (either sorptivity S or capillary length λ), and geometric considerations across these three models. While we ascertain that each 3D model developed distinct relationships of K_s to the steady-state slope b and geometric configurations, the fundamental principles governing these relationships are aligned.

As for the model proposed by Di Prima et al. (2021) (also known as BESTWR), this model stood out as distinct from the other models by incorporating water repellency and hydrophobicity into infiltration modeling (i.e., integrating a third parameter α_{wr}, in addition to K_s and S). This additional parameter α_{wr} models the impact of water repellency, distinguishing it from the classic concave shape depicted by other models and instead describing a convex shape in cumulative infiltration curves. From our analysis (Figures 4.3 and 4.4), Di Prima et al. (2021) fails in estimating reliable values of K_s and S when optimized simultaneously using the least square technique (i.e., scenarios 1 and 3). However, they provided accurate and reliable predictions of K_s and S under Scenario 2-TR where K_s is estimated as function of steady-state slope b, sorptivity S, and geometric factors (Figure 4.3), reducing the system from three unknows (K_s, S, and α_{wr}) to a

simpler system with two unknows (S and α_{wr}). This distinctive performance of Di Prima et al. (2021) under varying extraction techniques highlight the influence of infiltration dynamics on the complex interactions between K_s, S, and α_{wr}. During the early stages of infiltration, water repellency causes a delay in the wetting front advancement, leading to a convex shape in the cumulative infiltration curve. This complexity makes it challenging to optimize K_s and S accurately using only transient-state data with the varying influence of water repellency. As infiltration progresses, the impact of water repellency diminishes, allowing the soil to reach a more stable infiltration rate. Under steady-state conditions, effects of hydrophobicity are minimized, making it easier to estimate K_s accurately when related to the steady-state slope b, sorptivity S, and geometry. Additionally, integration of geometric factors in steady-state expressions helps to normalize effects of hydrophobicity, leading to more consistent and reliable K_s and S estimates.

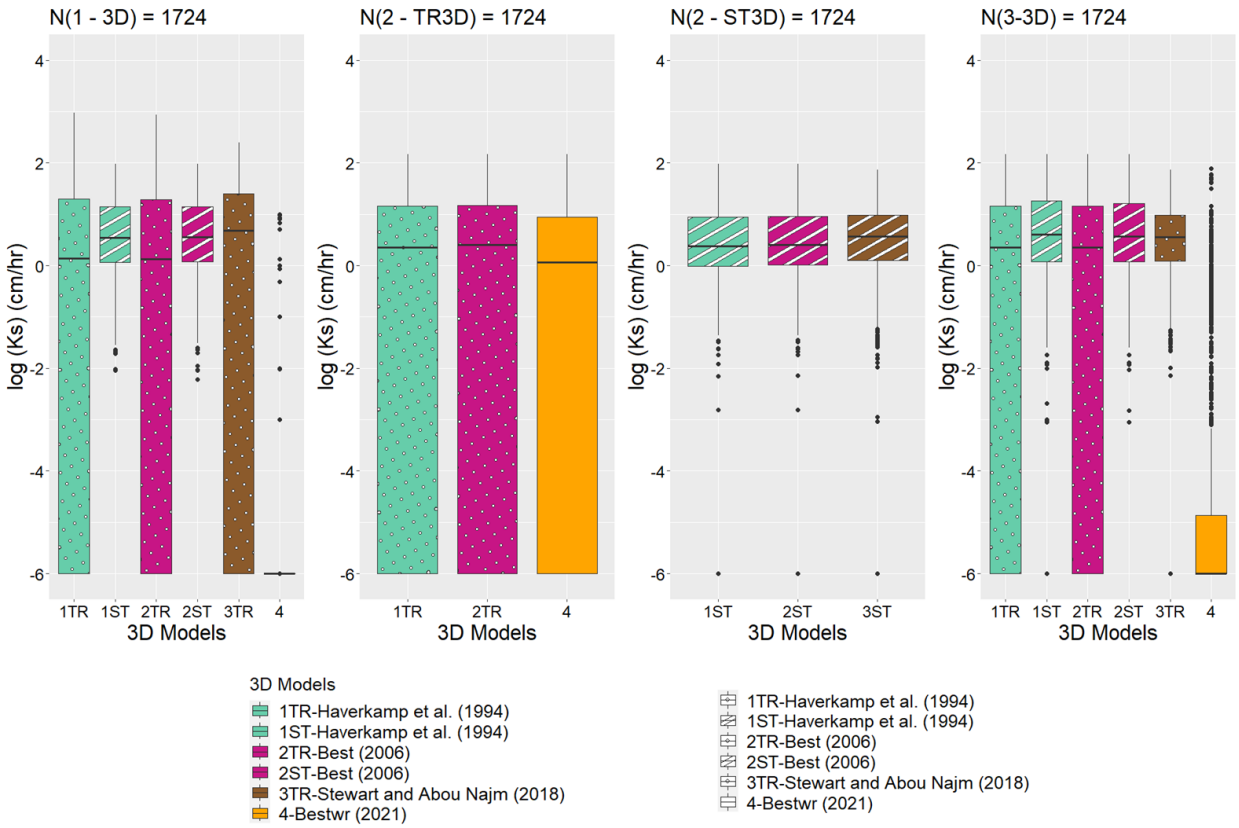

Figure 4.3: Boxplots illustrating the statistical variation of saturated hydraulic conductivity Ks ($cmhr^{-1}$) estimated across the experimental plots of total N=1724 per each 3D infiltration model. Models are ordered by the historical evolution of infiltration modeling attempts from the oldest (left) to the most recent (right).

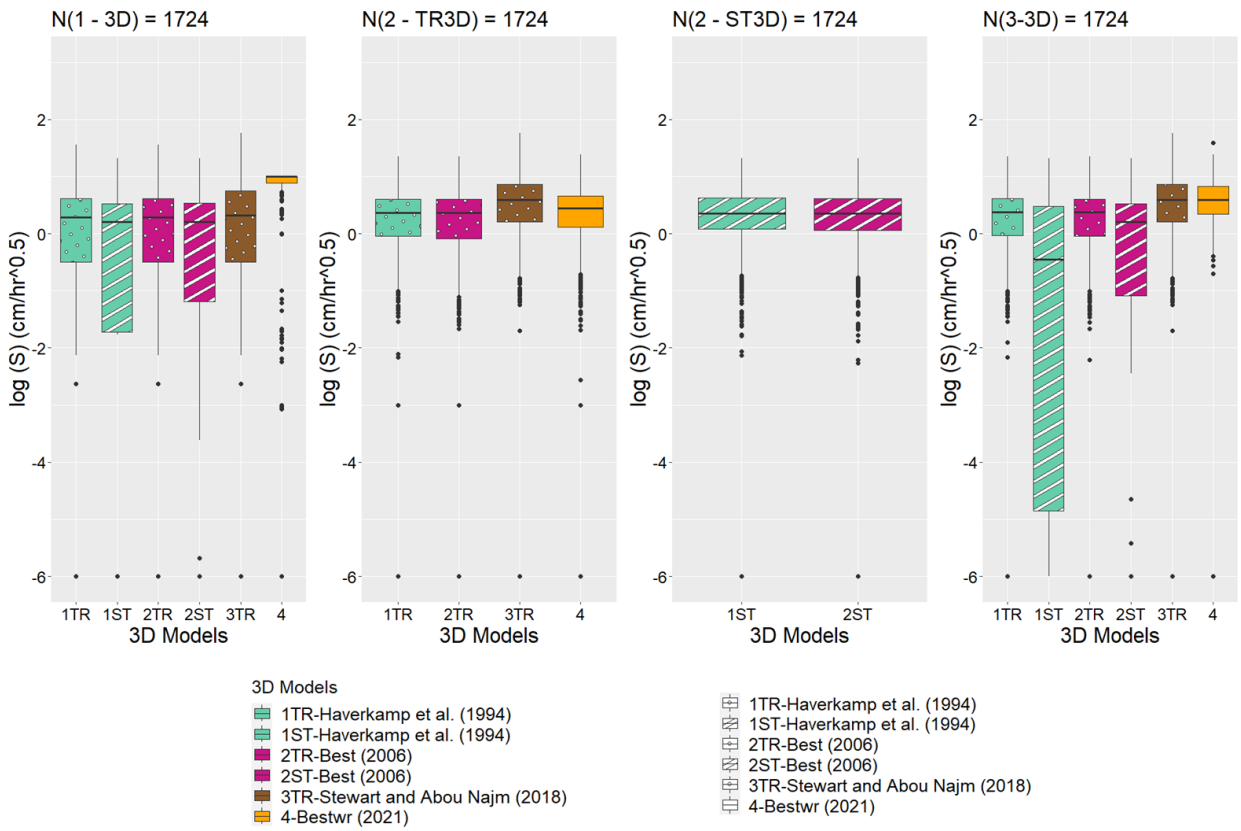

Figure 4.4: Boxplots illustrating the statistical variation of sorptivity S ($cmhr^{-0.5}$) estimated across the experimental plots of total N=1724 per each 3D infiltration model. Models are ordered by the historical evolution of infiltration modeling attempts from the oldest (left) to the most recent (right).

While the boxplots in Figures 4.3 and 4.4 effectively portrayed the degree of similarity and variability in the estimated infiltration characteristics, K_s and S, they do not capture every aspect of the underlying data.

4.4.2. Variability in K_s and S estimated values across 3D models and extraction methods per each infiltration experiment

To gain a deeper understanding, we explored K_s and S estimates across the four 3D infiltration models for each individual plot within the dataset, as depicted in Figures 4.5 and 4.6.

This detailed analysis provided a multifaceted view of the K_s and S estimates in each scenario, offering insights into the distributional characteristics, statistical variations, and outlier counts associated with each of the 3D infiltration models at the plot level. In both figures (i.e., Figures 4.5 and 4.6), the density plots on the left depicted the distribution of z-scores. Each z-score explains the distance from the mean (standard deviations) across four 3D infiltration models per infiltration plot. The graphical plots in the right segment provided a detailed examination of statistical variations within each experimental plot, with key statistical indicators including means (μ) highlighted in red, model-specific outliers highlighted in colors designated to each model, and +- standard deviation (σ) indicated by black horizontal lines. The barplots in the bottom summarized the total number of outliers observed in estimates for each of the 3D infiltration models. An outlier is defined as a data point (x) that deviates significantly from most other data points in the dataset. This deviation is determined based on a z-score falling outside the range of -2 to +2 where z is estimated using the following formula $z = \frac{x-\mu}{\sigma}$.

Figures 4.5 and 4.6 highlighted variability of K_s and S estimates across major experimental plots in Scenarios 1 and 3, although major data points representing K_s and S estimates for each model are clustered around the mean within the [-2,2] z-score range, with a minimal number of outliers depicted. This clustering suggests that models might produce statistically consistent estimates, but notable variability exists, which can be attributed to underlying physics behind each model. The variability in K_s and S estimates can be primarily attributed to the model proposed by Di Prima et al. (2021). The inclusion of the α_{wr} parameter, which accounts for water repellency and the resulting convex shape in cumulative infiltration curves, complicates the simultaneous optimization of K_s and S using transient-state data under Scenario 1 and 3, leading to greater variability in K_s and S estimates within each plot. As well, variability in predictions is more

pronounced across K_s compared to S estimates since, as stated before, estimates of K_s can be variable across the same model when using either transient- or steady-state equations/datasets; however, this discrepancy is less significant for S.

Variability in K_s and S decreased among models under Scenario 2 (2TR and 2ST) especially when predicting S, highlighting a more uniform behavior of the models in terms of K_s and S estimates under Scenario 2. Relating K_s and S together transforms the problem from a system with two unknowns (K_s and S) to one unknown (S) for non-hydrophobic soils, and from a system with three unknowns (K_s, S, and α_{wr}) to two unknowns (S and α_{wr}) for water-repellent soils, mainly reducing the complexity imposed on the optimization. On one hand, anchoring K_s to steady-state conditions ensures that the steady-state slope of the cumulative infiltration curve reflects K_s dynamics. On the other hand, relating sorptivity and geometric factors to K_s play a significant role in K_s estimation across 3D models, reflecting the soil's ability to absorb water initially and affecting the shape of the wetting front. Therefore, our detailed plot-level analysis highlighted the importance of steady-state conditions in providing consistent and accurate infiltration characteristics, especially in complex soil conditions affected by water repellency.

Interestingly, we deciphered in Figure 4.5 a spike around $K_s = 1e^{-06}\ cmhr^{-1}$ across Haverkamp et al. (1994), BEST, and BESTWR models under Scenario 2-TR, encompassing 457 plots (i.e., 27% of plots). This spike suggests that the optimizer in Scenario 2-TR which is constrained by the condition $S_i \leq \sqrt{\frac{b_i r_i \Delta\theta_i}{\gamma}}$ (as shown in the first two rows of Table 4.2 under Scenario 2-TR), was consistently converging to this maximum value across these models, leading to K_s to be equal to minimal value set at $1e^{-06}\ cmhr^{-1}$. This indicates that the optimizer might be overly restrictive when transient-state expressions were applied using transient-state data, constraining the

predictions of a realistic range of K_s values that reflect actual soil properties. However, we plotted Figure 4.7 to check whether the extraction technique (i.e., Scenario 2-TR) is causing this spike, which can point to potential limitations or biases when such models (i.e., Haverkamp et al. (1994), BEST, and BESTWR) are applied. Figure 4.7 compared Scenarios 1 and 3 (i.e., conventional optimization techniques) versus Scenario 2 (2TR and 2ST) regarding the estimates of K_s within the 457 plots across the models developed by Haverkamp et al. (1994), BEST, and BESTWR. The spike was again depicted under the other two scenarios, pinpointing potential limitations behind the models' concepts and algorithms that depict the transient state infiltration behavior rather than the extraction technique itself. In contrast, steady-state expressions of these models showed a more realistic range of K_s predictions, which can better reflect the actual soil-water structure.

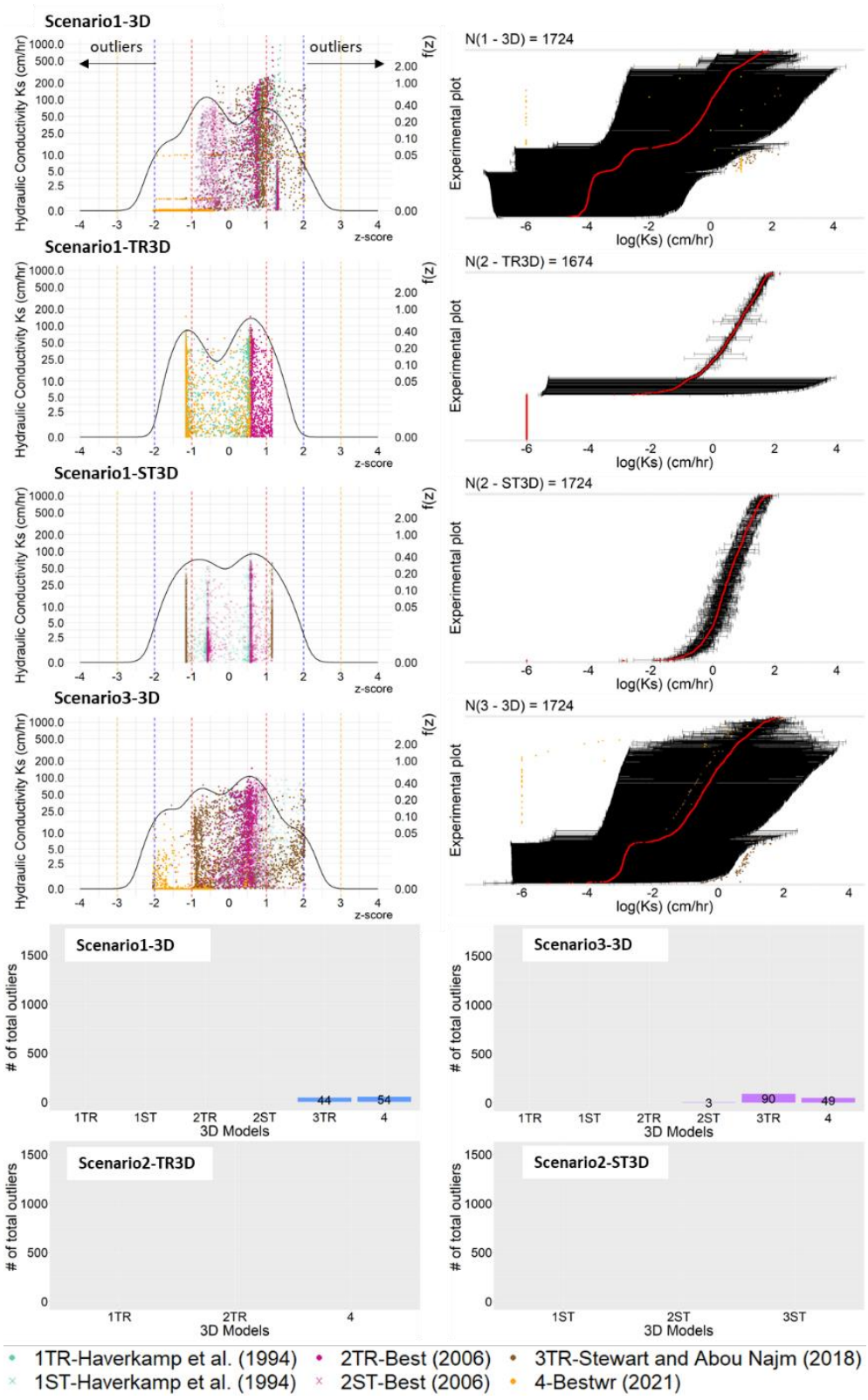

Figure 4.5: Graphical representing of the variability, skewness, and outliers in the estimates of K_s (cmhr^{-1}) at the plot level per each 3D infiltration model.

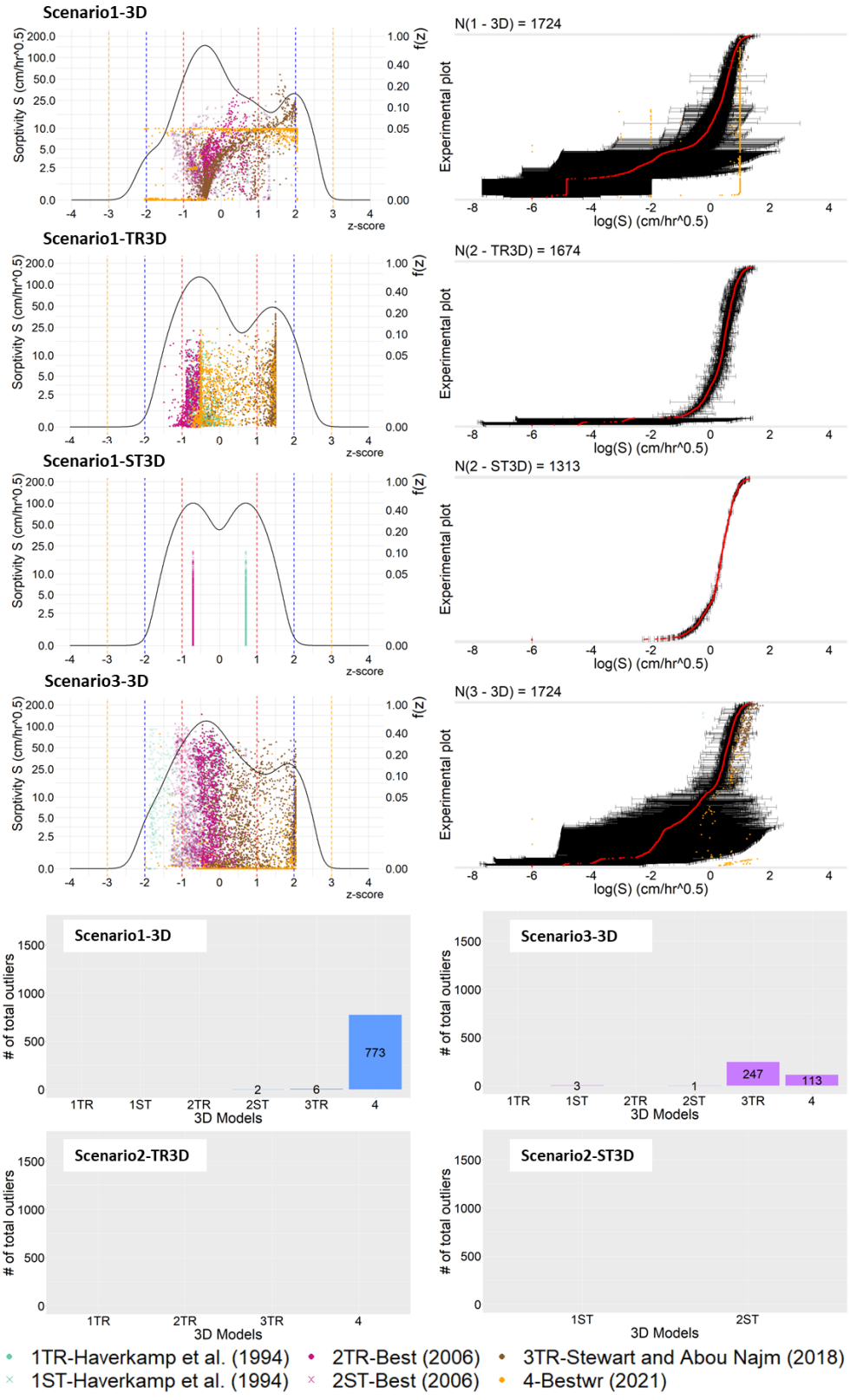

Figure 4.6: Graphical representing of the variability, skewness, and outliers in the estimates of S (cmhr$^{-0.5}$) at the plot level per each 3D infiltration model.

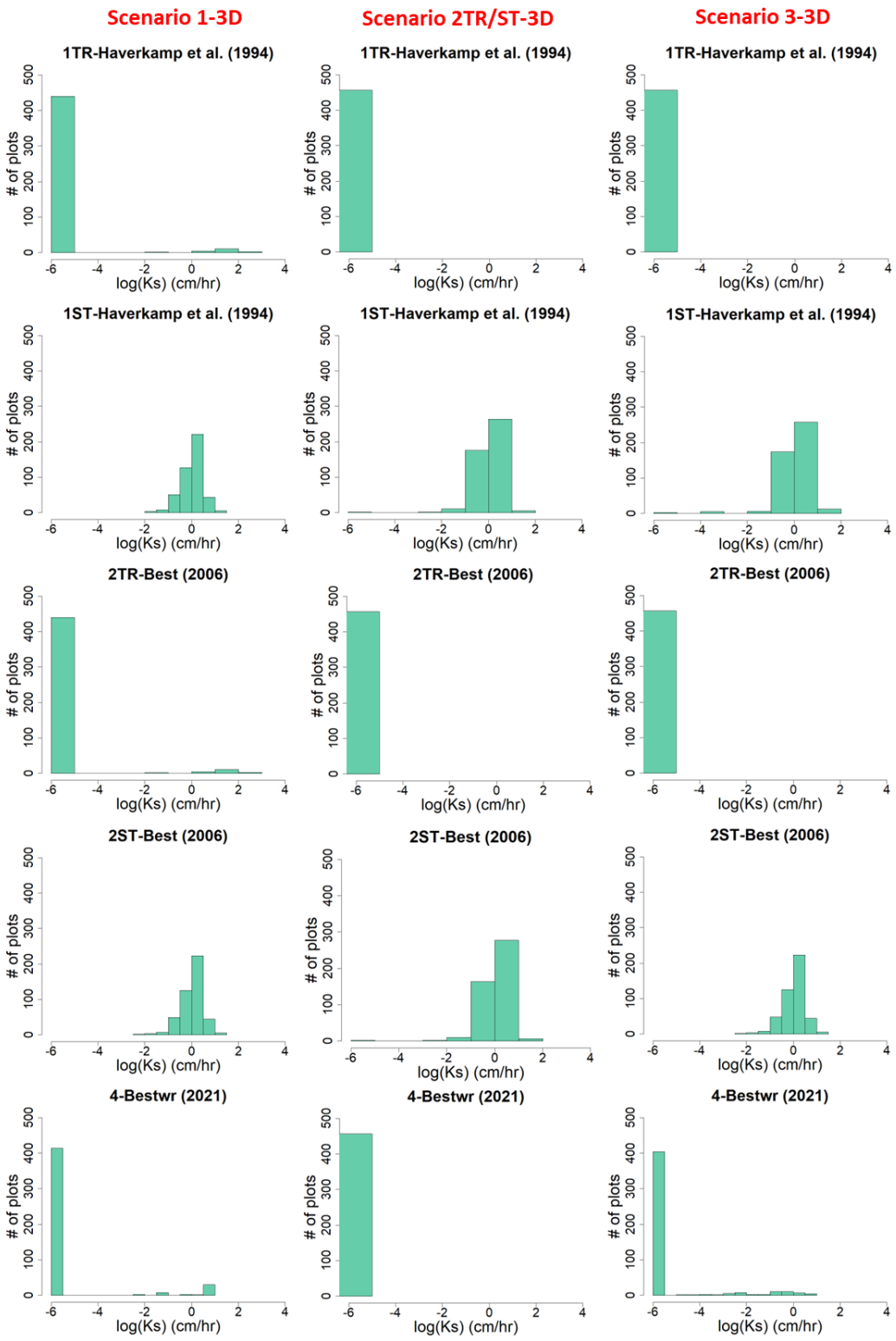

Figure 4.7: Histograms representing the statistical variation of saturated hydraulic conductivity K_s ($cmhr^{-1}$) per each 3D infiltration model across N=457 plots that exhibited minimal values of K_s (10^{-6} $cmhr^{-1}$) by the three models under Scenario 2-TR including Haverkamp et al. (1994), BEST, and BESTWR

It is worth noting that the transient-state expressions of 3D models are applicable to transient data comprising N=1674 experiment plots, compared to the total or steady-state data comprising N=1724 plots. This discrepancy is due to 50 infiltration tests in our dataset that did not undergo a transition phase and were already under saturation conditions. However, since this number represents only a negligible 3% of the total dataset, it will not affect the statistical comparison between transient- and steady-state expressions.

Another notable observation regarding the number of estimates is illustrated under Scenario 2-ST, where the estimation of K_s and S from Haverkamp et al. (1994) and BEST models resulted in NA values. This issue led to fewer estimates (N=1313) than the expected 1724 estimates (Figures 4.5 and 4.6). Upon investigation, we plotted corresponding cumulative infiltration curves and found these curves to be convex or non-uniform in shape. Since these models were designed to depict the classic concave shape of cumulative infiltration curves, they failed in generating finite estimates of K_s and S. This is especially problematic because the intercept c (Equation [6]) of the linear cumulative curve at steady state is negative. Given that S is estimated using the intercept c (as shown in the first two rows of Table 4.2 under Scenario 2-ST), the root mean square of a negative value is infinite, leading to an inability of these models to produce valid estimates under such conditions. This finding underscored the need to apply other models under these specific conditions. Even if finite values of K_s and S were estimated across these models using other extraction techniques, limitations are evident from the classic models. At this stage, Scenario2-ST has proved efficient in depicting the inability of models to produce valid estimates in cases where infiltration curves deviate from the expected concave shape. For accurate and reliable estimation of soil hydraulic properties under conditions of water-repellency, alternative models that can handle such deviations are necessary.

4.4.3. Performance of 3D infiltration models

Our analysis revealed that Scenarios 1 and 3 exhibited relatively better performance compared to Scenario 2 in predicting cumulative infiltration I (cm) across Haverkamp et al. (1994), BEST, and Stewart and Abou Najm (2018) models. Specifically, Scenario 1 demonstrated the lowest Normalized Root Mean Squared Error (NRMSE), the highest value of R^2, and the highest Correlation Coefficient (CC) to estimate infiltration compared to Scenarios 2 and 3 (Figure 4.8).

However, when considering BESTWR model, Scenarios 1 and 3 led to infiltration predictions with very low accuracy (NRMSE > 50 and R^2<0). Interestingly, BESTWR showed significantly better predictions under Scenario 2-TR. This indicates that for BESTWR model, estimating infiltration using transient-state data and relating K_s to the steady-state slope b, sorptivity S, and geometry (Scenario 2-TR) resulted in better predictions compared to other scenarios.

Now one could suggest the following hypothesis based on the observed performance of these models on cumulative infiltration I predictions: "Scenario 1 can be applied to estimate K_s and S from Haverkamp et al. (1994), BEST, Stewart and Abou Najm (2018) models while Scenario 2-TR can be used to estimate K_s and S from BESTWR".

However, it's crucial to acknowledge that while key evaluation parameters provide valuable insights into the overall performance of infiltration models under our analysis scenarios, they do not capture whether K_s and S adhere to the physical principles of infiltration theory. We observed that if we follow the suggested hypothesis, a wider range of behaviors will be exhibited by Haverkamp et al. (1994), BEST, Stewart and Abou Najm (2018) under Scenario 1 compared to other scenarios, as illustrated in Figure 4.9. Specifically, 60% and 46% of the experimental plots under Scenario 1 showed a magnitude (max-min) exceeding the mean value across K_s and S

estimates, respectively. Convergence issues were encountered as previously discussed when transient-sate expressions were applied to estimate K_s and S under this scenario. Therefore, while the model's performance metrics might appear favorable, the underlying physical realism and robustness of the parameter estimates could be compromised. Therefore, careful consideration and possibly further refinement of the models and scenarios are necessary to ensure both accurate and physically meaningful predictions of soil hydraulic properties.

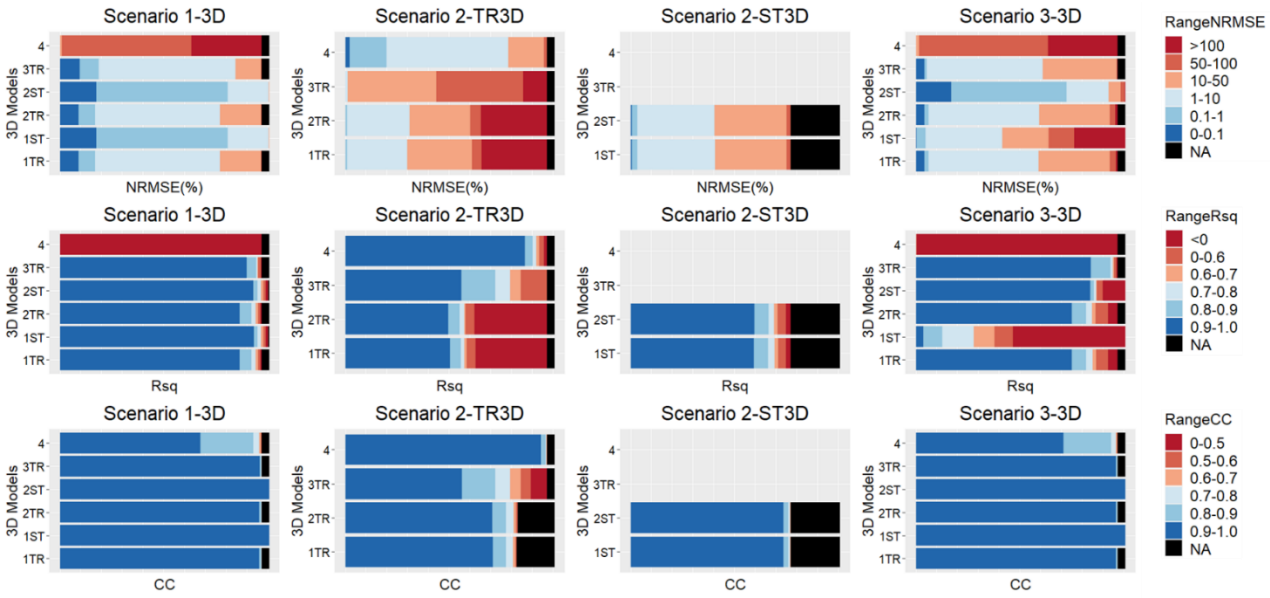

Figure 4.8: Range plots illustrating the performance of 3D infiltration models across 1724 experimental plots using three key model performance parameters: Normalized Root Mean Squared Error (NRMSE), R-squared value (R^2), and Coefficient of Correlation (CC).

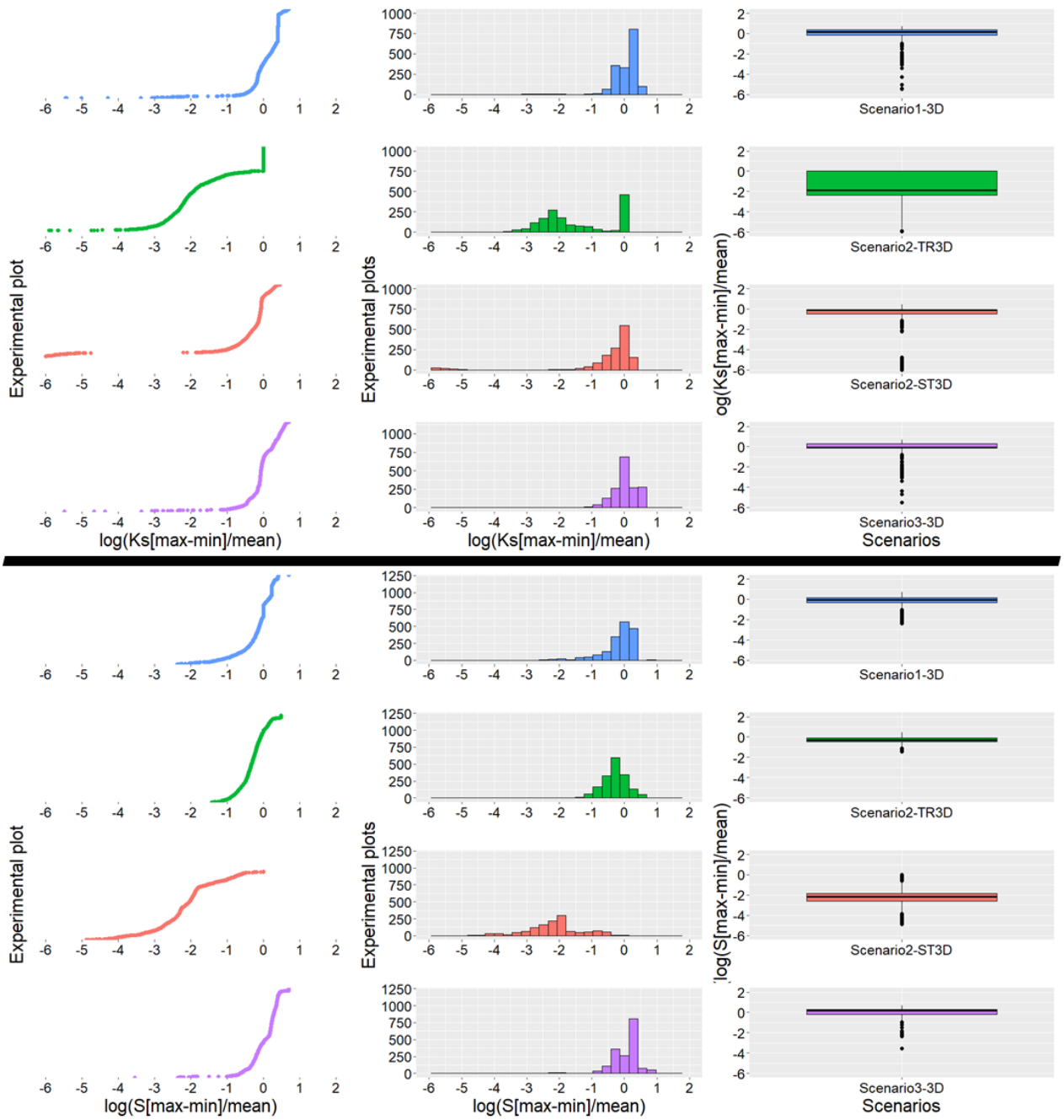

Figure 4.9: Graphical visualization of the statistical variation of the magnitude (max-min)/mean estimated from the saturated hydraulic conductivity K_s ($cmhr^{-1}$) and sorptivity S ($cmhr^{-0.5}$) values per each experimental plot across 1724 experimental plots among 3D infiltration models of non-hydrophobic soils

4.4.4. Infiltration models for water-repellent soils

Both, Abou Najm et al. (2021) and Di Prima et al. (2021) were developed as physical infiltration frameworks to account for water repellency in soils that depict convex cumulative infiltration curves.

Abou Najm et al. (2021) pioneered the addition of a soil water-repellency parameter α_{wr} (T^{-1}) and thus proposed the scaling factor $(1 - e^{-\alpha_{wr}t})$ that can be incorporated to any infiltration model as an attempt to mimic infiltration behaviors of water-repellent soils. Abou Najm et al. (2021) further developed a modified version of classic two-term Philip's equation (Philip, 1957b) (also known as WR) by integrating the scaling factor $(1 - e^{-\alpha_{wr}t})$ to develop an analytical equation describing one-dimensional (1D) cumulative infiltration in hydrophobic soils.

Di Prima et al. (2021) expanded upon the existing BEST method (Lassabatere et al., 2006) and developed an analytical equation (also known as BESTWR) by incorporating the scaling factor $(1 - e^{-\alpha_{wr}t})$ proposed by Abou Najm et al. (2021) as an attempt to mimic three-dimensional (3D) infiltration behaviors of water-repellent soils.

At this level, we carried out a statistical analysis on the performance of these two models in terms of their capabilities or limitations in estimating reliable values of the soil water-repellency parameter α_{wr} (T^{-1}), and therefore characterizing the convex shape of cumulative infiltration curves (Figures 4.10 and 4.11).

As shown in Figure 4.10, WR demonstrated a relative consistency in α_{wr} predictions across varying extraction techniques. 84% to 93% of the infiltration plots showed favorable Normalized Root Mean Squared Error (NRMSE) of less than 10% between Scenario 3, and Scenarios 1 and 2-TR, respectively. Additionally, the WR model was able to effectively characterize the shape of

cumulative infiltration curves. WR predicted lower values of α_{wr} converging to zero for infiltration plots exhibiting a convex shape, and relatively higher values converging to infinity for infiltration plots exhibiting a concave shape (Figure 4.11). α_{wr} parameter captures the initial resistance of water-repellent soils to infiltration, with values approaching zero as the water repellency effect dominates. In contrast, for non-repellent soils or soils where the water repellency diminishes quickly, α_{wr} values are higher, reflecting the quicker transition from initial to steady-state infiltration rates.

As for BESTWR, this model did not generate statistically significant values of α_{wr} under scenarios 1 and 3 with high NRMSE values indicating less reliable predictions. However, the model succeeded in providing reliable and comparable predictions of α_{wr} with those obtained through WR model under Scenario 2-TR, where the model was able to effectively characterize the shape of cumulative infiltration curves, with 75% of the infiltration plots showing favorable NRMSE of less than 10%. Therefore, while BESTWR model might struggle under certain extraction techniques, the model can still provide reliable α_{wr} estimates under specific conditions (like Scenario 2-TR), highlighting the importance of selecting appropriate scenarios for model application.

These findings suggest that the scaling factor proposed by Abou Najm et al. (2021) could be a versatile tool for characterizing soil water repellency and its impact on infiltration dynamics. The addition of the soil-water repellency parameter α_{wr} aligns well with the physical expectations of how water-repellent and non-repellent soils behave under infiltration conditions.

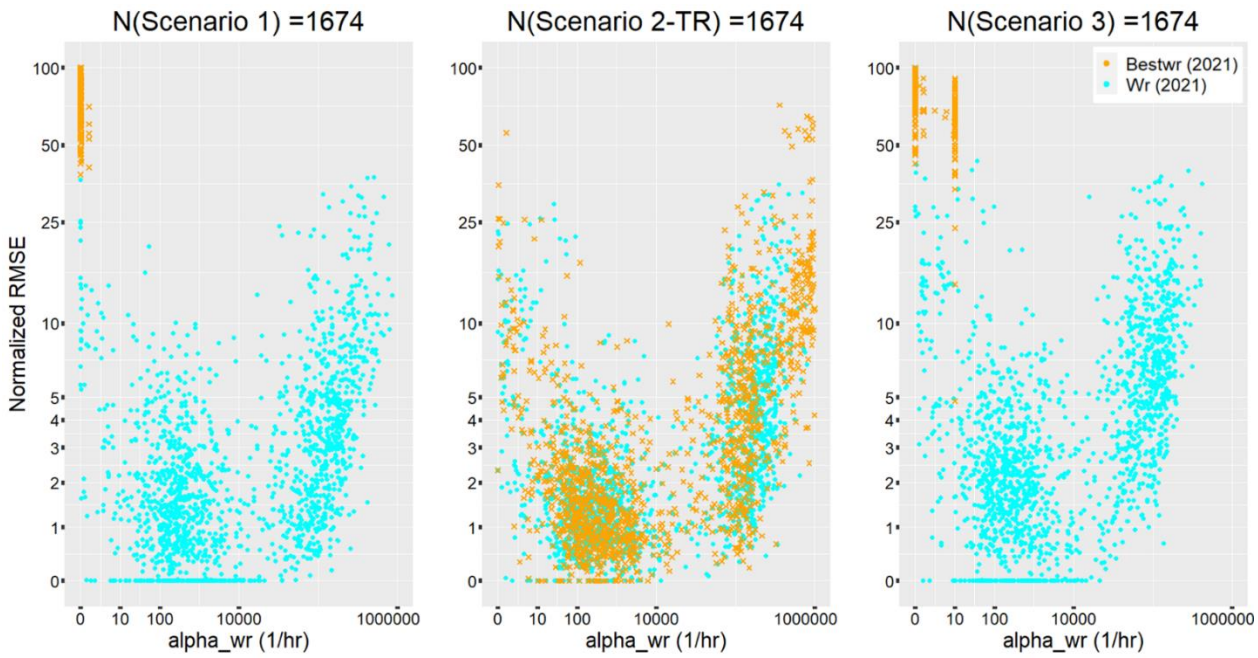

Figure 4.10: Normalized mean squared error (NRMSE) error as function of α_{wr} (cm^{-1}) parameter estimated by (1D) and (3D) infiltration models of water-repellent soils, including WR (2021) and BESTWR (2021) respectively, across N=1674 infiltration plots.

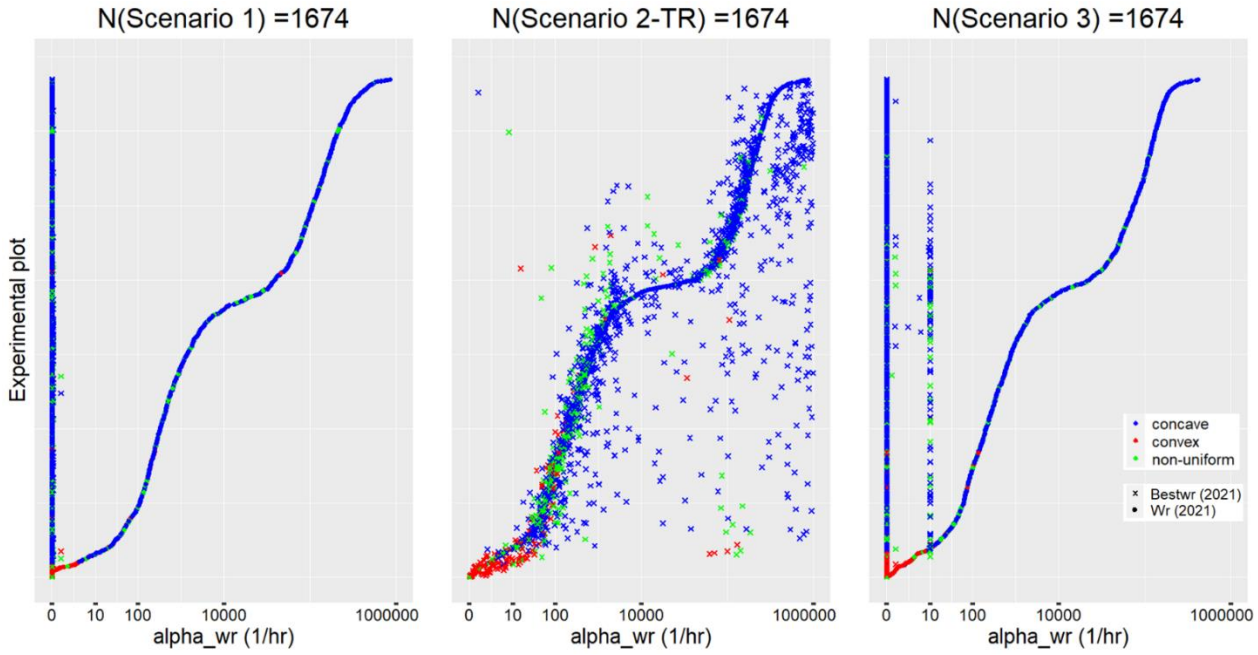

Figure 4.11: Distribution of α_{wr} (cm^{-1}) parameter estimated by (1D) and (3D) infiltration models of water-repellent soils, including WR (2021) and BESTWR (2021) respectively, as function of the shape of cumulative curves (concave, convex, and non-uniform) across N=1674 infiltration plots

4.5. Conclusion

Compared to 1D models, 3D models offer greater accuracy in situations involving varied soil textures, layering, or significant radial where infiltration is not strictly vertical such as in heterogeneous soils. However, significant efforts have been dedicated to the development and evaluation of 1D infiltration models compared to 3D modeling due to the greater complexity, computational demands, and data requirements associated with 3D modeling efforts. To this end, we carried out a metadata analysis to shed light on the strengths and limitations of 3D models to depict the infiltration behaviors of both non-hydrophobic and water-repellent soils, while studying the variability and uniqueness associated with estimated saturated hydraulic conductivity and sorptivity in the context of four different 3D infiltration models and three different extraction techniques illustrated by three scenarios. Scenario 1 optimized simultaneously for the two parameters, K_s and S, using each model's equation. Scenario 2 unified K_s across all models, as the steady-state slope of the cumulative infiltration curve at end times, and further optimized for S using each model's equation. Scenario 3 represented a dual optimization which optimized for K_s and S using each models' equation while minimizing the infiltration error and the difference between K_s and the steady-state slope of the cumulative infiltration curve. Our detailed analysis of 3D models and the different scenarios with their impact on infiltration characteristics, K_s and S, provided valuable insights into the trade-offs and considerations involved in 3D model's selection and extraction techniques for soil-water parameter estimation.

In summary, our analysis revealed both expected similarities and notable variabilities in the infiltration characteristic estimates across different 3D models and extraction techniques. The observed similarities and variabilities highlight the importance of understanding the specific contexts and conditions under which 3D different models are applied. For instance, Haverkamp et

al. (1994) and BEST models have provided similar estimates under varying extraction techniques, underscoring their shared foundations. However, the variability within each model's transient and steady-state expressions for K_s highlights the need for careful model selection based on specific infiltration conditions. Sorptivity S proved to be more consistent across these variations, providing a reliable measure of initial infiltration behavior. Compared to transient-state expressions, steady-state expressions of Haverkamp et al. (1994) and BEST revealed greater consistency and thus more reliable estimates of K_s, recommending their application in the context of K_s estimation.

Furthermore, Scenario 2 (i.e., where K_s is related constrained by steady-state conditions and related to sorptivity and geometry) has been shown to provide reliable estimates of K_s and S across different 3D models and is therefore recommended as an extraction technique. By relating K_s and S together, the problem is transformed from a system with two unknowns (K_s and S) to one unknow (S) for non-hydrophobic soils, and from a system with three unknowns (K_s, S, and α_{wr}) to two unknowns (S and α_{wr}) for water-repellent soils, reducing numerical complexity. In addition, the close alignment in K_s predictions between 3D models describing homogeneous soils, including ST-Haverkamp et al. (1994), ST-BEST, and Stewart and Abou Najm (2018), under Scenario 2-ST suggests a high level of consistency in defining K_s as function of the steady-state slope b, soil's sorptive capacity (either sorptivity S or capillary length λ), and geometric considerations across these three models. Scenario 2-ST has further demonstrated a remarkable capability in depicting the inability of models including Haverkamp et al. (1994) and BEST to produce valid estimates under conditions of water-repellency, enforcing researchers to apply alternative models, such as the BESTWR model under such conditions, which can handle water-repellency. Concluding with BESTWR, this model also shows more realistic predictions under Scenario 2, proving to be suitable for soil water parameter estimation in hydrophobic soils.

4.6. References

Basset, Christelle; Abou Najm, Majdi; Angulo-Jaramillo, Rafael; Bagarello, Vincenzo; Ghanbarian, Behzad; Di Prima, Simone; Iovino, Massimo; Lassabatere, Laurent; Stewart, R. (2023). Conceptual and empirical approaches to characterize infiltration: A literature review (under review). *Vadose Zone Journal*.

Bayabil, H. K., Dile, Y. T., Tebebu, T. Y., Engda, T. A., & Steenhuis, T. S. (2019). Evaluating infiltration models and pedotransfer functions: Implications for hydrologic modeling. *Geoderma*. https://doi.org/10.1016/j.geoderma.2018.11.028

Di Prima, S., Castellini, M., Abou Najm, M. R., Stewart, R. D., Angulo-Jaramillo, R., Winiarski, T., & Lassabatere, L. (2019). Experimental assessment of a new comprehensive model for single ring infiltration data. *Journal of Hydrology*, *573*, 937–951.

Di Prima, S., Stewart, R. D., Abou Najm, M. R., Ribeiro Roder, L., Giadrossich, F., Campus, S., Angulo-Jaramillo, R., Yilmaz, D., Roggero, P. P., Pirastru, M., & Lassabatere, L. (2021). BEST-WR: An adapted algorithm for the hydraulic characterization of hydrophilic and water-repellent soils. *Journal of Hydrology*. https://doi.org/10.1016/j.jhydrol.2021.126936

Elrick, D. E., Reynolds, W. D., & Tan, K. A. (1988). A new analysis for the constant head well permeameter technique. *Proceedings of the Conference on Validation of Flow and Transport Models for the Unsaturated Zone, New Mexico*, *23*, 26.

Fodor, N., Sándor, R., Orfanus, T., Lichner, L., & Rajkai, K. (2011). Evaluation method dependency of measured saturated hydraulic conductivity. *Geoderma*. https://doi.org/10.1016/j.geoderma.2011.07.004

Jačka, L., Pavlásek, J., Pech, P., & Kuráž, V. (2016). Assessment of evaluation methods using infiltration data measured in heterogeneous mountain soils. *Geoderma*. https://doi.org/10.1016/j.geoderma.2016.04.023

Lassabatere, L., Angulo-Jaramillo, R., Soria-Ugalde, J. M., Šimůnek, J., & Haverkamp, R. (2009). Numerical evaluation of a set of analytical infiltration equations. *Water Resources Research*. https://doi.org/10.1029/2009WR007941

Minasny, B., & McBratney, A. B. (2007). Estimating the water retention shape parameter from sand and clay content. *Soil Science Society of America Journal*, *71*(4), 1105–1110.

Mirzaee, S., Zolfaghari, A. A., Gorji, M., Dyck, M., & Ghorbani Dashtaki, S. (2014). Evaluation of infiltration models with different numbers of fitting parameters in different soil texture classes. *Archives of Agronomy and Soil Science*, *60*(5), 681–693.

Mishra, S. K., Tyagi, J. V, & Singh, V. P. (2003). Comparison of infiltration models. *Hydrological Processes*, *17*(13), 2629–2652.

Nie, W., Ma, X., & Fei, L. (2017). Evaluation of Infiltration Models and Variability of Soil Infiltration Properties at Multiple Scales. *Irrigation and Drainage*. https://doi.org/10.1002/ird.2126

Philip, J. R. (1990). Inverse solution for one-dimensional infiltration, and the ratio A/K1. *Water*

Resources Research. https://doi.org/10.1029/WR026i009p02023

Rahmati, M., Latorre, B., Lassabatere, L., Angulo-Jaramillo, R., & Moret-Fernández, D. (2019). The relevance of Philip theory to Haverkamp quasi-exact implicit analytical formulation and its uses to predict soil hydraulic properties. *Journal of Hydrology*. https://doi.org/10.1016/j.jhydrol.2019.01.038

Rahmati, M., Weihermüller, L., Vanderborght, J., Pachepsky, Y. A., Mao, L., Sadeghi, S. H., Moosavi, N., Kheirfam, H., Montzka, C., Van Looy, K., Toth, B., Hazbavi, Z., Al Yamani, W., Albalasmeh, A. A., Alghzawi, M. Z., Angulo-Jaramillo, R., Antonino, A. C. D., Arampatzis, G., Armindo, R. A., … Vereecken, H. (2018). Development and analysis of the Soil Water Infiltration Global database. *Earth System Science Data*. https://doi.org/10.5194/essd-10-1237-2018

Reynolds, W. D., & Elrick, D. E. (1990). Ponded Infiltration From a Single Ring: I. Analysis of Steady Flow. *Soil Science Society of America Journal*. https://doi.org/10.2136/sssaj1990.03615995005400050006x

Shukla, M. K., Lal, R., & Unkefer, P. (2003). Experimental evaluation of infiltration models for different land use and soil management systems. *Soil Science*, *168*(3), 178–191. https://doi.org/10.1097/00010694-200303000-00004

Sihag, P., Tiwari, N. K., & Ranjan, S. (2017). Estimation and inter-comparison of infiltration models. *Water Science*, *31*(1), 34–43.

Smettem, K. R. J., Parlange, J. Y., Ross, P. J., & Haverkamp, R. (1994). Three-dimensional analysis of infiltration from the disc infiltrometer: 1. A capillary-based theory. *Water Resources Research*. https://doi.org/10.1029/94WR01787

Stewart, R. D., & Abou Najm, M. R. (2018). A Comprehensive Model for Single Ring Infiltration I: Initial Water Content and Soil Hydraulic Properties. *Soil Science Society of America Journal*. https://doi.org/10.2136/sssaj2017.09.0313

Vand, A. S., Sihag, P., Singh, B., & Zand, M. (2018). Comparative evaluation of infiltration models. *KSCE Journal of Civil Engineering*, *22*, 4173–4184.

White, I., & Sully, M. J. (1987). Macroscopic and microscopic capillary length and time scales from field infiltration. *Water Resources Research*. https://doi.org/10.1029/WR023i008p01514

Wu, L., & Pan, L. (1997). A Generalized Solution to Infiltration from Single-Ring Infiltrometers by Scaling. *Soil Science Society of America Journal*. https://doi.org/10.2136/sssaj1997.03615995006100050005x

Wu, L., Pan, L., Mitchell, J., & Sanden, B. (1999). Measuring Saturated Hydraulic Conductivity using a Generalized Solution for Single-Ring Infiltrometers. *Soil Science Society of America Journal*. https://doi.org/10.2136/sssaj1999.634788x

CHAPTER 5: How does soil structure affect water infiltration? A meta-data systematic review

5.1. Abstract

Soil structure is a key attribute of soil quality and health that significantly impacts water infiltration. Structure can be significantly altered by natural or anthropogenic drivers including soil management practices and can in turn impact soil infiltration. Those changes in soil structure are often complex to quantify and can lead to conflicting impacts on water infiltration into soils. Here, we present a narrative systematic review (SR) of the impacts of soil structure on water infiltration. Based on inclusion and exclusion criteria, as well as defined methods for literature search and data extraction, our systematic review led to a total of 153 papers divided into two sets: experimental (131) and theoretical (22) papers. That implied a significant number of in-situ and field experiments that were conducted to assess the impacts of soil structure on water infiltration under the influence of different land uses and soil practices. Analysis of the metadata extracted from the collected papers revealed significant impacts of soil structure on water infiltration. Those effects were further attributed to land use and management, where we demonstrate the impact of three unique categories: soil amendments, crop management and tillage. Furthermore, significant correlations were established between infiltration rate and soil structural properties, with R^2 values ranging from 0.51 to 0.80 and for saturated hydraulic conductivity and soil structural properties, with R^2 values ranging from 0.21 to 0.78. Finally, our review highlighted the significant absence of and the need for theoretical frameworks studying the impacts of soil structure on water infiltration.

5.2. Introduction

Soil structure refers to the hierarchical grouping and arrangement of soil particles (sand, silt, clay, organic and inorganic particles) into porous compounds forming aggregates which can vary in size and shape from small clusters through to large blocks (Dexter, 1988; Lal, 1991; Kay and Angers, 2001). Some soils build a large, solid, structureless mass (referred to as massive); and others consist of small, porous aggregates that tend to have a uniform rounded shape – referred to as granular, a desirable structure for the growth of crops (Coughlan et al., 1991; Levine et al., 1996). These aggregate arrangements develop a strong structural influence on the ability of soil to absorb and hold water during irrigation and rainfall events (Franzluebbers, 2002; Pagliai et al., 2004; Di Prima et al., 2021; Abou Najm et al., 2021).

Over the last 40 years, soil structure has received growing interest and broader audience as a dynamic soil factor affecting soil-water movement at multiple scales (Hamblin, 1986; Abou Najm et al., 2010; Sanders et al., 2012). Furthermore, expanded efforts in conservational practices, from no-till to cover crops to soil amendments and others, have led to significant impacts on soil structure. Those impacts, however, were the results of myriads of complex and interconnected factors, often resulting in conflicting soil responses. As a result, several studies have investigated the role of soil structure, with both its inherent and induced variations, on water infiltration (Lepore et al., 2009; Rahmati, 2017). However, no studies, to our knowledge, have compared previous findings in the structured approach of a "systematic review". A systematic review is a review that conducts a literature search to answer a clearly formulated question by applying predetermined inclusion and exclusion criteria used to identify and eventually analyze the collected data from the most relevant research.

Here, we aim to conduct a meta-analysis systematic review (SR) that investigates the impacts of soil structure on water infiltration. Therefore, the primary research question that best follows this approach is: *How does soil structure affect water infiltration?*

5.3. Methodology

Our systematic review follows the approach developed by the Center for Evidence-Based Conservation (CEBC) which answers a research question through a literature search followed by data extraction based on a defined set of 'inclusion criteria'. The research question for this systematic review (*how does soil structure affect water infiltration?)* was formulated according to the PECO (Population/Exposure/Comparator and Outcomes) model as described by the CEBC's protocol. Three different database sources (Scopus, ScienceDirect and googlescholar.com) were used in the review including peer reviewed journal articles and other scientific documents, but only peer reviewed journal articles published in English were considered. Table 5.1 shows the data sources and the keywords used in building the literature search.

Table 5.1: Literature search: publishing sources and keywords

Publishing sources	**Keywords**	**Number of Records** *(on May 8, 2020)*
Scopus	("soil structur*" OR "soil infiltra*" OR "soil aggregate*") AND (structur* OR aggregat*) AND infiltra*	1,524
ScienceDirect	("soil structure" OR "soil infiltration" OR "soil aggregation") AND (structure OR aggregation) AND infiltration	266
Google scholar	Same as in ScienceDirect	22[a]

*Wildcard characters (*and?) are not supported in ScienceDirect and Google Scholar.*

[a]Using Google scholar, we included 22 out of 17,400 results which are the most relevant and unique retrieved records.

Once collected, we exported all these references into Mendeley software which can also check for any duplication in references. The first filtering process was carried out in Mendeley based on the title of the database, followed by the second screening based on the reading of screened abstracts.

At the end, the remaining literature went through a full-text review after being selected and tabulated in MS Excel spreadsheets. As a result, the literature gathered consisted of 1,812 records, narrowed down to a total of 1,544 references after duplicates were removed. The title-screening lowered the number to 854 followed by the abstract-screening which led to a final of 462 references. Figure 5.1 provides a flow chart summarizing the screening process.

Among the 462 records that passed the title and abstract screening, 84% (387) of the literature assessed the direct or indirect impacts of soil structure on water infiltration upon studying the influence of different land uses on hydraulic and structural soil properties through in-situ and field experiments. Furthermore, 7% (32) of the retrieved literature consisted of theoretical papers relating water infiltration/flow to soil structure through previously or newly developed models; and the remaining 9% (43) were review papers. Then, the screened papers were subjected to full text reading and exclusion criteria. The exclusion criteria covered papers that did not have a clear treatment/control system, did not report infiltration or soil texture data, and did not show a clear concise description of models relating infiltration/flow to soil structure. Finally, a total of 153 papers passed the exclusion criteria and were analyzed. Those papers were divided into two sets, experimental (131) and theoretical (22). Two comprehensive summary tables were built, one for each set, including the title, the author, and the publication year of each paper in MS Excel spreadsheets.

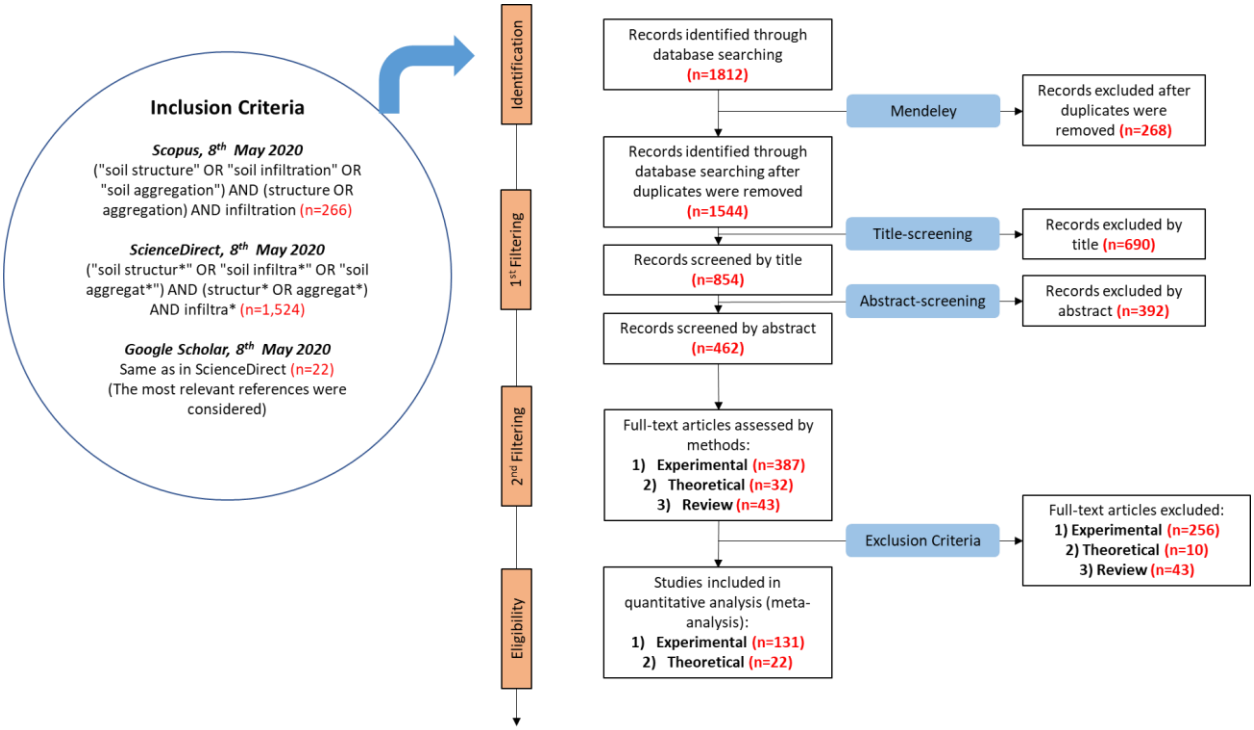

Figure 5.1: Flowchart of describing the steps of the literature search, the inclusion and exclusion criteria and the quality assessment

5.4. Results and Discussion

Here, we present a summary of the lessons learned and different compilations and integrations of data gathered from the 153 selected papers (131 experimental and 22 theoretical). We first observed that the results were dominated by field-scale experimental studies comparing field responses under different soil practices or treatments with the purpose of studying changes in water infiltration and soil structure. We also noted a significant absence of theoretical efforts to describe soil structural attributes as impacted by different land uses, and we will get back to this point towards the end of this study.

To start, we plotted the historical distribution of the gathered research as identified by our inclusion criteria (Figure 5.1), which goes back to 1953 (Figure 5.2). However, while reviewing the research's evolution over the years, we found that almost no literature on structure was published between 1953 and 1980 (or the significance of structure was not highlighted at the Title or Abstract levels). Most modeling effort in that period seemed clustered around modeling soil as a homogeneous medium (no structure), possibly because the technology and computational capabilities back then limited the ability to visualize or characterize soil structural features. After 1980, the frequency of research increased gradually, especially during the last decade, which can be attributed to improvements in visualization and computational technologies, as well as experimental capabilities across the years. Simultaneously, attention to soil structure and its impact on important soil ecohydrological functions as well as on physical and biogeochemical interactions related to water distribution in soils gained a lot of momentum, particularly with increased interest in phenomena like preferential flow (Beven and Germann, 1982; Abou Najm et al., 2010) and the biogeochemical cycling of carbon, nitrogen, and phosphorous among other elements.

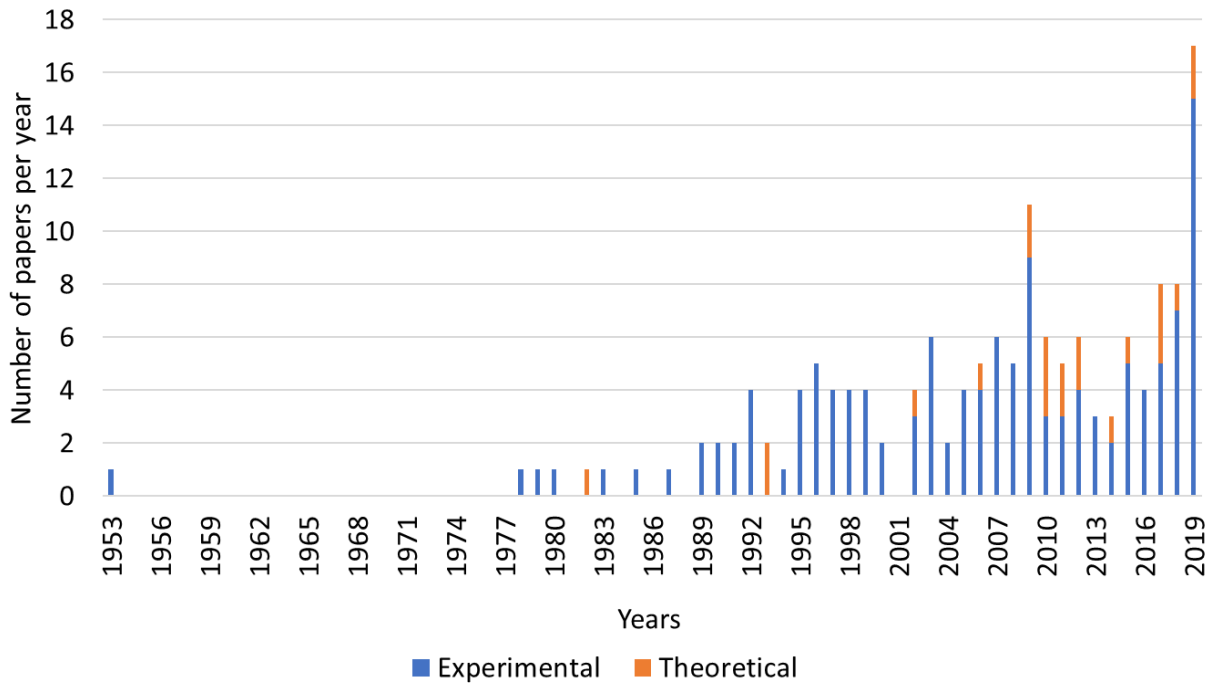

Figure 5.2: Historical distribution of the screened literature

Hereafter, we will assess the experimental efforts that demonstrated evidence of the impact of soil structure on infiltration. Those efforts also led to the realization and need for the development of theoretical frameworks assessing the role of soil structure on infiltration modeling. The assessment first included the 131 experimental papers (Figure 5.1) and then was followed by a summary and synthesis of all the other 22 modeling and theoretical papers that focused on incorporating structure into infiltration modeling.

5.4.1. General Characteristics of the Experimental Set

Detailed analysis of the 131 experimental papers led to the extraction of 800 unique plot datasets (N=800). A unique plot was extracted from a paper only when infiltration data was available on a treatment (typically soil management) and a control. Each plot includes the results of soil physical

and structural characterization as well as results from infiltration experiments (location, period, and type of experiment).

First, we reported data descriptive of the location and the study period of the run experiments. The review included case studies from 15 major countries (Figure 5.3) where most of the studies were conducted in USA (22%), China (15%), Australia (8%), and Israel (7%).

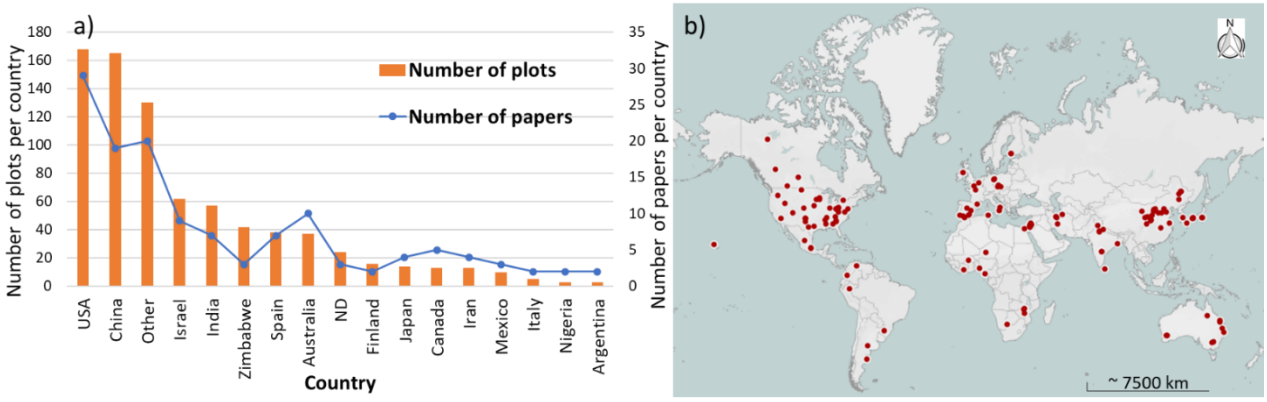

Figure 5.3: a) Combined Bar and line graph illustrating the geographical distribution of the screened literature by the number of plots and papers per country, respectively (ND=Not Determined), b) Geographical map illustrating the exact geographic location of all sampling plots based on latitude and longitude coordinates extracted from the literature

According to the review, most experimental studies (35%) on soil structure were performed over a period of less than 5 years (Figure 5.4). This is probably related to the fact that typical research projects have a duration of less than 5 years. This is a major limitation to the advancement of our understanding of soil structure as changes take much longer time to develop.

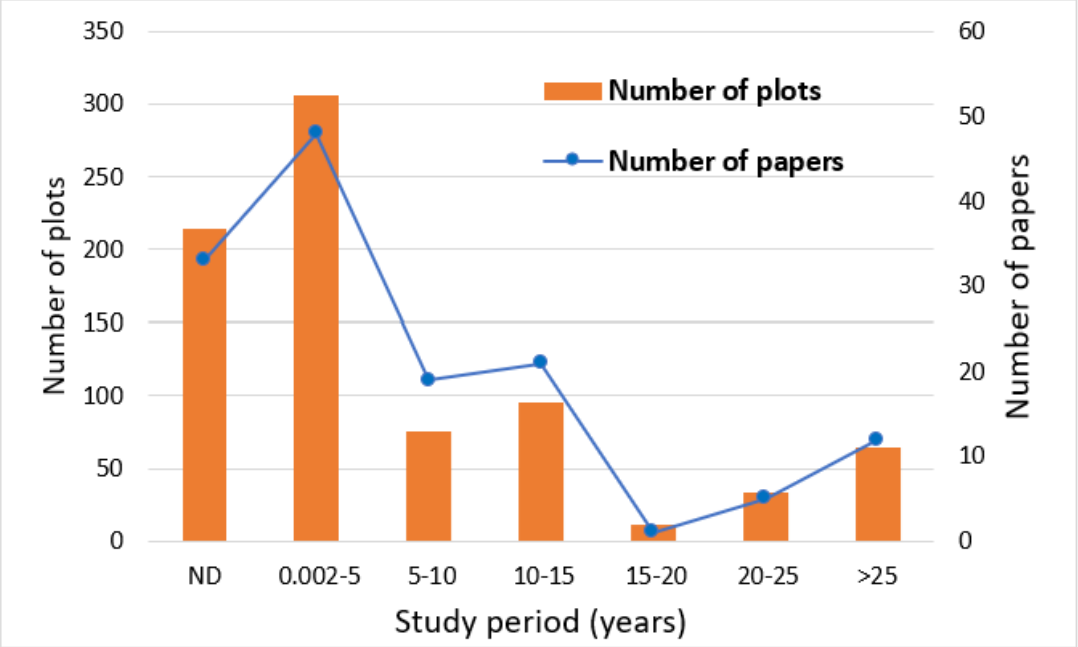

Figure 5.4: Distribution of the final screened literature based on the study period (ND=Not Determined)

Then, we conducted a detailed analysis of data indicative of soil textural, structural, and physical attributes under different types of soil management. The 800 plots covered the full range of soil texture, as identified by the USDA soil texture triangle (Figure 5.5), from coarse to fine particles.

About 30% (highlighted in red in Figure 5.5) of those soils were described only by their soil texture class without reporting their particle size distribution (i.e., %sand, silt, and clay).

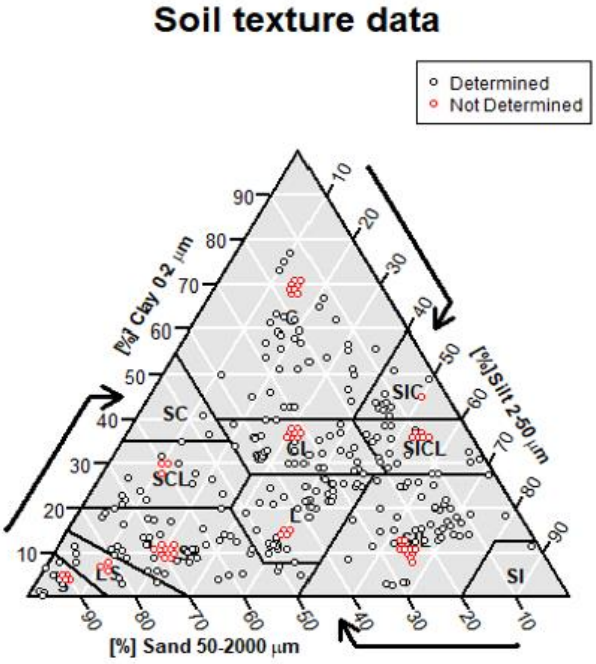

Figure 5.5: Distribution of soil particle sizes in the final screened literature (N=800). Points in black are based on exact reported values (% of sand, silt, and clay) while points in red are arbitrarily located around the center of a textural class, in the absence of detailed texture data.

The soil structure, on the other hand, was characterized by the following soil properties: bulk density, penetration resistance, porosity (total, capillary, and non-capillary), % of macro-, meso-, and micropores, aggregate mean weight diameter (MWD), geometric mean diameter (GMD), dry-aggregation degree (DAD), % of water stable aggregates (WSA) (>0.25mm), stability and instability index, macro-aggregation index, % of dry aggregates (>2mm, 1-2mm and <1 mm), % of soil organic matter (SOM), and carbon (SOC). It was also characterized by the following

physical properties relating to water infiltration: infiltration rate (initial, mean, final/steady), saturated and unsaturated hydraulic conductivity, sorptivity, infiltration depth and time to ponding. Although all studies reported the change in structural and physical soil properties under the effects of different land uses, data attributes reported in each paper were different. This resulted in a heterogeneous database with larger datasets for certain attributes compared to others, as summarized in Figure 5.6.

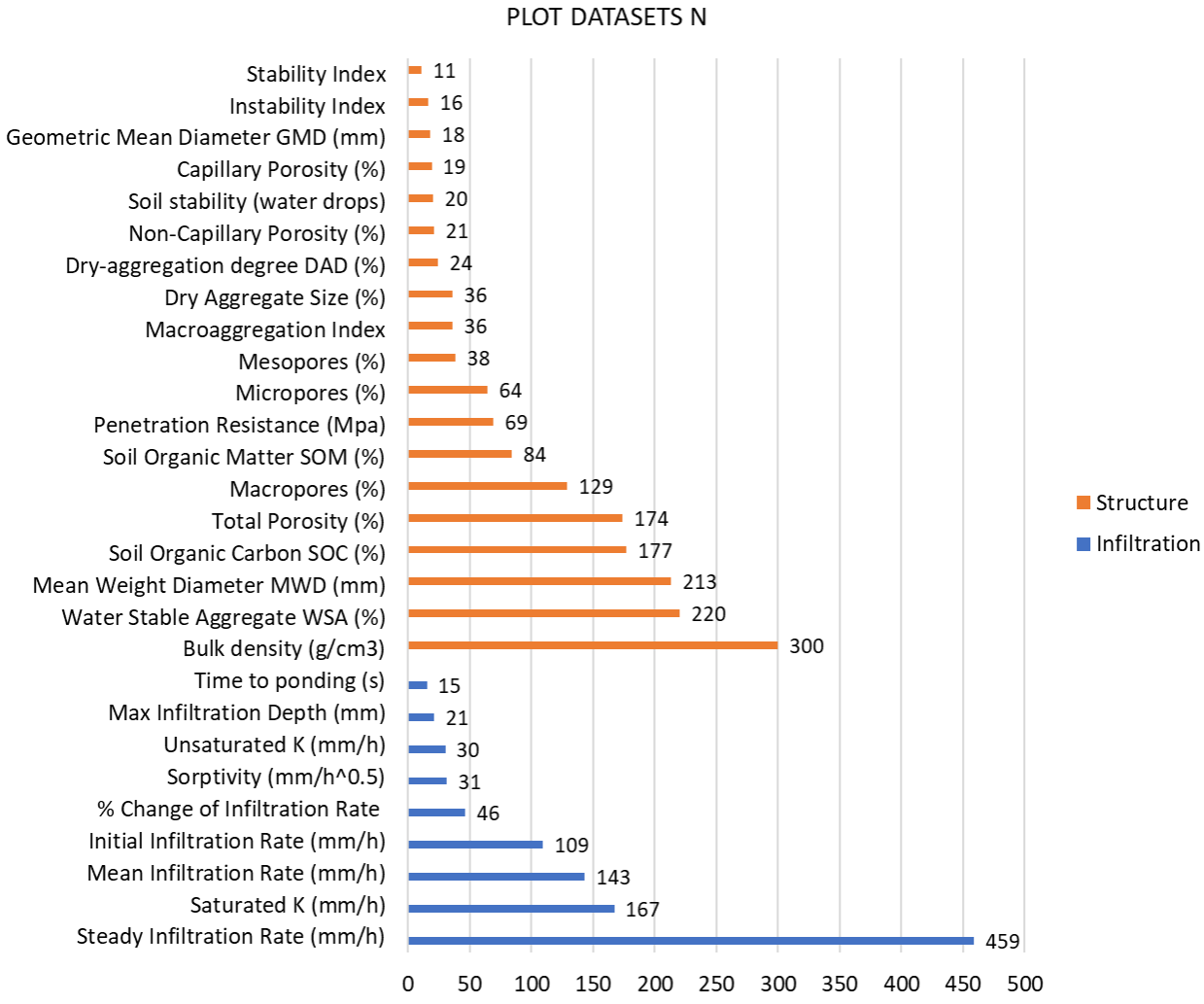

Figure 5.6: Number of plot datasets (N) with reported measured soil structure and infiltration attributes, derived from the full dataset N=800.

Therefore, we based our analysis on the following soil attributes showing the highest number of descriptive plots (Figure 5.6): infiltration rate (initial, mean, and steady) (mm/h), bulk density (g/cm^3), mean weight diameter MWD (mm), water stable aggregates WSA (%), soil organic carbon SOC (%), and total porosity (%). Hereafter, we assumed that soil organic matter is made up of 60% organic carbon, i.e., SOC = 0.6*SOM. The first detailed assessment of these selected soil attributes explored the effects of different soil practices on soil structure and water infiltration. Figure 5.7 shows the range of different soil practices assessed in literature that alter soil structure and infiltration. Across the full dataset (N=800), a total of 226 plots (28%) investigated the induced changes in soil structure and water infiltration under soil amendments treatment (including compost, manure, and conditioners), followed by 191 (24%) and 87 (11%) plots studying tillage and crop management (including cultivation, vegetation, and cover crops), respectively.

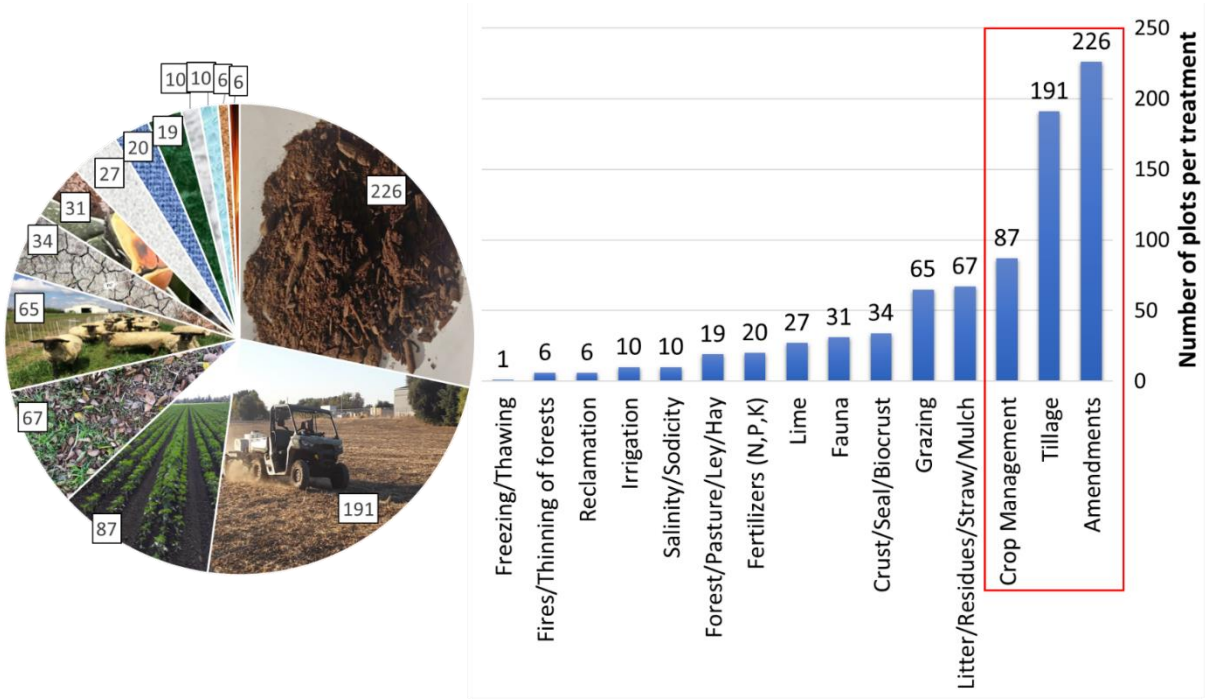

Figure 5.7: Distribution of soil management practices generated from the gathered literature (N=800)

5.4.2. Effects of soil management practices on soil structure and water infiltration

The following is a summary of the effects of these different soil management practices (treatments) on soil structure and water infiltration. Based on the reported data, we analyzed those effects using Treatment vs. Control plot comparisons and effect size analysis to understand the potential effects of soil management practices on soil structure and water infiltration.

5.4.2.1.Treatment vs. Control (T vs. C) plots

We plotted Treatment vs. Control (T vs. C) on scatter graphs to illustrate the implication of soil amendments (Figure 5.8), tillage (Figure 5.9) and crop management (Figure 5.10) on six soil attributes: infiltration rate, bulk density, porosity, MWD, WSA, and SOC. Infiltration was reported either as initial infiltration rate, mean, or steady state while porosity was reported as either total, macro, or micro. Points above the 1:1 line indicate an increasing effect induced by the represented treatment while points below the line represent a decreasing effect on the attribute between the treatment and the control. Points on the 1:1 line indicate that the treatment has no significant effect on that attribute, meaning that the control and the treatment revealed the same value for that specific attribute. Each graph (Figures 5.8, 5.9, and 5.10) is coupled with the USDA soil texture triangle that illustrates the particle size distribution of the corresponding soils. Note that the infiltration rate had to be log-transformed in all datasets for a better data visualization.

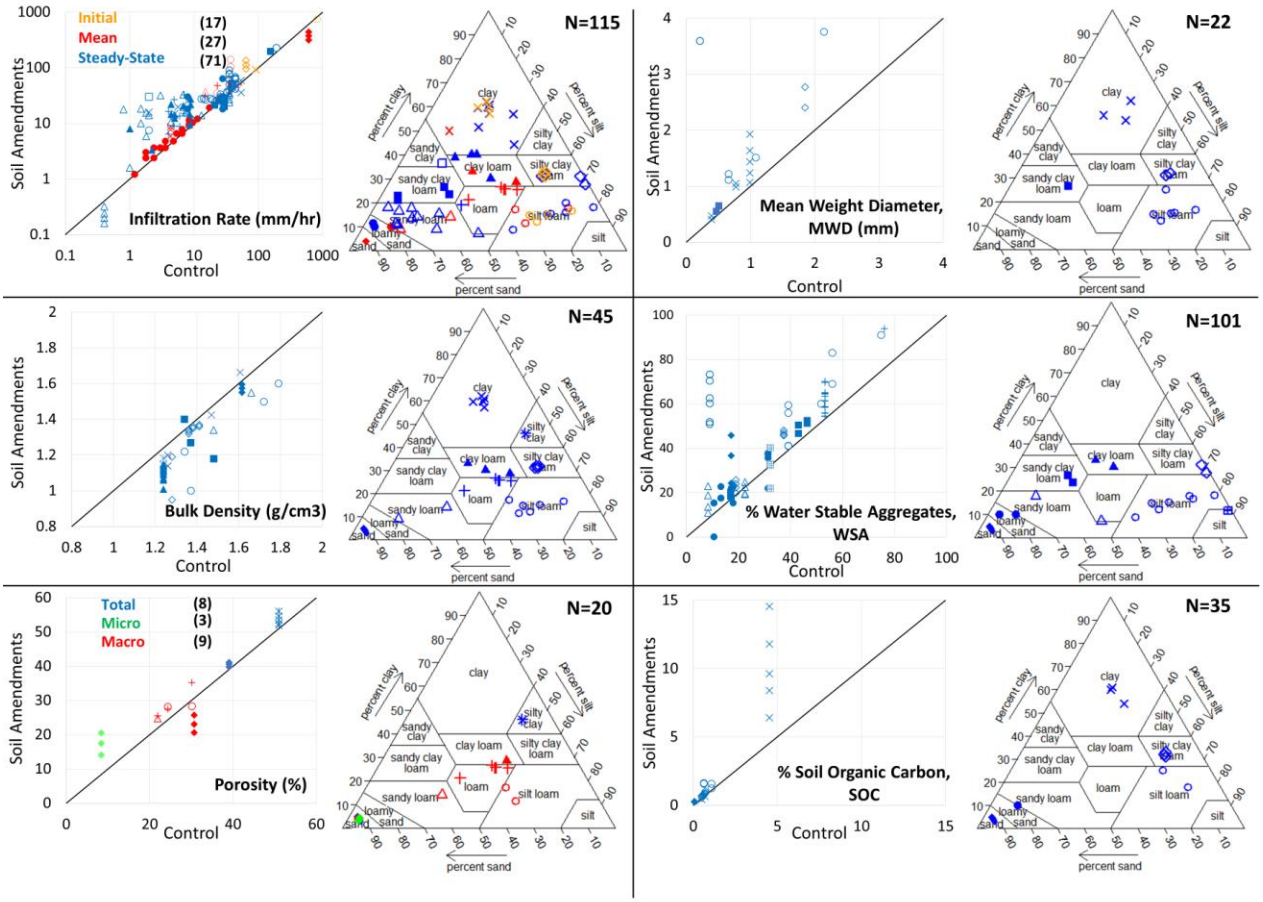

Figure 5.8: Effect of soil amendments (N=226 out of 800) on soil structure using Treatment vs. Control scatter graph, coupled with a 1:1 line. Six soil attributes (infiltration rate, bulk density, porosity, MWD, WSA, and SOC) are plotted comparing soil amendments impact compared to the control values. N is the number of plot datasets for each of the six attributes, derived from the sub database N=226 with soil amendments.

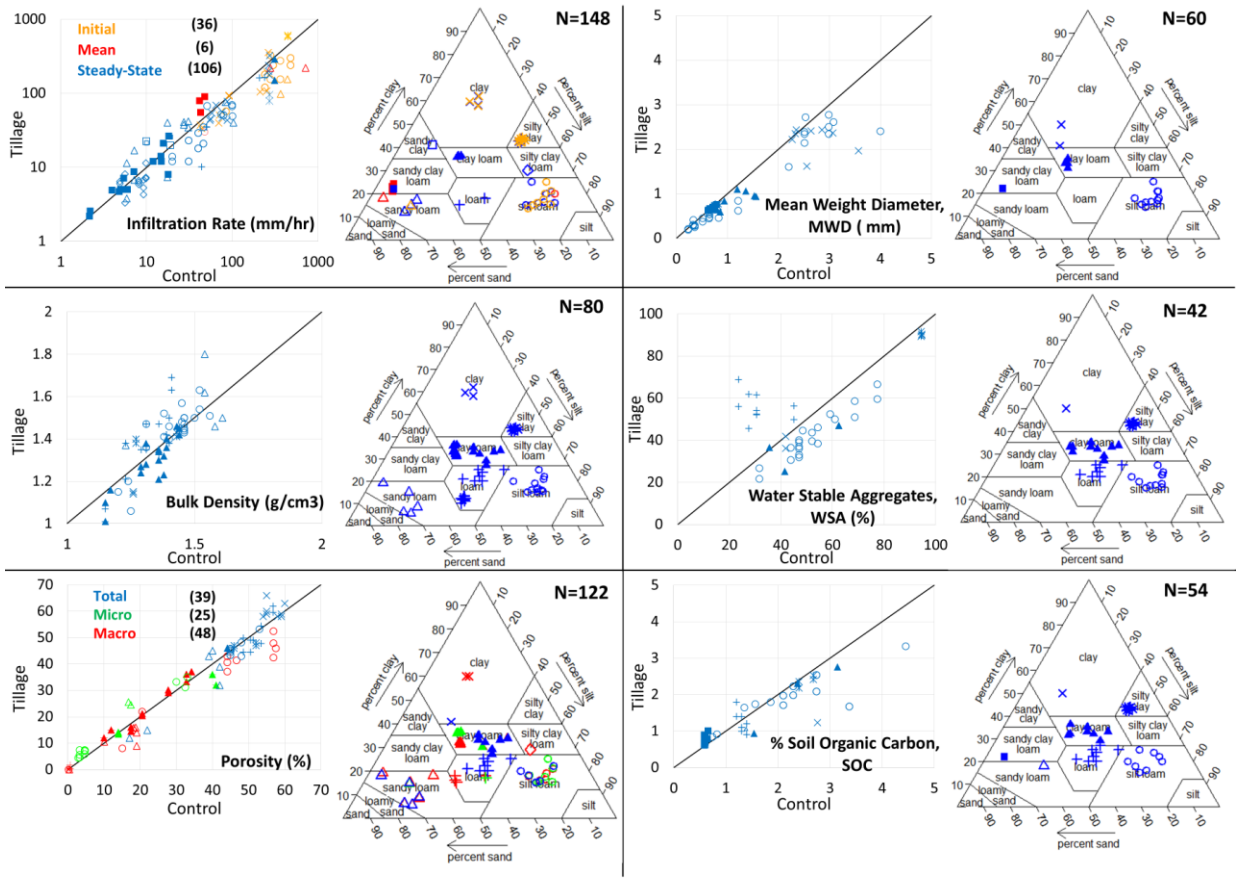

Figure 5.9: Effect of tillage (N=191 out of 800) on soil structure using Treatment vs. Control scatter graph, coupled with a 1:1 line. Six soil attributes (infiltration rate, bulk density, porosity, MWD, WSA, and SOC) are plotted comparing soil tillage impact compared to the control values. N is the number of plot datasets for each of the six attributes, derived from the sub database N=191 with tillage.

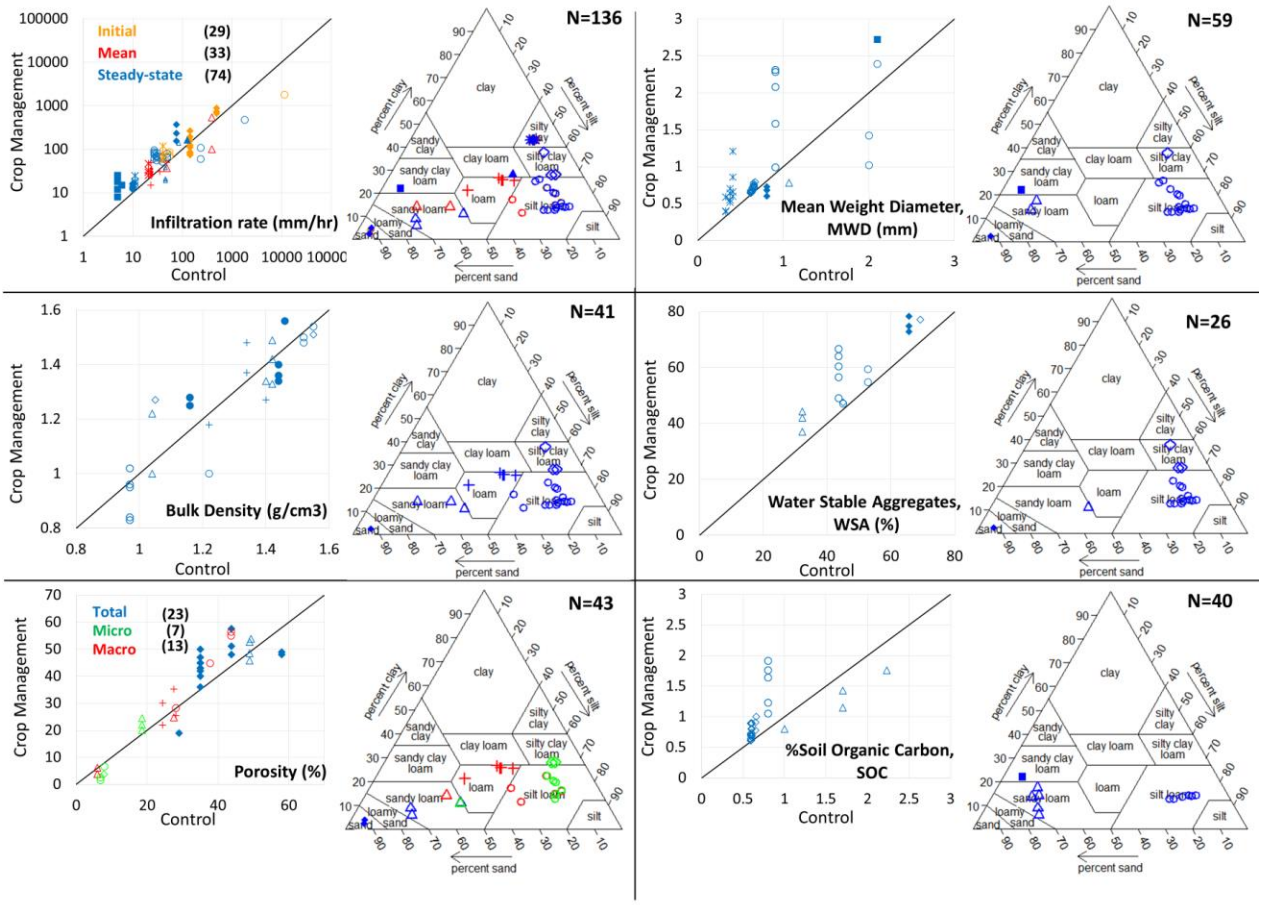

Figure 5.10: Effect of crop management (N=87 out of 800) on soil structure using Treatment vs. Control scatter graph, coupled with a 1:1 line. Six soil attributes (infiltration rate, bulk density, porosity, MWD, WSA, and SOC) are plotted comparing crop management impact compared to the control values. N is the number of plot datasets for each of the six attributes, derived from the sub database N=87 with crop management.

5.4.2.2.Effect Size Analysis

An alternate approach of analyzing the treatments' effects on soil structure and water infiltration was the determination of an effect size - a quantitative measure of the magnitude of the treatment effect. The effect size, ES, is calculated as the following response ratio:

$$ES = \frac{X_{treatment}}{X_{control}}$$

Where X represents the value of the structural and physical soil attributes.

Three distinct scenarios emerge based on the obtained ES value:

1. $ES > 1$ indicates an increase, or a positive response to treatment.
2. $ES < 1$ indicates a decrease, or a negative response to treatment.
3. $ES = 1$ indicates no response to treatment.

Note that a positive response reflects only an increase in value in treatment compared to control, and this does not necessarily mean an improvement to soil or infiltration conditions (Ex.: increase in bulk density is a sign of compaction). The effect sizes associated with each of the top three treatment categories (soil amendments, tillage, and crop management) in particular, and all treatments in general, for the selected soil attributes (infiltration rate, bulk density, porosity, MWD, WSA, and SOC) were presented in tabular form (Table 5.2), as well as graphically displayed using boxplots (Figure 5.11).

Table 5.2: Statistical summary of the effect sizes (Treatment: Control) associated with each treatment for each of the selected soil attributes in the data set

Soil Attributes	Mean	Standard Deviation	Sample Size	Mean	Standard Deviation	Sample Size	Mean	Standard Deviation	Sample Size	Mean	Standard Deviation	Sample Size
Infiltration Rate												
Initial	1.410	0.458	17	0.782	0.302	36	1.496	0.688	29	1.207	0.576	109
Mean	1.224	0.265	27	1.125	0.662	6	1.413	0.486	33	1.644	2.755	143
Steady-State	2.104	3.417	71	0.864	0.281	106	2.085	1.044	74	1.716	1.957	459
Porosity												
Total	1.048	0.028	8	0.983	0.081	39	1.163	0.213	23	1.035	0.168	174
Micro	2.078	0.385	3	1.207	0.359	25	0.782	0.432	7	1.121	0.374	64
Macro	0.995	0.198	9	0.966	0.845	48	1.047	0.235	13	1.008	0.597	129
Bulk Density	0.911	0.068	45	1.016	0.091	80	0.966	0.100	41	0.982	0.09	300
MWD	3.549	5.534	22	0.852	0.142	60	1.388	0.513	59	1.232	0.607	213
WSA	2.263	2.194	101	1.068	0.558	42	1.269	0.166	26	1.664	1.612	220
SOC	1.705	0.915	35	0.972	0.286	54	1.436	0.228	40	1.498	2.016	258

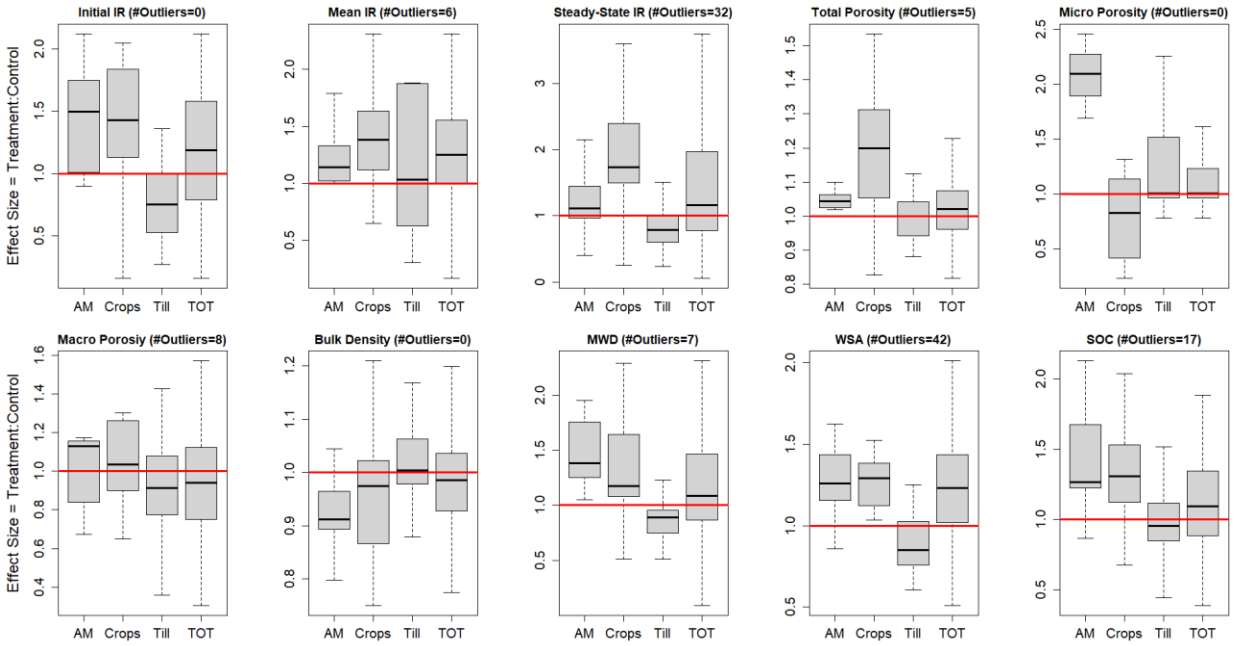

Figure 5.11: Boxplots of the effect sizes associated with each treatment (AM = soil amendments, Crops = crop Management, Till = tillage, TOT = Total Treatments) for each of the selected soil attributes in the data set. The margin line, highlighted in red, corresponds to an effect size of 1 (i.e., no response to treatment). If the variable median lies above the red line, the variable attribute indicates a positive response to treatment and vice versa. Extreme outliers that distort the scale of a boxplot were excluded, with their numbers indicated atop the appropriate boxplot.

In addition, we generated 95% confidence intervals for the effect sizes ES of the soil attributes within each treatment and we then plotted the resulting confidence intervals and effect sizes in forest plots in Figure 5.12 representing a) soil amendments, b) crop management, and c) tillage. These forest plots show a horizontal line representing the 95% confidence intervals of the attribute's result, with each end of the line representing the boundaries of the 95% confidence interval, and a vertical line known as the "line of null effect". This line is placed at ES=1, with the right side favoring the treatment (ES>1) while the left side favoring the control (ES<1). It is particularly important to check whether the horizontal line crosses the "line of null effect" or not. If the horizontal line does not cross the line of null effect, the null value (ES=1) does not lie within

the 95% confidence interval, and therefore, the studied treatment illustrates a statistically significant effect on the assessed treatment at the 5% significance level (irrespective to which side the data is). In other words, there is only a 5% risk of concluding that **a statistically significant difference exists between the treatment and its control when there is no actual difference.**

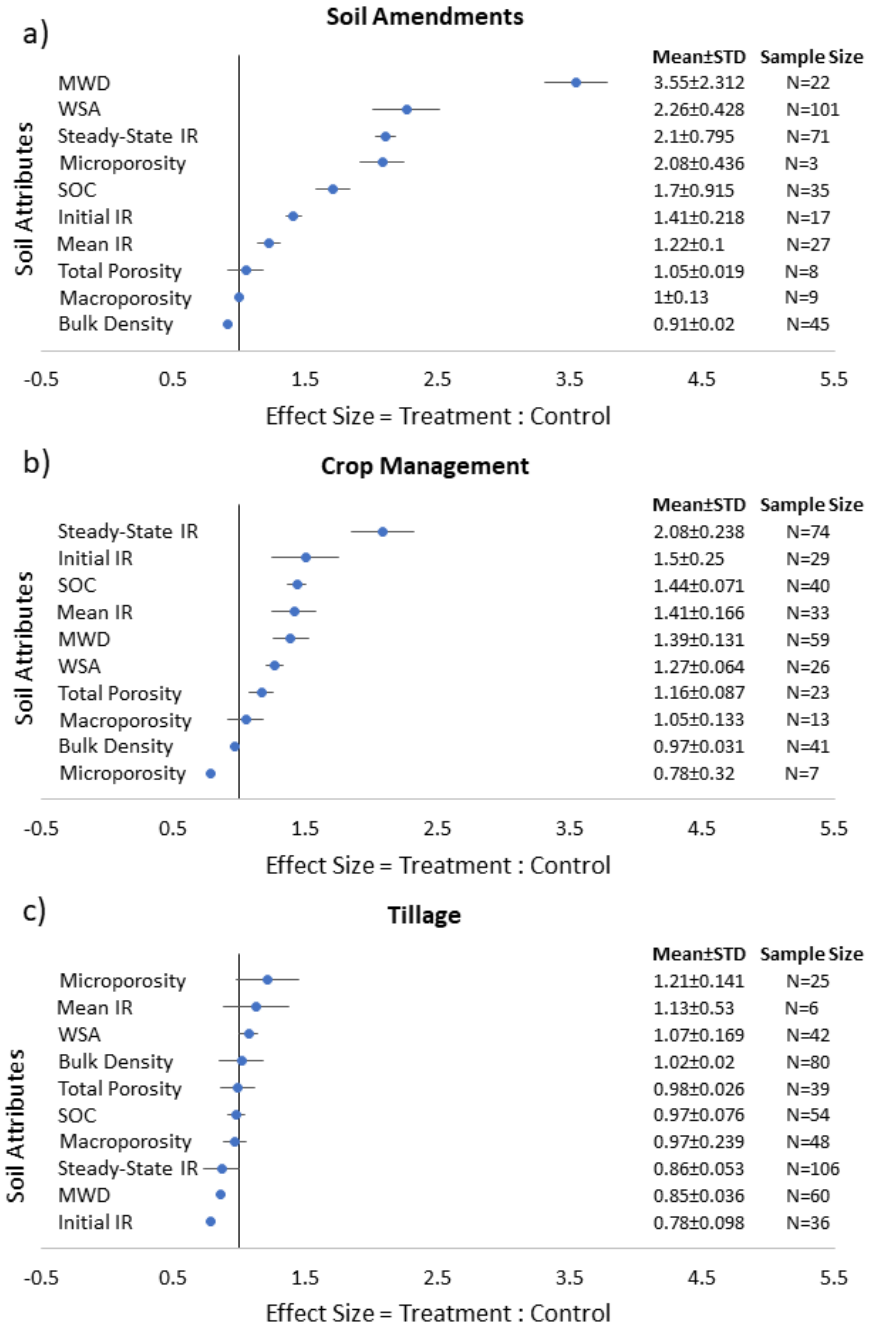

Figure 5.12: Forest plot showing the effect of a) soil amendments, b) crop management, and c) tillage on the selected soil attributes. The horizontal lines represent the 95% confidence intervals for each attribute, and the vertical line represents the "line of null effect" (ES=1). The right side of the null effect line (ES>1) favors the treatment while the left side (ES<1) favors the control. N is the number of plot datasets derived from the sub database N=226, 191, and 87 out of 800, respectively for a), b), and c).

5.4.3. Interpretation of the effects of Soil Treatments on structure and Infiltration

Figures 5.12 (a and b) show the positive effect of both soil amendments and crop management on soil structure and water infiltration, with statistical significance at 5% significance levels for approximately all included soil attributes. This is also demonstrated in Figures 5.8 and 5.10 for all different types of soils, as indicated by points above the 1:1 line comparing soil amendments and crop management to their control, respectively.

As for tillage, a statistically significant decline in mean weight diameter (MWD) as well as initial and steady-state infiltration rate (IR) was observed across tilled soils (Figure 5.12c). This effect is demonstrated also in Figure 5.9 where most of the data points representing these attributes lie below the 1:1 line indicating a decreasing effect induced by tillage, particularly in finer soils. That decline partly reflects the effect of using heavy farm machinery and artificial disturbance which leads to a poorer soil structure as compared to no-till practices (Nyamadzawo et al., 2007, Kahlon et al., 2013, Chen et al., 2016, Nouri et al., 2019, Melman et al., 2019). Figure 5.12c shows six soil attributes crossing the ES=1 line (demonstrated also by more scatter in Figure 5.9 corresponding to those attributes as compared to MWD for example), indicating no particular response to tillage, suggesting that some attributes may be more sensitive to soil particle size differences than others (Figure 5.9). Referring to Figure 5.12c, these attributes have effect sizes with 95% confidence intervals overlapping around the value of 1. That means no statistical significance can be reported with respect to their response to tillage at the 5% significance level. Clearly, the analysis conducted above (i.e., Table 5.2 and Figures 5.8 to 5.12) highlighted significant variations in the physical and structural soil attributes under the studied treatments. To this end, we plotted Figure 5.13 to summarize the treatments' effects on soil structure and water infiltration.

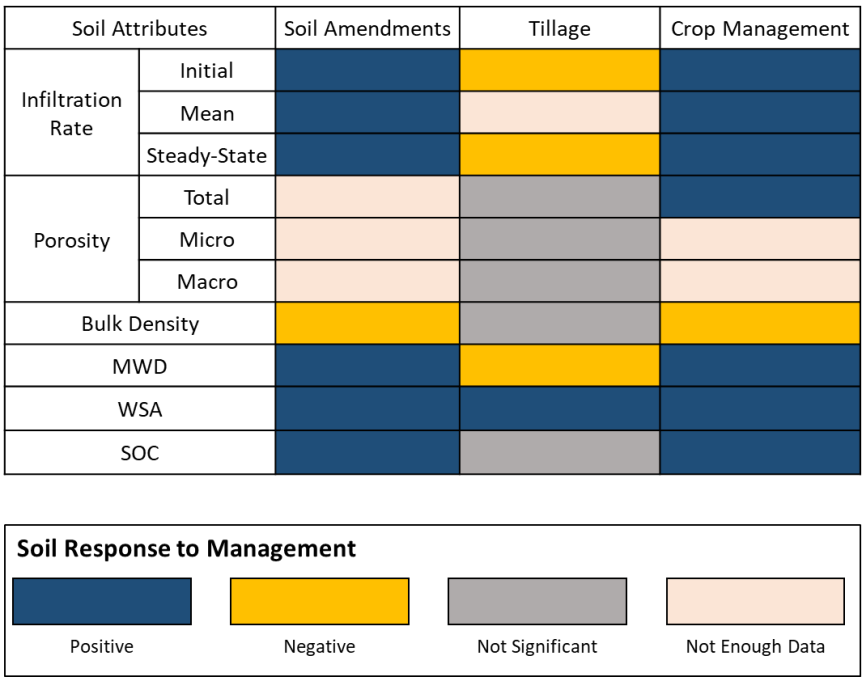

Figure 5.13: Summary of treatments' effects on soil structure and water infiltration at the 5% significance level

As shown in Figure 5.13, this systematic review gathers enough meaningful data indicating statistically significant effects of both, soil amendments and crop management on water infiltration and soil structure, resulting in increased infiltration rate, mean weight diameter (MWD), water stable aggregates (WSA), soil organic carbon (SOC), and reduced soil bulk density. However, there was not enough data to support that there is a significant response of porosity to soil amendments and crop management. Furthermore, this systematic review shows that tillage negatively impacts water infiltration (initial and steady state) and mean weight diameter, while it can increase the % of water stable aggregates. And, given that the effects of tillage on bulk density, soil porosity and soil organic carbon are not statistically significant, it is not so obvious to draw one comprehensive conclusion around the effects of tillage on soil structure.

5.4.4. Effect of Soil Structure on Infiltration Rate

To assess the change in water infiltration as function of soil structure, we explored the correlations between steady infiltration rate and soil structural attributes. To this end, we plotted the steady infiltration rate (mm/h) as a function of a) mean weight diameter (MWD, mm), b) water stable aggregates (WSA, %), c) total porosity (%), and d) SOC (%) in Figure 5.14 under different soil practices and their respective control. Also, we plotted in Figure 5.15 the steady infiltration rate as a function of soil bulk density – a structural property that exhibited a high number of points in our dataset. Each graph (Figures 5.14 and 5.15) is coupled with the USDA soil texture triangle that illustrates the particle size distribution of the corresponding soils. Note that steady infiltration rate, plotted on the y-axis, is log-transformed in all figures, and fitted to the best-fit curve for a better data visualization.

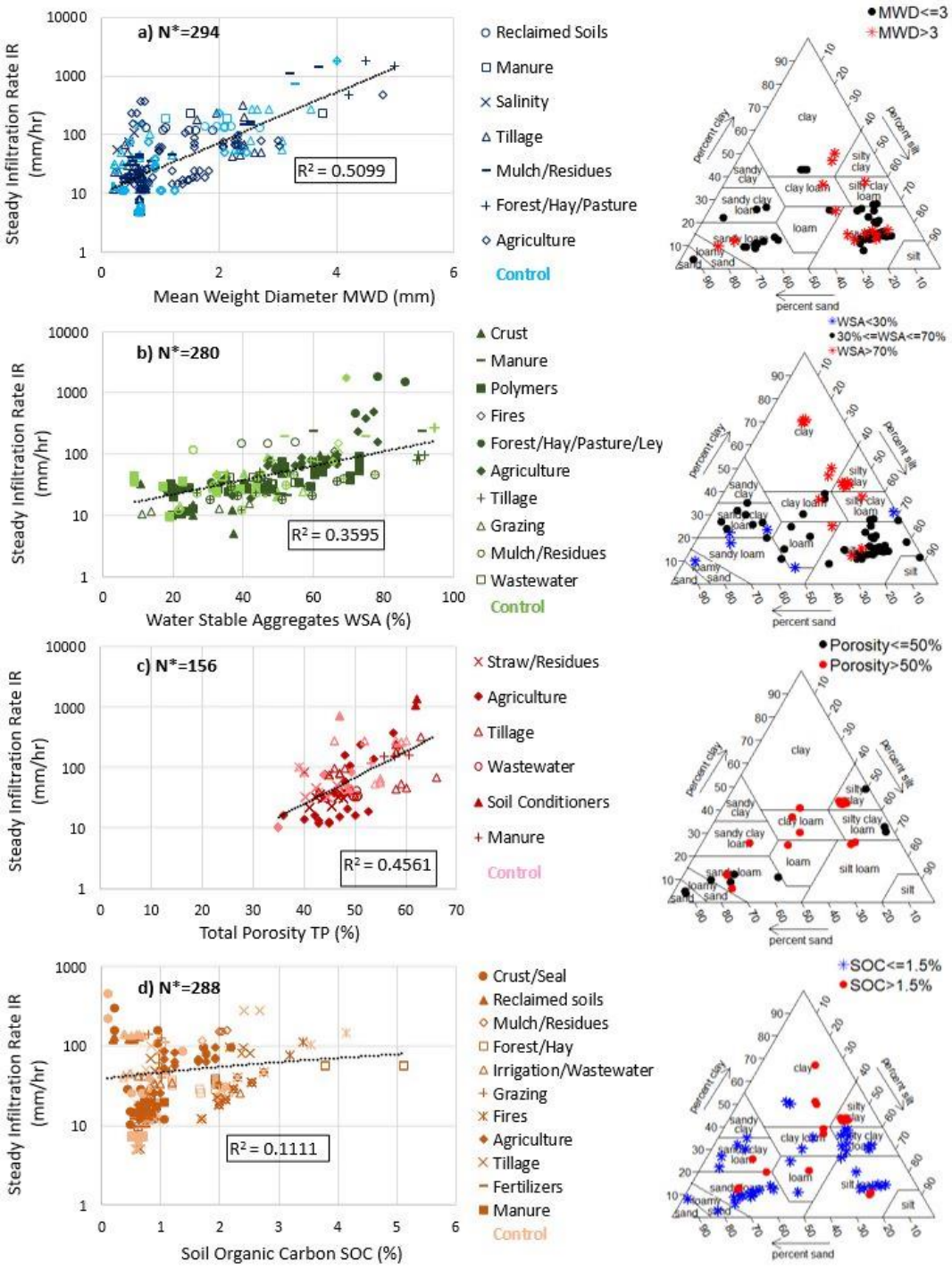

Figure 5.14: Steady infiltration rate IR (mm/hr) as function of a) mean weight diameter MWD (mm), b) water stable aggregates WSA (%), c) total porosity TP (%), and d) soil organic carbon SOC (%) for different soil practices and their respective control. N^* is the number of data points of the attributes (both treatment and control values) that exist in the same plots N (N^*=2N).

The data in Figure 5.14a indicates that steady infiltration rate is directly proportional to mean weight diameter MWD of soil aggregates with a reasonably fitted R^2 of 0.5099. Infiltration tends to increase as mean weight diameter increases, particularly for MDW > 1mm, and with $MWD >$ 3mm stimulating much higher infiltration rate than lower MWD. We further noticed that soils with $MWD > 3$ have a finer texture with higher clay and silt contents compared to soils with lower MWD. Despite their fine texture, these soils show the highest infiltration rate because fine particles can act as cementing agents for aggregation, resulting in a higher mean weight diameter compared to coarse materials. The high infiltration rate in these soils is therefore attributed to the effect of soil structure, a characteristic that profoundly affects water infiltration. Fine-textured soils with well-developed structure enhance water infiltration, whereas infiltration can be hindered in coarse-textured soils without a defined and stable structure, and especially if compacted. For instance, sandy loams have a strong tendency of structural degradation through compaction (Nawaz et al., 2013; Huang and Hartemink, 2020). That supports the notion that studying soil texture alone, without considering soil structure, is not enough for an effective assessment of soils' infiltration characteristics.

For water stable aggregates (WSA), Figure 5.14b shows no clear change in the steady infiltration rate as function of the % of water stable aggregates at lower values (WSA < 30%). For WSA varying between 30 and 70%, the steady infiltration rate seems to follow an increasing linear trend with the increase in % of water stable aggregates. An increase in the slope of this relationship seems possible above this range (WSA > 70%) thus indicating a nonlinear relationship overall. To interpret these clusters, we first assessed the particle size distribution of the studied soils over the three considered ranges of WSA. We noticed that soils with a very low WSA (< 30%) have a coarse texture composed of loamy sand, sandy loam, or sandy clay loam. On the other hand, soils

with higher WSA (> 70%) consist of fine textures ranging from clay loam, silty clay loam, silty clay to clay. As for soils with an intermediate WSA (between 30 and 70%), these soils are the most diverse and abundant among the data collected; they are mixed, but mostly of silty loam texture. These results were predictable due to the impact of soil texture on water stable aggregates. Fine textured soils have much greater surface area per unit volume ratio compared to soils with coarser particles. This helps in maintaining a stronger binding of soil particles and thus increases WSA. The highest infiltration rate in these fine-textured soils resulted from their high % of water stable aggregates, which again highlights the strong correlation between soil structure and water infiltration.

With respect to total porosity, a positive correlation (R^2 = 0.46) was found between the steady infiltration and total porosity data, as shown in Figure 5.14c. Increasing total soil porosity from 35 to 65% corresponds to an increase in the steady infiltration rate from 10 gradually up to 1000 mm/hr. With respect to soil texture data, the increase in total porosity concurs with an increase in the percentage of fine particles (silt and clay). Soils with porosity greater than 50% show the highest fines content which decreases as porosity goes below 50%. Figure 5.14c supports the significant influence of soil structure on water infiltration by showing that a high porosity is in favor of enhancing water infiltration only in well-structured soils.

Last but not least, Figure 5.14d displays a high overall variability in steady infiltration rate (IR, mm/hr) as function of soil organic carbon SOC (%). No significant trends were shown, but increased values of infiltration rate can be observed at higher values of soil organic carbon, particularly for SOC > 1.5%. A marginally slight increase in SOC does not necessarily influence soil structure and infiltration rates (Sastre et al., 2018). However, a significant increase in soil organic carbon is often associated with increased aggregation, physical stability, and permanent

pore development (Nyamadzawo et al., 2007; Jemai et al., 2012). Noellemeyer et al. (2008) showed that SOC turnover led to a loss of aggregation, and accordingly, soil hydraulic properties were negatively impacted in the longer term. The soil texture data in Figure 5.14d indicates that soils with high SOC (> 1.5%) have higher clay content as compared to soils with low carbon content (SOC < 1.5%). Clayey soils favor high carbon stocks due to the stabilizing and cementing properties of clays physically protecting soil organic carbon from microbial activity (Green et al., 2000; Noellemeyer et al., 2008).

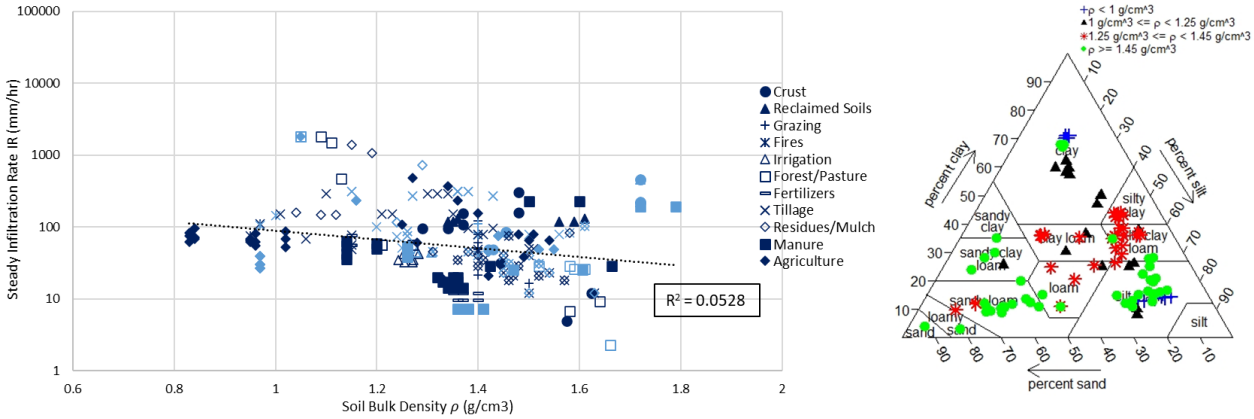

Figure 5.15: Steady infiltration rate IR (mm/hr) as function of soil bulk density ρ_b (g/cm³) for different soil practices and their respective control. N^* is the number of data points of the attributes (both treatment and control values) that exist in the same plots N (N^*=2N=306).

The data in Figure 5.15 shows a negative but weak relationship between soil bulk density and infiltration rate. For the most part, the steady infiltration rate is inversely related to soil bulk density, implying that a high bulk density can be an indicator of a low infiltration rate. But this figure still emphasizes the importance of addressing soil structure beyond bulk density given the fact over the wide range of bulk density for which the same or similar steady infiltration rate is observed. A representation of correlation between steady infiltration rate and bulk density is illustrated in the context of the USDA soil texture triangle which displays the particle size

distribution of soil groups classified into the following four categories of bulk density in descending rank: (1) $\rho_b \geq 1.45\ g/cm^3$, (2) $1.25 \leq \rho_b < 1.45\ g/cm^3$, (3) $1 \leq \rho_b < 1.25\ g/cm^3$ and (4) $\rho_b < 1\ g/cm^3$. High-density soils lie down at the base of the triangle while soils with low density are clustered at the mid-right to the top of the triangle. Coarse-textured soils (sandy soils) are more prone to high bulk density. Assuming same particle density, sandy soils have smaller porosity values (0.25-0.4) as compared to silt (0.35-0.5) and clayey soils (0.4-0.7) (Yu et al., 1993; Hillel, 2003). Given that bulk density is inversely related to total porosity, we can typically emphasize that coarse-textured soils are generally more dense than fine-textured soils.

5.4.5. Can Soil Structure Predict Infiltration Rate?

We performed a multilinear regression analysis using R software to build on the statistical correlations we explored and see if a combination of soil structural attributes can be used to predict infiltration rate. Our regression analysis led to the development of several pedo-transfer functions (PTFs) predicting steady infiltration rate (IR, mm/hr) as function of particle size distribution (PSD, % sand, silt, and clay) and four soil structural attributes: MWD (mm), WSA (%), soil bulk density ρ_b (g/cm^3), and soil organic carbon SOC (%) (Table 3). We reported PTFs that led to statistically significant results and came because of a wide number of data points N^* (referring to the number of data points for each attribute and including both the values under treatment and control in the same plots). As a result, we disregarded the PTFs with a considerably low R-squared value ($R^2 <$ 0.5) and low N^* (< 100).

Accordingly, our shortlisted PTFs had reasonable R^2 ranging from 0.51 to 0.80, and a number of data points N^* ranging from 100 to 294 (each representing a unique plot). The developed PTFs were further illustrated in Figure 5.16 which plots the observed vs. predicted values of steady IR (mm/hr) to emphasize the accuracy (with R^2 values of 0.51-0.80) and reliability (with CV values

lower than 27%) of our predictions. A very important observation from Table 5.3 is that SOC improved the predictability of IR. This is a very significant finding implying that IR is not a static soil parameter, but rather a dynamic one that changes according to the dynamics of soil organic carbon. Therefore, our results show that soil structure, with its dynamic, time- and scale-dependent behavior, can predict water infiltration. More importantly, this allows for a water infiltration predictive tool that is dynamic and can account for changes in water infiltration properties as function of dynamic changes in soil structure that can result from varied land or soil management. As such, those PTFs can capture changes in water infiltration rate because of variations in the dynamic soil structural properties including mean weight diameter, % of water stable aggregates, bulk density, and soil organic carbon. In addition, involving the changes in soil texture improves the predictability of IR, which again supports the notion that soil structure and soil texture together, lead to a stronger assessment of soils' infiltration characteristics.

Table 5.3: Pedo-transfer functions (PTFs) predicting steady IR (mm/hr) as function of PSD (%sand, silt, and clay) different soil structural attributes, MWD (mm), WSA (%), bulk density BD (ρ_b, g/cm^3), and soil organic carbon SOC (%). Only PTFs that have an R-squared value $R^2 \geq 0.5$ and a number of data points $N^* \geq 100$ were considered.

Response Y	Variables X	Equation	R^2	N^*
Steady IR (mm/hr)	MWD (mm)	$logIR = 2.33 + 0.98MWD$	0.5099	294
	MWD (mm) + SOC (%)	$logIR = 1.42 + 1.14MWD + 0.57SOC$	0.5679	172
	MWD (mm) + WSA (%)	$logIR = 1.88 + 0.59MWD + 0.026WSA$	0.696	128
	MWD (mm) + SOC (%) + ρ_b (g/cm^3)	$log(IR) = 2.55 + 0.81MWD - 0.19SOC + 0.55\rho_b$	0.704	100
	Including PSD			
	MWD (mm) + Sand (%)	$logIR = 2.73 + 1.05MWD - 0.013Sand$	0.7121	166
	MWD (mm) + Silt (%)	$logIR = 1.68 + 1.08MWD + 0.012Silt$	0.7125	166
	MWD (mm) + Clay (%)	$logIR = 2.08 + 1.19MWD - 0.009Clay$	0.6638	198
	MWD (mm) + SOC (%) + Sand (%)	$logIR = 2.67 + 1.59MWD - 0.6SOC - 0.015Sand$	0.7406	120
	MWD (mm) + SOC (%) + Silt (%)	$logIR = 1.47 + 1.52MWD - 0.49SOC + 0.014Silt$	0.7524	120
	MWD (mm) + SOC (%) + Clay (%)	$logIR = 3.4 + 1.12MWD + 0.29SOC - 0.097Clay$	0.8007	120
Log is natural logarithm (i.e., base *e*)				

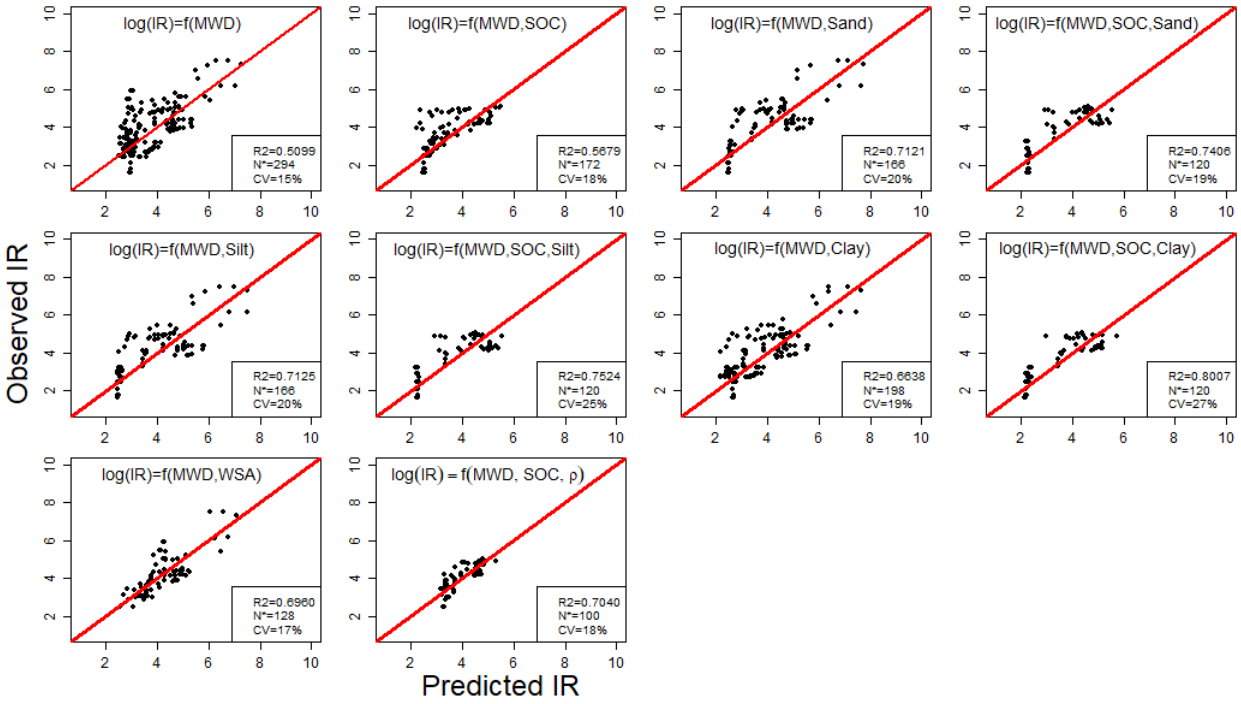

Figure 5.16: Observed vs. predicted values of steady infiltration rate IR (mm/hr) by each developed PTF with the corresponding equation, R^2, number of data points N^*, and coefficient of variation CV (%).

5.4.6. Can Soil Structure Predict Hydraulic Conductivity?

As we obtained accurate and reliable PTFs predicting steady infiltration rate IR in soils, we were further interested in exploring significant correlations relating the hydraulic conductivity K_{sat} (mm/h) to soil structural properties. As such, we applied a similar multilinear regression approach in R (Table 5.4).

Table 5.4: Pedo-transfer functions (PTFs) predicting saturated hydraulic conductivity K_{sat} (mm/h) as a function of different soil structural attributes, MWD (mm), bulk density BD (ρ_b, g/cm^3), and soil organic carbon SOC (%).

Response Y	Variables X	Equation	R^2	N^*
Ksat (mm/hr)	MWD (mm)	$log(K_{sat}) = -1.19 + 1.38MWD$	0.2067	112
	MWD (mm) + SOC (%)	$log(K_{sat}) = -1.11 + 2.67MWD - 0.29SOC$	0.3467	82
	MWD (mm) + SOC (%) + ρ_b (g/cm^3)	$log(K_{sat}) = 13.65 + 1.65MWD - 3.46SOC - 5.67\rho_b$	0.7824	64

Only three developed PTFs were able to predict the hydraulic conductivity K_{sat} (mm/h) as a function of soil structural properties. Also, these PTFs were less accurate than the previously developed functions relating infiltration rate (IR) with soil structural properties (Table 5.3). The difference in results between IR and K_{sat} predictions can be partly attributed to the significantly large difference in data points representing the two variables in our dataset (N^*=932 compared to N*=334 data points descriptive of IR and K_{sat}, respectively). However, there was one significant correlation reported for predicting K_{sat} (mm/h) as function of three structural properties (MWD, mm), bulk density (BD, g/cm^3), and soil organic carbon (SOC, %) with a significant R^2 of 0.7824. Despite the low number of corresponding data points (N^*=64), this correlation highlights reliable and promising K_{sat} predications as function of soil structure attributes that we can further enhance when larger datasets are available. Interestingly, this correlation provided a PTF that can successfully predict K_{sat} without the need for soil texture information. In fact, we attempted to include soil texture (%sand, silt, or clay) to this PTF and the predictability of K_{sat} was not improved

for our dataset. This finding can have significant implication on the parameterization of hydrologic models and shows the importance of soil structure in predicting K_{sat}.

5.4.7. Theoretical set

Finally, we evaluate the second dataset comprising the 22 theoretical papers that we obtained from the systematic review. Those papers were further divided into two categories: one category of 14 papers emphasized new models (Parlange et al., 1982; Helalia, 1993; Messing and Jarvis, 1993; Greco, 2002; Lepore et al., 2009; Li and Zhang, 2011; Tiktak et al., 2012; King and Bjorneberg, 2012; Braudeau and Mohtar, 2014; Coppola et al., 2015; Dong et al., 2017; Rahmati, 2017; Mohammadzadeh-Habili et al, 2018; Fatichi et al., 2020) and another category (8 papers) utilized developed models, particularly HYDRUS-1/2/3D, for water flow simulations (Germann and Hensel, 2006; Sander and Gerke, 2009; Laloy et al., 2010; Rajeswari et al., 2010; Zehe et al., 2010; Schwärzel et al., 2011; Xu et al., 2017; Belcaid et al., 2020).

Here, we want to highlight one of the most significant outcomes of this search, which is its inability to identify many of the classic contributions that assessed the effect of structure on infiltration. In fact, the search outcomes highlight the significant absence of and the need for modeling efforts to derive a comprehensive theoretical framework around different soil structural attributes that are impacted by different land uses. We realize that such a comprehensive framework is still an open research question. However, this research highlights that a wide literature review, using the general search criteria defined in Table 5.1, has missed a significant number of theoretical contributions that should have been included or captured. Those missing include papers that have developed models or theoretical frameworks for soil structure characterization and its influence on water infiltration (Ex.: Pachepsky and Rawls (2003); Jorda et al., 2015; Araya and Ghezzehei, 2019). For instance, Pachepsky and Rawls (2003) provided a quantitative characterization of the field soil

structure using pedo-transfer functions that show empirical relationships between soil structure and hydraulic properties. Also, Jorda et al. (2015) predicted the soil hydraulic conductivity from other more easily obtained soil and land characteristics (e.g., bulk density) in a study using 487 data points gathered from the literature. Later, Araya and Ghezzehei (2019) realized how difficult it is to accurately model the complex and non-linear relationships between soil structural variables and infiltration properties using physically based models or traditional statistical methods. Therefore, they developed new accurate PTFs which predict the saturated hydraulic conductivity K_s using machine learning ML, high performance computing, and a large database of over 18,000 soils. Their study opens an opportunity to revise the challenges encountered in soil structure characterization and therefore conduct future research that can engage our metadata of soil hydraulic and structural properties with the current progress in ML tools.

Yet, these papers (and many others, as the above three papers present a noncomprehensive list of other papers that should have been included) could not be retrieved from the literature sources in our search because they did not include the keywords "structure" and "infiltration" terms in their title and/or abstract. As a result, these papers could not make it through the initial literature screening of our systematic review. This shows that soil structure remains an underutilized term in soil physics; impacted by the lack of universally applicable and reliable quantitative measures of soil structure. This challenge exacerbates when structure is dynamically changing in space and time.

5.5. Conclusion

We presented a narrative systematic review (SR) of the impacts of soil structure on water infiltration. Following the (SR) methodology, we first formulated the primary research question entitled "how does soil structure affect infiltration?". Then, we conducted a literature search tailored to that question based on predefined inclusion criteria. Following our literature search, we screened the retrieved literature by title/abstract, and analyzed the extracted data. The total number of title- and abstract-screened literature including "soil structure" and "infiltration" retrieved from publishing sources (Scopus, ScienceDirect, and GoogleScholar) was 153 studies, divided into 131 experimental and 22 theoretical papers. Results have demonstrated the dominance of field-scale experimental studies comparing field responses under different soil practices or treatments over the modeling efforts studying the effects of soil structure on water infiltration. In addition, most of these studies are on the order of five years or less. This is probably attributed to the fact that typical research projects have a duration of less than 5 years. We identify this as a major limitation to the advancement of our understanding of soil structure as changes take much longer time to develop. Then upon analyzing the metadata extracted from the collected papers (N= 800 data points), our results suggested that land use (a variable that most directly impacts soil structure) profoundly affects water infiltration. More specifically, soil amendments and crop management improve water infiltration and soil structure, whereas tillage negatively impacts water infiltration (initial and steady state). As for the effects of tillage on soil structure, our data has demonstrated different responses of soil structural attributes to tillage. Our systematic review shows that tillage decreases the mean weight diameter, while it can increase the % of water stable aggregates. Consequently, significant correlations were established between infiltration rate and soil structural properties (such as bulk density, wet aggregate stability, mean weight diameter, organic carbon, and

porosity), highlighting the positive effects of improving soil structure on water infiltration. They also highlight the dynamic (temporal) nature of infiltration response, given that organic carbon (a dynamic property) showed an ability to improve the predictions of infiltration rate. In addition, soil structure and soil texture assessed together, lead to a stronger predictability of soils' infiltration characteristics than when each soil property is considered alone. Finally, this study highlights the need to utilize the growing availability of large databases along with accurate data-driven methods, to research new predictive data-science methods, and to direct future research efforts towards comprehensive theoretical frameworks around the understanding of the impacts of soil management on different soil hydraulic and structural attributes, and their corresponding impact on infiltration.

5.6. References

Abou Najm, M., J. D. Jabro, W. M. Iversen, R. H. Mohtar, and R. G. Evans (2010). New method for the characterization of three-dimensional preferential flow paths in the field, *Water Resources Research*, 46, W02503, doi:10.1029/2009WR008594

Abou Najm, M. R., Stewart, R. D., Di Prima, S., & Lassabatere, L. (2021). A Simple Correction Term to Model Infiltration in Water-Repellent Soils. *Water Resources Research*. https://doi.org/10.1029/2020WR028539

Araya, S. N., & Ghezzehei, T. A. (2019). Using Machine Learning for Prediction of Saturated Hydraulic Conductivity and Its Sensitivity to Soil Structural Perturbations. *Water Resources Research*. https://doi.org/10.1029/2018WR024357

Beven, K., & Germann, P. (1982). Macropores and water flow in soils. *Water Resources Research*. https://doi.org/10.1029/WR018i005p01311

Belcaid, A., Benaicha, M., Le Palec, G., & Draoui, A. (2020). Simulation of Water Infiltration Process into a Porous Unsaturated Soil: Application on Tangier's Bay Region-Morocco. *Geotechnical and Geological Engineering*. https://doi.org/10.1007/s10706-019-01024-7

Braudeau, E. F., & Mohtar, R. H. (2014). A framework for soil-water modeling using the pedostructure and Structural Representative Elementary Volume (SREV) concepts. *Frontiers in Environmental Science*, *2*(JUN). https://doi.org/10.3389/fenvs.2014.00024

Chen, Q., Kravchenko, Y. S., Li, H., Chen, S., & Zhang, X. (2016). Seasonal variation of physical and chemical properties in a black soil under No-till and conventional tillage in Northeast China. *Philippine Agricultural Scientist*, *99*(3), 277–282.

Coppola, A., Comegna, A., Dragonetti, G., Gerke, H. H., & Basile, A. (2015). Simulated preferential water flow and solute transport in shrinking soils. *Vadose Zone Journal*, *14*(9). https://doi.org/10.2136/vzj2015.02.0021

Coughlan, K. J., McGarry, D., Loch, R. J., Bridge, B., & Smith, G. D. (1991). The measurement of soil structure—some practical initiatives. *Australian Journal of Soil Research*. https://doi.org/10.1071/SR9910869

Dexter, A. R. (1988). Advances in characterization of soil structure. *Soil and Tillage Research*. https://doi.org/10.1016/0167-1987(88)90002-5

Di Prima, S., Stewart, R. D., Abou Najm, M. R., Ribeiro Roder, L., Giadrossich, F., Campus, S., Angulo-Jaramillo, R., Yilmaz, D., Roggero, P. P., Pirastru, M., & Lassabatere, L. (2021). BEST-WR: An adapted algorithm for the hydraulic characterization of hydrophilic and water-repellent soils. *Journal of Hydrology*. https://doi.org/10.1016/j.jhydrol.2021.126936

Dong, H., Huang, R., & Gao, Q.-F. (2017). Rainfall infiltration performance and its relation to mesoscopic structural properties of a gravelly soil slope. *Engineering Geology*, *230*, 1–10.

https://doi.org/10.1016/j.enggeo.2017.09.005

Fatichi, S., Or, D., Walko, R., Vereecken, H., Young, M. H., Ghezzehei, T. A., Hengl, T., Kollet, S., Agam, N., & Avissar, R. (2020). Soil structure is an important omission in Earth System Models. *Nature Communications*, *11*(1). https://doi.org/10.1038/s41467-020-14411-z

Franzluebbers, A. J. (2002). Water infiltration and soil structure related to organic matter and its stratification with depth. *Soil and Tillage Research*. https://doi.org/10.1016/S0167-1987(02)00027-2

Germann, P. F., & Hensel, D. (2006). Poiseuille flow geometry inferred from velocities of wetting fronts in soils. *Vadose Zone Journal*, *5*(3), 867–876. https://doi.org/10.2136/vzj2005.0080

Greco, R. (2002). Preferential flow in macroporous swelling soil with internal catchment: Model development and applications. *Journal of Hydrology*, *269*(3–4), 150–168. https://doi.org/10.1016/S0022-1694(02)00215-9

Green, V. S., Stott, D. E., Norton, L. D., & Graveel, J. G. (2000). Polyacrylamide Molecular Weight and Charge Effects on Infiltration under Simulated Rainfall. *Soil Science Society of America Journal*. https://doi.org/10.2136/sssaj2000.6451786x

Hamblin, A. P. (1986). The influence of soil structure on water movement, crop root growth, and water uptake. *Advances in Agronomy*. https://doi.org/10.1016/S0065-2113(08)60674-4

Helalia, A. M. (1993). The relation between soil infiltration and effective porosity in different soils. *Agricultural Water Management*, *24*(1), 39–47. https://doi.org/10.1016/0378-3774(93)90060-N

Hillel, D. (2003). *Introduction to environmental soil physics*. Elsevier.

Huang, J., & Hartemink, A. E. (2020). Soil and environmental issues in sandy soils. *Earth-Science Reviews*, *208*, 103295.

Jemai, I., Ben Aissa, N., Ben Guirat, S., Ben-Hammouda, M., & Gallali, T. (2012). On-farm assessment of tillage impact on the vertical distribution of soil organic carbon and structural soil properties in a semiarid region in Tunisia. *Journal of Environmental Management*. https://doi.org/10.1016/j.jenvman.2012.05.029

Jorda, H., Bechtold, M., Jarvis, N., & Koestel, J. (2015). Using boosted regression trees to explore key factors controlling saturated and near-saturated hydraulic conductivity. *European Journal of Soil Science*. https://doi.org/10.1111/ejss.12249

Kahlon, M. S., Lal, R., & Ann-Varughese, M. (2013). Twenty two years of tillage and mulching impacts on soil physical characteristics and carbon sequestration in Central Ohio. *Soil and Tillage Research*. https://doi.org/10.1016/j.still.2012.08.001

Kay, B. D., & Angers, D. A. (2001). 7 Soil Structure. *Soil Physics Companion*, 249.

King, B. A., & Bjorneberg, D. L. (2012). Transient soil surface sealing and infiltration model for bare soil under droplet impact. *Transactions of the ASABE*, *55*(3), 937–945.

Lal, R. (1991). Soil structure and sustainability. *Journal of Sustainable Agriculture*. https://doi.org/10.1300/J064v01n04_06

Laloy, E., Weynants, M., Bielders, C. L., Vanclooster, M., & Javaux, M. (2010). How efficient are one-dimensional models to reproduce the hydrodynamic behavior of structured soils subjected to multi-step outflow experiments? *Journal of Hydrology*, *393*(1–2), 37–52. https://doi.org/10.1016/j.jhydrol.2010.02.017

Lepore, B. J., Morgan, C. L. S., Norman, J. M., & Molling, C. C. (2009). A Mesopore and Matrix infiltration model based on soil structure. *Geoderma*, *152*(3–4), 301–313. https://doi.org/10.1016/j.geoderma.2009.06.016

Levine, E. R., Kimes, D. S., & Sigillito, V. G. (1996). Classifying soil structure using neural networks. *Ecological Modelling*. https://doi.org/10.1016/0304-3800(95)00199-9

Li, J. H., Zhang, L. M., & Li, X. (2011). Soil-water characteristic curve and permeability function for unsaturated cracked soil. *Canadian Geotechnical Journal*, *48*(7), 1010–1031. https://doi.org/10.1139/t11-027

Melman, D. A., Kelly, C., Schneekloth, J., Calderón, F., & Fonte, S. J. (2019). Tillage and residue management drive rapid changes in soil macrofauna communities and soil properties in a semiarid cropping system of Eastern Colorado. *Applied Soil Ecology*, *143*, 98–106. https://doi.org/10.1016/j.apsoil.2019.05.022

Messing, I., & Jarvis, N. J. (1993). Temporal variation in the hydraulic conductivity of a tilled clay soil as measured by tension infiltrometers. *Journal of Soil Science*, *44*(1), 11–24. https://doi.org/10.1111/j.1365-2389.1993.tb00430.x

Mohammadzadeh-Habili, J., Heidarpour, M., & Khalili, D. (2018). Effect of aggregate size and porosity of clay soils on the hydraulic parameters of the Green-Ampt infiltration model. *Journal of Hydrologic Engineering*, *23*(3). https://doi.org/10.1061/(ASCE)HE.1943-5584.0001628

Nawaz, M. F., Bourrié, G., & Trolard, F. (2013). Soil compaction impact and modelling. A review. *Agronomy for Sustainable Development*, *33*(2), 291–309. https://doi.org/10.1007/s13593-011-0071-8

Noellemeyer, E., Frank, F., Alvarez, C., Morazzo, G., & Quiroga, A. (2008). Carbon contents and aggregation related to soil physical and biological properties under a land-use sequence in the semiarid region of central Argentina. *Soil and Tillage Research*. https://doi.org/10.1016/j.still.2008.02.003

Nouri, A., Lee, J., Yin, X., Tyler, D. D., & Saxton, A. M. (2019). Thirty-four years of no-tillage

and cover crops improve soil quality and increase cotton yield in Alfisols, Southeastern USA. *Geoderma*, *337*, 998–1008. https://doi.org/10.1016/j.geoderma.2018.10.016

Nyamadzawo, G., Chikowo, R., Nyamugafata, P., & Giller, K. E. (2007). Improved legume tree fallows and tillage effects on structural stability and infiltration rates of a kaolinitic sandy soil from central Zimbabwe. *Soil and Tillage Research*, *96*(1–2), 182–194. https://doi.org/10.1016/j.still.2007.06.008

Pachepsky, Y. A., & Rawls, W. J. (2003). Soil structure and pedotransfer functions. *European Journal of Soil Science*. https://doi.org/10.1046/j.1365-2389.2003.00485.x

Pagliai, M., Vignozzi, N., & Pellegrini, S. (2004). Soil structure and the effect of management practices. *Soil and Tillage Research*. https://doi.org/10.1016/j.still.2004.07.002

Parlange, J. Y., Lisle, I., Braddock, R. D., & Smith, R. E. (1982). The three-parameter infiltration equation. *Soil Science*. https://doi.org/10.1097/00010694-198206000-00001

Rahmati, M. (2017). Reliable and accurate point-based prediction of cumulative infiltration using soil readily available characteristics: A comparison between GMDH, ANN, and MLR. *Journal of Hydrology*, *551*, 81–91. https://doi.org/https://doi.org/10.1016/j.jhydrol.2017.05.046

Rajeswari, M., Sankar, G. M., Ranghaswami, M. V., & Mishra, P. K. (2007). Screening of soil amendments for efficient water-holding capacity based on a rainfall-infiltration model in a vertisol. *Journal of Irrigation and Drainage Engineering*, *133*(5), 468–474. https://doi.org/10.1061/(ASCE)0733-9437(2007)133:5(468)

Sander, T., & Gerke, H. H. (2009). Modelling field-data of preferential flow in paddy soil induced by earthworm burrows. *Journal of Contaminant Hydrology*, *104*(1–4), 126–136. https://doi.org/10.1016/j.jconhyd.2008.11.003

Sastre, B., Marques, M. J., García-Díaz, A., & Bienes, R. (2018). Three years of management with cover crops protecting sloping olive groves soils, carbon and water effects on gypsiferous soil. *Catena*. https://doi.org/10.1016/j.catena.2018.07.003

Schwärzel, K., Carrick, S., Wahren, A., Feger, K.-H., Bodner, G., & Buchan, B. (2011). Soil hydraulic properties of recently tilled soil under cropping rotation compared with two-year pasture. *Vadose Zone Journal*, *10*(1), 354–366. https://doi.org/10.2136/vzj2010.0035

Tiktak, A., Hendriks, R. F. A., & Boesten, J. J. T. I. (2012). Simulation of movement of pesticides towards drains with a preferential flow version of PEARL. *Pest Management Science*, *68*(2), 290–302. https://doi.org/10.1002/ps.2262

Xu, X., Kalhoro, S. A., yuan Chen, W., & Raza, S. (2017). The evaluation/application of Hydrus-2D model for simulating macro-pores flow in loess soil. *International Soil and Water Conservation Research*, *5*(3), 196–201. https://doi.org/10.1016/j.iswcr.2017.05.010

Yu, C., Cheng, J. J., Jones, L. G., Wang, Y. Y., Faillace, E., Loureiro, C., & Chia, Y. P. (1993). *Data collection handbook to support modeling the impacts of radioactive material in soil*. Argonne National Lab.

Zehe, E., Blume, T., & Blöschl, G. (2010). The principle of "maximum energy dissipation": A novel thermodynamic perspective on rapid water flow in connected soil structures. *Philosophical Transactions of the Royal Society B: Biological Sciences*, *365*(1545), 1377–1386. https://doi.org/10.1098/rstb.2009.0308